February, 2017

Ph.D Dissertation

Design of replaceable reduced link sections for eccentrically braced frames

Graduate School of Chosun University

Department of Architectural Engineering

Major: Steel Structure and Earthquake Engineering

Daniel Yeshewawork Abebe

Design of replaceable reduced link sections for eccentrically braced frames

편심 브레이스 골조의 교체가능한 링크빔의 설계

February 24, 2017

Graduate School of Chosun University
Department of Architectural Engineering
Major: Steel Structure and Earthquake Engineering
Daniel Yeshewawork Abebe

Design of replaceable reduced link sections for eccentrically braced frames

Advisor: Professor Jaehyouk Choi (Dr. Eng.)

This dissertation is submitted to graduate school of Chosun University in partial fulfillment of the requirements for the degree of
Doctor of Philosophy
in
Architectural Engineering

October, 2016

Graduate School of Chosun University

Department of Architectural Engineering

Major: Steel Structure and Earthquake Engineering

Daniel Yeshewawork Abebe

The doctoral dissertation committee for Daniel Y. Abebe certifies that this is the approved version.

Committee:

Professor Jeong-oug Park, Chosun University
(Chair Committee)

Professor Chang-geun Cho, Chosun University
(Committee Member)

Professor Jae-hyouk Choi, Chosun University
(Committee Member)

Professor Sang-hoon Oh, Pusan National University
(Committee Member)

Professor Young-kyu Ju, Korea University
(Committee Member)

December, 2016

Graduate School of Chosun University

Content

List of Figures

CHAPTER 1

CHAPTER 2

CHAPTER 3

CHAPTER 4

CHAPTER 5

CHAPTER 6

CHAPTER 7

APPENDIX A

APPENDIX B

APPENDIX C

APPENDIX D

APPENDIX E

List of Tables

Chapter 3

CHAPTER 4

CHAPTER 5

CHAPTER 6

APPENDIX E

Nomenclature

e: link length
E: young's modulus
σ_y: yield stress
σ_u: ultimate stress
M_p: plastic end-moment
M_n: nominal end moment
V_p: plastic shear force
V_n: nominal shear strength
V_L: shear strength of link
V: shear strength of story
d: depth of link
t_f: flange thickness
t_w: web thickness
b_f: flange width
Z: plastic section modulus
Z_p^{rl}: plastic section modulus at center of the reduced link section
ρ: link length factor
γ: link rotation
γ_p: plastic rotation
γ_e: elastic rotation
θ_p: overall frame drift
γ_e: elastic rotation
R_y: the ratio of mean to normal material yield stress
θ_B: rotation of link in beam end
θ_C: rotation of link in column end
M_B: end-moment in column face
M_C: end-moment in beam face
k_B: spring constant in beam end
k_C: spring constant in column end
α: relative stiffness of column
β: relative stiffness of beam
R: Radius of cutoff
c: depth of cut at center of the reduced link section
σ_r: radial stress
σ_θ: tangential stress
$\sigma_{r\theta}$: shear stress
r: the distance from the hole center
τ: applied shear stress
θ: counter clockwise angle relative to a horizontal datum
γ_{tf}: tension filed angle
A_w: cross-sectional area of web
A_w^*: cross-sectional area of reduced web
D: Link Depth
d: effective link depth
V_p^{rw}: plastic shear for reduced web
n: number of perforation in a vertical alignment
ϕ: diameter of perforation
ρ_{rw}: reduced web link length factor
e_{rw}: reduced link length
ρ_{rl}: reduced web and flange link length factor
e_{rl}: reduced web and flange link length
V_p^{rl}: plastic shear strength of reduced web and flange link

Nomenclature (*continued...*)

M_p^{rl}: plastic end-moment of reduced web and flange link

K_e: elastic stiffness

G: Shear modulus

I: moment of inertia

Ω: overstrength factors

$V_{\max}$: maximum shear recorded

σ_{tr}: true stress

σ_e: engineering stress

σ_{eq}: equivalent stress

σ_m: mean stress

ε^{cr}: critical plastic strain

ε_e: engineering strain

ε^p: equivalent plastic strain

C_k and ψ: parameters of the model

σ_0: yield stress at zero equivalent plastic strain

Q_∞: maximum change in the size of the yield surface

v: the rate at which the size of the yield surface changes

σ_i^t: maximum tensile stress

σ_i^c: maximum compressive stress

$\Delta\varepsilon_p$: plastic strain range

K_T: initial stiffness of experimental result

K_A: initial stiffness of analytical result

I_f: failure index for monotonic loading

ε_t: tensile strain

ε_c: compresive strain

ε^*: critical plastic strain

λ: positive material parameter

I_f^*: cyclic failure index

E_l: cumulative energy dissipated

$ed\gamma$: link end plastic shear deformation

ξ_{eq}: equivalent viscous damping

$\xi_{eq,o}$: initial damping in the elastic range or viscous damping

$\xi_{eq,hyst}$: inelastic hysteresis damping.

t_e: thickness of end plate

τ_{tr}: stress triaxiality ratio

ε_y: yield strain

RI: Rupture Index

ε_y: yield strain

ε_{ij}: plastic strain components

σ_1: normal stresses in x

σ_2: normal stresses in y

σ_3: normal stresses in z

V_p': plastic shear considering the effect of flange

V_f: shear carried by the flanges

V_{ult}: ultimate shear force

ABSTRACT

Design of replaceable reduced link sections for eccentrically braced frames

Daniel Y. Abebe
Advisor : Prof. Jaehyouk Choi, Ph.D.
Department of Architectural Engineering
Graduate School of Chosun University

Eccentrically braced frames (EBFs) are lateral force resisting system developed to resist earthquake loads in a predictable manner. They are designed and detailed to have ductile behavior only in the link that yields either in shear or flexural or combined shear and flexural depending on the link length. The link should have the capacity of resisting load under repeated load so that the seismic energy will be absorbed.

The maintenance and repairing cost of the damaged members after earthquake is an expensive operation if the damaged member is not isolated from the main structures. The functionality of building may also be affected in the process of repairing the damaged members which will in turn increases the overall economic loss. However, if the dissipative members are isolated from the other structures, they can be maintained or replaced after an earthquake. These decreases the repairing cost and the interruption of building use won't affected. Thus, in existing conventional eccentrically braced frames, the active links was not isolated from other structural components. These can be taken as a main limitation of conventional eccentrically braced frames.

In order to address the limitation of contentional eccentrically braced frames, researchers came up with the concept of EBFs with removable links and a number of research work have been done on this issue. Researches shows that, in order to control the plastic deformation at the link, the link should be designed weaker in strength or less cross-sectional area than the collector beam. However; links with less cross-section with collector beam, results in difficulties during slab construction and may require deck support over replaceable links.

Link-to-column connection in eccentrically braced frames (EBFs), tend to fracture in the link flange prior to large link rotations due to column connection attracts greater moment because the axial stiffness of the column is stiffer than the flexural stiffness of the beam. AISC provisions also warns designers of this problem which is an indication it is an ongoing research.

In this research, replaceable links with reduced web section and links with reduced web and flange sections were proposed and investigated in order to address the limitations of EBFs listed above. The merit of the aimed links are: First, since the proposed links are isolated from the main structural components such as collector beam and columns, they are easily replaced or maintained in post earthquake. Second, these links have weaker in strength than the collector beam since the section is reduced but have equal cross-section which makes easer for the slab construction. Finally, the reduced sections of web reduces stress and strain values in the links flange at the connection. On the other hand, the perforations (holes) in web increases the plastic strain and stress at the edge of perforations, thus fracture is concentrated at the web so that the fracture at the link flange-to-column welds will be avoided.

The effectiveness of the proposed links were evaluated using non-linear finite element method and quasi-static loading test to evaluate the cyclic inelastic performance considering different parameters. The parameters considered includes: section compactness, percent of reduced web area, link length and effect of stiffeners. The effects of these parameters on the plastic rotation, overstrength factor and the deformation mode were presented. The results obtained from FE analysis and experiment shows that the replaceable links both with reduced web sections and reduced web and flange sections satisfies the plastic rotation level recommended by AISC—341-10 provision. Design equations were recommended for the proposed links considering the geometry and engineering mechanics. The equation were verified by the analysis and experimental results. In addition, the analysis model developed by different researchers were applied for the proposed links and it is found that the developed model can also applied for links with reduced sections.

ABSTRACT

편심 브레이스 골조의 교체가능한 링크빔의 설계

Daniel Y. Abebe
Advisor : Prof. Jaehyouk Choi, Ph.D.
Department of Architectural Engineering
Graduate School of Chosun University

편심브레이스프레임(Eccentrically braced frames (EBFs))은 지진하중에 견딜 수 있도록 개발된 구조물의 지진저항시스템 중의 하나이다. 편심브레이스프레임이 갖는 링크빔(Link beam) 구간은 전단, 휨, 또는 전단과 휨이 동시에 발생하는 구조물에 충분한 연성거동을 할 수 있도록 설계되어있다. 따라서 링크부분은 지진에너지가 흡수될 수 있도록 반복하중에 대해서 효과적으로 에너지가 흡수 될 수 있도록 설계되어야 한다.

한편 지진발생 후 부재에 손상이 발생한 경우, 손상 부재가 주요 구조물로부터 격리되지 않은 경우 주구조체 전체의 교체로 인해 유지보수비용 측면에서 많은 비용이 발생한다. 이는 건축물의 기능을 손상전의 상태로 복구하는 과정에서 경제적 손실을 증가시킨다. 그러나 링크빔이 다른 구조물로부터 격리되어 있는 경우, 지진 후에 손상된 부분만 간단히 교체함으로서 구조물 전체를 손상전의 상태로 복구하는 것이 가능하다. 이는 수리비용을 획기적으로 절감할 수 있으며, 대규모의 지진발생 이후에도 건축물을 즉시 사용할 수 있는 기능을 제공한다. 일반적으로 사용되는 기존의 편심브레이스 프레임의 링크빔 부분은 주구조체로부터 분리되어 있지 않아 교체 가능한 지진저항시스템으로서 복구에 한계를 가지고 있다.

기존의 편심 브레이스프레임의 한계를 해결하기 위해, 많은 연구자들은 교체 가능한 링크부를 갖는 EBF시스템을 개발하고자 다양한 디테일을 제안하고 그 구조적 성능검증을 위한 연구를 활발히 진행하고 있다. 지금까지의 연구 결과에 따르면 링크부의 소성 변형을 제어하기 위해서 링크빔의 재료강도를 약하게 하거나 링크빔에 연결된 컬렉터 빔에 비해 보의 높이를 작게 설계하는 것으로 해결책을 찾고 있다 .

그러나 콜렉터 빔과의 보의 높이를 감소시킨 링크빔은 슬래브를 시공하기가 어려우며, 교체 가능한 디테일을 형성하기 위해서 별도의 장치를 필요로 하고 있다.

한편, 편심 브레이스 프레임(EBF)이 기둥부재와 연결되어 될 때 기둥의 축 방향 강성이 보의 굽힘 강성보다 더 높을 경우 링크부의 회전능력이 충분히 발휘되기 전에 링크 플랜지에서 파손되는 경향이 있어 AISC 규정에서도 주의 깊은 사용을 권장하고 있다.

본 논문에서는 앞서 언급한 EBFs의 적용 한계를 해결하기 위해 웨브와 플렌지

의 단면적을 감소시켜 충분한 에너지소산능력을 발휘하면서도 시공성과 교체가능성을 확보된 새로운 형태의 링크부를 제안하였다. 제안된 링크빔에 대한 이점은 다음과 같다. 첫번째 보 또는 기둥과 같은 주요 구조요소로부터 분리가 가능하도록 설계되어 지진 후에도 쉽게 교체가 가능하다. 두번째 링크빔의 높이를 감소시킨 것이 아니라 웨브와 플랜지내의 단면적을 감소시킴으로 주요 보 부재보다 강도는 약해지지만 교차단면은 동일하게 유지되어 슬래브 시공을 원활하게 할 수 있다. 마지막으로 웨브와 플랜지의 단면적 감소비를 조절하여 링크부의 공칭강도를 자유롭게 설계 할 수 있다, 또한 링크 플랜지와 기둥간 용접부의 파괴를 방지하여 웨브의 오픈 홀 가장자리에서 응력집중이 발생하도록 유도할 수 있다.

제안된 링크의 성능을 확인하기 위해 section compactness , 웨브와 플랜지의 단면 감소량, 링크부의 길이, 보강재의 유무 등을 고려하여 비선형 유한요소해석과 정적가력실험을 실시하여 비탄성거동을 평가하였다. 특히, 링크부의 소성 회전 및 초과강도계수에 대해서 검토를 수행하였다. 본 논문에서 제안한 링크부에 대하여 FE해석과 재하실험결과를 검토한 결과, AISC—341-10 조항에서 제공하는 소성회전 등급을 만족하는 결과를 얻었다. 또한 제안한 링크부의 기하학적인 형상에 따른 설계식과 설계프로세스를 제안하고, 해석 및 실험적 검증을 수행하여 충분한 에너지소산능력을 가진 링크빔으로서의 적용 가능성을 확인하였다.

1. Introduction

1.1 General

In eccentrically braced frames the axial forces in the braces are transmitted to the columns through bending and shear in the beams, and, when designed and detailed correctly, the system possesses more ductility than concentrically braced frames (CBRs) while retaining the advantage of reduced horizontal deflections which braced systems have over moment resisting frames (MRFs). These combine the strength and stiffness of a concentric braced frame with the inelastic performance of a special moment-resisting frame. Link beams in eccentrically braced frames develop good inelastic behavior because yielding in the link beam occurs well before brace buckling or inelastic deformation of the columns, and this yielding permits large inelastic deformations and great energy dissipation during severe earthquakes.

Eccentrically braced frames (EBFs) have been used in building and other civil engineering structures since first evaluated by Roeder & Popov in 1978. Examples of buildings constructed using eccentrically braced frames are shown in Fig. 1.1. Eccentrically braced frames (EBFs) evaluated ed by Popov which now called traditional or conventional EBFs was where the link beam is either welded on the collector beams or link beam and collector beams are monolithic elements. In order to prevention or to mitigate the disaster caused by earthquakes, engineers recommend different design techniques and philosophy. Structural damage in buildings designed according to the dissipative design philosophy can be significant, even under moderate to severe earthquakes.

In this section of the dissertation, the limitations of both conventional eccentrically braced frames and EBFs with replaceable links will be discussed. In addition, the limitation of link-to-column connections in eccentrically braced frames (D-bracing EBFs) will be reviewed. The objectives of this dissertation and its scope will be presented including the organization of dissertation.

Fig. 1.1 Istanbul Bilgi University, Prep School Building

1.2 Statement of the problem

Repair of damaged members is an expensive operation and may affect the functionality of the building in general, which in turn increases the overall economic loss. Therefore a number of researchers are came up with the ideas about post-earthquake event that if the damage is controlled to certain dissipative members realized to be removable following an earthquake, the repair costs and time of interruption of building use can be reduced significantly.

In post-earthquake it is difficult to repair the damaged part since decapitating element wasn't isolated from the main structures. This phenomenon has been seen in different countries around the world where an earthquake occurred. For instance, Fig. 1.2 shows the failure of conventional eccentrically braced frames (EBFs) seen during Christchurch New Zealand earthquake series of 2010/2011.

S. Gardiner et al. and G.C. Clifton et al. reported an assessment following Christchurch earthquake series of 2010/2011 [36]. The failure of conventional eccentrically braced frames (EBFs) were seen during Christchurch New Zealand earthquake series of 2010/2011. As reported by G.C. Clifton et. al, (2012) Christchurch, New Zealand earthquake was the first event worldwide to push modern EBFs into the inelastic range and impacted on recently built EBFs from 3 to 22 storeys in height. For instance Fig. 1.2 (a) shows the photo of fractured link beam in Pacific Tower and Fig. 1.2 (b-c) failure of EBF Parking garage on St Asaph St and Antigua St, Christchurch New Zealand. As shown in Fig 1.2, the structures were resisted the seismic load according to the design.

From the assessments all EBFs failed during Christchurch earthquake series only the link beam damaged through repeated inelastic deformation and local buckling prior to the rest of structural elements. However, because of the fact that the EBFs used were conventional where the link and the collector beams are not isolated or the link elements were welded to the collector beam or to the columns, it is difficult to maintain or repair with out affecting the main structural components.

The maintenance of these frames is difficult. Courtesy of Sean Gardiner, CPG NZ Ltd, proposed a replacement of the active links of Fig. 1.2 (a) as shown in Fig. 1.3. They achieved by cutting out the active link and adjacent braces and collector beam and replacing these with the shop fabricated detail shown in Fig. 1.3 which is site welded to the existing stub collector beams and braces.

(a) Fractured EBF active link in Pacific Tower. *(Image Spiire New Zealand Ltd.)*

(b) Evidence of EBF link yielding

(c) Fractured link at lower level EBF

Fig. 1.2 Fractured link beams of conventional EBFs
[Photos by M. Bruneau and C Clifton]

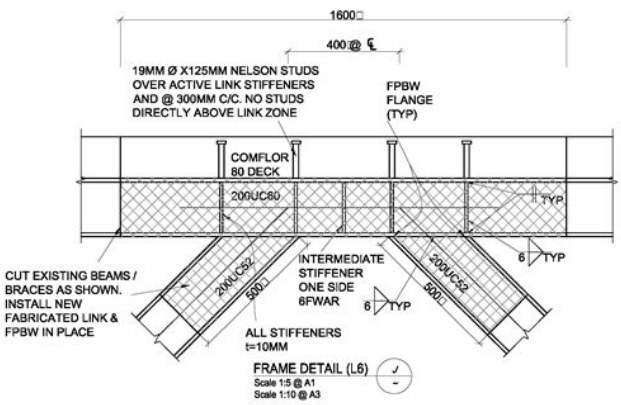

Fig. 1.3 The Proposed Replacement Detail.
(Courtesy of Sean Gardiner, CPG NZ Ltd)

Eccentrically braced frames with replaceable links addresses the limitations of traditional EBFs. Since the links are isolated from the main structural elements so that in post earthquake the damaged part (the link beam) can be replaced or maintained without affecting the functionality of the building. EBFs with replaceable links have been implemented in New Zealand as shown in Fig 1.4. The photo sources presented in Fig. 1.4 is (a) 335 Lincoln Rd Christchurch 3 Storey office building image courtesy of Ruamoko (b) 6 storey office/ parking building Hamilton image courtesy of Steltech Design Management Consultants and (c) 2 storey office building Christchurch Image courtesy of Spiire).

The concept and experimental investigation on bolted extended end-plate connections for eccentrically braced frames with link-to-column connection configuration was started in 1994 Ghobarah and Ramadan. The inelastic performance they found was similar to fully welded connections. Since then a number of research works have been done on EBFs with replaceable links and design recommendations have also been made like conventional EBFs.

The design procedures or the performance requirements for removable link elements are:

- They must be designed and detailed to achieve ≥ 0.08 radian plastic rotation (shear mode) and ≥ 0.02 radian plastic rotation (flexural mode) under the design level or greater earthquake.
- Inelastic demand must be limited to the link element so the link should have either weaker in strength or less in cross-sectional area than the collector beam.
- Ease of removal and replacement post earthquake

In the second requirement, in order to control the plastic deformation in EBFs with replaceable link beam, the link should be weaker in strength or less in cross-sectional area than the collector beam. The later, the difference in cross-section leads to some inconvenience during slab construction as shown in Fig. 1.5. As shown in the Fig. 1.5, the slab around the active replaceable link should be supported which can be taken as a limitation of EBFs with replaceable links.

Fig 1.4 New Zealand Examples of EBFs with Removable Links [1]

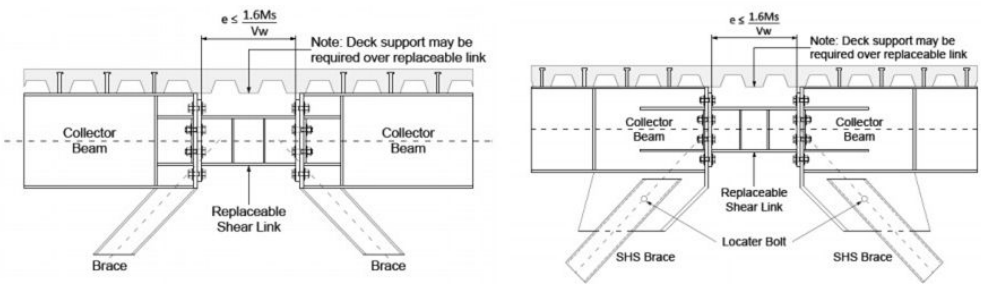

Fig. 1.5 Replaceable Link Configuration

(Kevin Cowie and Alistair Fussell, Steel Construction New Zealand Inc., 2013)

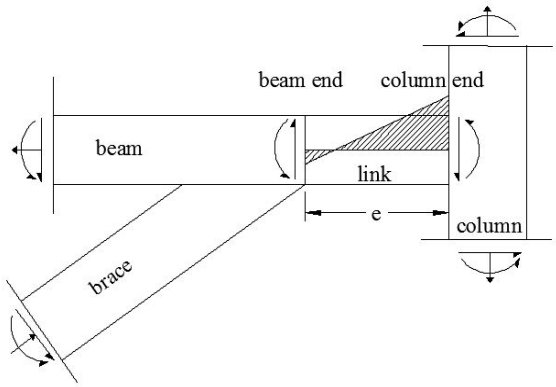

Figure 1.6 Link-to-Column Moment Distribution

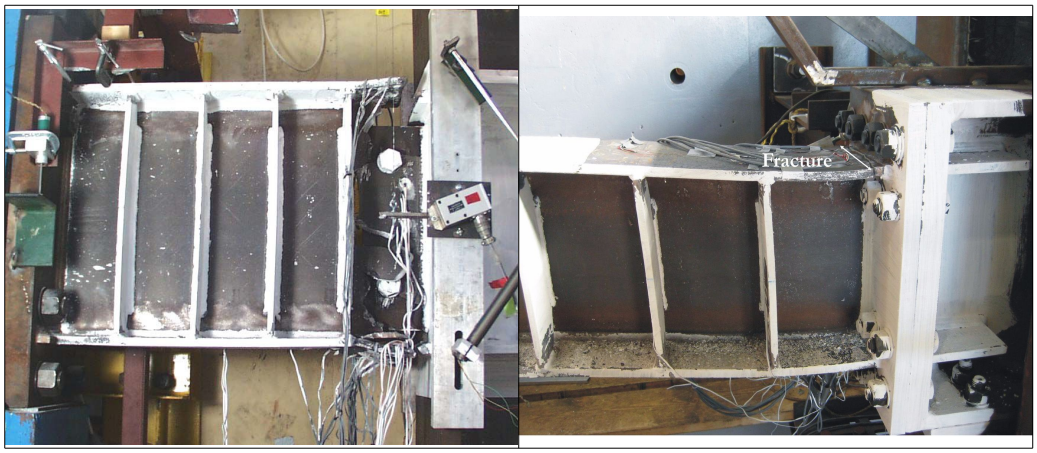

Failure of MWS specimen (Okazaki, 2010)

Failure of EPM-11A specimen (Nabil, 2010)

Fig. 1.7 Failure of link-to-column connections

The up to date limitation of EBF is in link-to-column connections as they un able to achieve the plastic rotation level. Studies show that welded link-to-column connections tend to fracture in the link flange prior to large link rotations. This is mainly because the fact that link-to-column connections in eccentrically braced frames (EBFs) must transmit large moments and shear forces to facilitate link rotation and the moment at the end of the column is bigger than the moment at the end of beam-brace. This is because the column connection attracts greater moment because the axial stiffness of the column is stiffer than the flexural stiffness of the beam. The moment distribution of link-to-column connection in

EBFs sis shown in Fig. 1.6. Fig. 1.7 shows the failure mode of welded flange of link-to-column connected links. The American Institute of Steel Construction (AISC) seismic provisions warn designers of the problems with link-to-column connections and indicate they are the subject of ongoing research.

The statements of problems in eccentrically braced frames discussed above will be summarized as follows:

1. there is a limitation to repair/replace/maintain the conventional eccentrically braced frames with out affecting the remaining structural components and the functionality of the building after earthquake
2. the design requirements of EBFs with replaceable links are either the links have to be weaker in strength or less in cross-section in order to control the plastic deformation at the link. this phenomenon leads to difficulties during slab construction.
3. link-to-column connections tend to fracture in the link flange prior to large link rotations. This is still an unsolved problem in link-to-column connections of EBFs.

In this study, this limitation will be addressed by using links having equal cross-section area with collector beam. In this study a new type of link is proposed which addresses some of the limitations of the existing EBFs with replaceable link. The proposed replaceable shear links are called replaceable shear links with perforated web shown in Fig. 1.3. The strength of proposed links have weaker than the collector beam because of the perforations provided. Two types of section were used i) replaceable links with perforated web fabricated from a W-section with end-plate connections and ii) replaceable links with perforated web fabricated from a C-section with web-bolted connections. The proposed shear links have been evaluated both analytically and experimentally.

1.3 Research Motivations, Objectives and Scope

1.3.1 Motivations and Objectives

Eccentrically braced frames (EBFs) were proposed as basic elements of structural typologies able to satisfy the objectives of the modern seismic design philosophy at a moderate expense. In EBFs, link beams have a fundamental role as the seismic dissipation depends on the link and the bracing guarantee high lateral stiffness and prevent severe damage during low intensity earthquakes. Attention needs to be paid to detail the link beams to ensure that there is a significant energy dissipation and a stable hysteretic behavior on the occurrence of strong ground motions. Numerous researches have been done to advance the performance as well as to make it ease during construction. As stated in sub-chapter 1.1, in order to control the plastic rotation at the link beam of EBFs, the replaceable link beam should have less cross-sectional area than collector beam which leads to difficulties during slab construction. The active link developed in this research addresses this limitations in a comprehensive manner.

Link-to-column connection in eccentrically braced frames (EBFs) transmit moment and shear force so that the link will have sufficient rotation to dissipate seismic energy. In conventional eccentrically braced frames, the welded link-to-column connections fractures at the link flange prior to large link rotations. In EBFs with replaceable link also this problem exists. As shown in Fig. 1.3, the link flange wended to the end plate connector failed. The reduction in web section enables to reduce the forces that could transfer to the flanges so that the connection will have enough strength to resist the rotation. Perforations in the web increases the plastic strain at the perforation edge but the stress and strain in the flange decreases. In this research these limitations are also tried to be addressed.

The main objective of this research formulates a general framework for the replaceable reduced link section used in eccentrically braced frames. The research started from the development of reduced link section followed by evaluation using analytical, theoretical and experimental approaches finally from the evaluation results design methods will be developed considering different parameters.

1.3.2 Research Scope

In order to achieve the above objective the following steps are involved:

1) Develop a replaceable reduced link section to be used in eccentrically braced frames.
2) Perform a preliminary non-linear finite element analysis in order to identify the general behavior of developed links and to identify the sensitive parameters. Validate that the replaceable links can achieve the required rotation demands as specified in the code and assess the overstrength factor. Some design equations are derived from the preliminary finite element analysis.
3) Conduct quasi-static loading test to verify the non-linear finite element analysis results.
4) Develop design methods and procedures for the replaceable reduced link section developed.

1.4 Organization of Dissertation

This dissertation includes eight different chapters.

Chapter 1 describes the limitations of the existing EBFs both traditional and EBFs with replaceable links. The motivation, objectives and scope of the research work also presented in this chapter.

Chapter 2 research background and literatures review on both conventional eccentrically braced frame and EBFs with replaceable links are reviewed in this section and other related literatures

Chapter 3 deals with the development and detail of proposed links. The design procedures of proposed links both reduced web section and reduced web and flange sections are presented in this section. The sensitive parameters have also been discussed in this chapter.

Chapter 4 presents the experimental investigation of proposed links to evaluate the plastic deformation capacity and the failure mode of developed links. The hysteresis response along with the failure mode and the summary of plastic rotation capacity of test specimens are presented in this section.

Chapter 5 discusses the finite element simulation of reduced link section for the preparation of further investigations. The conducted FE simulations results were compared with the experimental results in order to verify the accuracy of finite element simulation.

Chapter 6 presents the parametrical studies in order to include parameters that were not included in the experimental investigations including link-to-column connection. The plastic rotation capacity considering different variables are presented in this section. The required rotation demands as specified in the code and assess the over-strength factor of each analysis specimens considered are calculated.

Chapter 7 presents the summaries of design equation proposed along with the verifications with the experimental and analytical results. In addition, the analysis model for reduced link was proposed and the proposed analysis model is also verified by the experimental and analytical results.

Chapter 8 summarizes the findings of this research work and some recommendation for future studies were made in this section.

2. Background and Literature Review on EBFs

This chapter provides an overview of history and recent developments in the design of active links in steel eccentrically frames (EBFs) leading up to the reduced link concept. The historical background is briefly described, followed by general characteristics of active links up to date, the behavior of plate with holes under shear force and the concept of reduced link section application for eccentrically braced frame will be discussed.

2.1 History and Background of Eccentrically Braced Frames

Eccentrically braced frames (EBFs) can be viewed as a hybrid system between moment frames (high ductility and stable energy dissipation capacity) and concentrically braced frames (high elastic stiffness). EBFs combine the advantages and minimize the disadvantages of these two systems. This system was first developed in Japan in the early 1970s. In the United States, it was investigated at the system and component levels through a series of analytical and experimental studies at the University of California, Berkeley throughout the 1980s (*Roeder and Popov 1977; Hjelnstad and Popov 1983; Malley and Popov 1983; Kasai and Popov 1986; Ricles and Popov1987; Whittaker et al. 1987; Ricles and Popov 1989; Engelhardt and Popov 1992*).

The analytical and experimental studies at the University of California, Berkeley, and other research works confirmed the reliability of EBFs to resist horizontal actions. The link is designed to act as a fuse by yielding and dissipating energy while preventing buckling of the brace members. The links used to dissipate seismic energy so it should be designed and detailed to have stable hysteresis loops and predictable behavior. The commonly used framing systems are moment resisting frames (MRFs) and concentrically braced frames (CBFs).

MRFs have high ductility however they have low stiffness and CBFs have high stiffness but low ductility. EBFs can be defined as the combination of MRFs and CBFs as EBFs have high stiffness as CBFs and high ductility as in MRFs. The bracing members in the EBFs provide the high elastic stiffness characteristic of the CBFs, permitting code drift requirements to be met economically. Yet, under severe earthquake loading, properly

designed and detailed EBFs provide the ductility and energy dissipating capacity characteristic of MRFs. Fig. 2.1 shows the energy dissipation mechanism of moment resisting frames (MRFs), concentrically braced frames (CBFs) and eccentrically braced frames (EBFS). As shown in the figure, the EBFs has both ductile and stiffness. Consequently the number of civil applications of EBF is increasing day by day.

Different brace patterns are used in eccentrically braced steel frames. The possible patterns of EBFs are: V-bracing, K-bracing, X-bracing and Y-bracing as shown in Figure 2.2. The links in figure 2.2 is identified by the dimension e. EBFs have also advantages in the architectural perspective as it provides gaps for openings, doorways and windows.

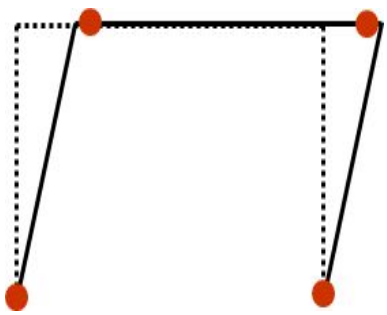

Moment resisting frames: High ductility

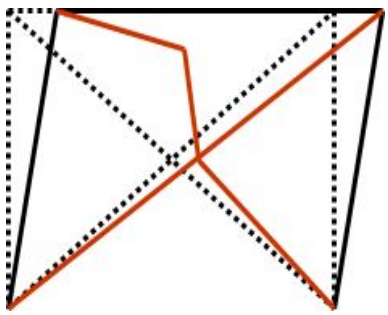

Concentrically braced frames: High stiffness

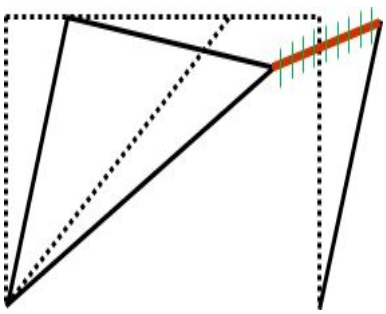

Eccentrically braced frames: Ductile and Stiff

Fig. 2.1 Energy dissipation mechanism of different framing systems.

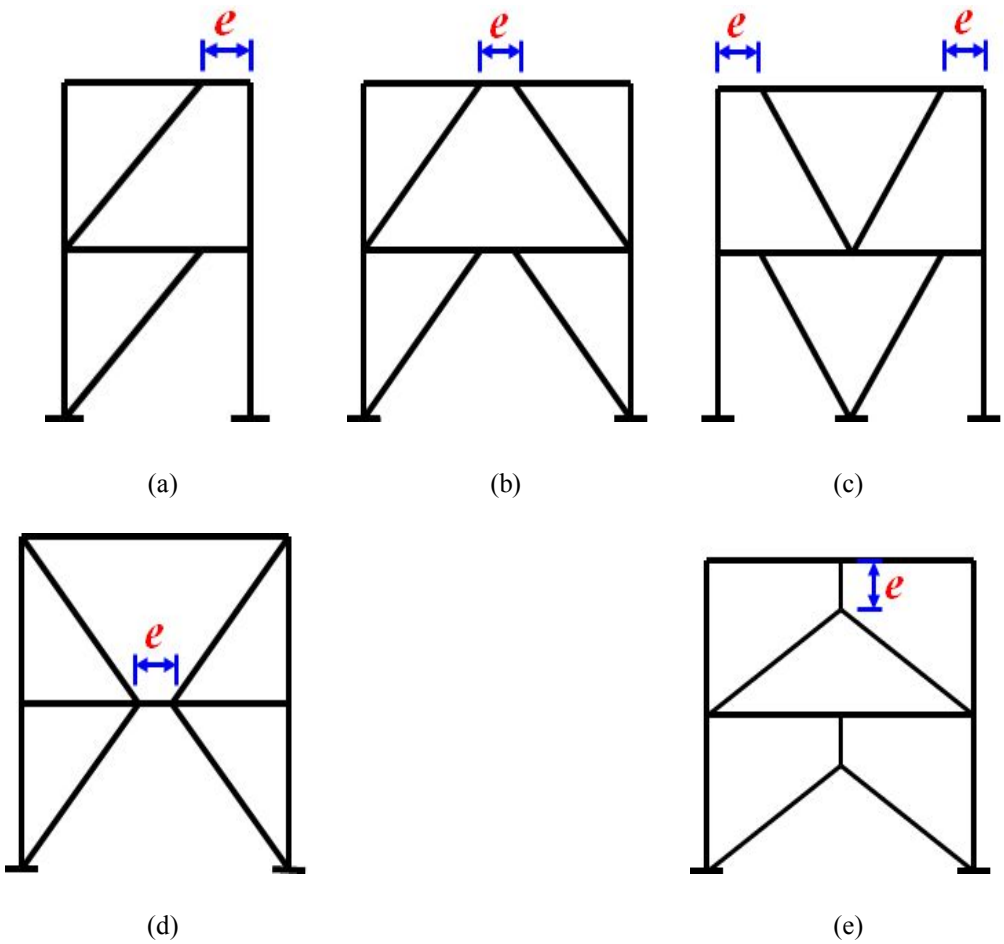

Fig. 2.2 Different Types of Eccentrically Braced Steel Frames: (a) D-Bracing; (b) K-Bracing; (c) V-Bracing; (d) X-Bracing; (e) Y-Bracing

2.2 General Behavior of EBFs

Eccentrically Braced Frames are associated with the desire of reaching to a bracing system which has laterally enough stiffness with significant dissipation of energy and also the ability of adjustment to huge seismic forces (Charles W. Roeder & P. Popov), (1978). The braces in EBFs are capable of resisting axial loads and the link has a flexural and shear forces. The qualitatively forces in EBFs under lateral loads are shown in Fig. 2.3 for collector beam, brace and links for diagonal bracing.

2.2.1 Requirements of Links in EBFs

The links must satisfy compactness requirements to ensure stable inelasticity within them. The flange width-to-thickness requirements are presented in Eqs. 2.1 for shear links and 2.2 for intermediate and flexural links, and the web slenderness criteria for all links in Eq. 2.3.

$$e \le \frac{1.6M_p}{V_p}: \quad \frac{b_f}{2t_f} < 0.38\frac{E}{F_y} \qquad \text{.....(2.1)}$$

$$e > \frac{1.6M_p}{V_p}: \quad \frac{b_f}{2t_f} < 0.30\frac{E}{F_y} \qquad \text{.....(2.2)}$$

$$\text{for } all\, link\, length: \quad \frac{d}{t_w} < 3.760\frac{E}{F_y} \qquad \text{.....(2.3)}$$

where e: link length, E: young's modulus, F_y: the yield strength, M_p: plastic moment, V_p: plastic shear force, d: depth of link, t_f: flange thickness and t_w: web thickness. The plastic shear and flexure will be discussed in the next section.

The link length classification mentioned as a shear link (short link), intermediate link, and flexural link (long link) depends on the link length factor. These non-dimensional link

length called link length factor (ρ) given by the ratio of link length to the ratio of plastic moment and plastic shear force as shown in Eq. 2.4.

$$\rho = \frac{e}{M_p / V_p} \quad \text{.....(2.4)}$$

The values of link length factor defined in Eq. (2.4) classifies the link in to three. these values are with the corresponding classification in Eq. (2.5):

Shear link	for $\rho \leq 1.6$:	.....(2.5)
Intermediate link	for $1.6 < \rho \leq 2.6$	
Flexural link	for $\rho > 2.6$	

The plastic shear and plastic moment used in Eq. (2.4) are defined in Eq. (2.6) and (2.7) respectively. The forces in the link, specifically is shown in Fig. 2.8. As shown in the figure, the link is capable of resisting flexural and shear force. The bending moment at equilibrium is calculated as e*V/2. Depending on the link length 'e' the plastic strength is controlled either by shear or flexure. For short link, the plastic strength is controlled by shear and for long links, the plastic strength is controlled by flexure. The corresponding shear and flexural strengths are given in equation below.

$$V_n = V_p = 0.6F_y(d - 2t_f)t_w \quad \text{.....(2.6)}$$

$$M_n = M_p = ZF_y \quad \text{.....(2.7)}$$

where F_y: the yield strength, d: depth of link, t_f: flange thickness and t_w: web thickness, Z: is the plastic section modulus.

2.2.2 Rotation Demand of Links

The rotation demand of link is one of the design determining factor in EBFs since the energy dissipation is accommodated by the links. The rotation demand of link is expressed in terms of energy dissipation mechanism of EBFs also known as the collapse mechanism. The link rotation angle is inelastic angle between the link and the beam outside of the link when the story drift is equal to the design story drift. For design purposes the inelastic link member rotations of EBFs must be quantified. This is most easily established through the use of an energy dissipation criterion, also commonly known as a collapse mechanism. Collapse mechanisms may be derived by assuming rigid plastic behaviour of the members. The link rotation angle along with energy dissipation mechanism of EBFs is illustrated in Fig. 2.3. The links shown in Fig. 2.3 with hatched yielded in shear and formed shear hinges.

The rotation demand of link in terms of the overall frame drift (θ_p) and bay length is given in Fig. 2.3 for respective EBFs types. The relationship of link rotation demand and the ratio of link length to bay length is given is shown in Fig. 2.4 for K-bracing frame. As shown in the figure, the rotation capacity of short link is high and the rotation of long link is less. The link rotation is increases rapidly as the link length decreases. However, plastic rotation demand presented in Fig. 2.4 shows that the links should not be too short to limit the plastic rotation demand.

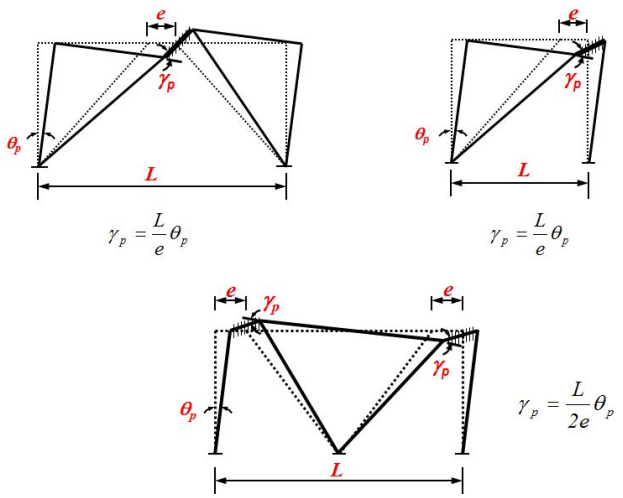

Fig. 2.3 Link rotation angle and energy dissipation mechanism of EBFs

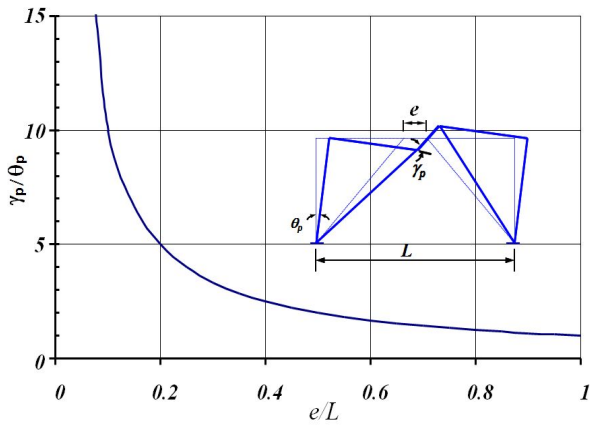

Fig. 2.4 Variation of link rotation demand with e/L (Popov and Engelhardt 1988)

The link rotation angle is the inelastic angle between the link and the beam outside of the link which is dependent on the link length factor defined in Eq. (2.4). The plastic link rotation capacity according to AISC for short link is 0.08rad, for long link 0.02rad and for intermediate link, the plastic link rotation is interpolated between 0.02 and 0.08rad which is summarized in Eq. (2.8).

γ=0.08rad	for $\rho \leq 1.6$:	.....(2.8)
interpolation 0.02 and 0.08 rad	for $1.6 < \rho \leq 2.6$	
γ=0.02rad	for $\rho > 2.6$	

2.2.3 Strength and forces in the link

The frame plastic capacity of eccentrically braced frames, for diagonal brace and K-brace is presented in Fig. 2.5 by Popov and Engelhardt in 1988. As shown in the figure, the strength of EBFs is affected by the link length (e) significantly. The relationship between link length and the frame plastic capacity is similar to the relationship between the plastic rotation and link length. As the link length decreases the frame plastic capacity increases rapidly and the finally becomes constant. The frame plastic capacity of K-bracing is more than twice than D-bracing for short links. As shown in the figure, the rate of increase rapidly for K-bracing as the link length decreases compared to D-racing. The rate becomes the same as the link length increases.

The shear strength of link (V_L) in terms of shear story is (V) is related as in Eq. (2.9) by Horne et al, 2001)

$$V_L = V^* \frac{h}{L} \qquad \text{.....(2.9)}$$

where h and L are the story height and bay length respectively.

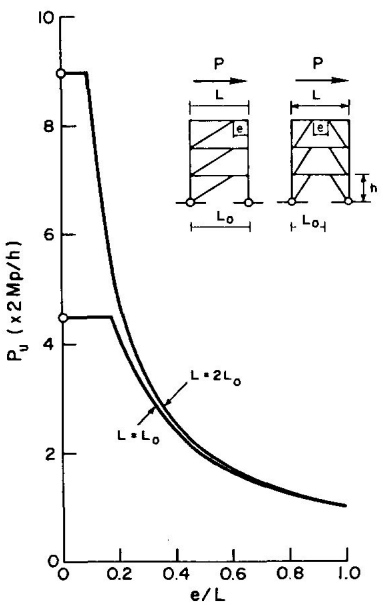

Fig. 2.5 Variation of frame plastic capacity with e/L

Equation (2.8) is derived from the force distribution in EBFs, bending moment (M), shear force (V) and axial forces (N) shown in Fig. 2.6. As shown from the figure that the link is subjected to high bending at its ends and high shear forces along the length. Depending on the link length, the yielding and hinge type is different short links from shear hinges with little yielding at its ends and if it is long, links from hinges at its ends. That is why the name stated in Eq. (2.5) is shear link for short link, and flexural link for long link.

In order to clearly understand the forces in links, the free body diagram of link is presented in Fig. 2.7 and based on static equilibrium, the relationship between shear force and bending moment will be:

$$V^{*}e = M_a + M_b \qquad \text{.....(2.10)}$$

For EBFs such as K-bracing type, the link end moments are equal, thus the relationship of shear and moment will be as shown in the last figure of Fig. 2.7.

$$V^{*}e = 2M \qquad \text{.....(2.11)}$$

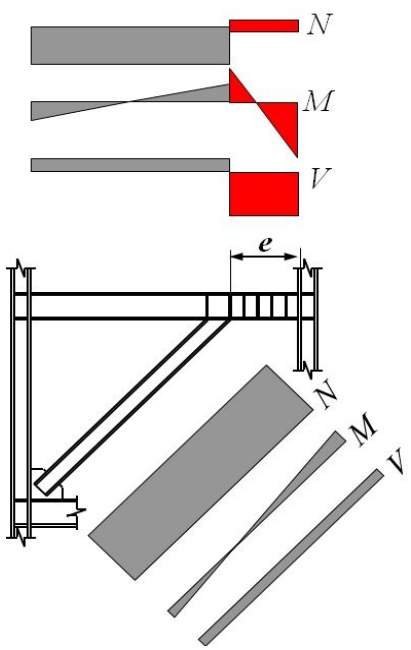

Fig. 2.6 Force distributions in eccentrically braced frames

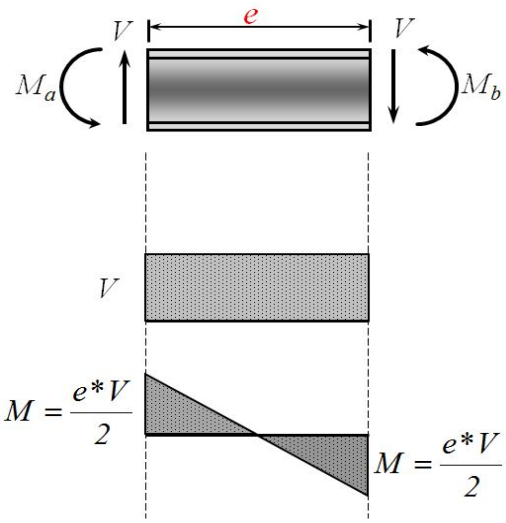

Fig. 2.7 Loading, shear and moment diagram of typical links

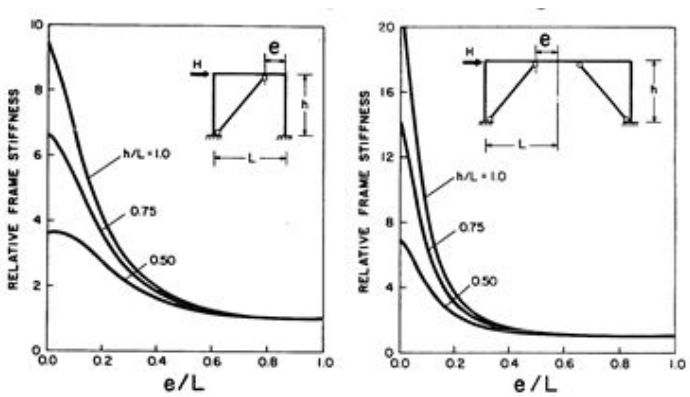

Fig. 2.8 Variation of elastic lateral stiffness with e/L for two simple EBFs (after Popov, Kasai and Engelhardt, 1987)

The behavior of eccentrically braced frames is determined or defined by the link length ratio. In order to clarify and explain the lateral stiffness of the EBFs it has been defined as a function of the ratio of link length to the beam length. When the link length is smaller and smaller, the stiffness becomes close to the stiffness of concentrically braced

frames. In reverse, as the link length increase, the stiffness becomes more ductile behavior approaching to the stiffness of an ordinary moment resisting frames as shown in Fig. 2.8.

2.3 Design Requirements of EBFs

The design requirements of links in EBFs including the link rotation angle, plastic shear strength and flexural strength have been discussed above. The lateral restraint against out-of-plane displacement and twist is required at the ends of the link to ensure stable inelastic behavior will be discussed in chapter 3. It is stated in standards that the ductility demands in EBF are concentrated in the links. Braces, columns and beams outside the link should have very little yielding in a properly designed EBF. According to AISC, the required strength of the diagonal brace and the beam outside of the link is based on the maximum forces that can be generated by the fully yielded and strain hardened link. The maximum forces, computed as the product of nominal shear strength of link and the overstrength factor and ratio of yields. The nominal shear strength of the link, V_n, is the lesser of that determined from the plastic shear strength of the link section or twice the plastic moment divided by the link length, as dictated by statics assuming equalization of end moments in the inelastic range of behavior is presented in Eq. (2.10).

$$V_n = \begin{cases} V_p & \text{for } e \le \dfrac{2M_p}{V_p} \\ \dfrac{2M_p}{e} & \text{for } e > \dfrac{2M_p}{V_p} \end{cases} \quad \text{.....(2.10)}$$

The required strength of the diagonal brace and beam outside of link can be taken as the forces developed by the following values of link shear and link end moment according to AISC is expressed in Eq. (2.11-2.12). The free body The ultimate shear force V_{ult} of link is given by Eq. (2.10) according to AISC.

for diagonal brace: $V_{ult} = 1.25 R_y V_n$ .....(2.11)

for beam outside link: $V_{ult} = 1.1 R_y V_n$ .....(2.12)

where V_n: is link nominal shear strength defined in Eq. (2.6), R_y accounts for the probable yield stress exceeding the minimum specified value, and the factor 1.3 applied to

the link nominal resistance is used to estimate the strain-hardening of link force magnitudes.

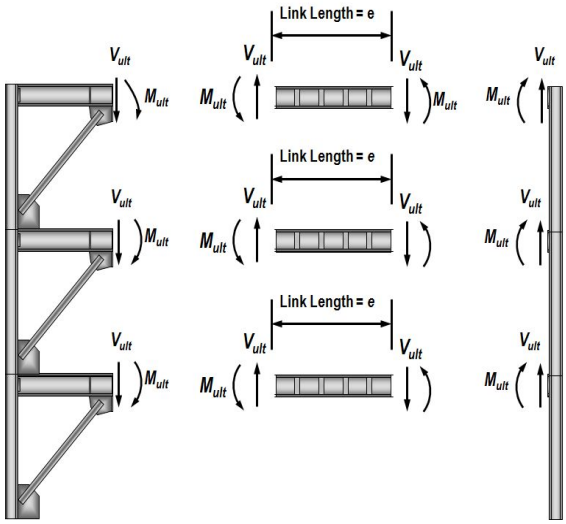

Fig. 2.9 Free body diagram of D-bracing 3 story EBF

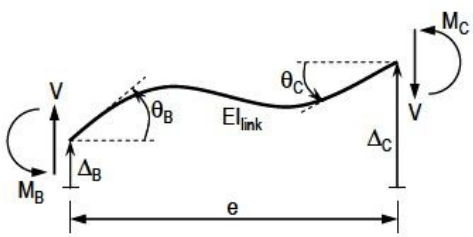

Fig. 2.10 Isolated link models ().

The forces developed in EBFs are shown in Fig. 2.9. As shown in the figure, the forces developed in links transferred to the other members. Thus, each member outside the link is designed as elastic for the maximum forces of link. The column required strength is forces generated in column when all links above level under consideration have developed their ultimate shear resistance (V_{ult}) and their ultimate flexural resistance (M_{ult}). The ultimate shear strength of can be taken $1.1R_y V_n$.

The other important portion of EBF is bracing connections, beam-to-column connections and link-to-column connections. The required strength of brace connections, at

both ends of the brace, shall be at least equal to the required strength of diagonal brace. Thus the design of bracing connections for forces (N and M) generated in braces by V_{ult} and M_{ult} of link shown in Fig. 2.3 and 2.9. The connection should also needs to be checked for axial compression forces of $1.1R_yN_n$, where N_n: is the nominal axial compression strengths of brace.

The link-to-column connections and beam-to-column connections construction of before the Northridge earthquake was similar. Therefore, the pre-Northridge link-to-column connections can have problems similar to those observed in beam-to-column connections in MRFs during the Northridge earthquake. The Provisions after Northridge earthquake contain specific requirements for link-to-column connections to ensure adequate ductility capacity.

The link-to-column connections should be designed for the maximum inelastic link rotation angle γ_p. It is known that the moment at the column face is bigger than the moment at collector beam face. This is because the column connection attracts greater moment because the axial stiffness of the column is stiffer than the flexural stiffness of the beam. For further understanding, the isolated link model is shown in Fig. 2.10. If the spring constants at each end of the link are taken as k_C and k_B, where C and B in Fig. 2.10 refers to the column end and beam end respectively, will be given as:

$$M_C = -k_C\theta_C$$
$$M_B = -k_B\theta_B \qquad \text{.....(2.12)}$$

where, M_C and M_B column end moment and beam end moments as shown in Fig. 2.10 respectively, θ_C and θ_B are the rotation of link in column end and beam end respectively. As discussed by Okazaki et al. A first order elastic analysis results in the following expression for the link end moment ratio as in Eq. (2.13) neglecting the shear deformation for simplicity.

$$\frac{M_C}{M_B} = \frac{\alpha(2+\beta)}{\beta(2+\alpha)} \qquad \text{.....(2.13)}$$

In the above equation, α and β are measures of the relative stiffness of the link and the rotational springs. These parameters are defined as follows:

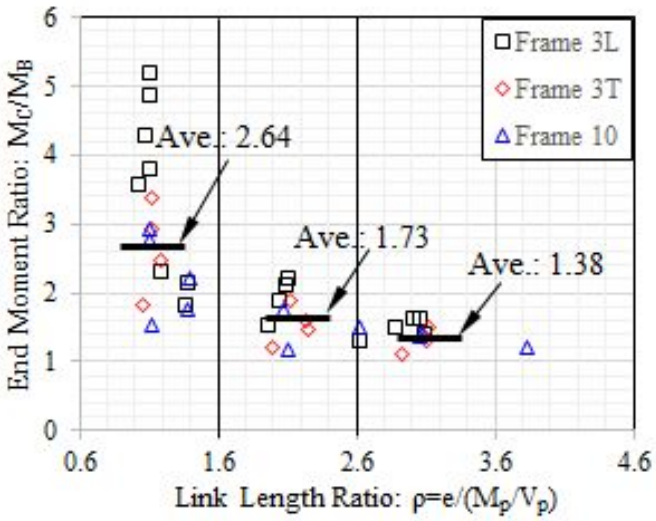

Fig. 2.11 End moment ratios estimated from elastic frame analyses

$$\alpha = k_C \frac{e}{EI_{link}}$$
$$\beta = k_B \frac{e}{EI_{link}} \qquad \text{.....(2.14)}$$

In the above equation, e is the link length and EI_{link} is the elastic flexural stiffness of the link section. Equations (2.13) and (2.14) show that the link end moment ratio, M_C / M_B, is a function of the end restraints and the flexural stiffness of the link itself.

The relationship between the ratio of end moments and link length factor is presented in Fig. 2.11 from the 2-D elastic frame analyses of EBFs for three different frames 3L, 3T and 10 correspond to three frames, two three-story frames and one ten-story frame, presented by Richards and Uang (2003). As shown in the Fig. 2.11, significant variation in end moment ratio is observed for shear links and as the link length increases the variation in end moment ratio decreases.

According to the provision, the cyclic tests for qualification of beam-to-column connections and link-to-column connections is different. Loading sequence for beam-to-column moment connections according to the provision is as specified below:

(1) 6 cycles at θ = 0.00375 rad
(2) 6 cycles at θ = 0.005 rad
(3) 6 cycles at θ = 0.0075 rad
(4) 4 cycles at θ = 0.01 rad
(5) 2 cycles at θ = 0.015 rad
(6) 2 cycles at θ = 0.02 rad
(7) 2 cycles at θ = 0.03 rad
(8) 2 cycles at θ = 0.04 rad

Continue loading at increments of θ = 0.01 rad, with two cycles of loading at each step.

Loading sequence for link-to-column connections according to the provision is as specified below:

(1) 6 cycles at γ_{total} = 0.00375 rad
(2) 6 cycles at γ_{total} = 0.005 rad
(3) 6 cycles at γ_{total} = 0.0075 rad
(4) 6 cycles at γ_{total} = 0.01 rad
(5) 4 cycles at γ_{total} = 0.015 rad
(6) 4 cycles at γ_{total} = 0.02 rad
(7) 2 cycles at γ_{total} = 0.03 rad
(8) 1 cycle at γ_{total} = 0.04 rad
(9) 1 cycle at γ_{total} = 0.05 rad
(10) 1 cycle at γ_{total} = 0.07 rad
(11) 1 cycle at γ_{total} = 0.09 rad

Continue loading at increments of γ_t = 0.02 rad, with one cycle of loading at each step.

2.4 Previous studies on EBFs

Numerous research works have been done on conventional EBF and EBF with removable links in the past four decades. The development of eccentrically braced frames (EBFs) and associated research was primarily conducted during the 1980s (Roeder & Popov 1978, Hjelmstad & Popov 1983, Popov & Malley 1983, Kasai & Popov 1986, Ricles & Popov 1987, Englehardt & Popov 1989). Roder and Popov (1977) conducted 2-D nonlinear dynamic analyses on a set of EBF CBF and MRF models to compare their performance under severe ground motions. The analyses indicated that EBFs perform well compared to the other framing system due to their combined high sti_ness and stable hysteretic behavior. Whittaker et al. (1987; 1989) examined the six story EBF-MRF dual structures by earthquake simulator tests of a).30-scale model. Although the structure exhibited excellent cyclic behavior, it was observed that the energy dissipation and story drift was concentrated in the lower stories. Ricles and Popov (1994) performed 2-D nonlinear dynamic analyses of a six-story four-bay EBF. The analyses demonstrated the excellent performance of the frame, where the links accounted for the majority of energy dissipation.

In 1970s a number building were designed as EBFs and MRFs as they were believed to be the most dependable seismic resistant systems because of their ability to ensure a stable ductile response during major earthquakes. However, during Northridge, California earthquake of January 17, 1994, extensive premature brittle fractures at the welded joints were found in more than 150 SMRF buildings. So many researchers raised question on the design procedure, the weld quality, and the construction practice of these moment resisting frames. Building owners and design engineers faced many unanswered questions related to the effective repair and rehabilitation procedures. These failures observed during Northridge, California earthquake first motivated researchers in the connections of MRFs. Different design and details for the repair of damaged connections were developed and its effectiveness of these connections was evaluated both experimentally and analytically and the expected ductility capacity could now be achieved.

Eccentrically braced frames (EBFs) with replaceable link beam addresses the limitation of conventional EBFs. In 1994 Ghobarah and Ramadan started the concept and experimental investigation on bolted extended end-plate connections for eccentrically braced frames with link-column connection configuration (Ghobarah & Ramadan 1994). The inelastic performance they found was similar to fully welded connections. In 2003 Balut and Gioncu

evaluated and identified for an improved dog-bone solution and they identified the advantage and disadvantage of replaceable dog-bone. They suggested that in order to control the formation of plastic mechanisms which provides a ductile behavior of steel frame, the dog-bone should be weaker or less cross sectional area than the connected beams so that it post-elastic deformation while the rest structural members remain in the elastic range. However, the disadvantage of using replaceable dog-bone according to Balut and Gioncu is the difference in section will make difference in yielding strength so that it needs exhaustive control (Balut & Gioncu 2003). The concept of dog-bone can also apply for removable active link.

Stratan and Dubina (2004) at the Politehnica University of Timisoara in Romania further performed tests on I-section replaceable links with bolted endplate connections for EBFs. However, the endplates were flush with the I-section top and bottom flanges, which resulted in observed failure in the connections. This highlights the need for appropriate design and detailing of the endplate connection to suppress ductile overload failure modes and the need for robust and relatively simple load paths through the connections.

The research works on EBF is still an undergoing process. Specially to over come the limitation of link-to-column connection, researches are undergoing since research has shown that link-to-column connections are prone to failure at low drift levels, due to their susceptibility to fracture at the link flange-to-column welds. The local stresses and strains at link-to-column connection in EBFs are more severe than those in moment resisting connections. Hence to enhance the ductility of link-to-column connections, researchers are given much attentions in this regards.

2.4.1 Okazaki et al. (2003, 2004, 2006a, 2006b, 2007 and 2009)

Extensive research and experimental testing on eccentrically braced frames (EBF) with ink-to-column connections has been conducted in the university of Texas at Austin. As it has been noted above, the design of link-to-column connections in seismic-resistant eccentrically braced frames remains an unresolved problem. Okazaki et al. tested large scale specimens under cyclic loading considering connection detail, link length, link section, and cyclic loading protocol as a parameters.

Six different connections were used by Okazaki et al. which are shown in Fig. 2.12 were tested using the test setup shown in Fig. 13 considering four different loading protocols. The protocols used were old AISC protocol, revised protocol, severe protocol and random protocol. The cyclic response and the photo captured after test was shown as an example in Fig. 14 for specimen of MWS. As shown in the figure, stable cyclic response was obtained, until during the loading cycle of γ = ±0:07 rad (γ_p= ±0:06 rad), both the top and bottom flanges fractured near the CJP groove weld.

Among the 23 tests conducted, sixteen specimens failed due to fracture of the link flange. Thus, the test results suggested that link-to-column connections are susceptible to fracture at the link flange welds, regardless of the link length. The summary of link rotation capacity of test specimens were presented ion Fig. 2.15. As shown in the figure, only two specimens satisfy the link rotation requirements of the AISC provision. The link rotation capacity plotted shows that the performance of the specimens depended on the connection type as well as on the link length. With increase in link length, the link-column specimens developed smaller inelastic link rotation. Whereas the PN- and MW specimens performed poorly, developing only about half of the required inelastic link rotations, the FF- and MW-specimens achieved greater rotations, although generally still falling short of the required rotation levels.

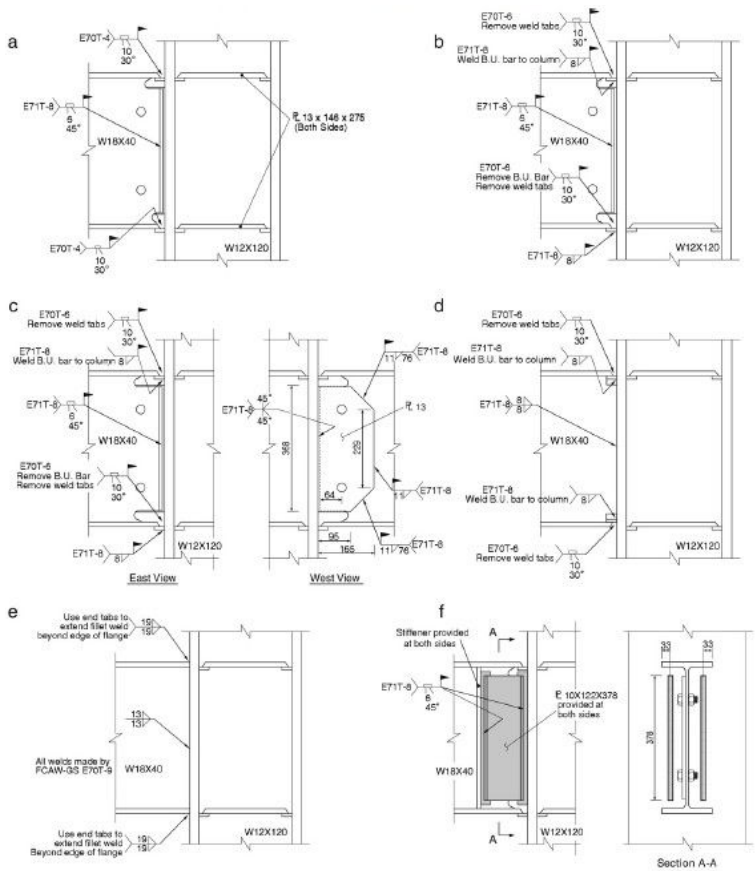

Fig. 2.12 Connection types used by Okazaki et al. (link stiffeners not shown): (a) PN-connection; (b) MW-connection; (c) FF-connection; (d) NA-connection; (e) AF-connection; and (f) SW-connection. (Dimensions in mm).

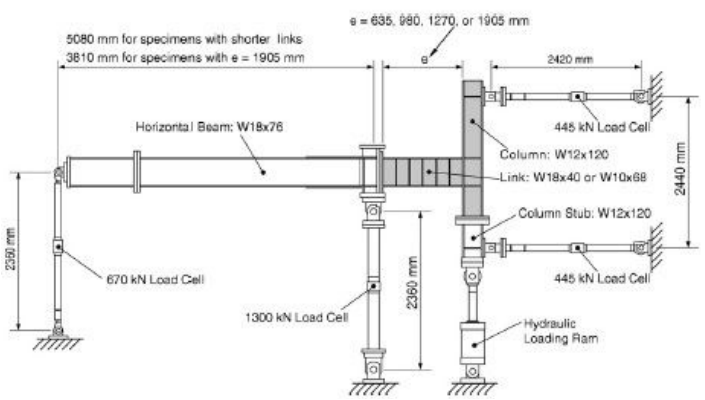

Fig. 2.13 Test setup (Okazaki et al.)

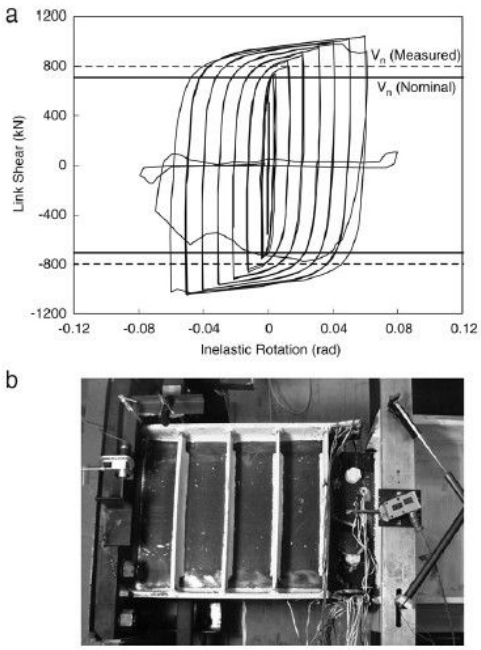

Fig. 2.14 Specimen MWS (a) cyclic response (b) link after test (Okazaki et al.)

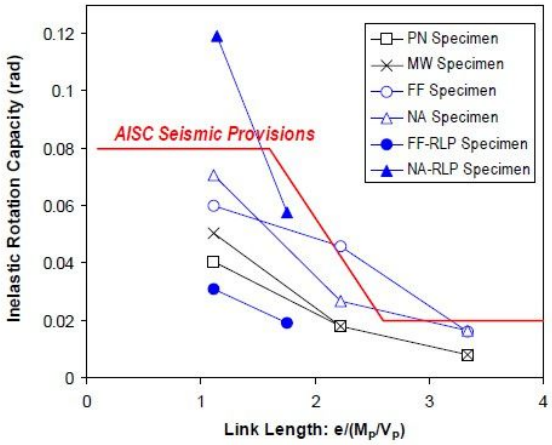

Fig. 2.15 Link rotation capacity (Okazaki et al.)

2.4.2 Nabil et al research

A series of experimental investigations on eccentrically braced frames (EBFs) with replaceable shear links was conducted in Canada in 2010 (*M. Nabil et al, 2010*). This research conducted by Nabil Mansour is presented in detail in his doctorate thesis. Generally two replaceable link types with different bolted connections were evaluated. These are:

i) W-sections (I sections) end plate connections, and
ii) Back-to-back channels with eccentrically loaded web connections and also shown in Fig. 2.16.

Nabil Mansour evaluated a shear link experimentally the local response of the replaceable links and characterize the global frame behavior considering a total of 13 full-scale shear links were tested at the University of Toronto and École Polytechnique de Montreal using the etst set up shown in Fig. 2.17. The replaceable shear link specimens qualify or meet the performance requirements of the steel structures standard if they achieve 0.08 rad plastic link rotation without fracture or severe strength degradation during a standard cyclical load test of 2005 AISC seismic provisions.

All link specimens tested at the University of Toronto and École Polytechnique de Montreal exhibited stable hysteretic shear yielding. Replaceable links with web-bolted connections exhibit a more pinched response, but because of the connection rotations, are able to sustain larger inelastic link rotations, on average γp=0.119radians and a maximum of γp=0.166radians. These specimens met and exceeded the ductility acceptance criteria of 0.08radian inelastic link rotation prescribed by both the Canadian Standards and 2005 AISC Seismic Provisions.

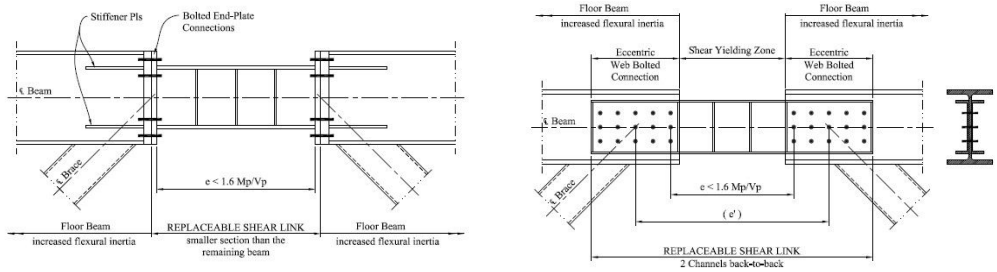

(a) Replaceable I-section link (b) Replaceable Back-to-back channels

Fig. 2.16 Specimen detail (N. Mansour et al. 2010)

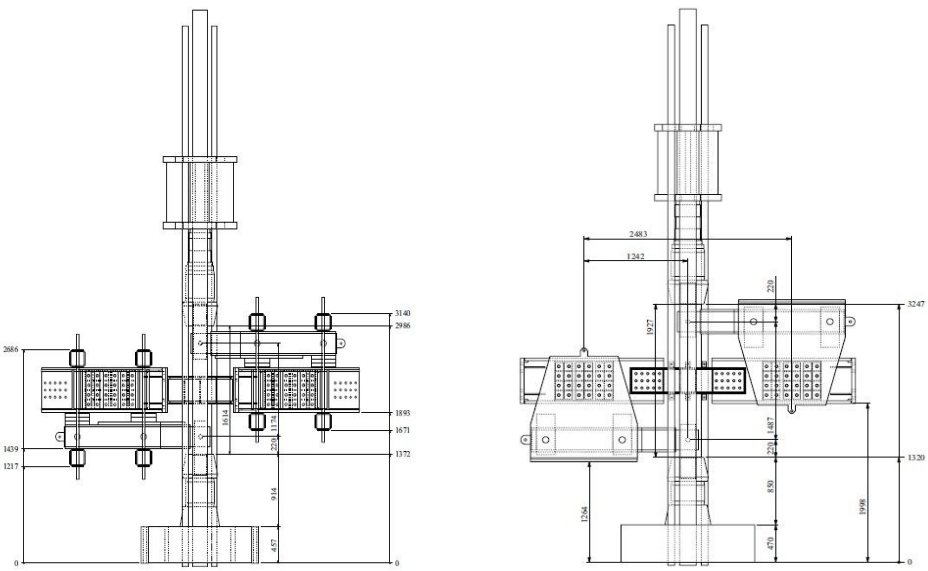

Fig. 2.17 Test setup (N. Mansour et al. 2010)

All link specimens (with exception to UT-2A, a bolted web connected link) tested at the University of Toronto and École Polytechnique de Montreal by Mansour, exhibited unstable hysteretic shear yielding as shown in Fig. 2.19. These specimens met and exceeded the ductility acceptance criteria of 0.08 radian inelastic link rotation prescribed by both the Canadian Standards and 2005 AISC Seismic Provisions.

End-plate connected shear replaceable links displayed a consistent full hysteretic response up to γ_p=0.104 radians, that is very similar to that in traditional EBF construction, where the yielding link beam is an integral component of the floor beam as shown in Fig. 2.18.

Replaceable links with web-bolted connections exhibit a more pinched response, but

because of the connection rotations, are able to sustain larger inelastic link rotations, on average γ_p=0.119 radians and a maximum of γ_p=0.166 radians.

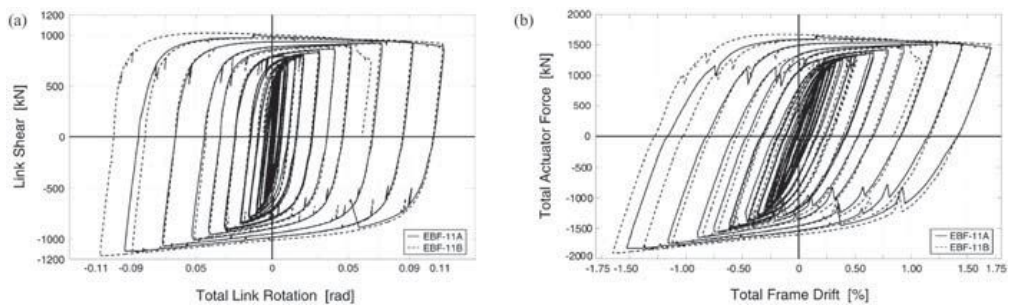

Fig. 2.18. Response of Replaceable Links with End Plates (Mansour, 2010)

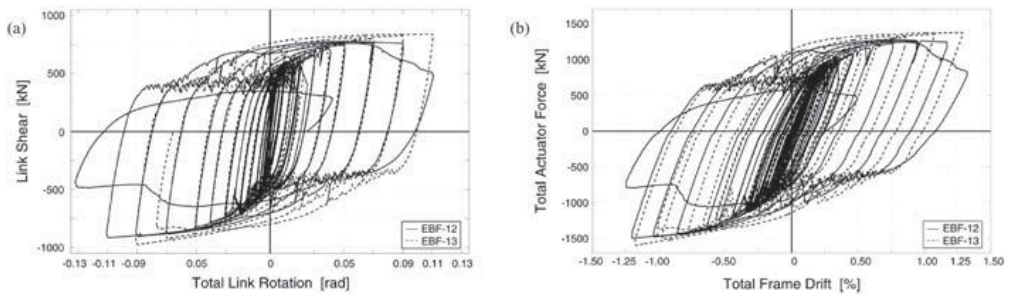

Fig. 2.19. Response of Replaceable Links with Back-to-back channels (Mansour, 2010)

2.4.3 Reduced Link Section

In order to address the limitation of link-to-column connections that do not develop the necessary ductility and are prone to connection fracture at low drift levels, Hauksdottir el al. 2008 come up with the application of the concept of reduced beam section as link to enhance the ductility. RBS has been used for MRF beam-to-volumn connections. Among RBS, the radius–cut is the only prequalified, field-welded connection in Prequalified Connections for use in Special Moment Resisting Frames SMRFs, although it should be noted that other connections may be qualified based on existing experimental data. Even hough AISC suggested that, RBS is not suitable for link-to-column connections due to the high moment gradient in links.

The prequalified radius-cut RBS connections are shown in Fig 2.20, prequalified based largely on work by Engelhardt et al. 1998 and Jones et al. 2002. The porpose of using the geometry shown in Fig. 2.20 is that the plastic hinge location in an SMRF beam is moved from the column face to the center of the RBS. The prequalified connections limits the dimensions a, b abd c in Fig. 2.21 as in Eq. (2.20) in terms of width beam flange (b_f) and beam depth (d):

$$\begin{aligned} 0.5b_f \le a \le 0.75b_f \\ 0.65d \le b \le 0.85d \\ 0.1b_f \le c \le 0.25b_f \end{aligned} \qquad \text{.....(2.13)}$$

However, previous research has shown that link-to-column connections do not develop the necessary ductility and are prone to connection fracture at low drift levels. Reduced beam sections (RBSs) have been proven to reduce strain concentrations at the ends of beams in MRFs and enhance ductility but have not been explored for use in EBF link-to-column connections where large moment gradients are present. This thesis investigates the application of RBSs in EBF links to enhance ductility.

The developed reduced link section is shown in Fig. 2.21. As stated above, in order to improve the ductility of EBF link-to-column connections is to reduce the plastic strain and localized deformation demands in the flanges at the end of the link by using a RLS. It is known that the end moment at the face of column is bigger than the end moment at the face of beam-brace. But for simplicity, Hauksdottir el al. 2008 neglects an unequality of these end moment differences. Hauksdottir el al. derived moment at the end of the link M_L, shown in Fig. 2.21 and the moment at the center of reduced link section as in Eq. (2.14) and (2.15 and 2.16) respectively.

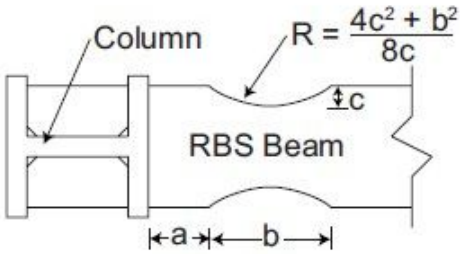

Fig. 2.20 Reduced beam section geometry

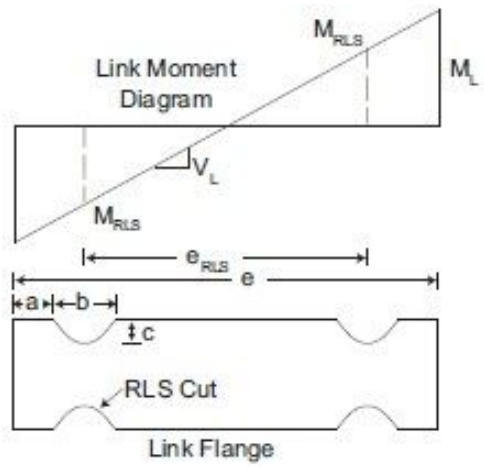

Fig. 2.21 Link moment distribution with reduced flange section

$$M_L = \xi M_p \quad \text{.....(2.14)}$$

$$M_{RLS} \le \xi \frac{M_p e_{RLS}}{e} \quad \text{.....(2.14)}$$

$$M_{RLS} \le \frac{Z_e}{Z} M_p \quad \text{.....(2.14)}$$

where

ξ = ratio of the moment at the end of the link to the plastic moment strength of the section.

Z = plastic section modulus for full beam cross-section

Z_e = plastic section modulus at center of the reduced link section

The plastic section modulus at the center of the reduced link section can be calculated according to Eq. 2.14.

$$Z_c = Z - 2ct_f(d - t_f) \quad \text{.....(2.14)}$$

where

c = depth of cut at center of the reduced link section

t_f = thickness of beam flange

d = depth of beam section

The ratio of moment at the end of link the plastic moment strength of the section was used as a parameter for studies done by Hauksdottir. The plastic rotation capacity of reduced link section evaluated by Hauksdottir analytically is summarized in Fig. 2.22. As shown in the figure, the analysis specimens satisfies the plastic rotation limit suggested by the AISC provision. Hauksdottir concluded from the FE analysis that the application of RLSs in EBFs is effective in reducing flange strains at the ends of all link types, though more effective for intermediate and flexural links than shear links.

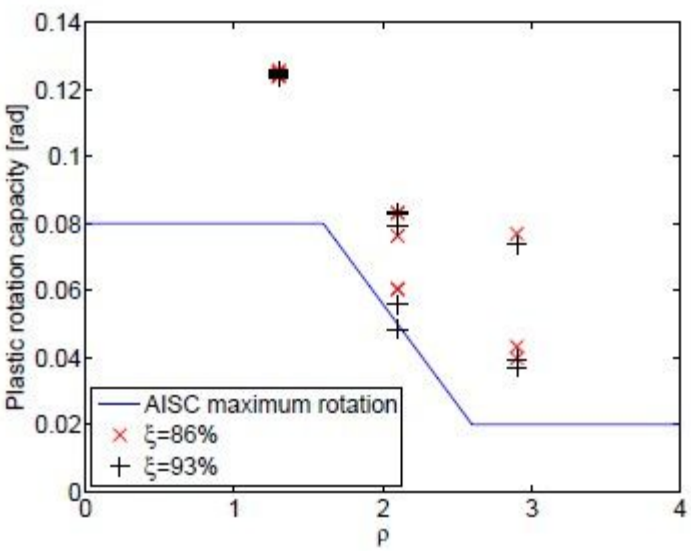

Fig 2.22 Plastic rotation versus link length factor (Hauksdottir, 2008)

2.5 The behavior of plates with circular hole under shear loading

It is important to understand the behavior of plates with circular hole under shear force to go through this dissertation. because in this research circular hole is included in the web of the link. These holes included in the link webs not only used to decrease the strength of links to use equal cross-section with the collector beam, they also control the failure at the web. The elastic theory indicates that holes will cause stress concentrations in the remaining material. The concept used in the in the reduced link section in this study is similar to the case of a thin plate in pure shear with a circular hole shown in Fig. 5.23.

The stresses in the plate can be derived from the classical solution for a thin plate with a circular hole in tension [Timoshenko]. The radial stress (σ_r), tangential stress (σ_θ) and shear stress ($\sigma_{r\theta}$) in the plate due to shear loading are:

$$\sigma_r = \tau\left(1 + \frac{3a^4}{r^4} + \frac{4a^2}{r^2}\right)\cos 2\theta \quad \text{.....(2.15)}$$

$$\sigma_\theta = -\tau\left(1 + \frac{3a^4}{r^4}\right)\cos 2\theta \quad \text{.....(2.16)}$$

$$\sigma_{r\theta} = -\tau\left(1 - \frac{3a^4}{r^4} + \frac{2a^2}{r^2}\right)\sin 2\theta \quad \text{.....(2.17)}$$

where: r, τ, a, and θ, are the distance from the hole center, applied shear stress, radius of the hole, and counter clockwise angle relative to a horizontal datum (see Fig. 2.23), respectively.

Fig. 2.24 shows the distribution of tangential stress (hoop stress) in the remaining plate. From Fig. 2.24, a tangential stress concentration of four times the applied shear stress can be seen at the edge of the hole. This is the concept how the fractures in links are controlled only in the web rather than in the flange connections that happened in case of link-to-column connection of EBFs.

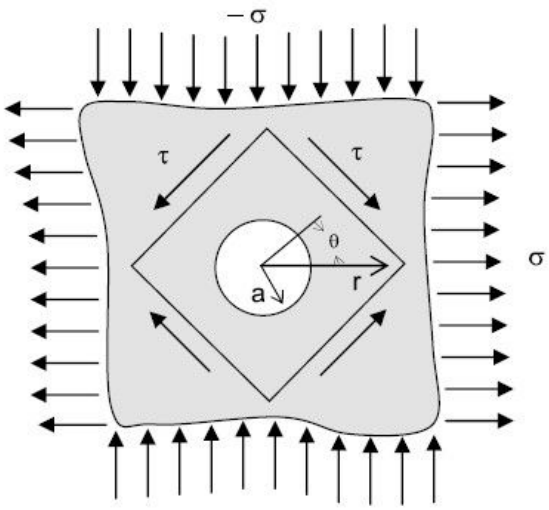

Fig. 2.23 Classical problem of infinite plate with circular hole subjected to shear loading.

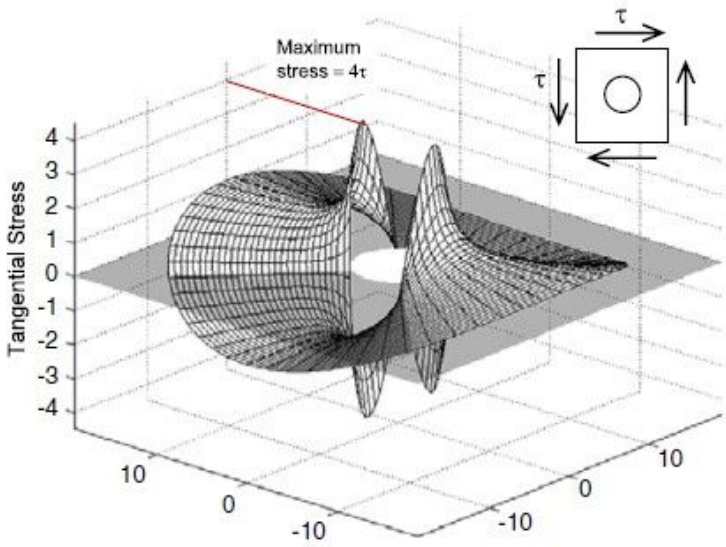

Fig. 2.24 Tangential stress distribution in a plate with a hole subjected to shear.

3. Development and design of replaceable reduced link sections

3.1 Development of replaceable reduced link section

The description along with a figure of the developed links are listed below. Generally the developed links are categorized in to two:

i. Replaceable links with reduced section fabricated from a W-section with end-plate connections and

ii. Replaceable links with reduced section fabricated from a C-section with web and flange-bolted connections.

The detail of developed active links 'links here after' are presented below.

3.1.1 Replaceable links with perforated web fabricated from a W-section with end-plate connections

The detail of the first link proposed is shown in Fig. 3.1. As shown in the figure, it is fabricated from W-section and the link is welded to the end plates both side. The end plates in which the links are welded to are connected to the beam section through bolted end-plate connections. The connection behavior and stiffness, which depend on the bolt size, end plate thickness and welding, are important to the design of EBF systems incorporating replaceable links. The addition of the horizontal stiffeners in the floor-beam sections adds stiffness to the floor-beam at the connections.

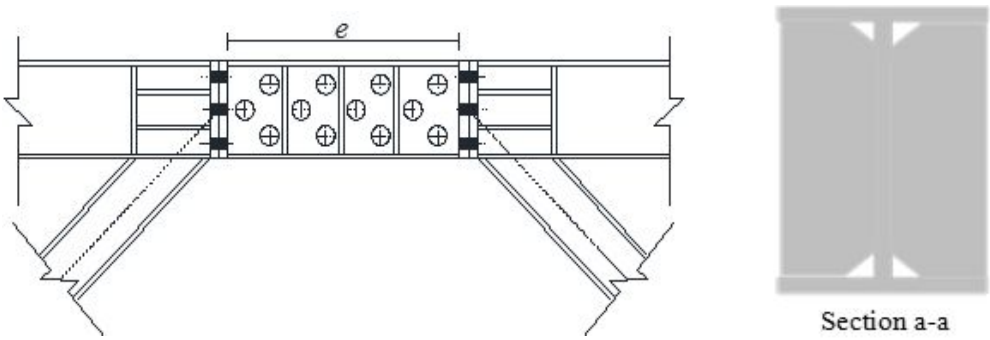

Fig. 3.1 Replaceable links with perforated web fabricated from a W-section with end-plate connections

3.1.2 Replaceable links with perforated web fabricated from a C-section with web and flange-bolted connections

The detail of the second link proposed is shown in Fig. 3.2. As shown in the figure, it is fabricated from C-sections are back-to-back connected to the web and flanges of the beam bolted to the web and flanges of link. The moment is transferred through top and bottom flange bolts, while the shear is transferred through concentric web-bolted connections. The research conducted by Nabil Mansour is the first research performed on the use of C-section beams as shear links, and the use of the web-bolted concept to connect the link to the collector beam. He developed and designed two types of C-section shear links, i) 2 channel-sections back-to-back eccentrically loaded web-bolted connections and ii) Built-up-channels section back-to-back with variable depth Shear Replaceable Link with web and flange connections. However in both cases of channel section link, he detailed and design a significant section difference between the link and collector beam in order to remove any interference with the floor deck. Both detailing option can be applied for perforated web channel; however in this research we concentrate on second detailing options with both web and flange are bolted to the floor beam. This detail involves two options: either bolting only web to the floor beam or bolting both web and flanges to floor beam. In the first option where only the web bolted with floor beam, the out of plane instability and connection detail of flanges needs to be evaluated.

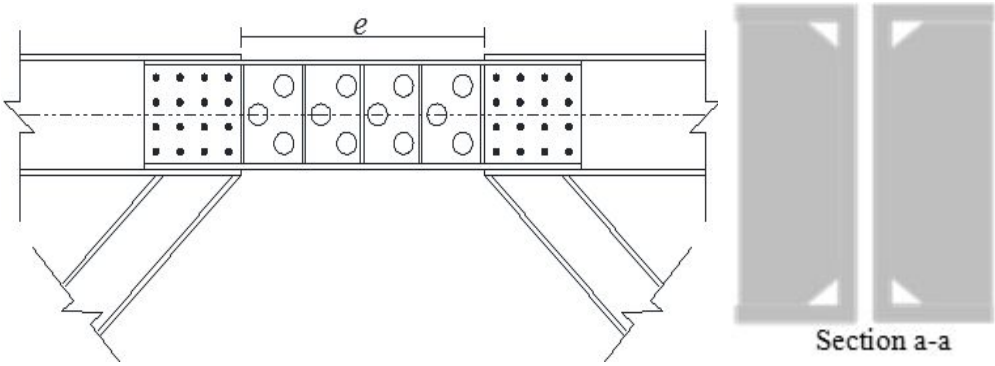

Fig. 3.2 replaceable shear links with perforated web fabricated from a C-section with web and flange-bolted connections

3.1.3 Replaceable links with perforated web and reduced flange section fabricated from a W-section with end-plate connections

The other detail of the proposed link is shown in Fig. 3.3. As shown in the figure, it is fabricated from C-section and the link is bolted to the web and flanges of the beams. The concept of reduced beam section for links in eccentrically braced frames to enhance the ductility of link-to-column connections is developed and evaluated by Jeffrey W. Berman in 2010 [37]. In this research, they suggested that links having various cross sections and lengths suggests that the reduced link section reduce the plastic flange strains at the link ends, which can improve the fracture life. Here, this concept is extended for replaceable link with perforated web. The reduced beam section is suitable for a beam that has flexural yielding occurring initially but can be less suitable for beams subject to shear yielding. Reduced flange section involves a decrease in moment at the face of the columns or in the moment transferred to the beam outside the link. By decreasing the moment in the beam outside the link, the stability of the beam improved and damage is reduced. Another advantage is that the RBS contains inelastic behavior within the link, which enables strict capacity design.

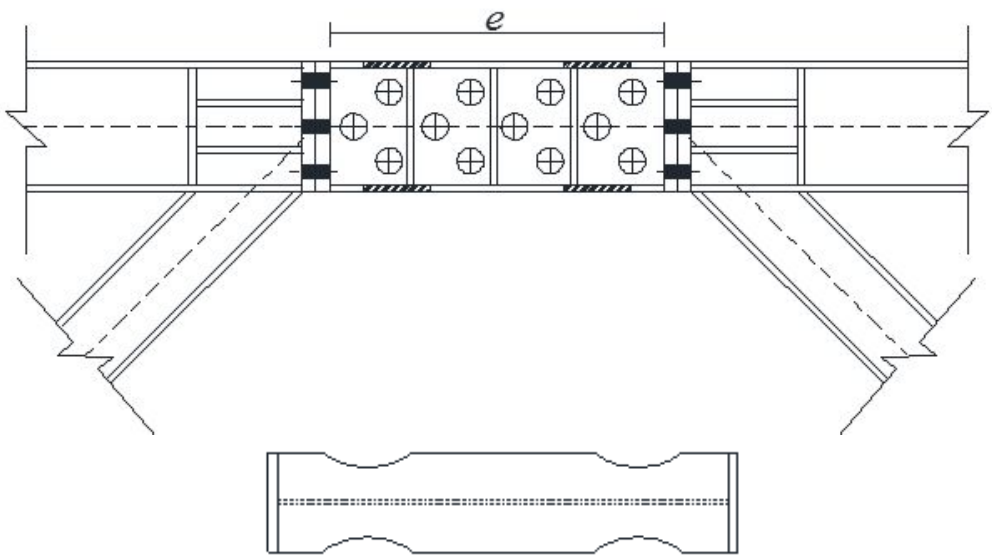

Fig. 3.3 Replaceable links with perforated web and reduced flange section fabricated from a W-section with end-plate connections

3.1.4 Replaceable links with perforated web and reduced flange section fabricated from a C-section with web and flange-bolted connections

The detail of the last link proposed is shown in Fig. 3.3. As shown in the figure, it is fabricated from C-section and the link is bolted to the web and flanges of the beams. Since the replaceable link section is a separate element from the rest of the beam, the potential of using built-up sections with relatively thin webs and thick flanges, can greatly optimize the design of the link and the entire EBF system. In all cases the link section thickness is different from collector beam. The connections in all links must be able to transfer and sustain the maximum forces that can be delivered by the fully yielded and strain hardened link.

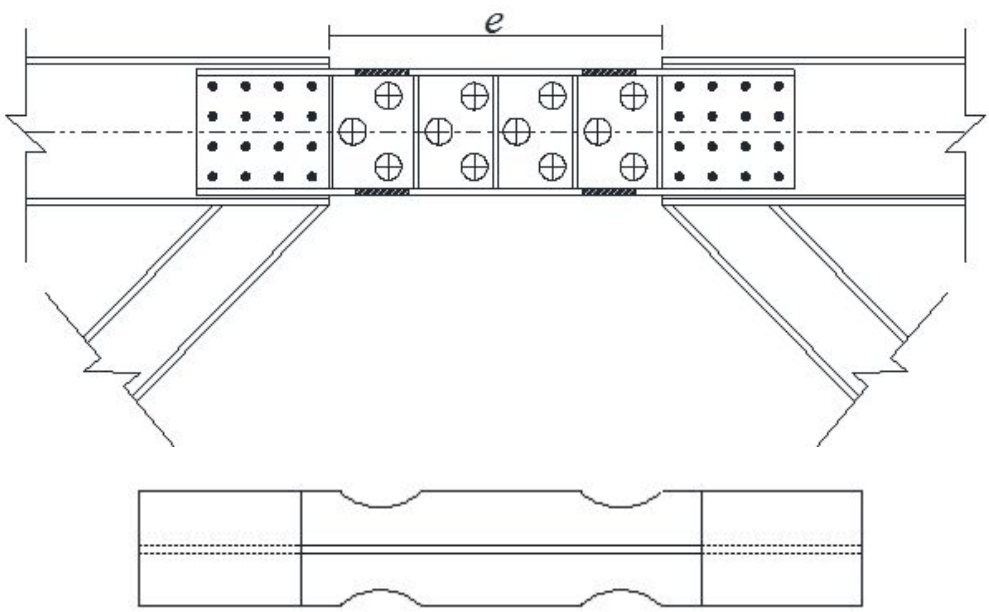

Fig. 3.4 replaceable shear links with perforated web and reduced flange section fabricated from a C-section with web and flange-bolted connections

3.2 Applications of developed links

The developed links can be installed as shown in Fig. 3.5. However, some of the links are not installed in all types of EBFs listed in Fig. 3.5. For instance, links fabricated from channel-section connected back-to-bach can not used in D-bracing type V-bracing type and vertical links. This is because channel section back-to-back connection details is with web bolting. Thus type 3.1.2 and 3.1.4 can not be used in link-to-column connection.

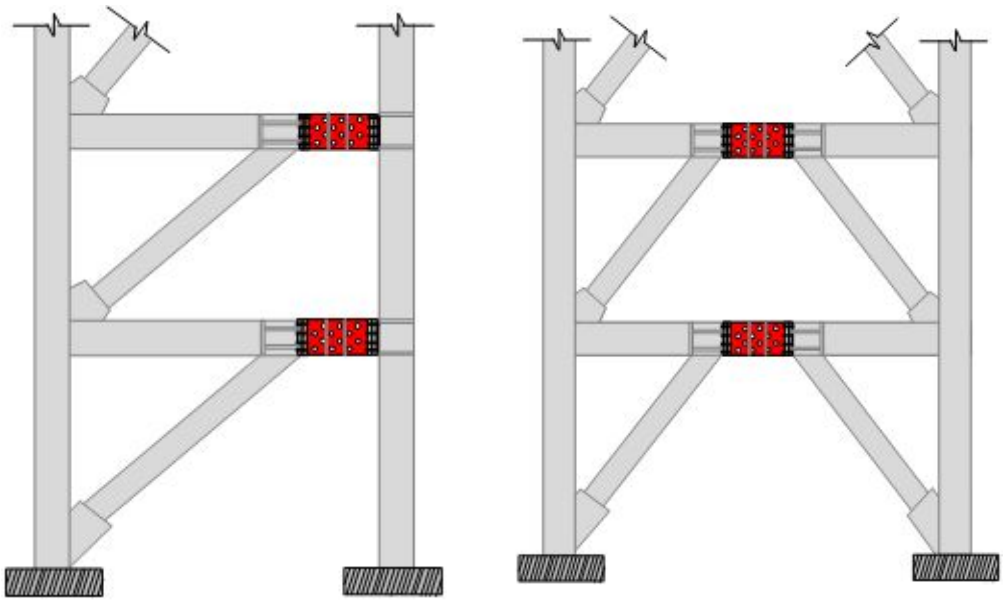

(a) D-braced frame (b) split-K braced frame

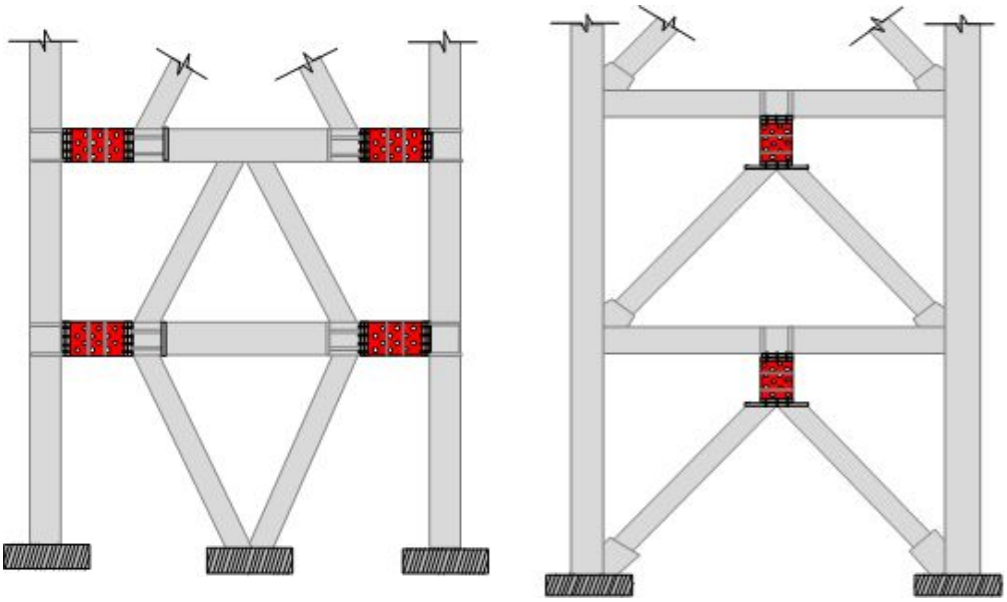

(c) V-braced frame (d) inverted Y-braced frame*

Fig. 3.5 Proposed Replaceable Shear links with perforated web fabricated from a W-section.

3.3 Design Procedure of reduced links section

The design and detailing of links needs a careful work as the over all building frame depends on the behavior of links. All structural members of EBFs are designed for forces developed in a fully yielded and strain hardened links i.e after the link beam goes through plastic deformation. Since a link with ductile detailing is capable of developing forces significantly greater than its nominal plastic strength, overstrength must be considered carefully when evaluating the link forces for capacity design of adjoining members. The inelastic action and damage is controlled primarily to the links in an appropriately designed eccentrically braced frames (EBFs). The design procedure of reduced section links categorized in to two: links with reduced web (perforated web) and involves two links with reduced both web and flange at the same time.

3.3.1 Arrangement of perforations

The inclination angle of perforations follows the tension field actions occurred under shear force. Different researchers recommended different equation to calculate the angle of tension filed actions.

3.3.1.1 Basler's Recommendation

Basler recommended the angle of tension filed action as in Equation (3.1) below.

$$\gamma_{tf} = \frac{1}{2} tan^{-1}\left(\frac{1}{b/d}\right) \qquad \text{.....(3.1)}$$

where γ: is the tension filed angle, b: width of plate and d: depth of plate.

3.3.1.2 Thorburn's Recommendation

Thorburn's recommended the angle of tension filed action as in Equation (3.2 and 3.3) below.

$$\gamma = \frac{1}{2} tan^{-1} \sqrt{\frac{1 + \frac{bt}{2A_c}}{1 + \frac{dt}{A_b}}} \quad \text{.....(3.2)}$$

$$\gamma = \frac{1}{2} tan^{-1} \left(\frac{b}{d} \right) \quad \text{.....(3.3)}$$

3.3.1.3 Timler's Recommendation

Timler's recommended the angle of tension filed action as in Equation (3.4 and 3.5) below.

$$\gamma = \frac{1}{2} tan^{-1} \sqrt{\frac{1 + \frac{bt}{2A_c}}{1 + dt\left(\frac{1}{A_b} + \frac{d^3}{360 I_c b} \right)}} \quad \text{.....(3.4)}$$

$$\gamma = \frac{1}{2} tan^{-1} \sqrt{\frac{1 + bt\left(\frac{1}{A_c} + \frac{a^3}{120 I_c b} \right)}{1 + dt\left(\frac{1}{2A_b} + \frac{b^3}{360 I_c b} \right)}} \quad \text{.....(3.5)}$$

Using all these recommendations, the calculated inclination angle ranges between $36^0 - 42^0$. We used inclination angle 39 and 40 for these preliminary analysis.

3.3.2 Design Procedure of Reduced Web (perforated web) Links Section

Links usually behave as short beams subjected to equal shear loads applied in opposite directions at the link ends. With this type of loading, the moment at each end is equal and in the same direction. The deformation of the link is an S shape with a point of counter flexure at mid-span. The moment is equal to 1/2 the shear times the length of the link at equilibrium for V-type braced EBFs. The shear and moment distribution of a link with a reduced web section (perforated web) is shown in Fig. 3.6. The perforation effect on shear force is significant where it decreases by the reduced web area. However, web section reduction (web perforation) has a slight or no effect on bending moment. The assumptions considered for this calculations are:

1. Equal end moment
2. The effect of web perforation on plastic moment was ignored for simplicity.

The plastic shear force of unreduced link is given by Eq. 3.6:

$$\begin{aligned} V_p &= 0.6\sigma_y A_w \quad \text{for shear yielding} \\ &= 2M_p/e \quad \text{for flexural yielding} \end{aligned} \qquad \text{.....(3.6)}$$

where σ_y: is the yield strength, e: link length, A_w: is the web cross-sectional area given in terms of the depth and flange and web thicknesses as in Eq. (3.7) and M_p: is the plastic end-moment expressed in Eq. (3.8)

$$A_w = (D - 2t_f)t_w \qquad \text{.....(3.7)}$$

$$\begin{aligned} M_p &= V_p e/2 \quad \text{for shear yielding} \\ &= \sigma_y Z_p \quad \text{for flexural yielding} \end{aligned} \qquad \text{.....(3.8)}$$

where Z_p: plastic section modulus. The plastic shear force of reduced link section is given by:

$$\begin{aligned} V_p^{rw} &= 0.6 f_y A_w^* \quad \text{for shear yielding} \\ &= 2M_p^{rw}/e_{rw} \quad \text{for flexural yielding} \end{aligned} \qquad \text{.....(3.9)}$$

where V_p^{rw}: is the plastic shear for perforated web, A_w^*: is the area of reduced web section given as in Eq. (3.10) and M_p^{rw}: is the plastic end-moment of reduced web link section expressed in Eq. (3.11)

$$A_w^* = (D - 2t_f - n\phi)t_w \qquad \text{.....(3.10)}$$

where ϕ: is the diameter of perforation, n: number of perforation in a vertical alignment.

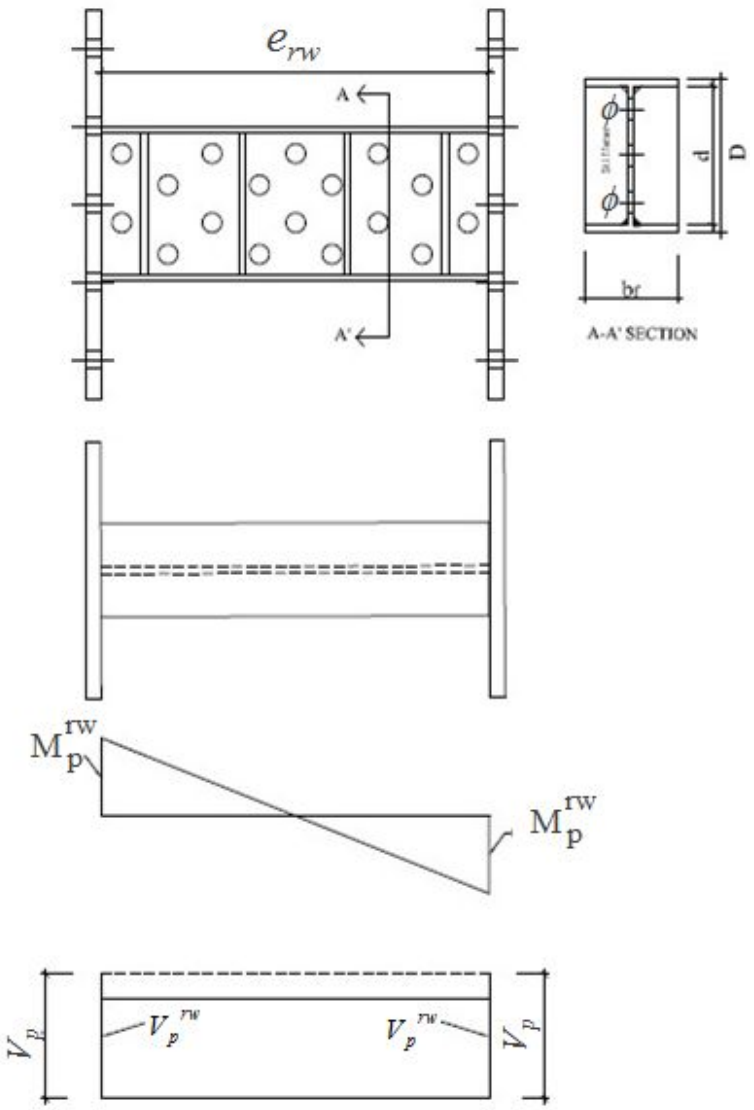

Fig. 3.6 Shear and moment distribution of reduced web link section

$$M_p^{rw} = V_p^{rw} e_{rw}/2 \quad \text{for shear yielding}$$
$$= Z_p^{rw} \sigma_y \quad \text{for flexural yielding} \qquad \text{.....(3.11)}$$

where Z_p^{rw}: is the plastic section modulus of reduced web section given by:

$$Z_p^{rw} = Z_p - \phi t_w \sum_{i=1}^{n} x_i \qquad \text{.....(3.12)}$$

where t_w: is the thickness of web, n: number of perforation in a vertical alignment and x_i: is the distance from the neutral axis to the centroid of the perforations.

The link length for reduced section is different from unreduced section as the plastic shear is decreased. The behavior of link depends on the link length ratio (non dimensional factor) ρ. which is given by Eq. (3.13) for reduced web section link:

$$\rho_{rw} = e_{rw} \frac{M_p^{rw}}{V_p^{rw}} \qquad \text{.....(3.13)}$$

where ρ_{rw}: non dimensional link factor, V_p^{rw}: plastic shear force, e_{rw}: link length of reduced web section, M_p^{rw}: plastic bending moment reduced web link defined in Eq. (3.11). The effect of web reduction on plastic end moment is small so it is ignored for simplicity. So that the plastic end moment for reduced web link and unreduced link is equal. From moment equilibrium of a link, the plastic end moment is expressed as in:

$$M_p = \frac{V_p^{rw} . e_{rw}}{2} \qquad \text{.....(3.14)}$$

$$M_p = \frac{V_p . e}{2} \qquad \text{.....(3.15)}$$

Equating Eq. (3.15) and (3.16):

$$\frac{V_p^{rw}}{V_p} = \frac{e}{e_{rw}} \qquad \text{.....(3.17)}$$

Combining Eq. (3.17) and Eq. (3.6-3.9):

$$e_{rw} = \frac{de}{1-n\phi} = \left(\frac{1}{1-\frac{n\phi}{d}}\right).e \qquad \text{.....(3.18)}$$

where ϕ: is the diameter of perforation, n: number of perforation in a vertical alignment and d: is the depth of link, e: is the length of unreduced link. Eq. (3.18) defines the relationship between the link length of reduced web section (e_{rw}) and unreduced link length (*e*).

It is known that the link type and behavior is depends on the link length factor. The same is true for reduced link section as well. Thus, depending on the link length factor, the type of links are:

Short link (Shear yielding link)

$$\rho_{rw} \leq 1.6 \qquad \text{.....(3.19)}$$

Intermediate link (Combined shear and flexural yielding link)

$$1.6 < \rho_{rw} < 2.6 \qquad \text{.....(3.20)}$$

Long link (Flexural yielding link)

$$\rho_{rw} \geq 2.6 \qquad \text{.....(3.21)}$$

In order to illustrate the equations expressed in Eq (3.18) the relationship between link length of reduced web and the diameter along with the number of openings in a vertical alignment is plotted as an example. Taking section H200x150xt_wx10 for instance, keeping the flange compactness constant, ($b_f/t_f = 15 < 0.76\sqrt{\frac{E}{F_y}} = 19$, compact section) and web compactness as a variable, $d/t_w = 20, 30, 40 < 2.45\sqrt{\frac{E}{F_y}} = 60$, all compact section) the plastic shear will be 316kN, 211kN and 158kN respectively and 102.3kNm, 97.6kNm and 95.2kNm plastic bending respectively.

Table 3.1 Link length design of H200x150xt_wx10

$\frac{d}{t_w}$	t_w (mm)	Z (mm^3) $(x10^5)$	V_p (kN)	M_p (kNm)	$\frac{M_p}{V_p}$(m)	ρ					
						1.0	1.6	2.0	2.4	2.6	3
						$e=\rho\frac{M_p}{V_p}$(mm)					
20	9	3.147	316	102.3	0.32	324	518	648	777	842	971
30	6	3.002	211	97.6	0.46	463	741	926	1112	1204	1390
40	4.5	2.929	158	95.2	0.60	603	964	1205	1446	1567	1808

The link length for unreduced section is summarized in Table 3.1 for different link length factor. The link length of reduced web section now calculated using Eq. (3.13). The calculated reduced link section length for $d/t_w = 30$ is summarized in Table 3.2 and 3.3 for number of openings n=1 and n=2 respectively. The corresponding plot of the reduced link section length and the opening diameter is presented in Fig. 3.7 for $d/t_w = 20, 30, 40$ and for both n=1 and 2. As shown in the figure, for all link type, the length of reduced link section increases with the diameter of opening. The number of opening has a significant effect on the length of reduced link section. The rate at which the length of reduced link section for n=2 is higher than n=1.

For each of the cross-sections expressed in Table 3.1, the reduced link length can be calculated using Eq. (3.18) considering different link length factor, diameter of perforations and number of perforations in a vertical alignment. For instance the reduced link length for $d/t_w = 30$ and n=1 is shown in Table 3.2. Similarly, the reduced link length for $d/t_w = 30$ and n=2 is presented in Table 3.3.

Reduced link length versus diameter of perforation for $d/t_w = 30$ and link length factor of 1.2 was plotted in Fig. 3.7. As shown in the figure, generally as the diameter of perforation increase the reduced link length also increases. And when the number of perforations in a vertical direction increase from one to two the rate at which the reduced link length increases with an increase of perforation diameter is high. Which indicates that the number of perforations has a significant effect of the behavior of links along with the perforation diameter. For links with cross-section of $d/t_w = 20$, $d/t_w = 30$ and $d/t_w = 40$ for different link length factor and number perforations in a vertical direction is plotted in Fig. 3.8.

Table 3.2 length of reduced web link section and diameter perforation relationship of d/t_w=30, for (n=1)

ρ	e (mm)	ϕ(mm)									
		0	5	10	15	20	25	30	35	40	45
		e_{rw}(mm)									
0.8	371	371	381	392	404	417	430	445	460	476	494
1	463	463	476	490	505	521	538	556	575	596	618
1.2	556	556	572	589	606	625	646	667	690	715	741
1.4	648	648	667	687	707	730	753	778	805	834	865
1.6	741	741	762	785	809	834	861	889	920	953	988
1.8	834	834	858	883	910	938	968	1001	1035	1072	1112
2	926	926	953	981	1011	1042	1076	1112	1150	1191	1235
2.2	1019	1019	1048	1079	1112	1146	1183	1223	1265	1310	1359
2.4	1112	1112	1143	1177	1213	1251	1291	1334	1380	1429	1482
2.6	1204	1204	1239	1275	1314	1355	1399	1445	1495	1548	1606
2.8	1297	1297	1334	1373	1415	1459	1506	1556	1610	1668	1729
3	1390	1390	1429	1471	1516	1563	1614	1668	1725	1787	1853

Table 3.3 length of reduced web link section and diameter perforation relationship of d/t_w=30, for (n=2)

ρ	e (mm)	ϕ(mm)									
		0	5	10	15	20	25	30	35	40	45
		e_{rw}(mm)									
0.8	371	371	392	417	445	476	513	556	606	667	741
1	463	463	490	521	556	596	641	695	758	834	926
1.2	556	556	589	625	667	715	770	834	910	1001	1112
1.4	648	648	687	730	778	834	898	973	1061	1167	1297
1.6	741	741	785	834	889	953	1026	1112	1213	1334	1482
1.8	834	834	883	938	1001	1072	1154	1251	1364	1501	1668
2	926	926	981	1042	1112	1191	1283	1390	1516	1668	1853
2.2	1019	1019	1079	1146	1223	1310	1411	1529	1668	1834	2038
2.4	1112	1112	1177	1251	1334	1429	1539	1668	1819	2001	2223
2.6	1204	1204	1275	1355	1445	1548	1668	1807	1971	2168	2409
2.8	1297	1297	1373	1459	1556	1668	1796	1945	2122	2335	2594
3	1390	1390	1471	1563	1668	1787	1924	2084	2274	2501	2779

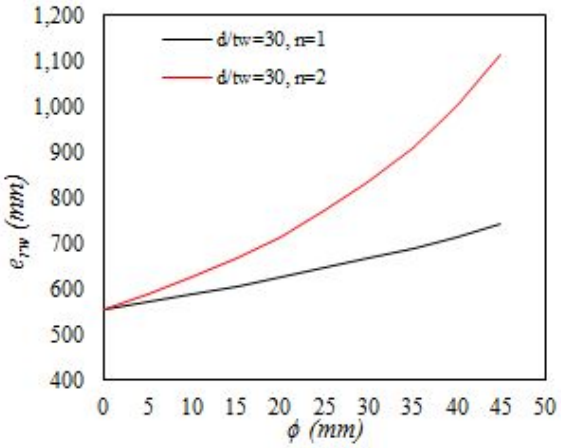

Fig. 3.7 Length of reduced web link section and diameter of perforation relationship for H200x150, ρ=1.2

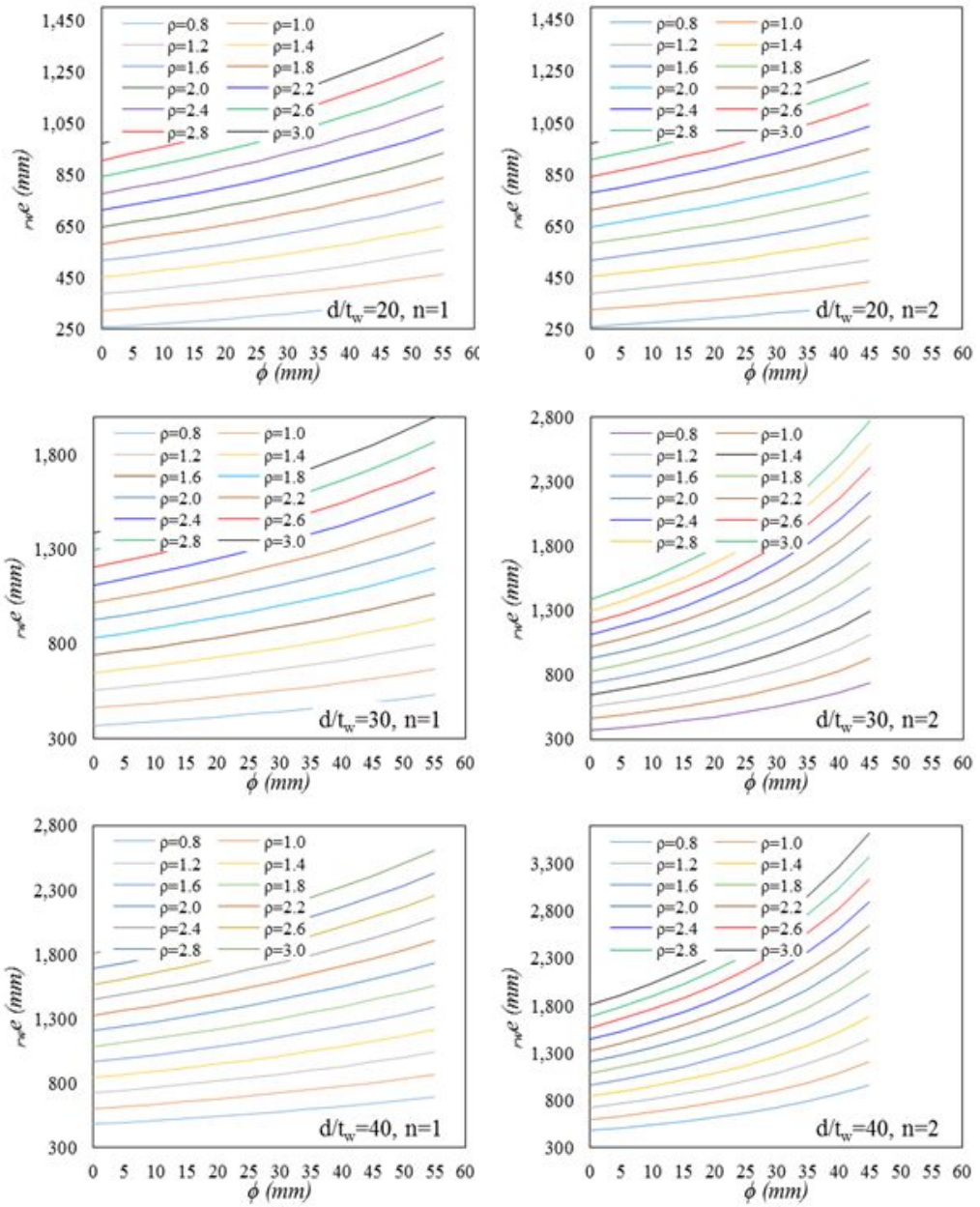

Fig. 3.8 Length of reduced web link section and diameter perforation relationship H200x150

3.3.2.1 Design Procedure of reduced web links

Taking the ratio of the plastic shear strength of unreduced and reduced links expressed in Eq. (3.6) and Eq. (3.9) is given by the Eq. (3.22), where the variables used are shown in Fig. 3.10. The plot of the relationship expressed in Equation 3.22 will be shown in Fig. 3.10.

$$\frac{V_p^{rw}}{V_p} = 1 - \frac{n\phi}{d} \qquad \text{.....(3.22)}$$

The general design procedure of reduced web link section is presented in a flow chart presented in Fig. 3.11. The design procedure presented in the flow chart is a general procedure for links with reduced web area.

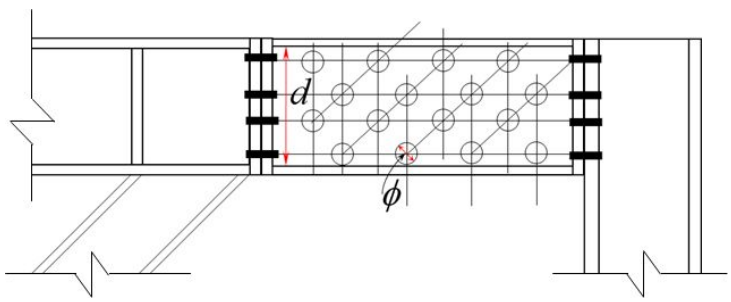

Fig. 3.9 Schematic detail of reduced web link

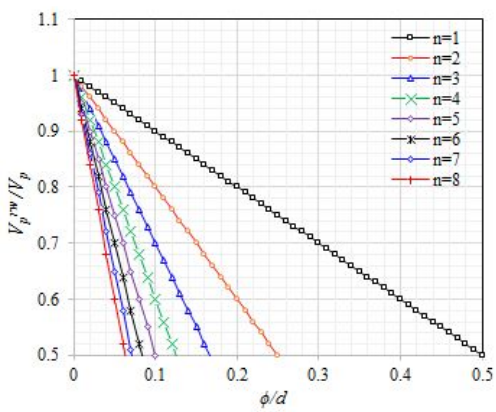

Fig. 3.10 plastic shear reduction vs diameter of perforation to depth ratio

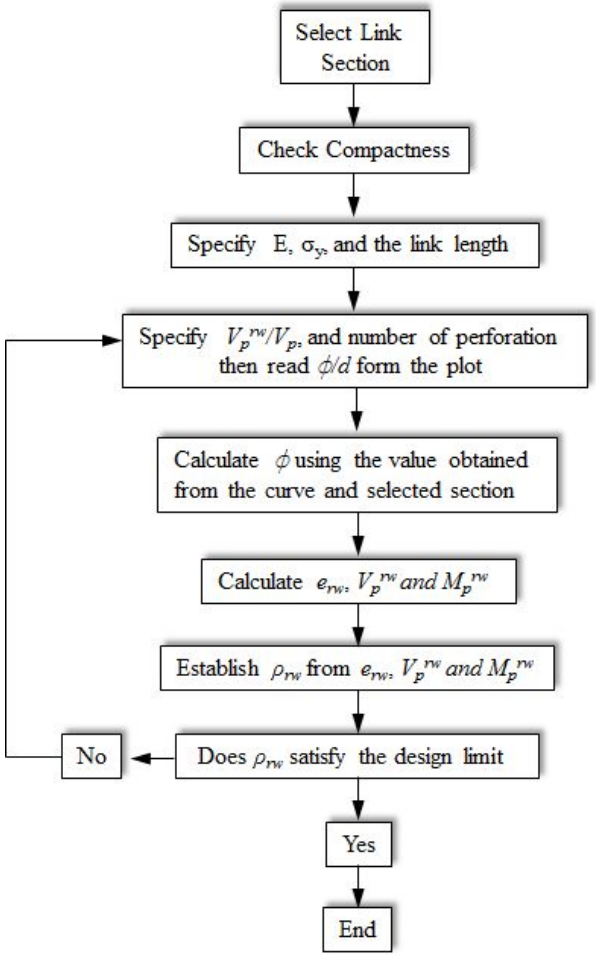

Fig. 3.11 A flow chart of the general design procedure of reduced web link section

The ratio of plastic shear strength of reduced and unreduced links might not go less than 0.5 in order to the link dissipates the seismic energy. Taking the lower limit of strength ratio as 0.5, the ratio of perforation diameter and depth of link can be read from the plot presented in Fig. 3.10. Looking at the design procedure presented in Fig. 3.11, if the calculated reduced link length factor, doesn't meet the design recommendation of standards, we can revise the strength ratio section.

3.3.3 Design Procedure of Reduced Web and Flange Links Section

The design and detailing of links needs a careful work as the over all building frame depends on the behavior of links. All structural members of EBFs are designed for forces developed in a fully yielded and strain hardened links i.e after the link beam go through plastic deformation. The shear and moment distribution of a link with a reduced web and flange section is shown in Fig. 3.12. In this case both plastic shear strength and flexural strength decreases. According to previous research on the behavior of RBS moment connections, the most practical cutout is a radius cut as shown in Fig. 3.13. The cutout radius is given:

$$R = \frac{4c^2 + b^2}{8c} \quad \text{.....(3.23)}$$

where b, and c are the flange design requirements expressed as in the following including 'a' the length from the end to the start of section reduction.

$$0.5b_f \leq a \leq 0.75b_f \quad \text{.....(3.24)}$$

$$0.65d \leq b \leq 0.85d \quad \text{.....(3.25)}$$

$$0.1b_f \leq c \leq 0.25b_f \quad \text{.....(3.26)}$$

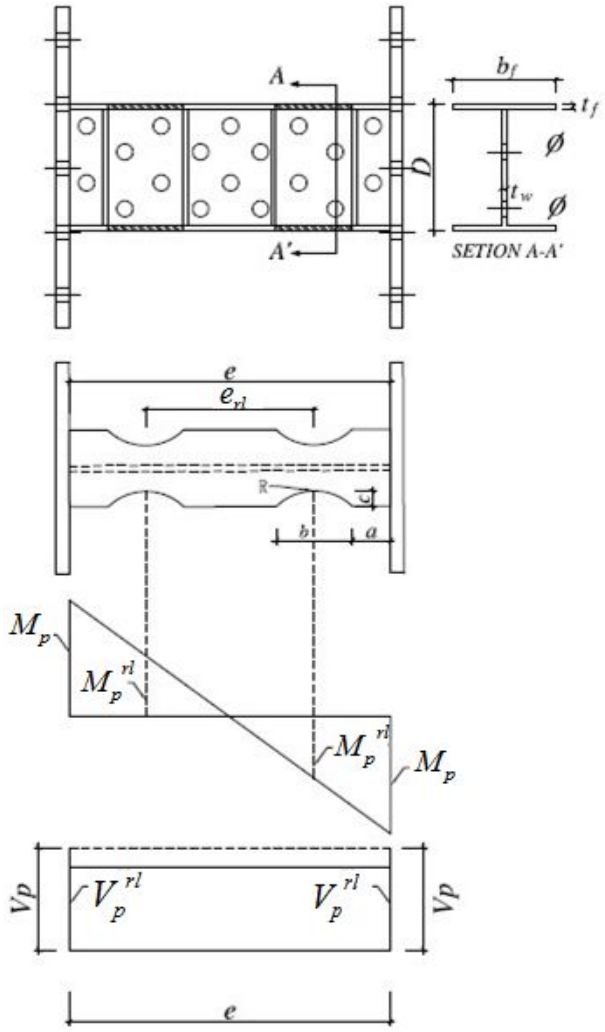

Fig. 3.12 Shear and moment distribution of reduced web and flange link section

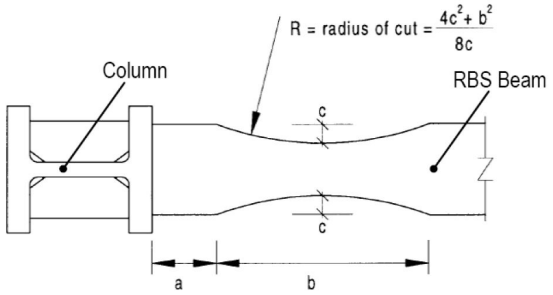

Fig. 3.13 Reduced beam section connection (Engelhardt et al. 1998)

By reducing the section, yielding and plastic hinge formation is forced to occur at the reduced beam section instead of at the end of the beam. Therefore, the highest stress and strain in the beam occur at the reduced beam section.

The link length for reduced section is different from unreduced section as the plastic shear is decreased. The behavior of link depends on the link length ratio (non dimensional factor) ρ. this time Eq. (3.13) is changed to Eq. (3.26) for reduced web and flange link section:

$$\rho_{rl} = \frac{V_p^{rl}.e_{rl}}{M_p^{rl}} \qquad \text{.....(3.26)}$$

where ρ_{rl}: non dimensional link factor, V_p^{rl}: plastic shear force, e_{rl}: link length of reduced web section, M_p^{rl}: plastic bending moment. The plastic shear force for reduced web and flange link section is calculated in the same way used in reduced web link section Eq. (3.9). Here it is possible to follow the same procedure to design a reduced web and flange link section. In this case also the link type depends on the link length factor, ${}_{rs}\rho \leq 1.6$, for short link, $1.6 < {}_{rs}\rho < 2.6$, for intermediate link and ${}_{rs}\rho \geq 2.6$, for long link. The plastic moment can be defined by:

$$\begin{aligned} M_p^{rl} &= \frac{e_{rl}\, V_p^{rl}}{2} \qquad \text{for shear yielding} \\ &= \sigma_y\, Z_p^{rl} \qquad \text{for flexural yielding} \end{aligned} \qquad \text{.....(3.28)}$$

where σ_y: is the yield strength, and Z_p^{rl}: is plastic section modulus at reduced section. The relationship between the plastic section modulus of unreduced section and reduced flange section is expressed in terms of c which is expressed in Eq (3.26) is given in Eq. 3.29), flange thickness and link depth.

$$Z_p^{rl} = Z_p - 2ct_f(d - t_f) - \phi t_w \sum_{i=1}^{n} x_i \qquad \text{.....(3.29)}$$

Ignoring the effect of web reduction for simplicity, the new plastic section modulus of reduced link section is shown in Eq. (3.30) is derived by (Heidrun 2008):

$$Z_p^{rl} = Z_p - 2ct_f(d - t_f) \quad \text{.....(3.30)}$$

The plastic end moment at equilibrium of a link for reduced and unreduced link section is given by Eq. (3.31) and (3.32) respectively.

$$M_p^{rl} = \frac{V_p^{rl}.e_{rl}}{2} \quad \text{for reduced link} \quad \text{.....(3.31)}$$

$$M_p = \frac{V_p.e}{2} \quad \text{for unreduced link} \quad \text{.....(3.32)}$$

Taking the ratio of Eq. (3.29) and (3.30):

$$e_{rl} = \frac{V_p.Z_p^{rl}}{V_p^{rl}Z_p}e \quad \text{.....(3.33)}$$

Substituting for plastic shear of links for unreduced and reduced link section in Eq. (3.31):

$$e_{rl} = \left(\frac{1}{1 - \frac{n\phi}{d}}\right).\left(\frac{Z_p^{rl}}{Z_p}\right).e \quad \text{.....(3.34)}$$

where n: is the number of opening in a vertical alignment, ϕ: is the diameter of opening, d: is depth of link. Substituting Eq. (3.33) in Eq. (3.34), the reduced link length will be:

$$e_{rl} = \left(\frac{1}{1 - \frac{n\phi}{d}}\right).\left(1 - \frac{2ct_f(d - t_f)}{Z_p}\right).e \quad \text{.....(3.35)}$$

Equation 3.35 can be applied for reduced web and flange link length if and only if the neutral axis of the cross-section is equal distance from the outer most fiber. The difference between the link length of reduced web and reduced web and flange link section is the ratio of plastic section modulus of reduced link to unreduced link as shown in Eq. (3.35).

In order to illustrate Eq. (3.35), the same specimen that is used to illustrate Eq. 3.18) was used. The relationship of the length of reduced web and flange link section and the diameter of open area for number of opening n=1 and 2 and flange section cutoff depth of 0.1b_f and 0.2b_f is presented in Table 3.4 - Table 3.7 for $d/t_w = 30$. Fig. 3.14 shows the relationship of reduced link length and diameter of perforations for $d/t_w = 30$ and link length factor 1.2 considering different number of perforations and cutout depth (c). As

shown in the figure, the effect of cutout depth (c) is on initial link length where the link length shifts up as the cutout depth increases. Whereas, the number of perforations affects the rate at which the link length increases with an increase of perforation diameter. The plot of this relationship is also presented in Fig. 3.15 for $d/t_w = 20, 30$ of number of opening n=1 and 2 and flange section cutoff depth of 0.1b_f and 0.2b_f.

Table 3.4 length of reduced web link section and diameter perforation relationship of d/t_w=30, for (n=1, c=0.1b_f)

ρ	e (mm)	ϕ(mm)									
		0	5	10	15	20	25	30	35	40	45
		e_{rl}(mm)									
0.8	217	217	223	230	237	244	252	261	270	279	289
1	271	271	279	287	296	305	315	326	337	349	362
1.2	326	326	335	345	355	366	378	391	404	419	434
1.4	380	380	391	402	414	427	441	456	472	489	507
1.6	434	434	447	460	474	489	504	521	539	558	579
1.8	489	489	502	517	533	550	567	586	606	628	651
2	543	543	558	575	592	611	630	651	674	698	724
2.2	597	597	614	632	651	672	693	716	741	768	796
2.4	651	651	670	690	711	733	756	782	809	837	868
2.6	706	706	726	747	770	794	819	847	876	907	941
2.8	760	760	782	805	829	855	882	912	943	977	1013
3	814	814	837	862	888	916	945	977	1011	1047	1086

Table 3.5 length of reduced web link section and diameter perforation relationship of d/t_w=30, for (n=1, c=0.2b$_f$)

ρ	e (mm)	ϕ(mm)									
		0	5	10	15	20	25	30	35	40	45
		e_{rl}(mm)									
0.8	175	175	180	185	191	197	203	210	217	225	234
1	219	219	225	232	239	246	254	263	272	282	292
1.2	263	263	270	278	287	296	305	315	326	338	350
1.4	307	307	315	325	334	345	356	368	381	394	409
1.6	350	350	360	371	382	394	407	420	435	450	467
1.8	394	394	405	417	430	443	458	473	489	507	526
2	438	438	450	464	478	493	509	526	544	563	584
2.2	482	482	496	510	526	542	559	578	598	619	642
2.4	526	526	541	556	573	591	610	631	652	676	701
2.6	569	569	586	603	621	641	661	683	707	732	759
2.8	613	613	631	649	669	690	712	736	761	788	818
3	657	657	676	696	717	739	763	788	815	845	876

Table 3.6 length of reduced web link section and diameter perforation relationship of d/t_w=30, for (n=2, c=0.1b$_f$)

ρ	e (mm)	ϕ(mm)									
		0	5	10	15	20	25	30	35	40	45
		e_{rl}(mm)									
0.8	217	217	230	244	261	279	301	326	270	279	289
1	271	271	287	305	326	349	376	407	337	349	362
1.2	326	326	345	366	391	419	451	489	404	419	434
1.4	380	380	402	427	456	489	526	570	472	489	507
1.6	434	434	460	489	521	558	601	651	539	558	579
1.8	489	489	517	550	586	628	676	733	606	628	651
2	543	543	575	611	651	698	752	814	674	698	724
2.2	597	597	632	672	716	768	827	896	741	768	796
2.4	651	651	690	733	782	837	902	977	809	837	868
2.6	706	706	747	794	847	907	977	1058	876	907	941
2.8	760	760	805	855	912	977	1052	1140	943	977	1013
3	814	814	862	916	977	1047	1127	1221	1011	1047	1086

Table 3.7 length of reduced web link section and diameter perforation relationship of d/t_w=30, for (n=2, c=0.2bf)

ρ	e (mm)	ϕ(mm)									
		0	5	10	15	20	25	30	35	40	45
		e_{rl}(mm)									
0.8	175	175	185	197	210	225	243	263	287	315	350
1	219	219	232	246	263	282	303	328	358	394	438
1.2	263	263	278	296	315	338	364	394	430	473	526
1.4	307	307	325	345	368	394	424	460	502	552	613
1.6	350	350	371	394	420	450	485	526	573	631	701
1.8	394	394	417	443	473	507	546	591	645	709	788
2	438	438	464	493	526	563	606	657	717	788	876
2.2	482	482	510	542	578	619	667	723	788	867	963
2.4	526	526	556	591	631	676	728	788	860	946	1051
2.6	569	569	603	641	683	732	788	854	932	1025	1139
2.8	613	613	649	690	736	788	849	920	1003	1104	1226
3	657	657	696	739	788	845	910	985	1075	1182	1314

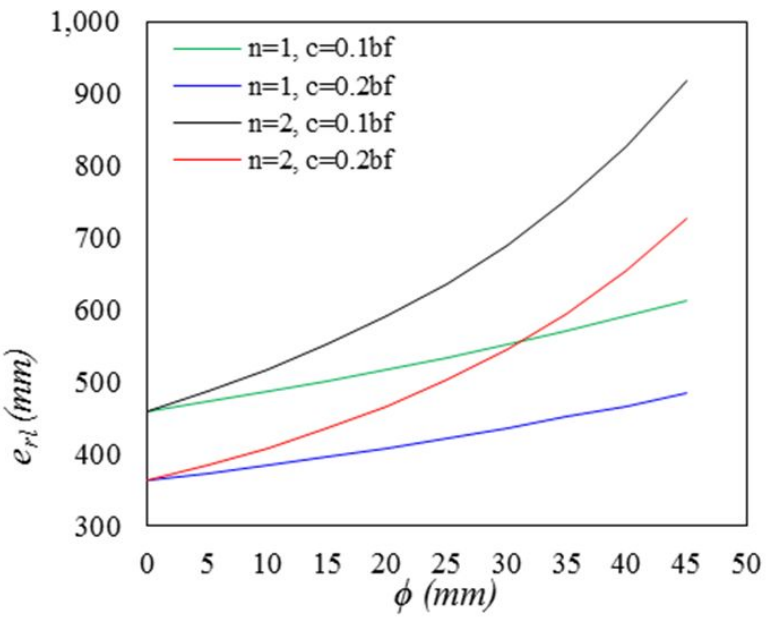

Fig. 3.14 Length of reduced web and flange link section and diameter perforation relationship H200x150, ρ = 1.2

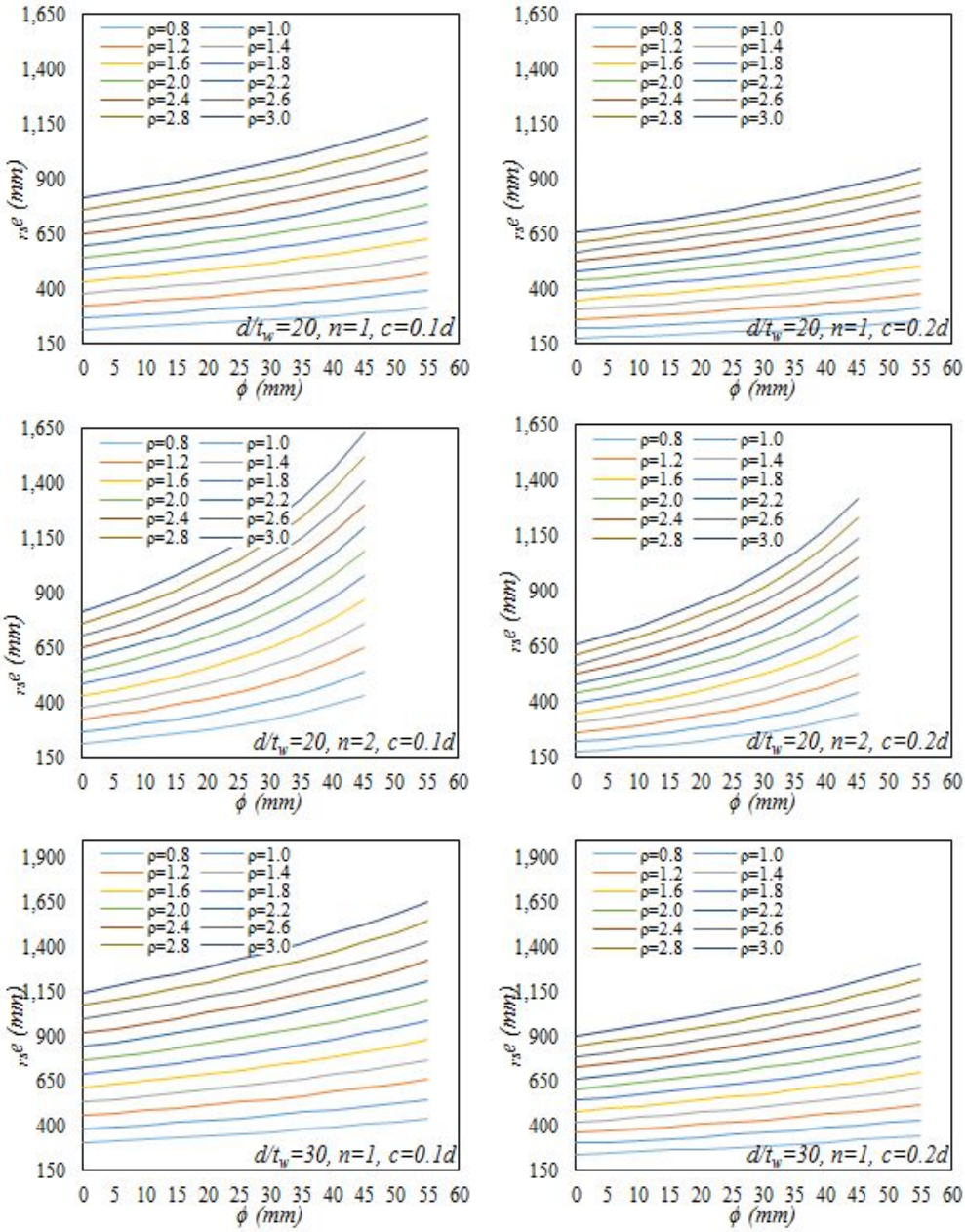

Fig. 3.15 Length of reduced web and flange link section and diameter perforation relationship H200x150

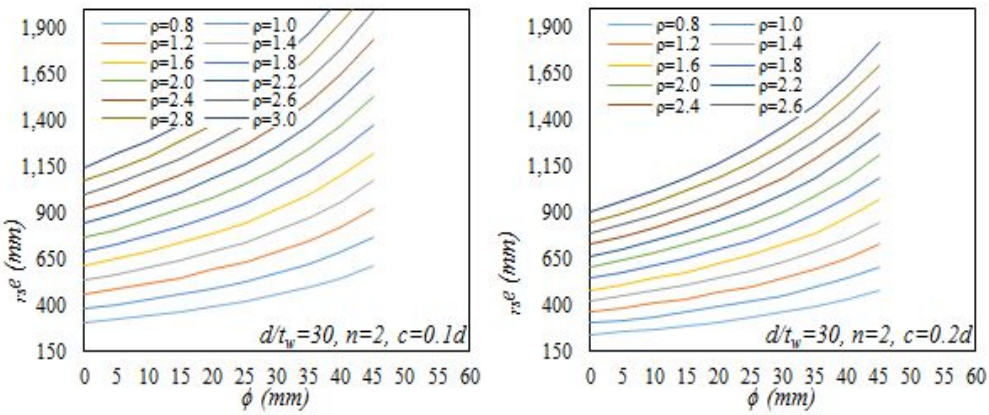

Fig. 3.15 Length of reduced web and flange link section and diameter perforation relationship H200x150 (*continued...*)

3.4 Summary

The equations derived in this chapters are very approximate since the assumptions taken for simplicity are significantly affect the design and details of links. The following summary was drawn from the derived equation.

For reduced web link section the sensitive parameter is the number of perforation in a vertical direction and the diameter of perforations. in both cases as the diameter of perforation increases the reduced link length also increases. However, the rate at which the reduced link length increase is higher when the number of perforations increases. The ratio of perforation diameter and link depth is requirements were set relative to the number of perforations and the ratio of reduced shear plastic strength and unreduced link. The ratio of plastic shear strength was assumed to be greater than 0.5, thus the corresponding the ϕ/d ratio can be set.

In the case of reduced flange and web section, the number of perforation in a vertical direction, the diameter of perforations and the depth of cut off plays an important role in the reduced link length. The change of reduced link length for the number of perforations 2 is very exponential compared to number of perforation 1. The effect of dimension c is seen at the initial reduced link length. For both c=0.1b$_f$ and c=0.2b$_f$ the rate of change of reduced link length is the same for both cases (n=1 and n=2).

4. Experimental Evaluation

4.1 Introduction

The specimens designed using the equations presented in Chapter 3 above have been evaluated through quasi-static loading test. The loading test was conducted in Chosun University, steel structure and earthquake engineering laboratory (SSEEL). A series of quasi-static cyclic loading tests was conducted as one of the key features of this research program. The main objective of these tests was to verify the proposed reduced link section can reach the required plastic rotation without significant damage and without deterioration of their load carrying capacity.

The tests were conducted only for W-sections with:

i) stiffened and unstiffened reduced web link section and

ii) stiffened and unstiffened reduced web and flange link sections. The specimens were made from a common structural steel called SS400 steel. Two different link lengths 300mm and 500mm were considered for experimental investigations. The percent of reduced web areas were also considered as a parameter for the experimental evaluation. The test results were used not only to evaluate the plastic deformation capacity and failure mode of reduced link but also used for calibrating nonlinear finite element analysis conducted for paramedical evaluations.

The designed specimens were constructed at HONAM steel manufacturing company, Gwangju, South Korea. The constraints in the test specimens design was the actuator capacity of loading test, which is 500 kN and the actuator hydraulic deformation capacity of ±100 mm and the developed test set-up system capacity in steel structure and earthquake engineering laboratory at Chosun University. Appropriate safety factor was taken in to account. For instance, the maximum shear force resistance capacity of test specimen should be less than 400 kN. The specimen should also inter in to plastic deformation within the deformation capacity of he actuator hydraulic deformation capacity.

The design of link and the connections are designed according to AISC-2010 seismic provisions. The test loading was conducted controlling the displacement and displacement protocol used was the revised protocol suggested in AISC Seismic Provisions for link beam evaluation. This experimental program also aimed to provide a better understanding of their behaviour.

The test program and process along with the test results are discussed in this chapter. The outlines of the test set-up, process and the detail of test specimens are discussed in section 4.2 including the cyclic loading sequence and instrumentations of test set-up with the design details and procedures of fabrications of all specimens. The hysteresis responses of test specimens and the failure or the buckling mode of loading test results were presented and discussed in section 4.3. The plastic rotation capacity, initial stiffness, cumulative rotation and other related variables are also discussed in this section.

4.2 Test plan and process

4.2.1 Detail of Test Specimens

A total of 9 test specimens was chosen for experiments considering different parameters including the percent of open areas, effect of stiffeners and link lengths with two cross-sections. Two of the cross-section geometries were selected from compact sections. The detail dimension of the test specimen is shown in Fig. 4.1. The specimens was chosen as the best compromise between specimen manufacturing ease and the developed test equipment system. The test specimen was designed using SS400 steel plate material with nominal yield stress $f_y = 310MPa$ was assumed for both flanges and webs. The test specimens consists of four components built-up together. These are: a perforated web, flanges with different compactness ratio and stiffeners and end plates all made of common mild steel SS400. The detail of each of the test specimens were presented in Fig. 4.1.

The flanges, the end plates are welded on the perforated plate which is used as a web. In addition the stiffeners for stiffened specimens are also welded on the perforated web and flanges. The CJP groove welds between flanges and perforated web were placed both side longitudinally. The groove welds between flanges and stiffeners and perforated web and stiffeners is also the same. With out some minor error, the connection details are made according to the design provided.

The selection criteria of test specimens were: first, the capacity of the actuator and test setup had to be sufficient to test the specimens to failure. Second, to consider the same link length with different geometries such as reduced web and reduced web and flange sections with and without stiffeners.

The specimen code along with the cross-sectional properties and detail of test specimen considered are summarized in Table 4.1. Sectional strength such as nominal plastic shear strength and plastic moment of the specimens are calculated from the geometries and equation presented in Section 3.3.2. The yield stress $f_y = 310MPa$ was used to calculate the cross-sectional strengths. The link length factor (ρ) for reduced section presented in the Table 4.1 is also calculated using the developed equations in Section 3.3.2. The codes illustrated in the Table, for instance RWS-S10S1 the first three letters stands for reduced web section, the letter after the – Stiffened, the number is for percent of reduced web area (10% reduced web area) and the last number is identifier.

Table 4.1 Summary of test specimens

Specimen ID	$\frac{b}{t_t}$	t_f	t_w	open area(%)	*e:* link length	Stiffener	V_p (kN)	M_p (kNm)	ρ	${}_{rs}\rho$
RWS-S10S1	9	10	8	10%	300mm	3@100	193.4	55.2	1.0	1.1
RWS-U10S1	9	10	8	10%	300mm	-	193.4	55.2	1.0	1.1
RWS-U15S1	9	10	8	15%	300mm	-	174.7	54.2	1.0	1.0
RLS-U5Sf1	13	9	8	5%	500mm	-	227.8	46.5	1.65	2.4
RLS-U10Sf1	13	9	8	10%	500mm	-	205.9	44.8	1.65	2.3
RLS-S5Sf1	13	9	8	5%	500mm	4	227.8	46.5	1.65	2.4
RLS-S10Sf1	13	9	8	10%	500mm	4	205.9	44.8	1.65	2.3
RWS-U5Sf1	13	9	8	5%	500mm	-	227.8	70.8	1.65	1.6
RWS-U10Sf1	13	9	8	10%	500mm	-	205.9	69.1	1.65	1.5
RWS-S5Sf1	13	9	8	5%	500mm	4	227.8	70.8	1.65	1.6
RWS-S10Sf1	13	9	8	10%	500mm	4	205.9	69.1	1.65	1.5
RWS-S10Sf2	13	9	7	10%	500mm	4	180.2	68.4	1.85	1.3
RLS-S10Sf2	13	9	7	10%	500mm	4	180.2	44.1	1.85	2.0

Spe-1 (RWS-U10S1)

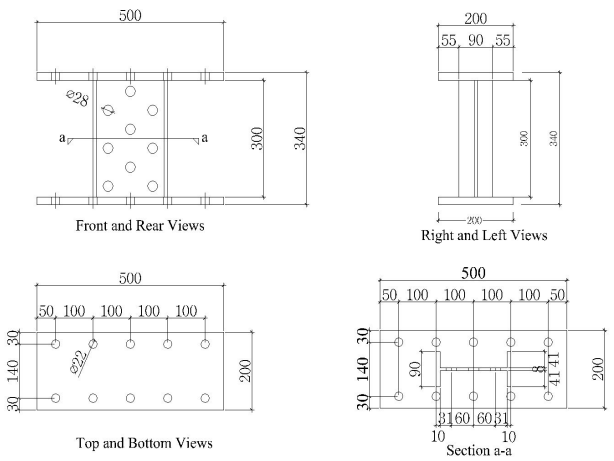

Spe-2 (RWS-U15S1)

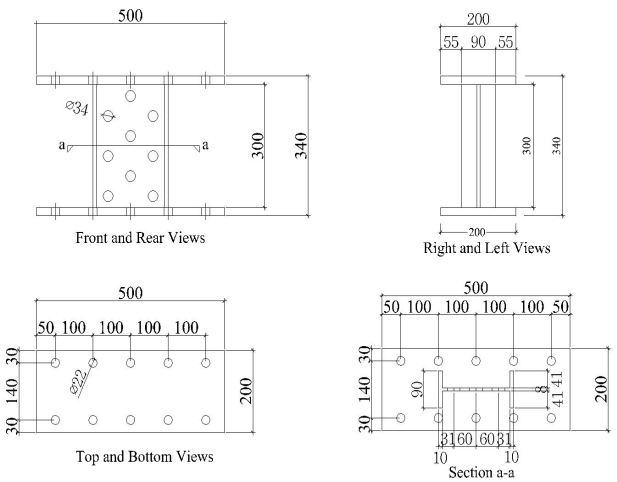

Fig. 4.1 Test specimen detail

Spe-3 (RLS-U5Sf1)

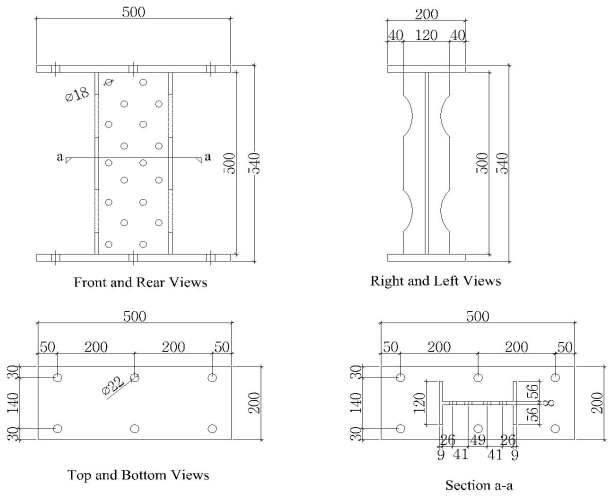

Spe-4 (RLS-U10Sf1)

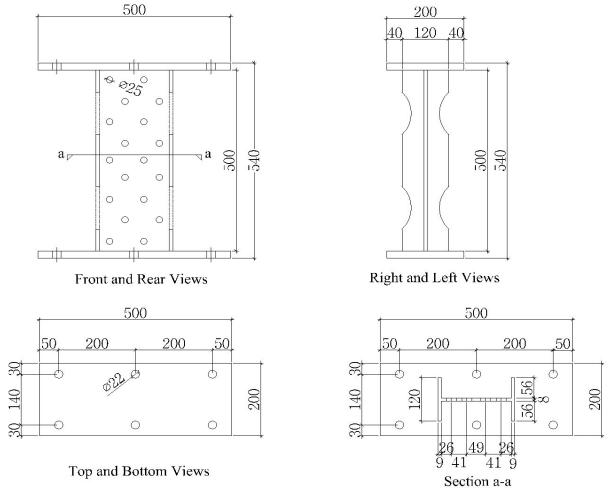

Fig. 4.1 Test specimen detail. *Continued...*

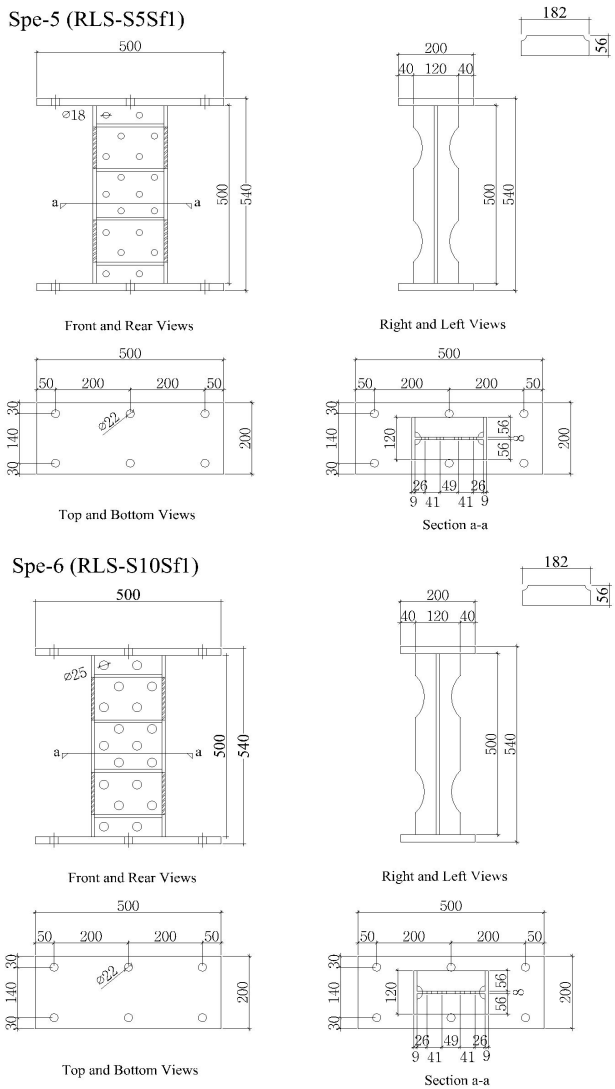

Fig. 4.1 Test specimen detail. *Continued...*

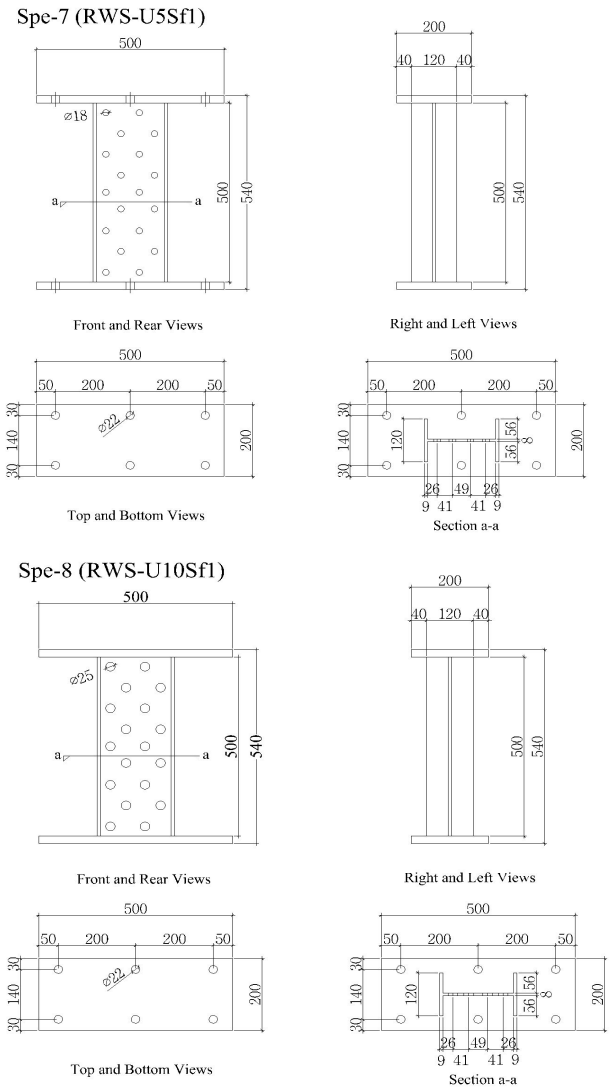

Fig. 4.1 Test specimen detail. *Continued...*

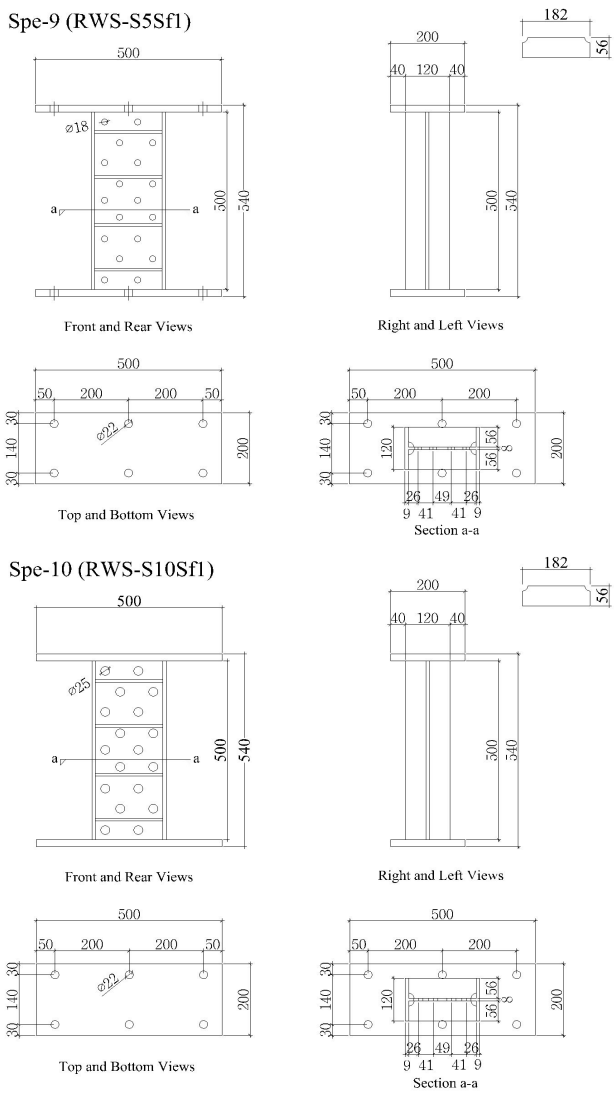

Fig. 4.1 Test specimen detail. *Continued...*

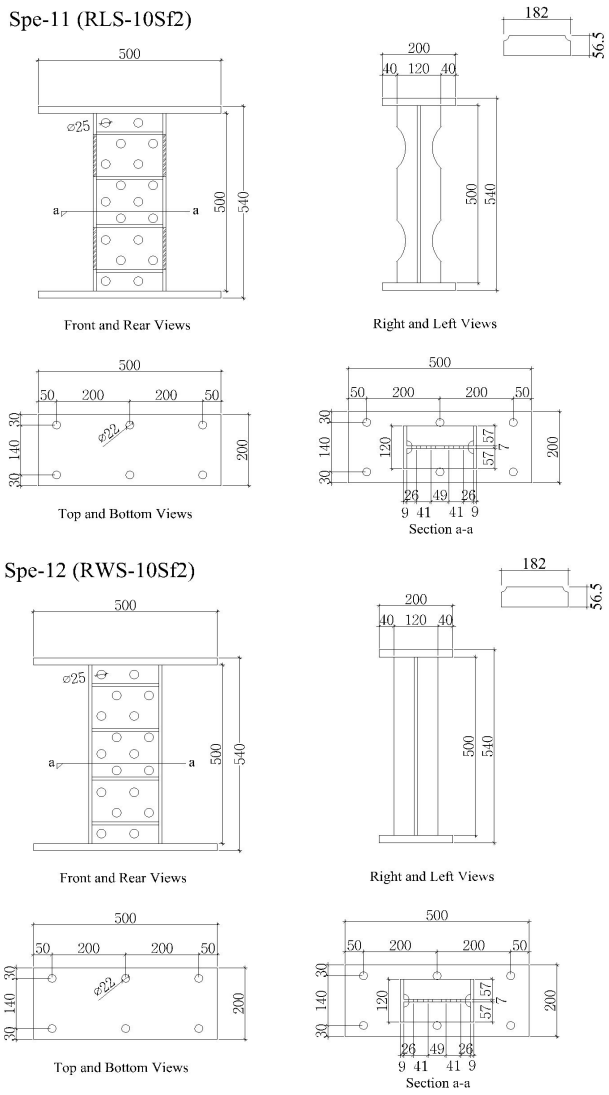

Fig. 4.1 Test specimen detail. *Continued...*

4.2.2 Material Property of test specimen

Coupon test under monotonic tension loading were performed on plates made from the plate material used to fabricate the various link cross-sections. Four different thickness plates where the test specimens were made was prepared for the tensile coupon test. The thicknesses of plates are, 7mm, 8mm, 9mm and 10mm. Three specimens were tested for each thickness to reduce the error arise during testing and average values were taken as a property. The coupon test specimens were designed according to KSB 0801-2007 (Korea Standards Association). The coupon test loading was conducted in DEA HO Machinery Co. LTD in Gwangju, South Korea in accordance with KS B 0802 (Korea Standards Association 2008b).

The applied load was recorded by a load cell mounted to DEA HO steel material testing machine and the strain was measured using strain gage mounted to the test specimen. The recorded yield and ultimate stresses for each material along with the ultimate strain are summarized in Table 4.1. In order to determine the yield stress the 0.2% offset method was used.Since the thickness of flange is the same (t_f=10mm), only one loading test was conducted for flange. For web, four different thicknesses have been considered for test specimens. The final failed coupon test results under monotonic tensile loading are shown in Fig. 4.2 for all thicknesses considered. The corresponding stress-strain relationship of the coupon test results were presented in Fig. 4.3.

Table 4.2 Summaries of Coupon test results

Flange	Yield strength σ_y @0.2%, (MPa)	Ultimate strength (σ_u)	Ultimate strain (ε_y) (%)
$t_1 = 10mm$	282.05	369.41	36
$t_2 = 10mm$	281.16	368.45	36.1
$t_3 = 10mm$	277.91	368.32	36.2
$t_1 = 9mm$	322.90	424.04	28.6
$t_2 = 9mm$	321.55	421.52	28.61
$t_3 = 9mm$	323.64	425.17	36.0
Web			
$t_1 = 8mm$	293.18	448.83	27.2
$t_2 = 8mm$	303.99	449.37	25.26
$t_3 = 8mm$	301.98	449.92	29.31
$t_1 = 7mm$	309.53	370.48	34.12
$t_2 = 7mm$	310.54	370.47	34.2
$t_3 = 7mm$	304.61	370.21	36.1

Fig. 4.2 Final failed results of coupon test specimens

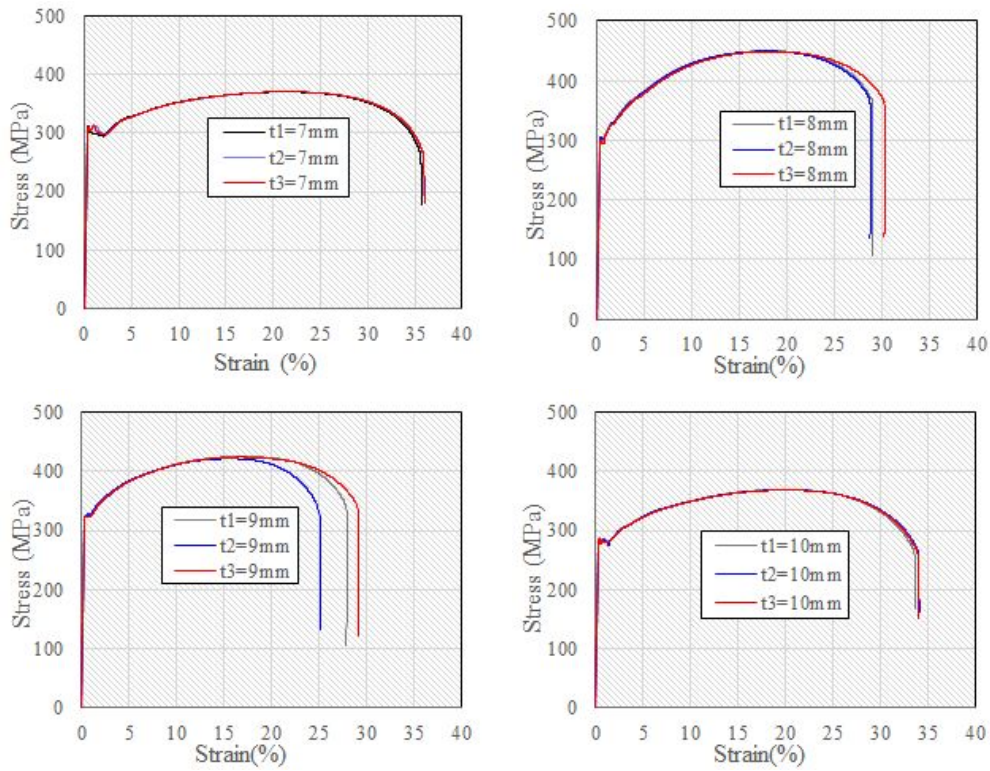

Fig. 4.3 Stress-strain relationship of coupon test result

4.2.3 Loading Test Equipment System

4.2.3.1 Test Subassemblage

Two loading system have been used. The loading test equipment system shown in Fig. 4.5 was used to produce the cyclic force and inelastic deformation demand for shear links having length of 300mm. The second option is for link length of 500mm. The base of loading frame of the test set-up was strong floor. The test frame stiffened at along its length by two H-section beams is strong enough to resist the applied load by the actuator. The test specimens are installed between fixed horizontal plate and loading beam supported by two pinned columns. The lower horizontal plate at which the test specimens bolted on the fixed on two H-section beams. The specimens are fastened by bolts in each side, thus the test specimen is fixed at lower end and free to translate along the longitudinal direction of loading beam. The two pinned columns that support the loading beam is used to resist axial loads supposed to be applied on the test specimens. In order to protect the rotation angle at the top of specimen, a pantograph was installed as shown in the equipment system. The axial force applied to test specimen is controlled by both end pined column used as counter weight of the loading beam. Horizontal cyclic load was applied by the actuator having a capacity of 500kN and displacement capacity of ±200 is mounted on the loading beam. Therefore, the test specimens are only exposed to shears.

The test setup system is shown in Fig. 4.4 - Fig. 4.6. Two test setup have been utilized depending on the length of link. The first option shown in Fig. 4.4, is for test specimen having clear length of 300mm. The 2^{nd} option shown in Fig. 4.5, for test specimen having length of 500mm. Fig. 4.6 shows the top view of test set-up.

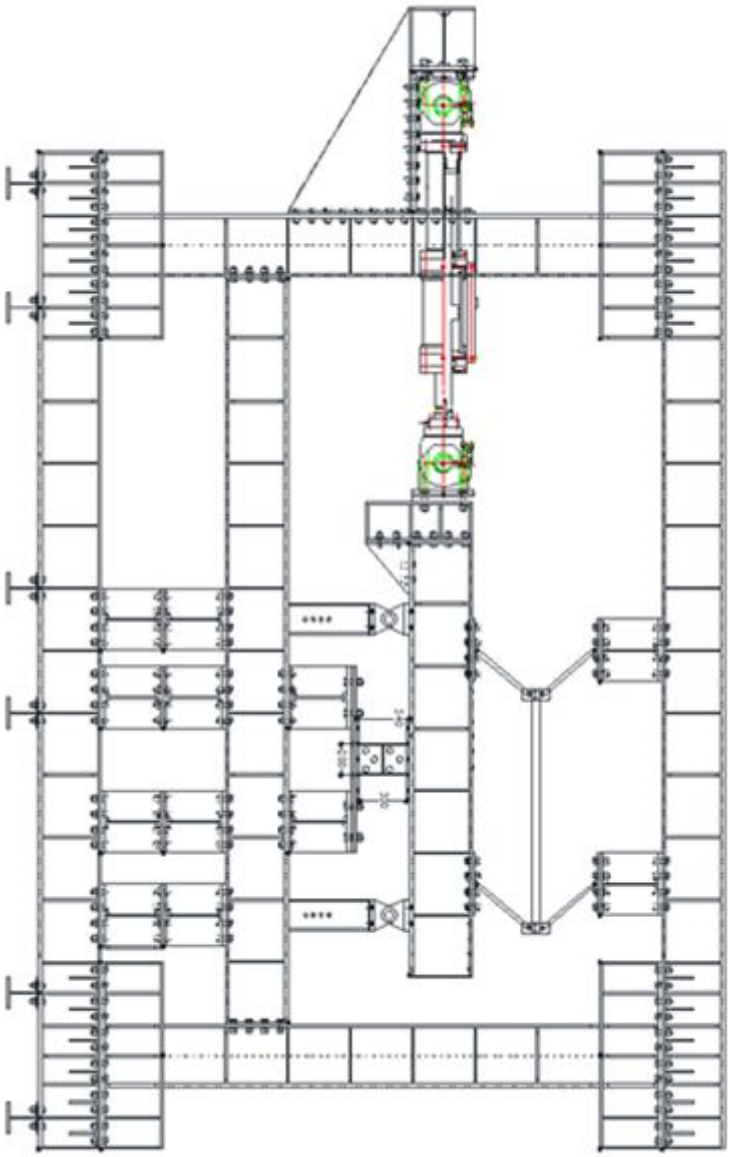

Fig. 4.4 Loading test set-up Elevation - option 1

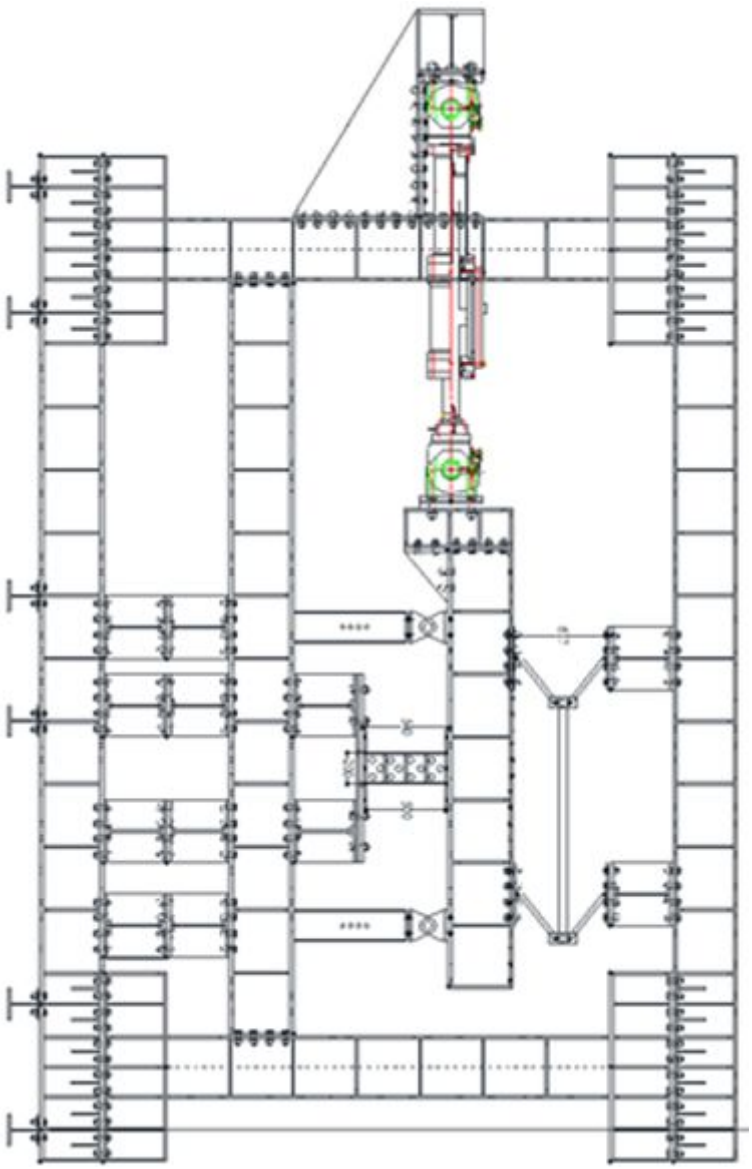

Fig. 4.5 Loading test set-up Elevation - option 2

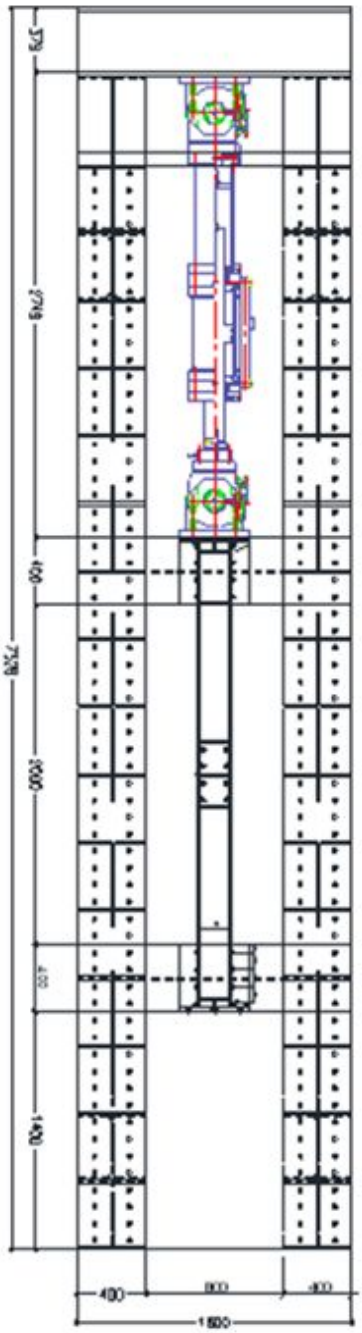

Fig. 4.6 Top view of test set-up

4.2.3.2 Instrumentation of Experiments

Total of 6 displacement meters are installed to measure displacements at different locations. The displacement meters, with an ID DT1 and DT3, was installed at the top end plate of test specimen and loading beam respectively to measure the displacement of maximum input amplitude. In order to measure any shakings at the fixed horizontal plate and the lower end plates of test specimens displacement meters with an ID of DT2 and DT4 was installed respectively on the lower end plate of test specimen and fixed horizontal plate. To capture any compression and tensile forces applied to the two columns pinned at both end and bolted at mid-height in sloted hole, displacement meters having an ID of DT6 and DT7 for the north column and south columns respectively were installed. Careful analysis needed in each test in order to find the exact displacement of test specimens for an input amplitude. Usually the difference between the displacements measured at upper and lower end plates of test specimens (DT1 and DT2) is the pure shear displacement of the test specimens. The detail of displacement installation location is shown in Fig. 4.7 on the second the test set up option. The displacement meters used in the test are shown in Fig. 4.8. Two different types displacement meters are used, the first has a capacity of ±50mm and the second displacement meter has a capacity of measuring ±100mm.

The loads applied on the test specimen and the deformations caused by the applied load was measured carefully. The loads are measured directly from the loading cell mounted in the actuator. This means, the force was measured through the actuator load cell directly and displacement externally controled measurements through laser displacement meters (laser displacement meter precision 0.05 mm). In order to eliminate errors the external displacement meters are installed at different locations as stated above.

All loading tests were recorded to look at the test specimens behavior during loading process. The digital camera having a resolution capacity of 4.3mega pixels were setup and recorded from east. The videos were helped to see the details of specimens from the start to finish.

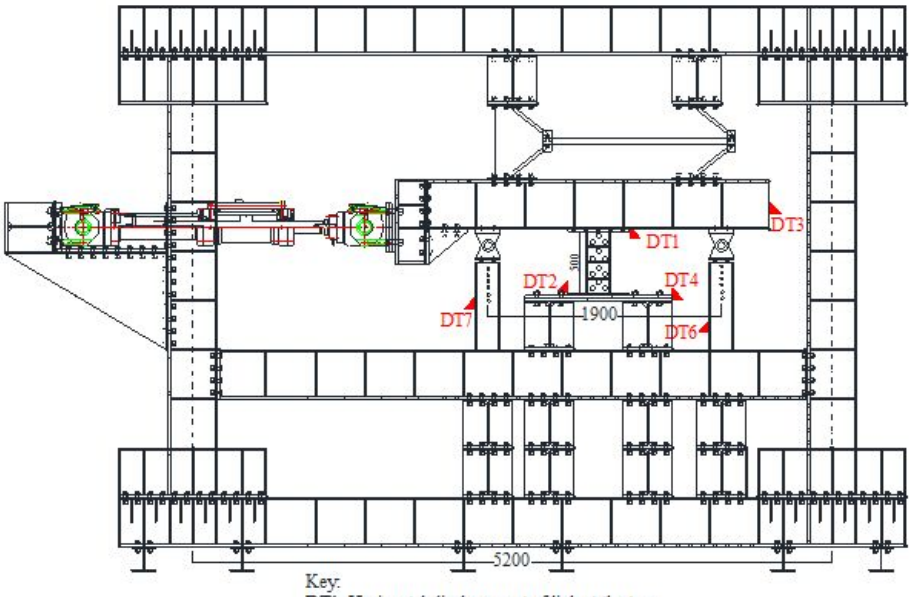

Fig. 4.7 Location of Displacement meters

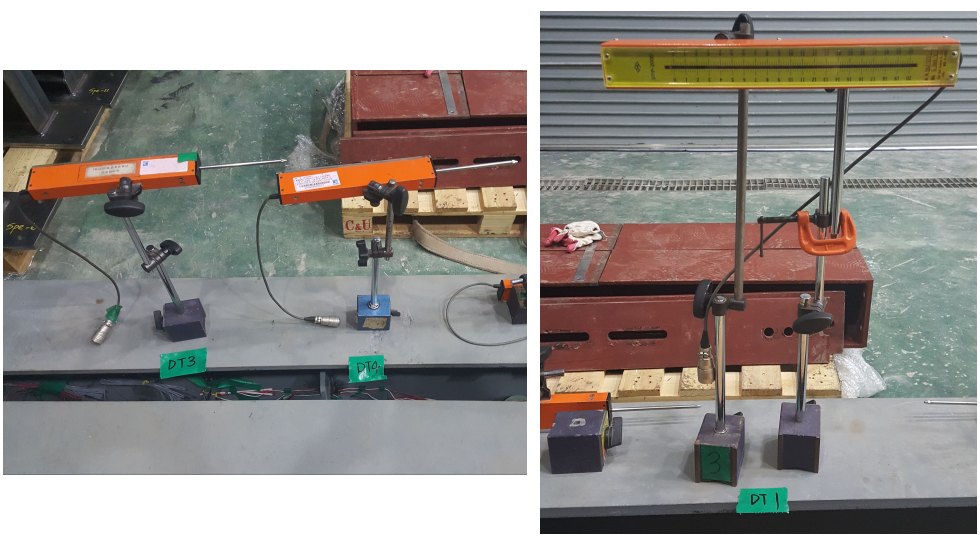

Fig. 4.8 Displacement meters

4.2.4 Loading Sequence

The loading sequence used to evaluate the test specimen is the revised protocol recommended in AISC-2010. Where it requires more cycles at lower rotation levels and fewer cycles at larger rotations compared to the protocol of the 2002 Seismic Provisions and severe protocol. The first four rotations have 6 cycles at 0.00375 rads, 0.005 rads, 0.0075 rads, and 0.01 rads, 4 cycles at 0.015 rads, and 0.02 rads, 2 cycles at 0.03 rads, one cycle at 0.04 rads and 0.05 rads, and then a single cycle at 0.02 rad increments from there. Displacement of the actuator was used as the control parameter during testing, which required that the specified rotation levels be converted into displacements using the link and setup geometries. The protocol used is shown in Fig. 4.9.

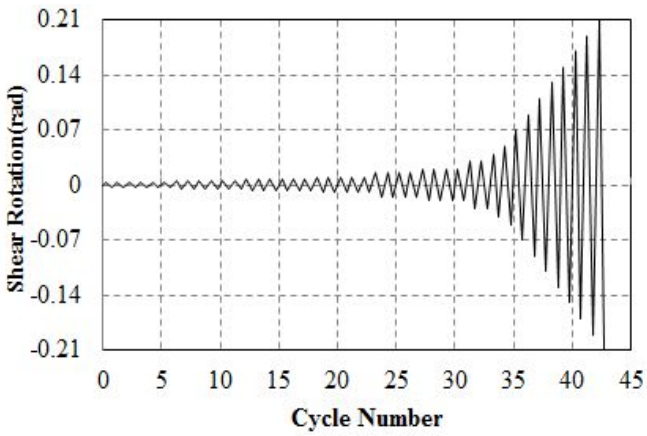

Fig. 4.9 Loading protocol

4.3 Test Results

The loading test results, the hysteresis response of each test specimens along with the failure mode, were presented in this section. From the recorded video, the cycle at which each test specimens stars to buckle and failed will be presented.

4.3.1 Observations on Each of Test Specimens

4.3.1.1 Links with reduced web section

As it has been stated in the considered specimens in this research work is categorized in to two. These are: links with reduced web and links with reduced web and flange section. The response of each specimens are presented here under. In this section links with reduced web section is presented.

RWS-S10S1

The first test was conducted on stiffened shear link with reduced 10% of web section. The hysteresis response, link shear versus shear rotation, is shown in Fig. 4.10 (a). In this test the specimen is loaded only up to the start of cracks and slight crack propagations. As shown in the Fig. 4.10 (a), the hysteresis curve is stable up to displacement of 45mm (0.15 rad) although the specimen is start to crack at the edge of reduced web link. The plastic rotation level of RWS-S10S1 is shown in the displacement protocol with a mark ▲ at which the crack and crack propagation starts as shown in Fig. 4.10 (b).

The displacement effect of the fixed plate measured by displacement meter of DT4 is higher compared to the displacement of both columns (DT6 and DT7) and the lower end plates of the test specimens (DT2) as shown in Fig. 4.11. The photos captured from the recorded video at the start of cracks around the edge of circular perforations is shown in Fig. 4.11. The crack is only seen at the edge of perforations all the welding and flanges do not shown any cracks.

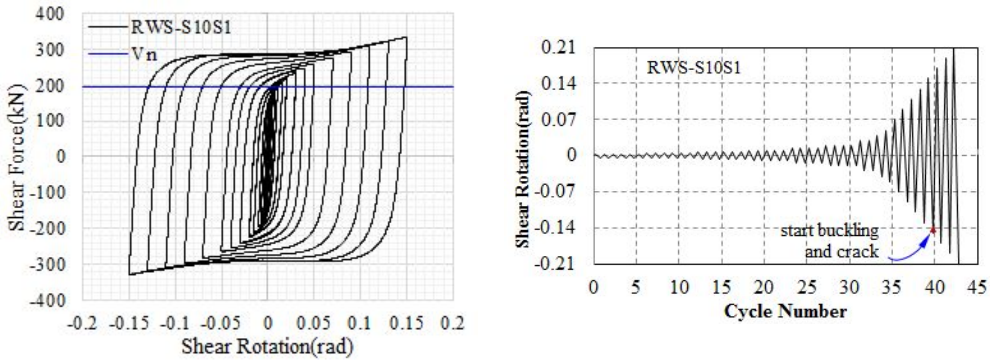

(a) Hysteresis curve of RWS-S10S1 (b) Loading history of RWS-S10S1

Fig. 4.10 Response of RWS-S10S1

Fig. 4.11 Deformed shape and cracks observed on RWS-S10S1

RWS-U10S1

RWS-U10S1 is the equivalent specimen of RWS-S10S1 where the first is unstiffened and 10% web area reduction whereas the later is stiffened. The hysteresis response, link shear versus shear rotation, is shown in Fig. 4.12. The specimen are loaded up to final failure. The start of buckling, crack and final failure is indicated both in the hysteresis curve and in the loading history. As shown in the hysteresis curve, the test specimen shows stable hysteresis loop before buckling and crack occurs after 0.11rad. One cycle after crack the final failure occurred and the shear response decreases rapidly after failure.

The photos captured from the recorded video at the start of cracks around the edge of circular perforations and the cracks propagates diagonally and finally fractured is shown in Fig. 4.13. The specimen failed diagonally in the angle of perforations i.e the failure follows the tension field action.

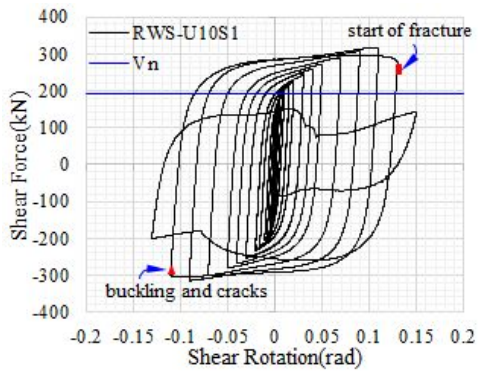

(a) Hysteresis curve of RWS-U10S1

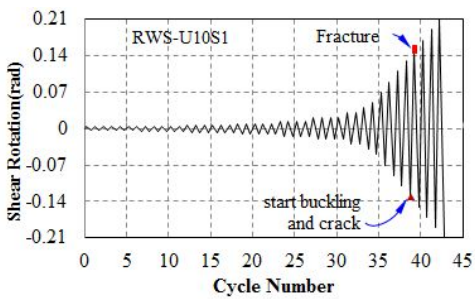

(b) Loading history of RWS-U10S1

Fig. 4.12 Response of RWS-U10S1

(a) buckling and crack of RWS-U10S1

(b) failure of RWS-U10S1

Fig. 4.13 Deformed shape and cracks observed on RWS-U10S1

RWS-U15S1

Fig. 4.14 shows the link shear force versus rotation hysteresis curve and the loading history for specimen RWS-U15S1. This specimen is unstiffened with 15% reduced web area. The buckling, crack and failure of RWS-U15S1 is at the cycle with specimens RWS-U10S1. Stable hysteresis response was observed up to buckling and cracks at the start of 2nd phase of 0.11rad. Finally the specimen failed at the beginning of 0.15 rad and the resisting capacity decreases rapidity. The photos captured from the recorded video at the start of cracks around the edge of circular perforations and the cracks propagates diagonally and finally fractured is shown in Fig. 4.15. Link specimen RWS-U10S1, this specimen also failed diagonally along the tension field action since both specimens are shear link and shear links are known by the yielding of the web prior to the flanges.

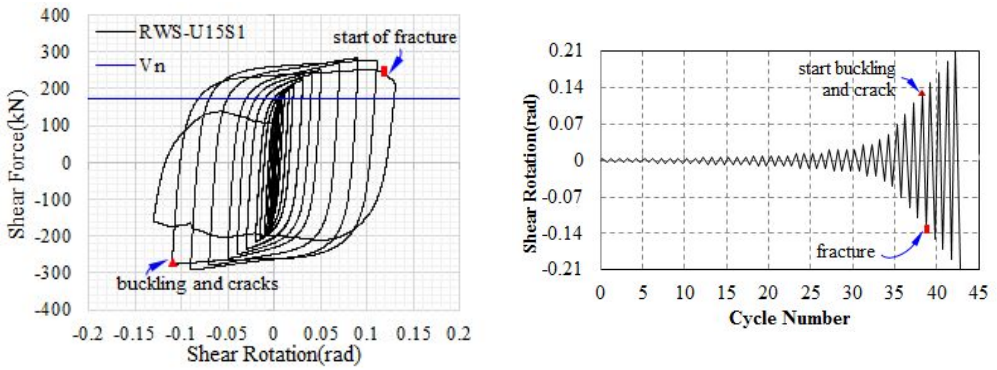

(a) Hysteresis curve of RWS-U15S1 (b) Loading history of RWS-U15S1

Fig. 4.14 Response of RWS-U15S1

(a) buckling and crack of RWS-U15S1 (b) failure of RWS-U15S1

Fig. 4.15 Deformed shape and cracks observed on RWS-U15S1

RWS-U10Sf1

The deformed shape of RWS-U10Sf1 test specimen is shown in Fig. 2.16. As shown in the deformed shape a small cracks at the edge of the perforations on the web was seen. In addition, a buckling of end plates was also observed indicated locations with yellow rectangle. This buckling of end plate affects the plastic rotation as the shear deformation recorded some how enlarged. Therefore some adjustments was made. In order to produce the adjustments, the deformation shape was modeled as shown in Fig. 2.17 (a). The external moment (M_{ext}) created by the applied load is given by:

$$M_{ext} = P*e \quad \text{.....(4.1)}$$

where P is the applied load from the actuator and e: link length. The external moment expressed in Eq. (4.1) decomposed to the compression (C) and tensile force (T) generated at the flanges of the specimen, which is expressed as in Eq. 4.2. The tension and compression forced are assumed equal so that

$$P*e = T*\frac{d}{2} + C*\frac{d}{2} = T*d \quad \text{.....(4.2)}$$

where d: is the depth of link. The uplifting deformation generated at the tensile force point load is given in terms of *a, b, l* which the dimensions are given in the Fig. 4.17 (b).

$$\delta = \frac{Ta^3b^3}{3EI\ell^3} \quad \text{.....(4.3)}$$

In order to calculate the net shear deformation of link specimen, the calculated deformation is deducted from the recorded displacements.

$$\Delta' = \Delta - 2\delta \quad \text{.....(4.4)}$$

where Δ' is the net shear displacement, Δ: is recorded shear displacement. Thus, the shear rotation of link is then calculated by dividing the net shear displacement by the link length.

The hysteresis response of RWS-U10Sf1 after adjustments were made is shown in Fig. 4.18 along with the loading history. As shown in the figure, the specimen shows stable hysteresis response up to over the rotation limit then finally the actuator stoped accidentally. The actuator stopped due to high temperature of pump beyond its limit which reached 80^0C before it stopped. The specimen attains the plastic rotation level suggested by the AISC-10 provision. Even though the loading test was not completed according to the imputed loading cycle on RWS-U10Sf1, the small cracks of specimen at the edge of openings was seen as shown on the magnified photos presented in Fig 4.16.

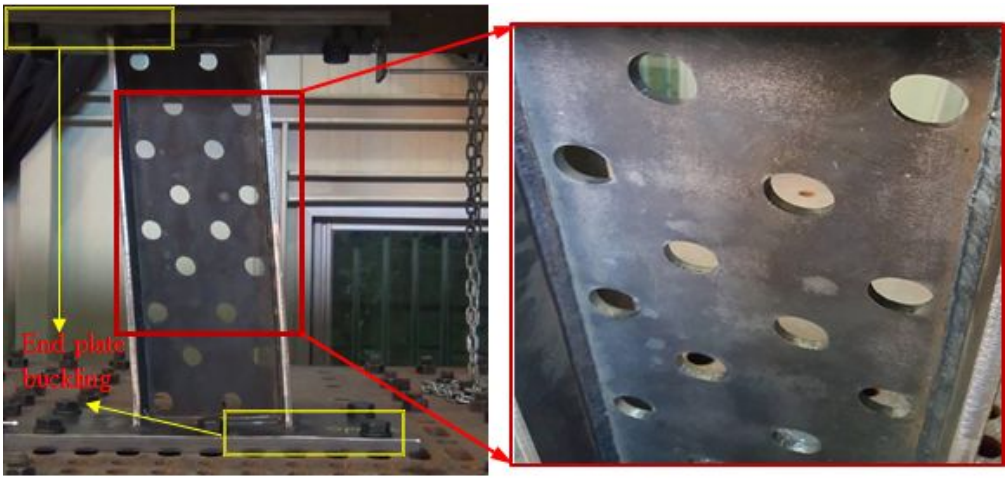

Fig. 4.16 Deformed shape and cracks observed on RWS-U10Sf1

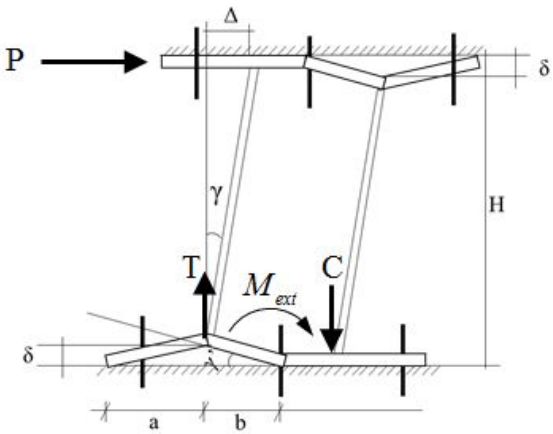

(a) deformed shape model

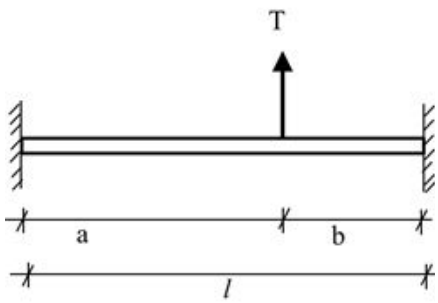

(b) end plate loading and boundary condition

Fig. 4.17. Deformed shape model

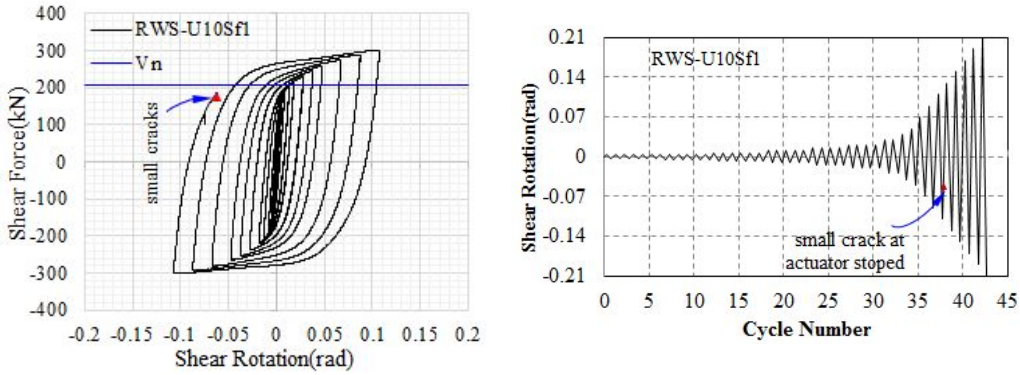

(a) Hysteresis Response of RWS-U10Sf1 (b) Loading history of RWS-U10Sf1

Fig. 4.18 Response of RWS-U10Sf1

RWS-S10Sf1

The hysteresis response of stiffened links with 10% reduced web section, RWS-S10Sf1 is shown in Fig. 4.19 along with the loading history. As shown in the figure, the specimen shows stable hysteresis response up to shear rotation of 0.15radian. During this test process also the actuator stoped due to high temperature of pump beyond its limit which is 80^0C. Even though the loading test wasn't completed according to the imputed loading cycle on RWS-S10Sf1, the small cracks of specimen at the edge of openings was seen as shown in Fig. 4.20. As shown in the figure, the end-plate buckling also observed therefore the shear displacement was adjusted just like RWS-U10Sf1 using the equations (4.1-4.4). The plastic rotation level was satisfied although the loading test wasn't completed.

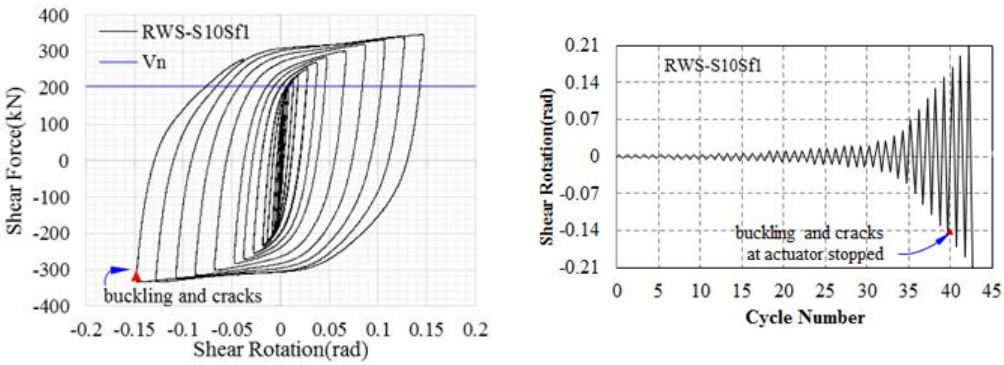

(a) Hysteresis Response of RWS-S10Sf1 (b) Loading history of RWS-S10Sf1

Fig. 4.19 Response of RWS-S10Sf1

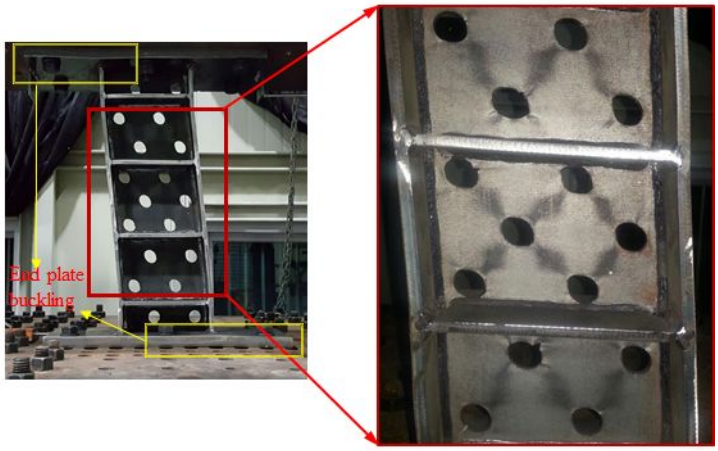

(a) buckling of RWS-S10Sf1 (b) Crack detail of RWS-S10Sf1

Fig. 4.20 Deformed shape and cracks observed on RWS-S10Sf1

RWS-S10Sf2

Fig. 4.21(a) shows the link shear force versus the adjusted rotation using Eqs. (4.1-4.4) hysteresis curve for specimen RWS-S10Sf2. As shown in the figure, the hysteresis response is stable. The corresponding loading history that shows the point at which the test specimen started buckling also presented in Fig. 4.21(b). But the test wasn't loaded up to the final failure as some inconvenience happened to the actuator motor and stopped before reached at the second cycle of shear rotation of 0.13rad. The actuator's motor was stopped because of the temperature attains above its maximum capacity. The capacity of the motor of actuator is 80^0C. The deformed shape of RWS-S10Sf2 is shown in Fig. 4.22. As shown in Fig. 4.22, buckling of end-plate is also observed for this specimen as well.

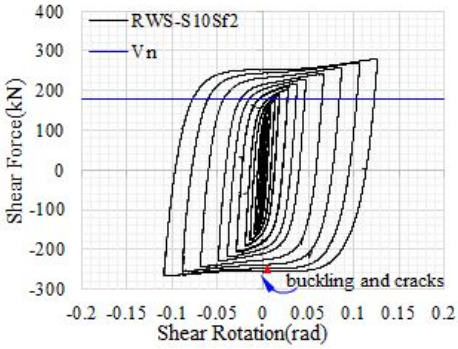

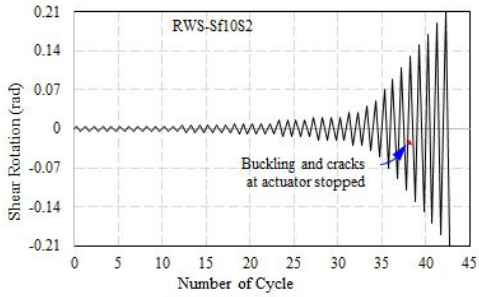

(a) Hysteresis Response of RWS-S10Sf2 (b) Loading history of RWS-S10Sf2

Fig. 4.21 Response of RWS-S10Sf2

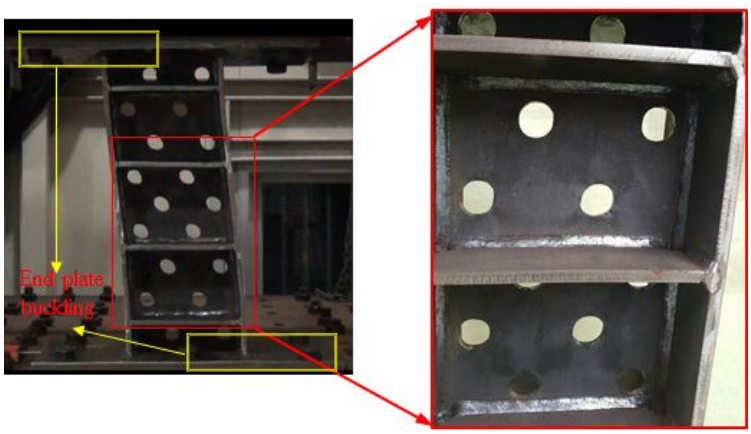

Fig. 4.22 Deformed shape and cracks observed on RWS-S10Sf2

4.3.1.2 Links with reduced web and flange section

The loading test response of test specimens of links with reduced web and flange section is presented in this section for three specimens tested.

RLS-U10Sf1

The hysteresis response of unstiffened intermediate links with 10% reduced web and flange section, RLS-U10Sf1 is shown in Fig. 4.23. As shown in the Fig. 4.23, the hysteresis response is stable up to shear rotation angle of 0.11rad where strength degradation due to buckling and cracks at the edge of holes. When the shear rotation reaches at 0.15rad the started crack continuos and finally failed.

The first yielding and cracks were occurred on the edge of web panel opening at which the flanges were reduced as it is shown in the Fig. 4.24. Compared to the equivalent links with reduced web (RLS-U10Sf1) the yielding and the crack starting location is different. This is the indication of the effect of flange reduction in links.

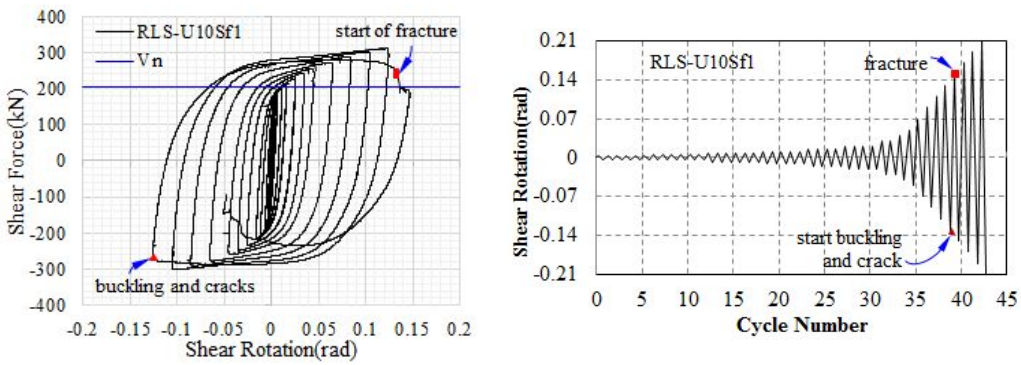

(a) Hysteresis curve of RLS-U10Sf1 (b) Loading history of RLS-U10Sf1

Fig. 4.23 Response of RLS-U10Sf1

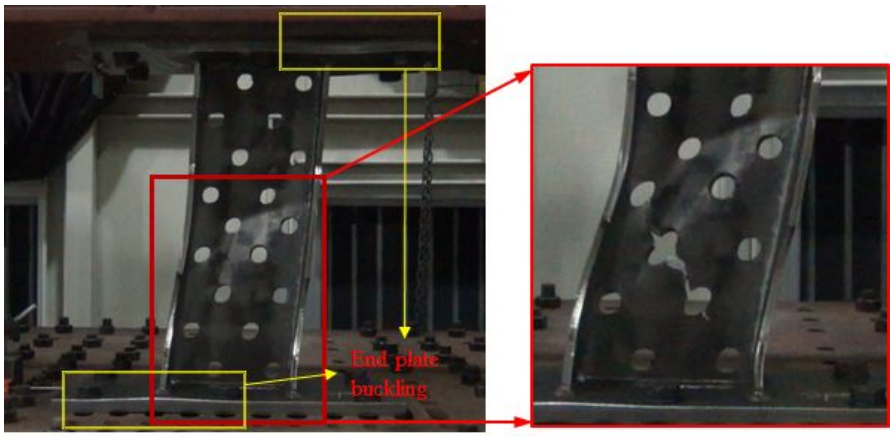

(a) buckling and crack of RLS-U10Sf1 (b) failure of RLS-U10Sf1

Fig. 4.24 Deformed shape and cracks observed on RLS-U10Sf1

RLS-S10Sf1

The hysteresis response of stiffened intermediate links with 10% reduced web area and reduced flange section, RLS-S10Sf1, is shown in Fig. 4.25 along with the loading history. Stable hysteresis response was obtained as shown in the Fig. 4.25 up to shear link rotation of 0.15radian. The hysteresis behavior is similar with specimen of only reduced web area, RWS-S10Sf1. However, when we look at the deformed and the failed specimen, the behavior is quit different. Here, the fracture is concentrated at the web where the flanges are reduced. In addition a plastic hinge was formed at reduced flange which indicates that stiffened reduced web and flange link section it is possible to control the location of plastic hinge as shown in Fig. 4.26.

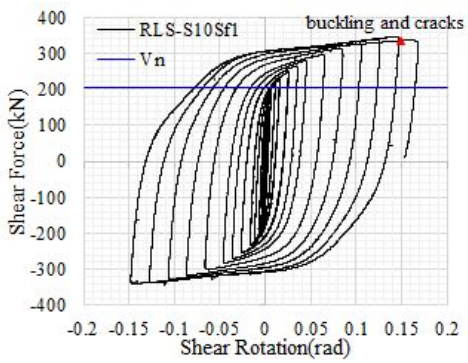

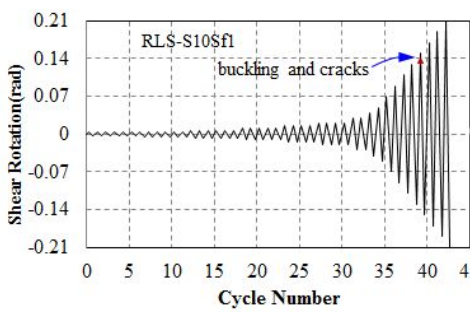

(a) Hysteresis curve of RLS-S10Sf1 (b) Loading history of RLS-S10Sf1

Fig. 4.25 Response of RLS-S10Sf1

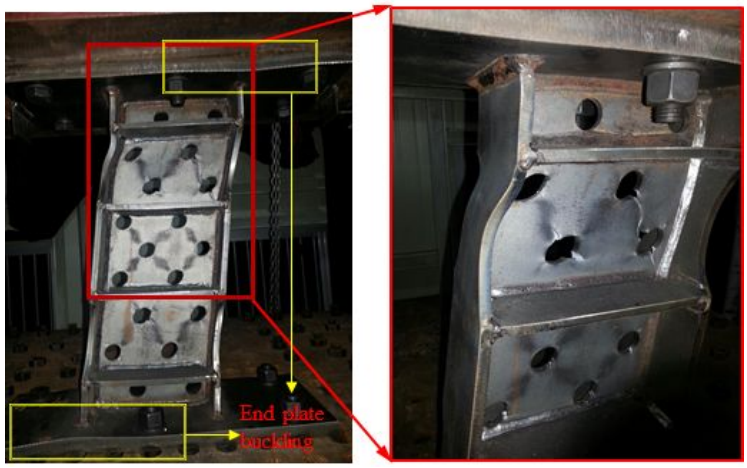

(a) buckling and crack of RLS-S10Sf1 (b) failure of RLS-S10Sf1

Fig. 4.26 Deformed shape and cracks observed on RLS-S10Sf1

RLS-S10Sf2

The hysteresis response of stiffened intermediate links with 10% reduced web and flange section, RLS-S10Sf2 is shown in Fig. 4.27. As shown in the Fig. 4.27, the hysteresis response is stable up to shear rotation angle of 0.15rad. Even though deformation and cracks are observed on the test specimen as shown in Fig. 4.28, the hysteresis response is quit stable. The first yielding and cracks were occurred on the edge of web panel opening at which the flanges were reduced as it is shown in the Fig. 4.28. Compared to the equivalent links with reduced web (RLS-S10Sf2) the yielding and the crack starting location is different. This is the indication of the effect of flange reduction in links.

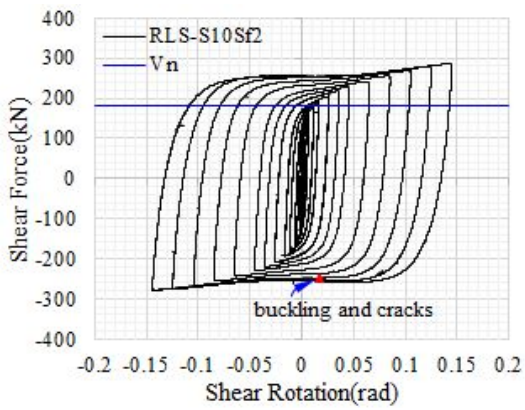

(a) Hysteresis curve of RLS-S10Sf2

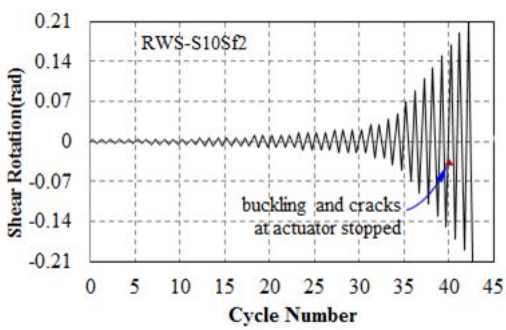

(b) Loading history of RLS-S10Sf2

Fig. 4.27 Response of RLS-S10Sf2

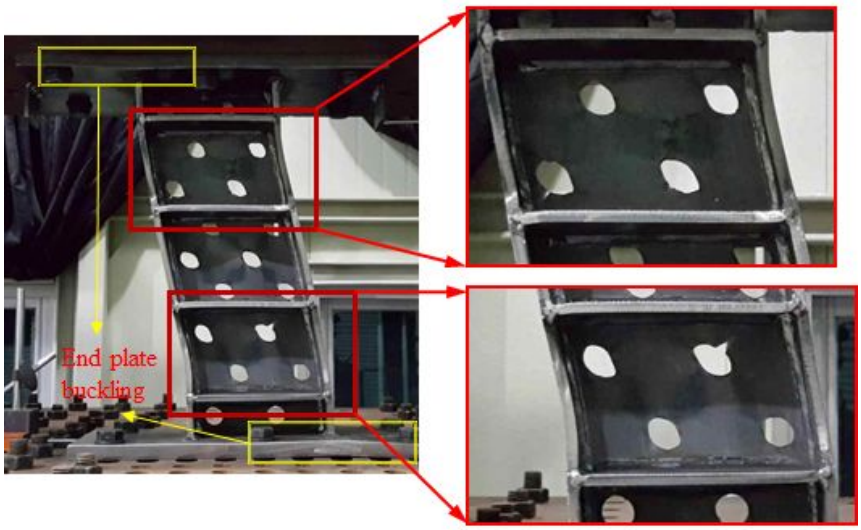

Fig. 4.28 Deformed shape and cracks observed on RLS-S10Sf2

4.3.2 Cumulative Inelastic Rotation

The cumulative inelastic rotation, $\Sigma\gamma_p$, of each test specimens was calculated. The cumulative plastic rotation is defined as the sum of the increments in inelastic link rotation associated with each half loading cycle. The sum of plastic rotation can be expressed as in Eq. (4.5) in a positive shear and negative shear of has a positive and negative as shown in Fig. 4.29 which is taken from test specimen of RWS-U15S1.

$$\sum\gamma_p = \gamma_{p,1} + \gamma_{p,2} + ... + \gamma_{p,m-1} + \gamma_{p,m} \quad \text{.....(4.5)}$$

where $\Sigma\gamma_p$ is the cumulative plastic rotation, and $\gamma_{p,1}$, $\gamma_{p,2}$, ... $\gamma_{p,m-1}$ and $\gamma_{p,m}$ are the plastic rotation of 1st, 2nd, $(m-1)^{th}$ and m^{th} respectively as shown in Fig. 4.29. The computation of cumulative plastic rotation based on the hysteretic relation of all test specimens are shown in Fig. 4.30. As shown in the Fig. 4.30, the cumulative plastic rotation of RWS-U10Sf1 is smaller than all other test specimens this is due to the fact during experiment test specimen RWS-U10Sf1 is stopped un expectedly before the loading test completed. For other test specimens, the cumulative plastic rotation is above unity and stiffened specimens shows better cumulative plastic rotation compared to unstiffened links. Comparing specimens with reduced web and reduced web and flange links, the cumulative plastic rotation is reduced web and flange links has slightly bigger cumulative plastic rotation. Cumulative plastic rotation is important parameter for seismic energy dissipating members. The effect of each parameter considering for test specimens on the cumulative plastic rotation is presented in under including the effect of stiffeners and percent of reduced web area.

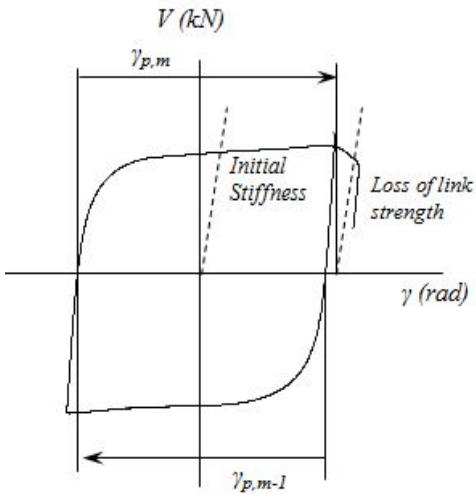

Fig. 4.29 Computation of cumulative inelastic rotation (example shown for specimen RWS-U15S1)

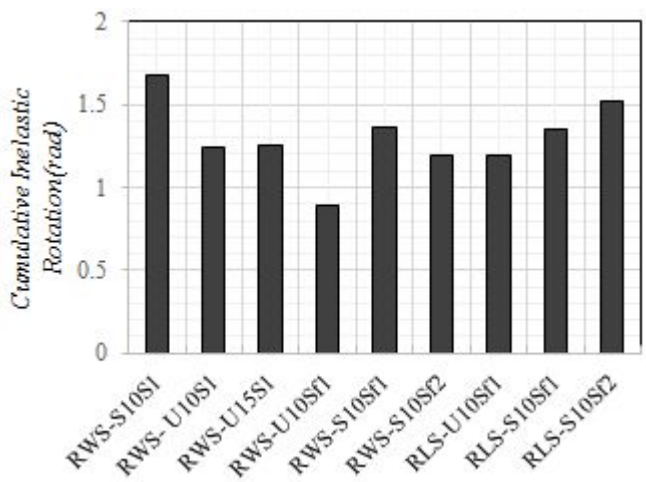

Fig. 4.30 The cumulative plastic rotation of test specimens.

4.3.3 Effect of Stiffeners

Looking at the loading test results of both the hysteresis response and the deformed shape with cracks and the final failed specimen one can see the difference clearly the effect of stiffeners on the links. In all unstiffened specimens shows relatively less plastic rotation capacity. This is because during the loading process, the specimens buckle out-of-plane in unstiffened specimens and stiffeners prevents the out-of-plane buckling and produce stable and large deformation.

Fig. 4.31 (a) shows the comparison of hysteresis response and initial stiffness of stiffened and untiffened reduced web shear links. As shown in the Fig. 4.31 (a), the hysteresis response of stiffened reduced web shear link shows stable hysteresis characteristics compared to untiffened reduced web shear link. The maximum shear force resisting capacity is also slight difference. The initial stiffness has no apparent difference between stiffened and unstiffened reduced web shear links.

The comparison of hysteresis response as well as initial stiffness of reduced web intermediate link is presented in Fig. 4.31 (b). As shown in the figure, the hysteresis response of stiffened intermediate reduced web link is higher shear link rotation capacity than unstiffened intermediate reduced web link. The maximum shear resistance of stiffened intermediate reduced web link is about 40kN higher than unstiffened intermediate reduced web link. The initial stiffness has no apparent difference for stiffened and unstiffened intermediate reduced web link. The same results were obtained for intermediate links with reduced web and flange intermediate links with intermediate reduced web link as shown in Fig. 4.31 (c). The cumulative plastic rotation comparison of stiffened and unstiffened is shown in Fig. 4.32 (a-c). As shown in Fig. 4.32 the cumulative plastic rotation of stiffened and unstiffened links shows that the cumulative plastic rotation of stiffened links is bigger than unstiffened links.

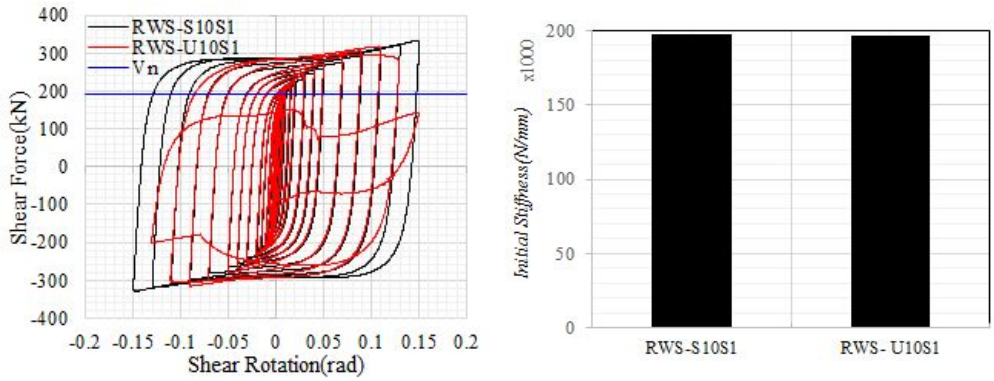

(a) Comparison of hysteresis response and initial stiffness of stiffened and unstiffened reduced web shear links

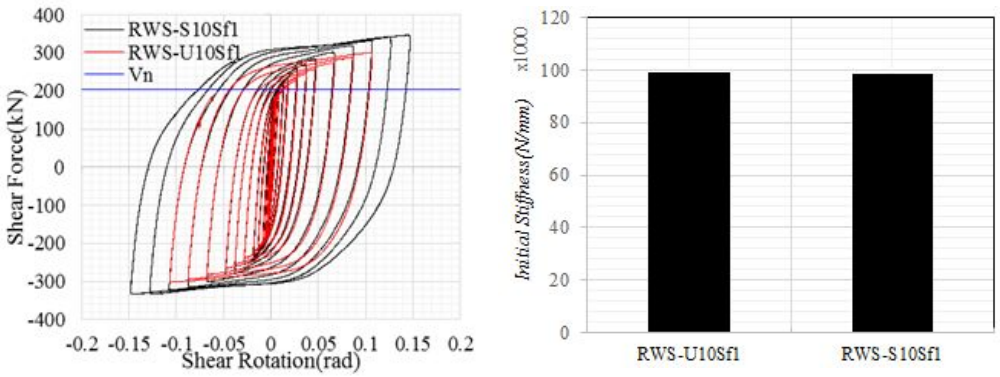

(b) Comparison of hysteresis response and initial stiffness of stiffened and unstiffened reduced web intermediate links

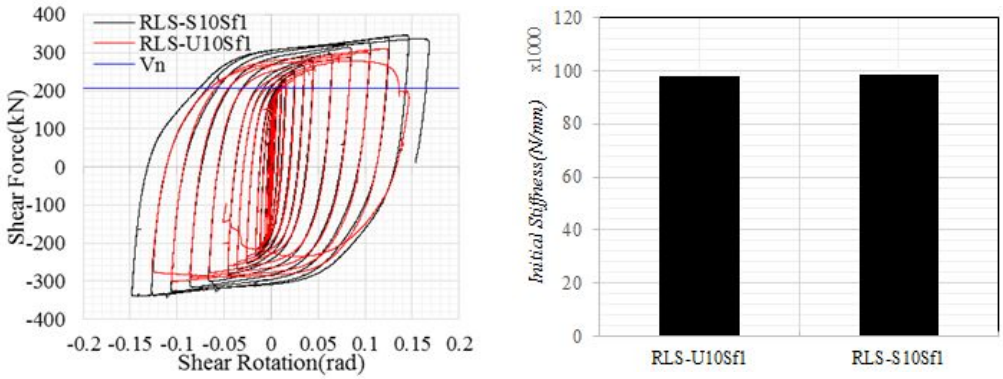

(c) Comparison of hysteresis response and initial stiffness of stiffened and unstiffened reduced web and flange intermediate links

Fig. 4.31 Effect of stiffeners on hysteresis and initial stiffness

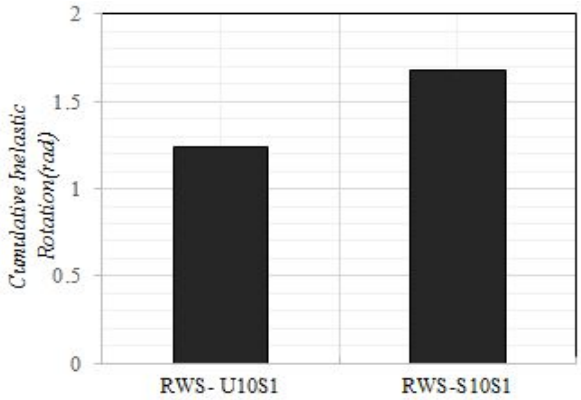

(a) Comparison of cumulative plastic rotation of stiffened and unstiffened reduced web shear links

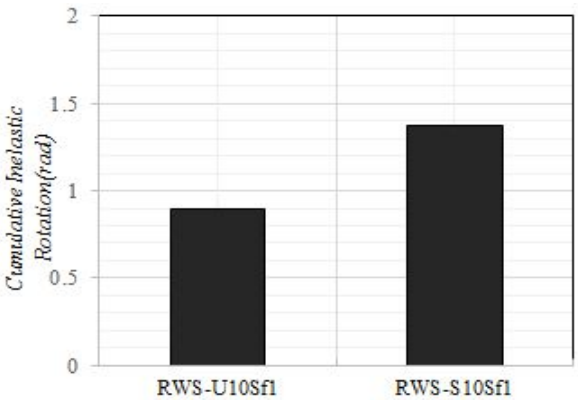

(b) Comparison of cumulative plastic rotation of stiffened and unstiffened reduced web intermediate link

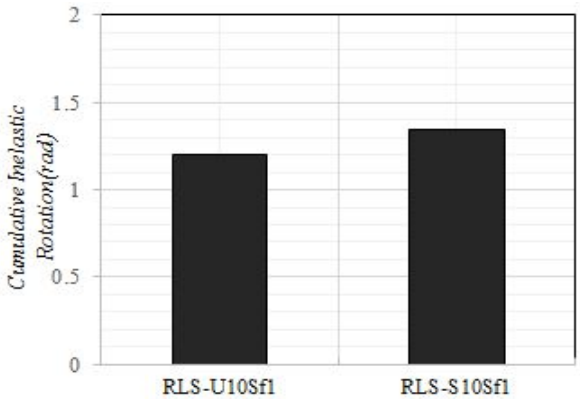

(c) Comparison of cumulative plastic rotation of stiffened and unstiffened reduced web and flange intermediate links

Fig. 4.32 Effect of stiffeners of cumulative plastic rotation

4.3.4 Effect of Percent Reduced Web Area

In order to see the effect of percent of reduced web area on the behavior of links, the hysteresis response of 10% and 15% reduced web unstiffened shear links were compared as shown in Fig. 4.33(a). Looking at the figure the comparison of hysteresis responses, the link rotation of 10% reduced web area and 15% reduced web area is the same including the rotation at which strength degradation occurred is also at the same point. The maximum shear resisting capacity of 10% reduced web area is 34.86kN bigger than the maximum shear resistance of 15% reduced web area.

The comparison of initial stiffness of 10% and 15% reduced web area is presented in Fig. 4.33(b). Looking at the comparison of initial stiffness of 10% and 15% reduced web area, initial stiffness of 10% reduced web area is bigger than 15% reduced web area which expected.

The comparison of cumulative plastic rotation of percent of open area is presented in Fig. 4.33 (c). As shown in the Fig. 4.33 (c), the cumulative plastic rotation of 10% and 15% reduced web links, is the equal. Thus, the percent of web reduction has no significant effect on the cumulative plastic rotation as shown in the Fig. 4.33(c).

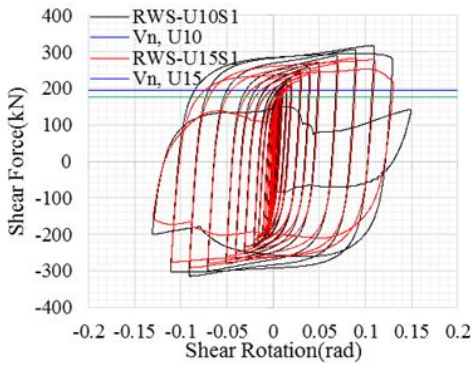

(a) Comparison of hysteresis curve

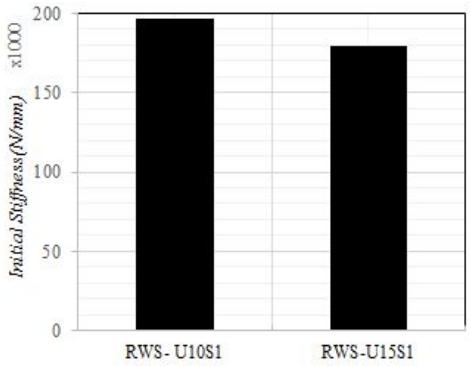

(b) Comparison of initial stiffness

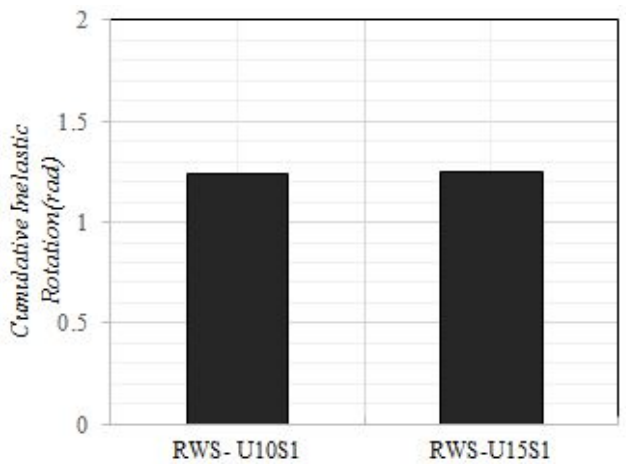

(c) Comparison of cumulative plastic rotation

Fig. 4.33 Effect of percent of reduced web area on hysteresis, initial stiffness and comparison of cumulative plastic rotation

4.4 Summary of Experimental Results

4.4.1 Plastic Rotation Capacity

The loading test results are summarized in Table 4.3 below. As shown in the table the target plastic shear rotation calculated from the AISC-2010 provision and the measures shear rotation from the experiment is presented. The plastic rotation which is calculated as the difference of total shear rotation and elastic rotation. The AISC Seismic Provisions evaluate the performance of the link in terms of the inelastic component of the link rotation angle, γ_p. In this research, γ_p is evaluated as follows:

$$\gamma_p = \gamma - \frac{V}{eK_e} \quad \text{.....(4.5)}$$

where γ_p: plastic rotation, γ: is the total shear rotation angle, V: is the link shear force, e: link length, K_e: elastic stiffness which is defined using Timoshenko beam theory as presented in Eqs. (4.6) and (4.7). [*C. K. Gulec et al, 2011, Malley JO et al., 1983*]:

$$K_e = \frac{12EI}{e^3(1+2\beta)} \quad \text{.....(4.6)}$$

$$\beta = \frac{6EI}{GA_w e^2} \quad \text{.....(4.7)}$$

where: E is the modulus of elasticity of steel, I is the moment of inertia of the cross-section, G is the shear modulus for steel, and A_w is the web area equal to the product of the reduced link depth $(d-n\phi)$ and web thickness (t_w).

The comparison of plastic rotation of test data collected from Hjelmstad and Popov 1983, Malley and Popov 1984, Kasai and Popov 1986, Ricles and Popov 1986, Engelhardt and Popov 1989, Ramadan and Ghobarah 1995, McDaniel et al. 2003, Okazaki and Engelhardt 2007, Okazaki et al. 2009, Dusicka et al. 2010 and Mansour et al. 2011 with the current research is presented in Fig. 4.34. As shown in the figure, the reduced link

section shows a plastic rotation much above the required limit. The observed buckling, cracks and failure of the test specimens are also presented in the table. The cracks started at the reduced web around the hole in all specimens considered. Which proves that the proposed links acts according to the assumed behavior.

Table 4.3 Summary of test specimens

Specimen ID	Target plastic shear γp (rad)	Measured shear rotation (rad)	$\Omega = \frac{V_{max}}{V_p}$	Observed buckling/cracks/failure
RWS-S10S1	0.080	0.1503	1.722	Cracks around web holes
RWS-U10S1	0.080	0.1296	1.643	Fracture of web
RWLS-U15S1	0.080	0.1274	1.619	Fracture of web
RWS-U10Sf1	0.08	0.1102	1.46	Cracks around web holes
RWS-S10Sf1	0.08	0.150	1.665	Cracks around web holes
RWS-S10Sf2	0.08	0.126	1.532	Cracks around web holes
RLS-U10Sf1	0.038	0.1247	1.511	Fracture of web
RLS-S10Sf1	0.038	0.1523	1.681	Fracture of web and local-buckling of flange at reduced section
RLS-S10Sf2	0.056	0.1508	1.587	Fracture of web and local-buckling of flange at reduced section

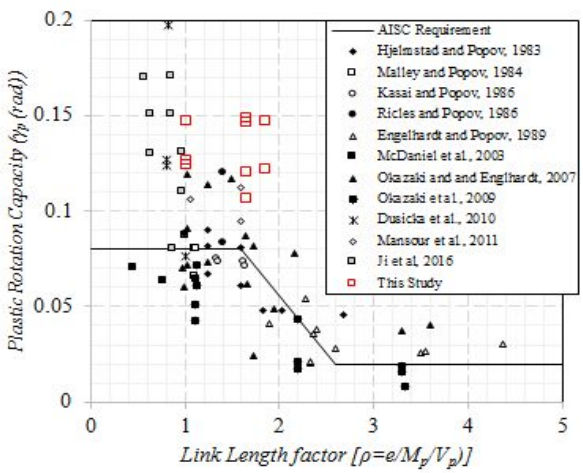

Fig. 4.34 Plastic rotation capacity versus the link length factor

4.4.2 Overstrength Factor (Ω)

Overstrength factors, OSF, are necessary to realize the capacity design approach in which a strength hierarchy is established within a structure so that some ductile “primary” “protected” elements are discouraged from yielding. These protected elements are generally designed for the maximum (or overstrength) force capacity which can be generated by the primary elements. Overstrength factors are multiplied by the specified or nominal primary element strength as part of determining the required strength of the protected elements. If the overstrength value is too high, uneconomic structures will result, if it too low, an undesirable mechanism may result. The overstrength factor is the ratio of maximum recorded shear forces to the plastic shear strength as expressed in Eq. (4.8).

$$\Omega = \frac{V_{\max}}{V_p} \qquad \text{.....(4.8)}$$

where Ω: is the overstrength factor, $V_{\max}$: is the maximum shear force, V_p: is the plastic shear. The over-strength factors existing links given in the 2005 AISC Seismic Provisions [19] are based on an assumed overstrength factor of 1.5 obtained in the previous experiments. However, researchers recommend that the overstrength factor recommended in AISC-05 is conservative for intermediate and long in accordance with European specification of structural section links' design. Amin Mohebkhah and Behrouz Chegeni recommended the strain hardening overstrength factor (Ω) calculated from finite element analyses is in a range of about 1.53–1.77 (average 1.60) for short links, about 1.29–1.46 (average 1.37) for intermediate and 1.39–1.41 (average 1.40)for long links. It can be seen that, the overstrength factor decreases as the length ratio increases for short and intermediate links and then increases a little for long links again. Richards and Uang then suggest that the cyclic hardening parameter defined above should vary with link length factor as:

$$\Omega = \begin{cases} 1.44 & \rho \le 1.6 \\ 1.44 - 0.4(\rho - 1.6) & 1.6 < \rho < 2.6 \\ 2.7/\rho & \rho \ge 2.6 \end{cases} \qquad \text{.....(4.9)}$$

The research works of Amin Mohebkhah and Behrouz Chegeni and Richards and Uang and the recommendation of AISC is different. Fig. 5.35 summarizes data from link tests Hjelmstad and Popov 1983, Malley and Popov 1984, Kasai and Popov 1986, Ricles and Popov 1986, Engelhardt and Popov 1989, Ramadan and Ghobarah 1995, McDaniel et al. 2003, Okazaki and Engelhardt 2007, Okazaki et al. 2009, Dusicka et al. 2010, Mansour et al. 2011 and the oversterngth factor calculated for test specimens in this study. The collected data is plotted the ratio V_{max}/V_n against the link length ratio in the range of 0.47–4.37. Vn is the inelastic strength of the link, and was calculated as the smaller of V_p or $2M_p/e$, where V_p and M_p were computed using the actual measured dimensions and actual measured yield strengths of steel. The overstrength factor of 1.5, suggested by Popov and Engelhardt (1988), is somewhat conservative for shear links with a length ratio of over 1.0. It was suspected that the substantially larger overstrength in very short shear links had two causes. The first cause is the shear resistance of flanges (Itani 2002 Richards 2004). The second is the cyclic hardening effect of web steel under large inelastic strains (Kasai et al. 2004).

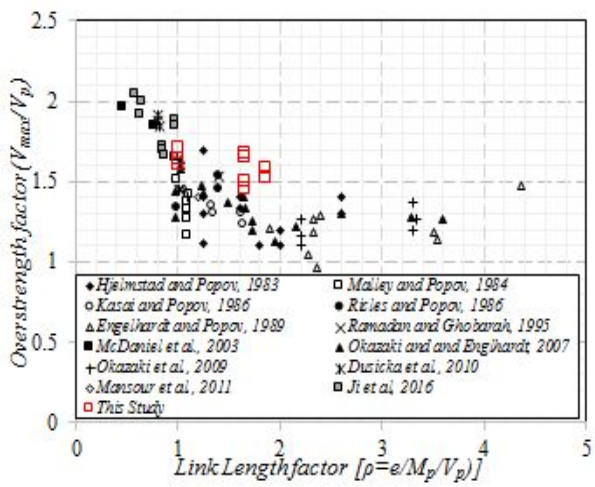

Fig. 4.35 Overstrength factor versus the link length factor

4.4.3 Equivalent Viscous Damping

The concept of viscous damping is generally used to represent the energy dissipated by the structure in the elastic range. An early proposal to model the inelastic behavior with a parameter proportional to the velocity was made by Jacobsen [1930, 1960]. He approximated the non-linear friction behavior to a power of velocity. This was initially used to compute the response of single-degree-of-freedoms systems (SDOF) when subjected to sinusoidal loads. Housner [1956] and Jennings [1964] carried out some investigation in order to extent the concept to other hysteresis systems. The concept of equivalent viscous damping is explained briefly emphasizing the main assumptions. The viscous damping coefficient in two parts:

$$\xi_{VD} = \xi_{eq,o} + \xi_{eq,hyst} \quad \text{.....(4.10)}$$

where $\xi_{eq,o}$ corresponds to the initial damping in the elastic range or also known as energy dissipation resulting from viscous damping and $\xi_{eq,hyst}$ corresponds to the equivalent viscous damping ratio that represents the dissipation due to the inelastic hysteresis behavior. The initial damping in the elastic range or energy dissipation resulting from viscous damping is generally assumed to be 5% [M. J. N. Priestley & D. N. Grant]. Chopra, 1995 suggested that the viscous damping for elastic range is between 2% and 5%. Viscous damping in elastic range or strain energy in a cycle is given by:

$$E_{SO} = \frac{1}{2} V_{\max} \delta_{\max} \quad \text{.....(4.11)}$$

where δ: is the displacement (loading amplitude), $V_{\max}$ and $\delta_{\max}$: is the maximum shear force and displacement respectively. The other important terminology in seismic dissipating elements is effective stiffness. (k_{eff}). The effective stiffness is defined as in Eq. (4.12) in terms of $V_{\max}$, $V_{\min}$ and $\delta_{\max}$, $\delta_{\min}$ are the maximum and minimum shear force and displacement respectively as shown in Fig. 4.36 (a).

$$k_{eff} = \frac{|V_{\max}| - |V_{\min}|}{|\delta_{\max}| - |\delta_{\min}|} \quad \text{.....(4.12)}$$

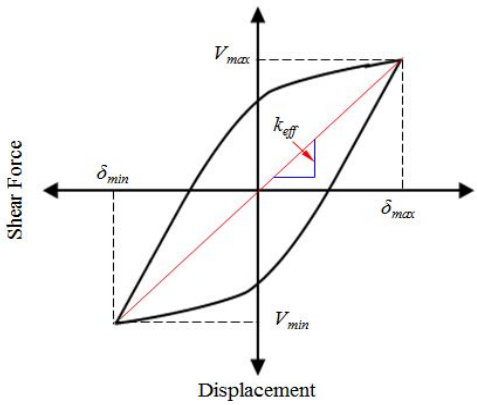

(a) Definition of effective stiffness

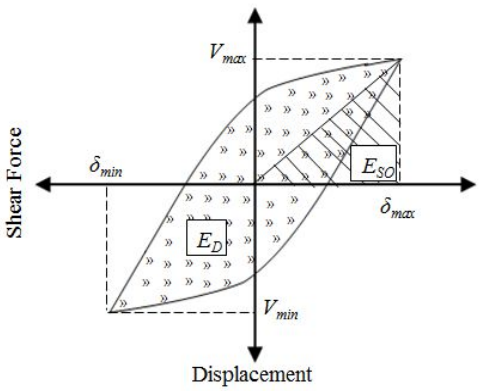

(b) Definition of energy loss in a cycle (E_D) and strain energy (E_{SO})

Fig. 4.36 Effective stiffness and energy dissipated in a cycle

The inelastic hysteresis behavior also called the damping ratio is to equate the energy dissipation in a vibration cycle of the actual structure and an equivalent viscous damping. For an actual structure the force-displacement relation obtained from an experiment under cyclic loading with displacement amplitude δ, is determined such a relation is shown schematically in Fig. 4.36 (b). The energy dissipated in the actual structure is given by the area E_D enclosed by the hysteresis loop. Equating this to the energy dissipated in viscous damping given by Eq. (4.13).

$$\xi_{eq} = \frac{1}{4\pi}\frac{E_D}{E_{SO}} \quad \text{.....(4.13)}$$

where E_D and E_{SO} are respectively the energy dissipated in a cycle and strain energy given in Eq. (4.11).

The damping ration and effective stiffness for test specimens were calculated for each specimens and a comparison have been made for the matching specimens. Fig. 4.37 shows the comparison of damping ratios and effective stiffness of RWS-S10S1 and RWS-U10S1, stiffened and unstiffened shear link. As shown in the figure, unstiffened shear link has bigger damping capacity at large deformation. The situation is reversed i. e. stiffened link has bigger damping capacity compared to unstiffned shear link at the elastic and low deformation of specimen, as shown in Fig. 4.37 (a) and (c). The damping ratio of stiffened and unstiffened shear link ranges from 10.7%-50.7% and 4.12%-52.67% respectively.

The effective stiffness of stiffened and unstiffened shear link decreases with equal rete as the shear deformation (number of cycle0 increases. Stiffened shear link (RWS-S10S1) shows slight bigger effective stiffness compared to unstiffened shear link (RWS-U10S1) Fig. 4.37 (a) and (b). The effective stiffness of both stiffened and unstiffened shear link ranges from 7.33kN/mm-149.kN.mm and 7.4kN/mm-159.35kN/mm respectively.

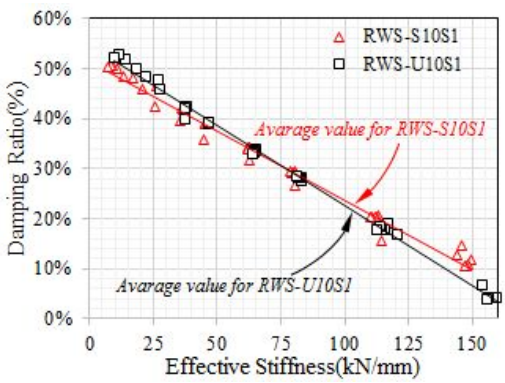

(a) Comparison of damping ratio and effective stiffness of RWS-S10S1 and RWS-U10S1

Fig. 4.37 Effect of stiffeners on effective stiffness and damping ratio of shear links

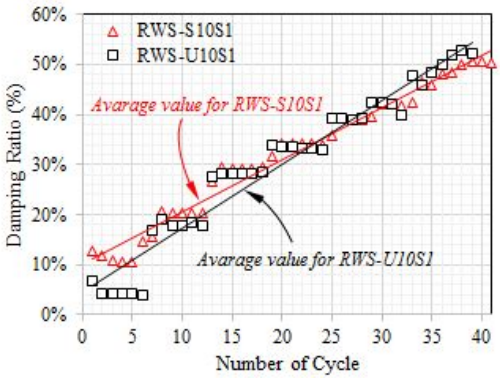

(b) Comparison of effective stiffness versus number cycle of RWS-S10S1 and RWS-U10S1

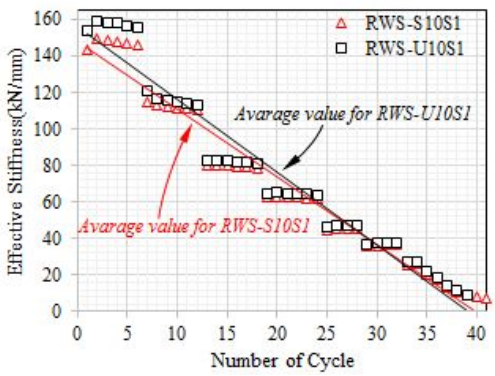

(c) Comparison of damping ratio versus number cycle of RWS-S10S1 and RWS-U10S1

Fig. 4.37 Effect of stiffeners on effective stiffness and damping ratio of shear links (*continue...*)

The effect of web reduced area on damping ratio and effective stiffness is presented in Fig. 4.38. As presented in figure, the damping ratio of 10% reduced web area is bigger compared to 15% reduced web area. As shown in the a linear decreement was observed in the relationship between damping ratio and effective stiffness shown in Fig. 4.38(a). The damping ratio of specimen having 15% reduced web area is high at large deformation (at bigger cycle) compared to specimen having 10% reduced web area as shown in Fig. 4.38 (b). The damping ratio of specimen having 10% reduced web area and 15% reduced web area shear link ranges from 4.12%-52.67% and 7.217%-50.92% respectively.

The effective stiffness of specimens with 10% reduced web area has generally shown bigger compared to 15% reduced web area. However, at large displacement both specimen have equal effective stiffness as shown in Fig. 4.38(c).

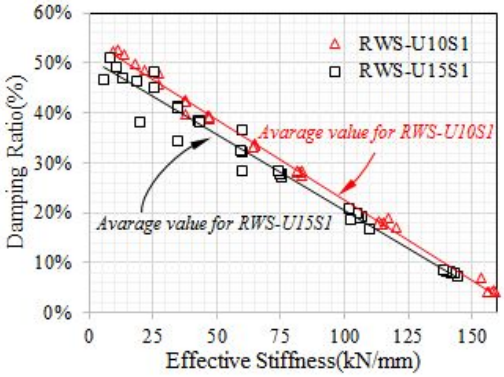

(a) Comparison of damping ratio and effective stiffness of RWS-U10S1 and RWS-U15S1

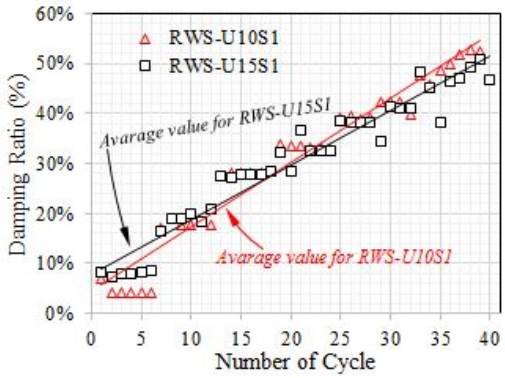

(b) Comparison of damping ratio versus number cycle of RWS-U10S1 and RWS-U15S1

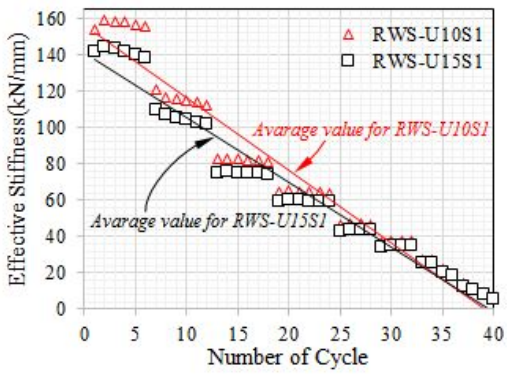

(c) Comparison of effective stiffness versus number cycle of RWS-U10S1 and RWS-U15S1

Fig. 4.38 Effect of % reduced web area on effective stiffness and damping ratio of shear links

4.5 Summary

In order to evaluate the plastic deformation capacity as well as the failure mode of reduced web link and reduced web and flange link section quasi static loading test was carried out. The following summaries was drawn from the obtained results of experimental investigations.

All link types, both shear and intermediate links, considered for experiments satisfied the plastic rotation limit specified in AISC seismic provision (AISC-341-10). Even though both stiffened and unstiffend links satisfied the plastic rotation limit, stiffened links shows higher plastic deformation capacity compared to unstiffened links for both shear and intermediate links. This is usually due to the fact that stiffeners provide stability to both web and flanges. Because looking at the deformed and/or fractured test specimens, local buckling of flanges was noticed in unstiffened links. In addition, in and out-of-plane buckling of web was also observed in unstiffened links which finally leads to fracture of web.

The deformation shape and failure mode of test specimens during and after loading test has been presented. Cracks and fractures was started at the edge of reduced web (at the edge of holes in the web) for all test specimens considered. This actually proves that the stress and plastic strains are concentrated at the edge of the holes when links are loaded in shear. The cracks started at the edge of holes propagates and finally leads to facture of web.

The percent of reduced web area has an effect on the maximum shear resisting capacity and initial stiffness. The higher the percent of web reduction the lesser the maximum shear resistance and initial stiffness. For the specimens considered 10% reduced web area and 15% reduced web area of unstiffened shear link have the same plastic rotation capacity. The same failure mode was also the noticed for 10% and 15% reduced web area shear links.

The damping ratio of stiffened and unstiffened links is in the same range but at large deformation, unstiffened links have high damping ratio compared to stiffened links and reverse results were obtained for the deformation less that the rotation limit. However, effective stiffness of unstiffened links are higher almost in all cycle compared to stiffened links. The percent of reduced web area has also an effect on the damping ratio. Thus, 10% reduced web area has higher damping ration at large deformation than 15% reduced web area. The effective stiffness of 10% reduced web area is greater than 15% reduced web area.

5. Non-linear FE Analysis

5.1 General

The behavior of developed reduced link section was studied by nonlinear finite element simulation. The ABAQUS platform was used for all of the continuum modeling of the proposed active links. The main objective of this analytical study were:

1. to extend the experimental investigations conducted to include the specimens type not included in the experimental investigation.
2. to study the effectiveness of finite element simulation to evaluate the proposed reduced link section
3. once the analytical investigations was calibrated and verified through experimental results, different parameters was considered including link-to-column connections, in the next Chapter 6 if non-linear finite element models of EBFs links demonstrates nice predictions of active links behavior under cyclic loading.

In this chapter, the detail of FE analysis modelling procedures and calibration method was presented including material modeling, meshing used, boundary and loading conditions. The comparison of the failure and deformed shape of test and analysis model as well as comparing the hysteresis response of analysis and test results were presented. In addition, the plastic rotation and cumulative energy of both results were also included in this section.

Different calculation method of plastic rotation for analysis model was presented because failure analysis was not include in the FE model so that the hysteresis response of analysis model some times keep stable even under large deformation. Thus, different indexes were considered in order to limit the total shear rotation.

5.2 Finite Element Analysis

5.2.1 Material Modeling

The structural steel components are modeled as an elastic–plastic material. With elastic and plastic options, the yield and ultimate tensile strength obtained firstly from the results of the coupon tests called engineering data should be converted into the true stress and plastic strain with appropriate input format for ABAQUS. The engineering data can be converted to true data using the following equations (Eq. (5.1) and Eq. (5.2) for stress and strain respectively.

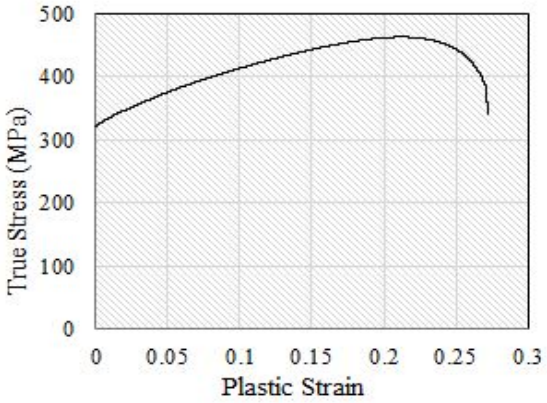

(a) Average true stress versus plastic strain relationship for 7mm thick steel plate

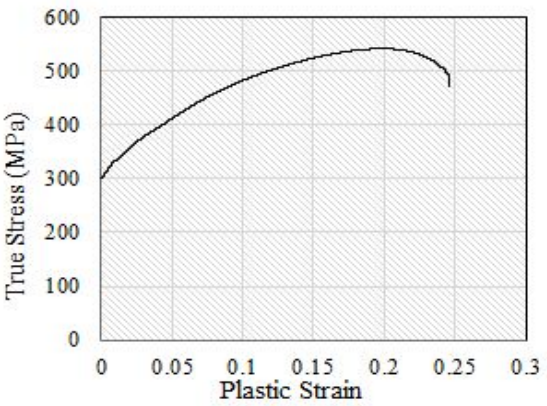

(b) Average true stress versus plastic strain relationship for 8mm thick steel plate

Fig. 5.1 Average true stress versus plastic strain relationship

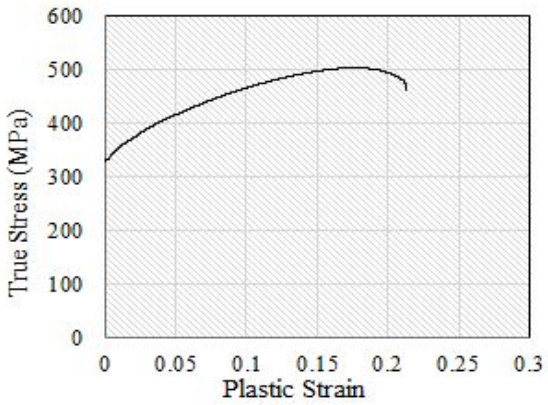

(c) Average true stress versus plastic strain relationship for 9mm thick steel plate

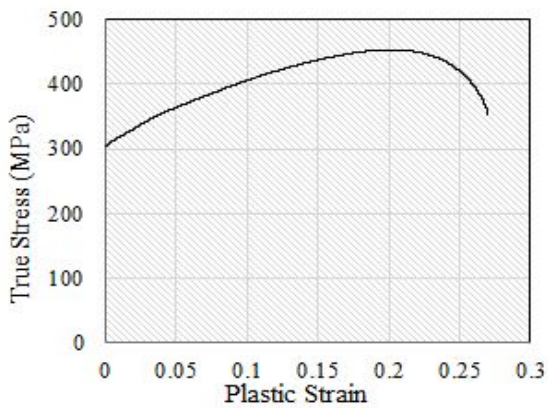

(d) Average true stress versus plastic strain relationship for 10mm thick steel plate

Fig. 5.1 Average true stress versus plastic strain relationship *(continue...)*

$$\sigma_{tr} = \sigma_e (1 + \varepsilon_e) \quad \text{.....(5.1)}$$

$$\varepsilon_{tr} = \ln (1 + \varepsilon_e) \quad \text{.....(5.2)}$$

where σ_{tr}: true stress, σ_e: engineering stress, ε_{tr}: true strain, ε_e: engineering strain

The average true stress and plastic stain of converted engineering data or coupon test results were plotted for all thicknesses are shown in Fig. 5.1. For finite element analysis the material properties shown in Fig. 5.1 was used as an input.

The important parameter to be considered in the plastic range of steel material in the large deformation modeling is the effect of strain hardening characteristics. Strain hardening is a phenomenon which results in an increase in hardness and strength of a metal subject to plastic deformation (cold working) at temperatures lower than the recrystallization range. There are three different types of strain hardening models used commonly. These are: isotropic, kinematic and combined isotropic and kinematic strain hardening.

Isotropic strain hardening: where the yield surface remains the same shape but expands with increasing stress. Kinematic hardening yield surface remains the same shape and size but merely translates in stress space. The isotropic model implies that, if the yield strength in tension and compression are initially the same, i.e. the yield surface is symmetric about the stress axes, they remain equal as the yield surface develops with plastic strain. In order to model the Bauschinger effect, and similar responses, where a hardening in tension will lead to a softening in a subsequent compression, one can use the kinematic hardening rule. The third commonly used strain hardening model is combined isotropic and kinematic model. Most of structural steel materials exhibit cyclic softening/hardening behavior, which can be described by superposition of isotropic hardening to a kinematic hardening rule which allows both movement and enlargement of initial yield surface. All these three hardening models was tried in this research but kinematic and combined hardening model were found better hardening model for link evaluation. However, in some cases stress enlargement was observed so combined hardening model is used in this research.

Looking at the analysis results comparing with experimental results, it is noted that further calibration is needed. Thus, calibration of cyclic material hardening in ABAQUS was considered using the coupon test results as an initial inputs for yielding and plastic strain.

5.2.1.1 Calibration of a cyclic material hardening model

Looking at the test results, the hysteresis curve shows an expansion as the loading amplitude increases. Thus, special parameters needs to be considered in the combined hardening model. Some adjustments of material input variables was implemented to come up with a calibrated analysis model for reduced link section. Hence in the elastic-plastic analysis, ABAQUS provides a numerical material law to simulate the behavior of metallic material under cyclic loading. The theory of cyclic plasticity provides a mathematical description of stress and strain in plastically deformed solids under cyclic loading which is based on the work by Lemaitre and Chaboche. In this model, the von Mises yield criterion and an associative flow rule are assumed. The characteristics of a material are defined by a combined isotropic/kinematic hardening model. The model consists of a nonlinear kinematic hardening component and an isotropic hardening component. The kinematic component of the model defines the change of backstress and isotropic hardening stress are shown in Eqs. (5.3) and (5.4), respectively. The back stress indicates the movement of the yield surface or kinematic hardening stress and isotropic hardening stress indicates the increase of radius of the yield surface.

$$\alpha = \frac{C_k}{\psi}\left(1 - e^{-\psi\varepsilon^p}\right) + \alpha_1 e^{-\psi\varepsilon^p} \quad \text{.....(5.3)}$$

$$\sigma_i = \sigma_0 + Q_\infty\left(1 - e^{-v\varepsilon^p}\right) \quad \text{.....(5.4)}$$

where the above equations, ε^p is the equivalent plastic strain and Ck and γ are the parameters of the model. σ_0 is the yield stress at zero equivalent plastic strain (defined in this study as the 0.01% proof stress), Q_∞ is the maximum change in the size of the yield surface and v is the rate at which the size of the yield surface changes as plastic strain increases.

For isotropic hardening the size of the yield surface in the i^{th} cycle σ_i can be obtained from Eq. (5.5) and the corresponding equivalent plastic strain is given by Eq. (5.6) in the elastic rage shown in Fig. 5.2.

$$\sigma_i = \frac{\sigma_i^t - \sigma_i^c}{2} \quad \text{.....(5.5)}$$

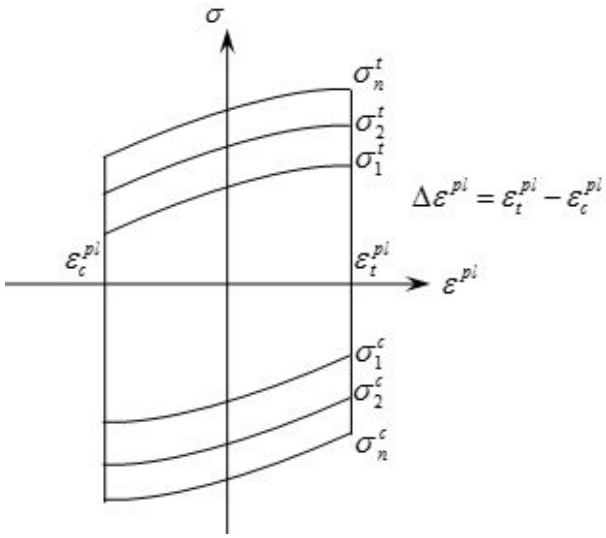

Fig. 5.2 Calibration of isotropic hardening component (K.H. Nip et al. 2010)

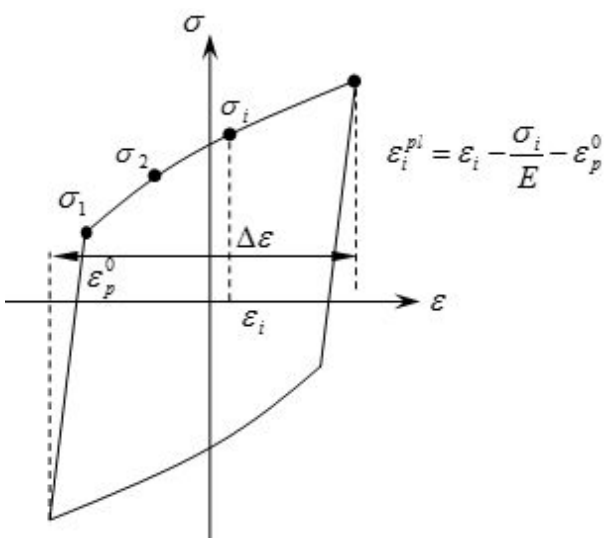

Fig. 5.3 Calibration of kinematic hardening component (K.H. Nip et al. 2010)

$$\varepsilon_i^p = \frac{1}{2}(4i-3)\Delta\varepsilon_p \quad \text{.....(5.6)}$$

where σ_i^t is the maximum tensile stress and σ_i^c is the maximum compressive stress, $\Delta\varepsilon_p$ is the plastic strain range. In the same way, the equivalent plastic strain for kinematic hardening is given by as shown in Fig. 5.3.

$$\varepsilon_i^p = \varepsilon_i - \frac{\sigma_i}{E} - \varepsilon_p^0 \quad \text{.....(5.7)}$$

In the finite element analyses, the steel material used the model for metals subjected to cyclic loading. This model adopts Von Mises yield criterion and considers both isotropic and kinematical hardening. The back stress and isotropic hardening stress are shown in Eqs. (5.8) and (5.9) respectively (*K. Deng et al. 2013, 2014, 2015*). The back stress indicates the movement of the yield surface, and isotropic hardening stress indicates the increase of radius of the yield surface.

$$\alpha = \sum_{k=1}^{n} \frac{C_k}{\gamma_k}\left(1 - e^{-\gamma_k \varepsilon^{-pl}}\right) \quad \text{.....(5.7)}$$

$$\sigma^0 = \sigma/0 + Q_\infty\left(1 - e^{-v\varepsilon^{-pl}}\right) \quad \text{.....(5.7)}$$

where ε^{-pl} is the equivalent plastic strain and C_k and γ_k are the parameters of the model. Q∞ represents the limit of the isotropic hardening stress and v represents the speed of steel hardening. σ|0 represents the initial yield stress and is given in Fig. 5.1 which is identical with the material for physical tests and converted to true value. The elastic module is 205 GPa and the Poisson's ratio is 0.3, n is assumed to be 4, and the associated C_k and γ_k (k = 1, 2, 3, 4) are determined based on the stress strain curve obtained from the coupon test. The details about the parameters adopted for the material model are given in Table 5.1. Coupon test results of the steel materials and the fitting of the numerical material law are presented in Fig. 12. In coupon test the max plastic strain is limited at 0.02.

Table 5.1 Material parameters used for numerical model

C_1	γ_1	C_2	γ_2	C_3	γ_3	C_4	γ_4	Q_∞
22000	500	1600	200	6000	250	600	30	$1.7x10^8$

5.2.1.2 Meshing Type and Size Used

Both solid and shell models have been tried for the proposed links using ABAQUS. The comparison of results shows that there is no apparent difference in modeling but the computational time for solid model is higher compared to shell model. The shell models were meshed with shell elements are used to model the web and flanges with elements called S4R. Many researchers have been used shell model for shear link without perforations. The S4R is a four-node doubly curved, reduced integration shell element with hourglass control. It can accommodate finite strains and large rotations. S4R element has several hourglass modes that may propagate over the mesh as shown in Fig. 5.4 (a). The shell element type "S4R" has been used for the web, flange and stiffeners. It has four nodes with six degrees of freedom per node, 3 translational and 3 rotational. The geometry of each shell model corresponded to the centerline dimensions of a prototype link. Different mesh densities have been tried to obtain reliable results, i.e., to not over-predict strength or stiffness by more than approximately 5%. The effect of mesh size was also presented before selecting the appropriate mesh size. The loading plates (end plates) are modeled using solid elements using ABAQUS C3D8R elements shown in Fig. 5.4(b). The mesh size of end plates has no effect on both globally (load displacement response) and locally (demand on the boundary elements) since they are modeled as a rigid element.

The mesh size were selected by trial and error. Considering accuracy of results comparing with the test results, computational time and the stress and strain distribution of analysis specimen.

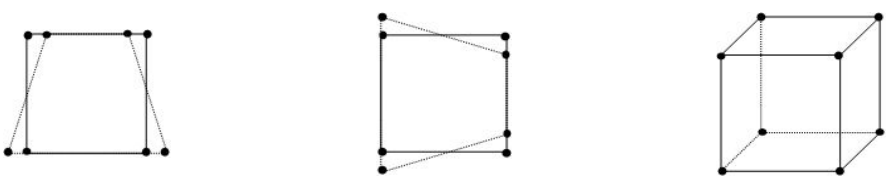

(a) S4R shell elements (b) C3D8R solid element

Fig. 5.4 Types of meshes

5.2.2 Loading and Boundary Condition

The boundary condition has a significant effect on the behavior and type of evaluation we intend to do. The boundary condition used follows the behavior of links in EBFs and the boundary condition used in experimental investigations. Boundary conditions were applied by constraining all degrees of freedom of the nodes at both ends of the link to master nodes placed at the centroid of the cross-section at each link end. Two types of boundary conditions were applied in the evaluation of links analytically. The first option, which is shown in Fig. 5.5, is fixing both displacement and rotation in all direction and allowing translation in the other end only in the loading direction as shown in Fig. 5.5 (a) (*M. Ohsaki et al. 2012*). The deformed shape of the first option of boundary condition is shown in Fig. 5.5 (b). The second option, which is shown in Fig. 5.6, is one end was restrained both displacement and rotations except translation in the link's axial direction and the other end was restrained against all displacement and rotation except the vertical translation as shown in Fig. 5.6 (a) (*Richard et al. 2006*). The deformed shape of the second option boundary condition is shown in Fig. 5.6 (b). Both boundary condition can express the real behaviour of links in EBFs. However, the second option is used in this study and it is the widely used boundry condition in many researchers as it shows the more logical and best explains the deformed shape of links in EBFs under lateral loading.

Loading was applied in the vertical direction of the second option as shown in Fig. 5.6. There are two types of loading, the first loading type is conducted by controlling the forces applied on the specimen. The second type of loading protocol is conducted by controlling the displacement. In this study, the constant strain loading is implemented and the revised AISC-2010 loading history shown in Fig. 5.7 is used.

The loading protocol in the finite element analysis includes 6 cycles of link rotation γ at an amplitude of 0.00375 radians, 6 cycles of link rotations γ at an amplitude of 0.005 radians, 0.0075 radians and 0.01 radians, 4 cycles of link rotations γ at an amplitude of 0.015 radians and 0.02 radians, 2 cycles of link rotation γ at an amplitude of 0.03 radians, 1 cycle of link rotation γ at an amplitude of 0.04 radians, 1 cycle of link rotation γ at an amplitude of 0.05 radians, and the following each cycle of link rotation γ increased in the amplitude by 0.02 radians up to the limit on the actuator or the specimen failure whichever came first.

The 3D meshed analysis model for stiffened intermediate links of specimens with reduced web and reduced web and flange section (RWS-S10Sf1 and RLS-S10Sf1) is presented in Fig. 5.8 (a) and (b) respectively.

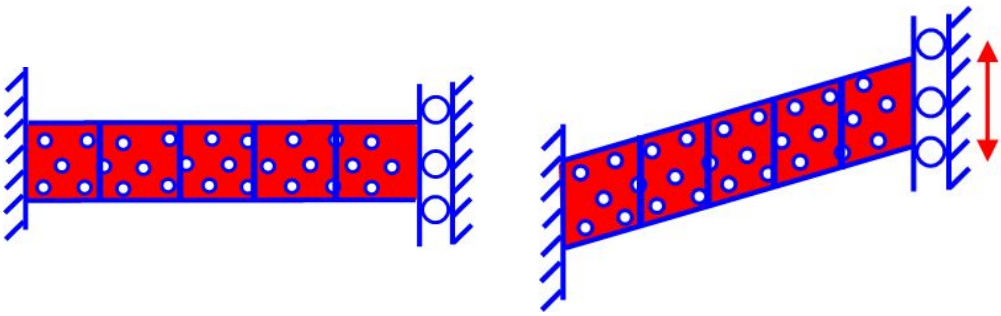

(a) Boundary Condition – Option 1 (b) Deformed shape of Option 1

Fig. 5.5. Finite-element model boundary conditions (Option 1)

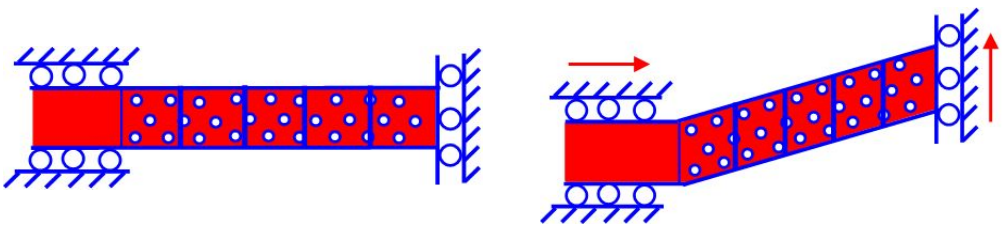

(a) Boundary Condition – Option 2 (b) Deformed shape of Option 2

Fig. 5.6 Finite-element model boundary conditions (Option 2)

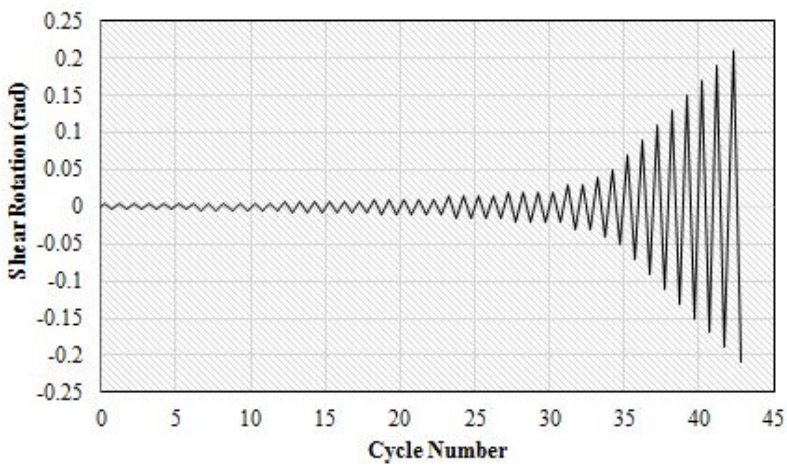

Fig. 5.7 Revised AISC-2010 loading protocol

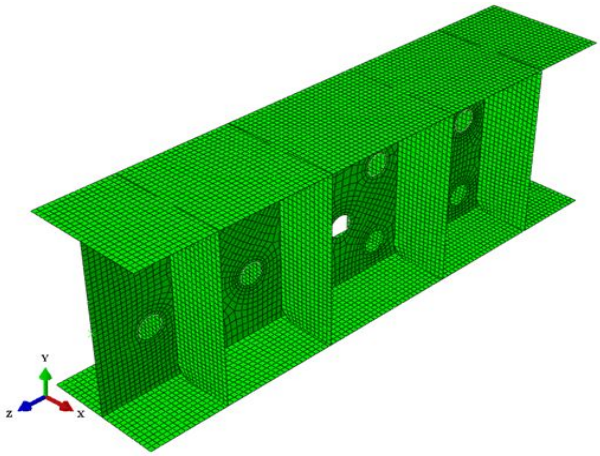

(a) Analysis model of RWS-S10Sf1

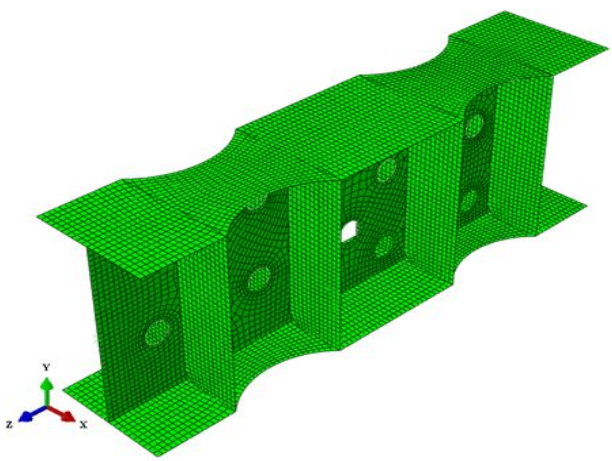

(b) Analysis model of RLS-S10Sf1

Fig. 5.8 3D meshed analysis model

5.3 Comparison of Analysis and Test results

The comparison of analysis and experimental results for considered specimens are presented in this section. The hysteresis response, deformation and/or the failure mode, plastic deformation capacity and the cumulative energy calculated from the hysteresis responses are presented. In order to develop a material parameter it is important first to compare the hysteresis curves of analysis and quasi-static loading results.

5.3.1 Hysteresis response and failure/deformation modes

The hysteresis response and the failure and/or deformation mode of link in EBFs is important. The seismic energy dissipation of eccentrically braced frames depends on the hysteresis performance and behavior of links. The stability of hysteresis response even in large displacement or plastic deformation capacity of links are important to dissipate the seismic energy. For some of the specimens considered in the test and analysis specimens are presented in detail.

5.3.1.1 Reduced web link sections

RWS-S10S1, RWS-U10S1 and RWS-U15S1

The comparison of analysis and experimental results of hysteresis response of RWS-S10S1 specimen is shown in Fig. 5.9(a) where the solid black line represent the test result and the black broken line represents the FE analysis results. As shown in the figure, the test result shown an expansion in the hysteresis loops as the loading amplitude increase specially in elastic range. There is also some unfitness in the bouncing region of both reloading in the positive and negative amplitude but with acceptable error. The maximum shear load resisting capacity of the test and analysis results agreed well. Generally, the plastic range of the hysteresis curve is in a good agrement. The main problem is in elastic range. The hysteresis response is stable for both cases up to 0.15 rad which is greater than the required shear rotation for shear links as the limit plastic rotation is 0.08 rad.

For unstiffened 10% reduced web area link section, RWS-U10S1, the comparison of analysis and experimental results of hysteresis response is shown in Fig. 5.9(b). The hysteresis response of both results agrees well in elastic range however the bouncing effect in both elastic and plastic zone has some differences. The maximum shear force is also well agreed. The test specimen failed earlier or the strength degradation of test specimen stated earlier compared to analysis model. The test specimen started buckled and strength degradation started at 0.11 rad and on the next cycle 0.13 rad the specimen failed/fractured at the link web. The resisting capacity of analysis specimen degrades at 0.13 rad which is the failure point for test specimen.

The comparison of hysteresis response for specimen with 15% reduced web area, RWS-U15S1 is shown in Fig. 5.9(c). The same results with RWS-U10S1 were obtained for RSW-U15S1 including the strength degradation point of analysis and test results. The maximum shear resisting capacity decreases compared to RWS-U10S1.

The comparison of deformed shape of analysis specimen with final deformed shape of test specimen is shown in Fig. 5.10 (a). In the test specimen some cracks at the edge of holes was observed. The comparison of deformed shape of analysis model and test specimen for RWS-U10S1 is presented in Fig. 5.10(b).

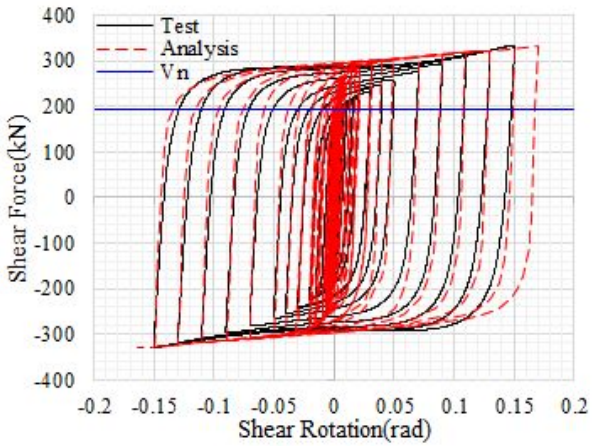

(a) Comparison of test and analysis results of hysteresis response for specimen RWS-S10S1

Fig. 5.9 Comparison of test and analysis results of hysteresis response for specimen e=300mm

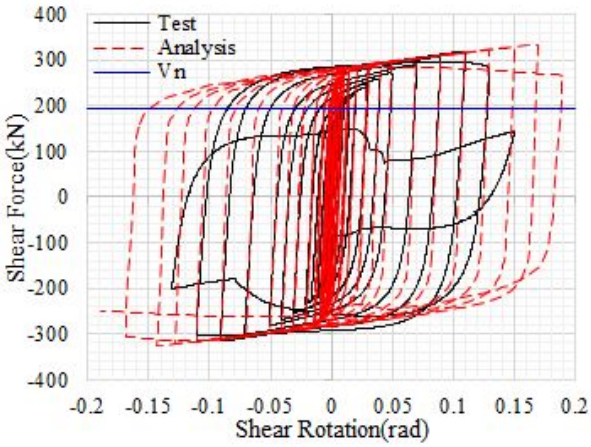

(b) Comparison of test and analysis results of hysteresis response for specimen RWS-U10S1

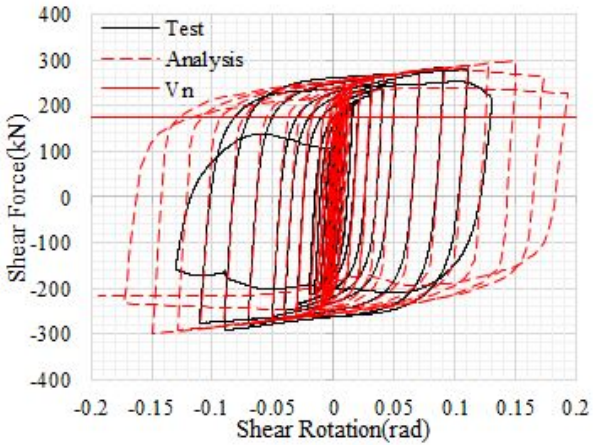

(c) Comparison of test and analysis results of hysteresis response for specimen RWS-U15S1

Fig. 5.9 Comparison of test and analysis results of hysteresis response for specimen e=300mm *(Continue...)*

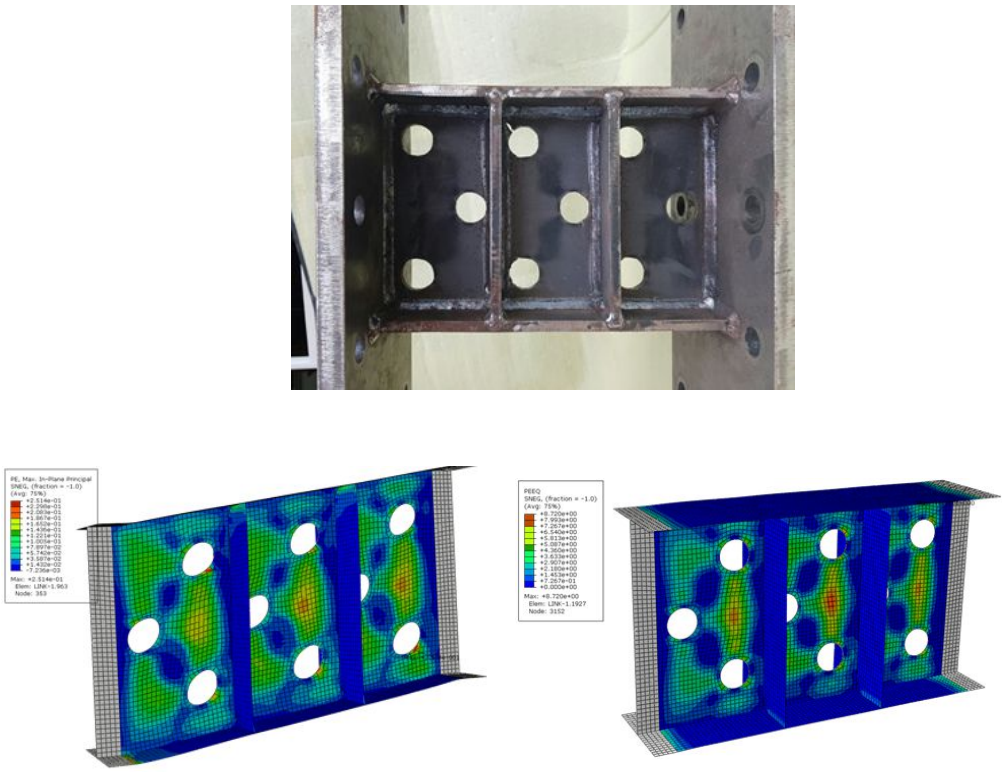

(a) Comparison of deformed shape of RWS-S10S1 specimen

Fig. 5.10 Comparison of deformed shape of reduced web link-300mm

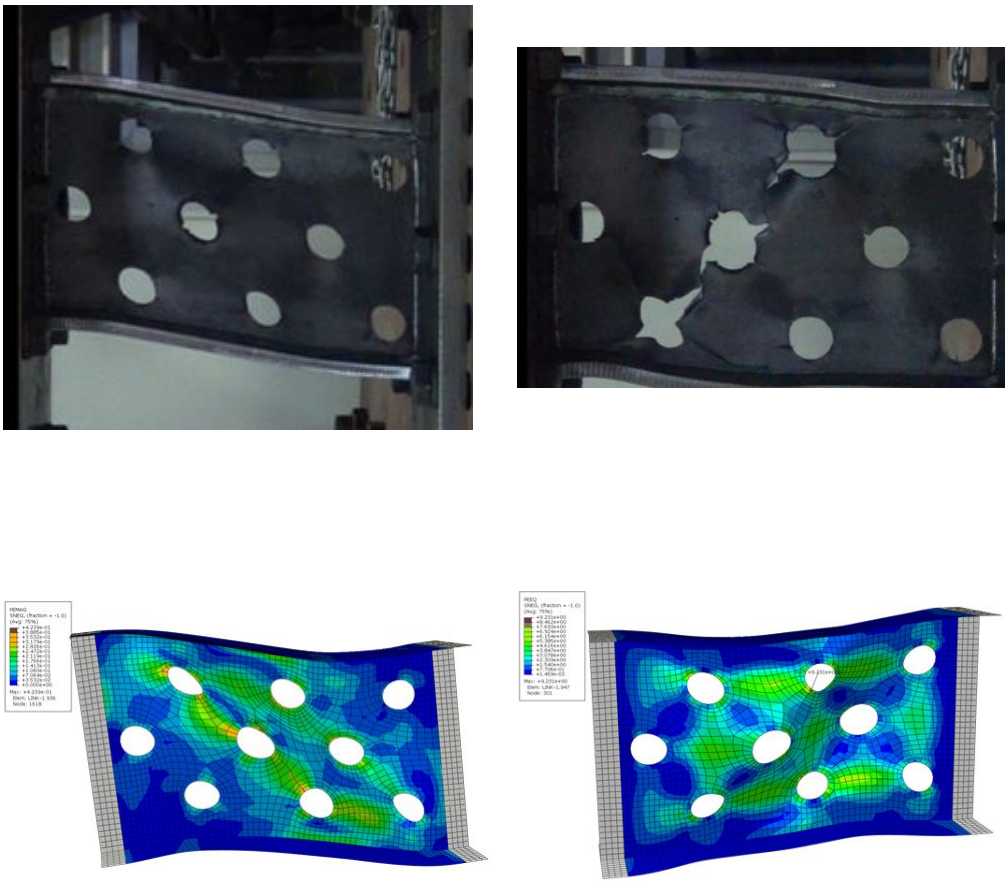

(b) Comparison of deformed shape of RWS-U10S1 specimen

Fig. 5.10 Comparison of deformed shape of reduced web link-300mm. *Continued...*

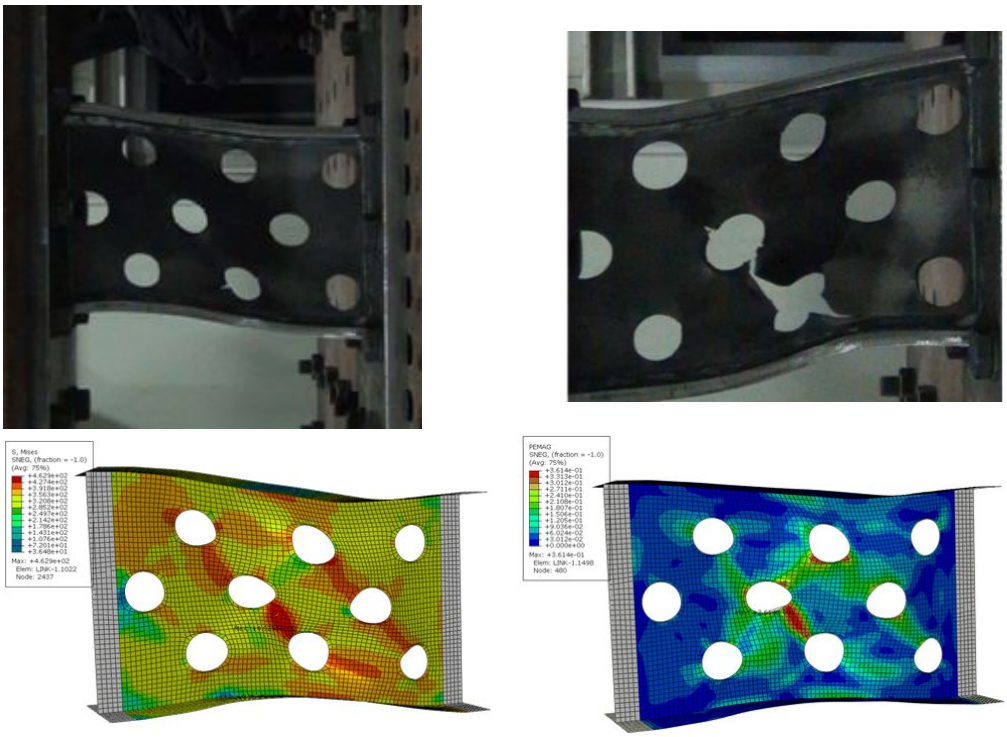

(c) Comparison of deformed shape of RWS-U15S1 specimen

Fig. 5.10 Comparison of deformed shape of reduced web link-300mm. *Continued...*

RWS-S10Sf1, RWS-U10Sf1 and RWS-S10Sf2

The comparison of analysis and experimental results of hysteresis response of RWS-S10Sf1, RWS-U10Sf1 and RWS-S10Sf2 specimens are presented in this section. The comparison of hysteresis response is presented in Fig. 5.11. As shown in the figure, the hysteresis response of analysis and test specimens almost equal maximum shear resistance and the plastic deformation capacity also matches well. However, as shown in the plotted curve, the bouncing effect don't agree. The elastic range of test and analysis agrees well.

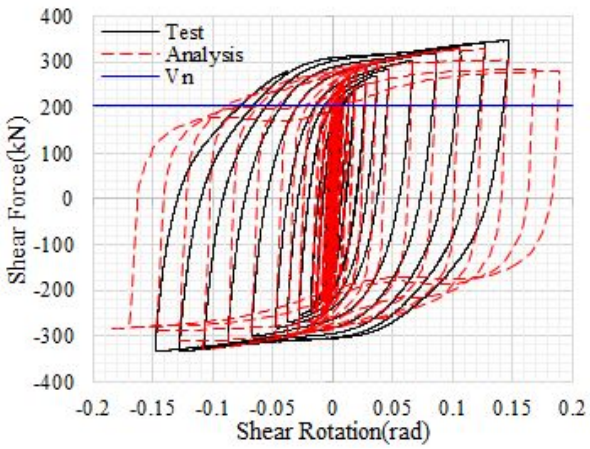

(a) Comparison of test and analysis results of hysteresis response for specimen RWS-S10Sf1

Fig. 5.11 Comparison of test and analysis results of hysteresis response for specimen reduced web link =500mm

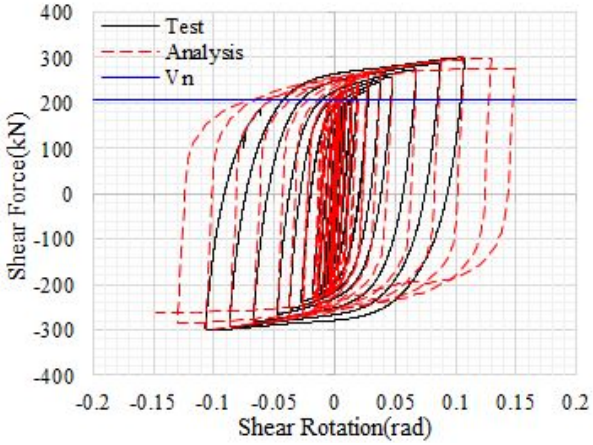

(b) Comparison of test and analysis results of hysteresis response for specimen RWS-U10Sf1

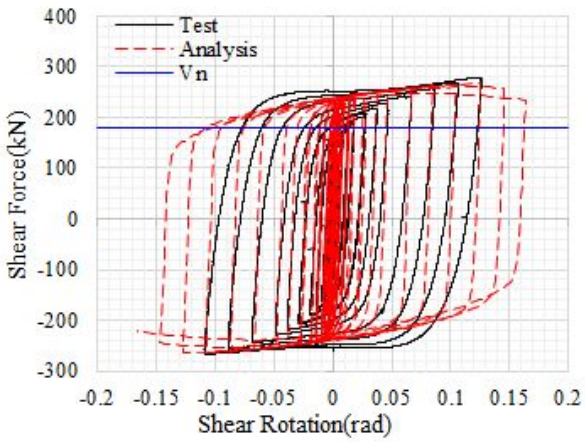

(c) Comparison of test and analysis results of hysteresis response for specimen RWS-S10Sf2

Fig. 5.11 Comparison of test and analysis results of hysteresis response for specimen reduced web link =500mm. *Continued...*

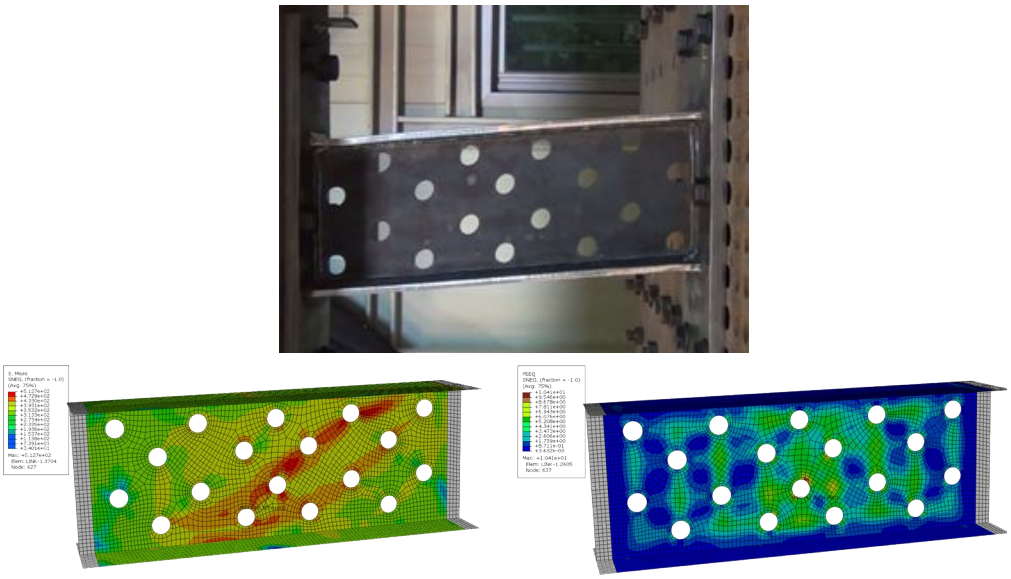

(a) Comparison of deformed shape of RWS-U10Sf1 specimen

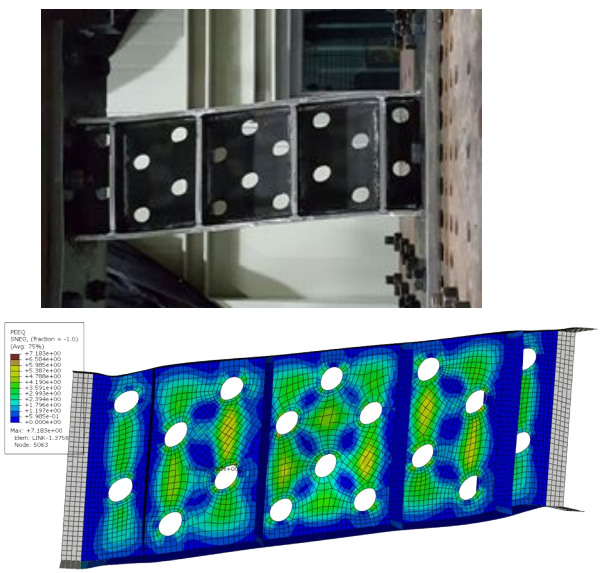

(b) Comparison of deformed shape of RWS-S10Sf1 specimen

Fig. 5.12 Comparison of deformed shape of reduced web link =500mm.

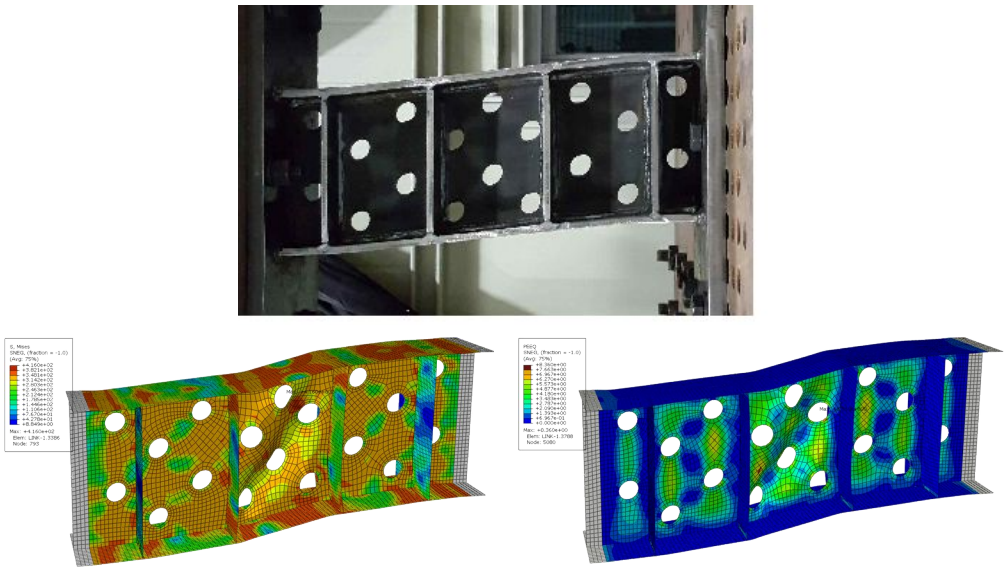

(c) Comparison of deformed shape of RWS-S10Sf2 specimen

Fig. 5.12 Comparison of deformed shape of reduced web link =500mm. *Continued...*

5.3.1.2 Reduced web and flange link sections

RLS-S10Sf1, RLS-U10Sf1 and RLS-S10Sf2

The comparison of analysis and experimental results of hysteresis response for reduced web and flange link sections are presented in Fig. 5.13. As shown in the figures, the maximum shear force resisting capacity of analysis and test results are in good agreement. However, the bouncing effect in both unloading and reloading wasn't agreed much. In all cases, the elastic range as far as the stiffness concerned, the analysis and test results agrees well.

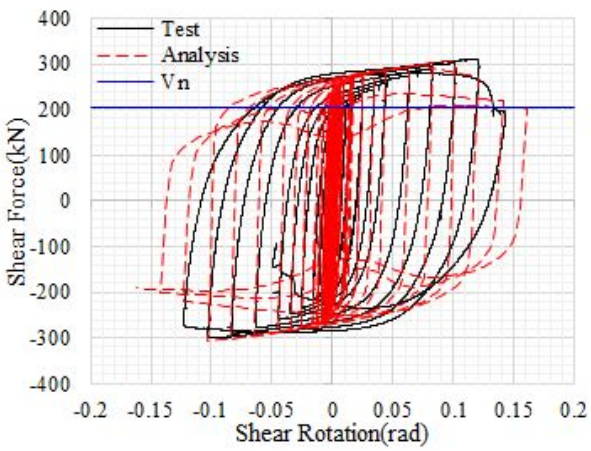

(a) Comparison of test and analysis results of hysteresis response for specimen RLS-U10Sf1

Fig. 5.13 Comparison of test and analysis results of hysteresis response for specimen reduced web and flange link section-500mm.

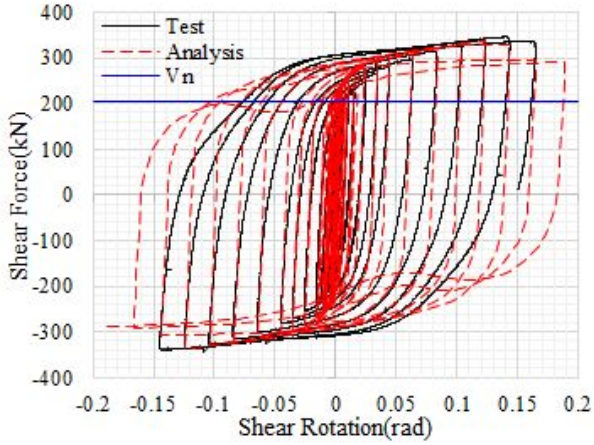

(b) Comparison of test and analysis results of hysteresis response for specimen RLS-S10Sf1

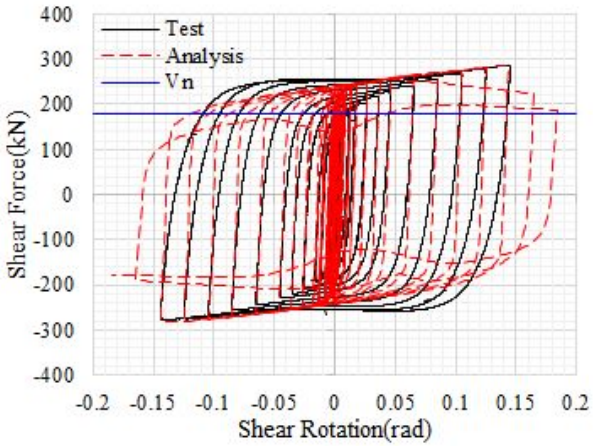

(c) Comparison of test and analysis results of hysteresis response for specimen RLS-S10Sf2

Fig. 5.13 Comparison of test and analysis results of hysteresis response for specimen reduced web and flange link section-500mm. *(Continued...)*

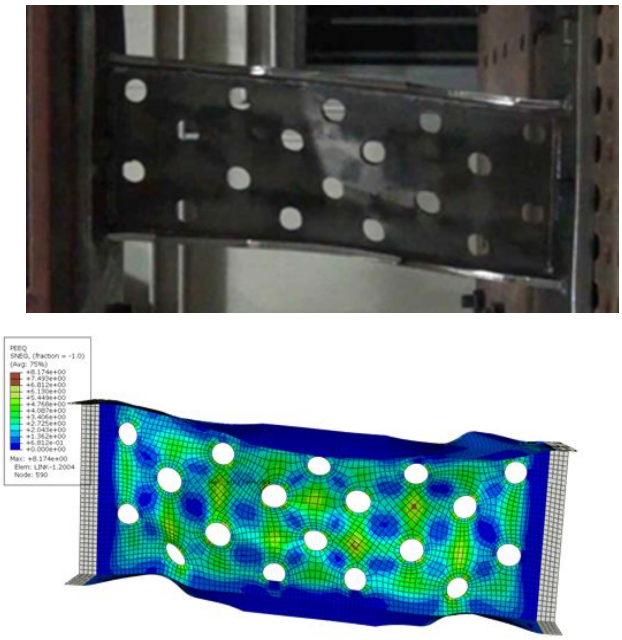

(a) Comparison of deformed shape of RLS-U10Sf1 specimen

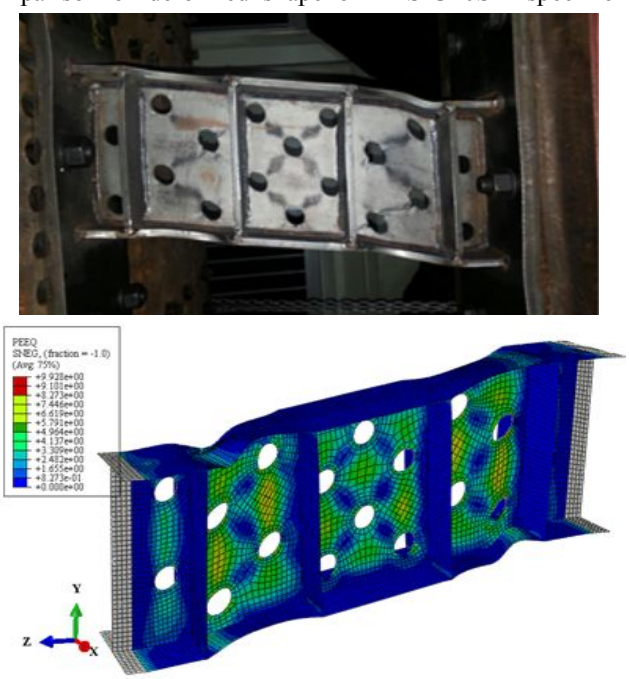

(b) Comparison of deformed shape of RLS-S10Sf1 specimen

Fig. 5.14 Comparison of deformed shape of reduced web and flange link section-500mm.

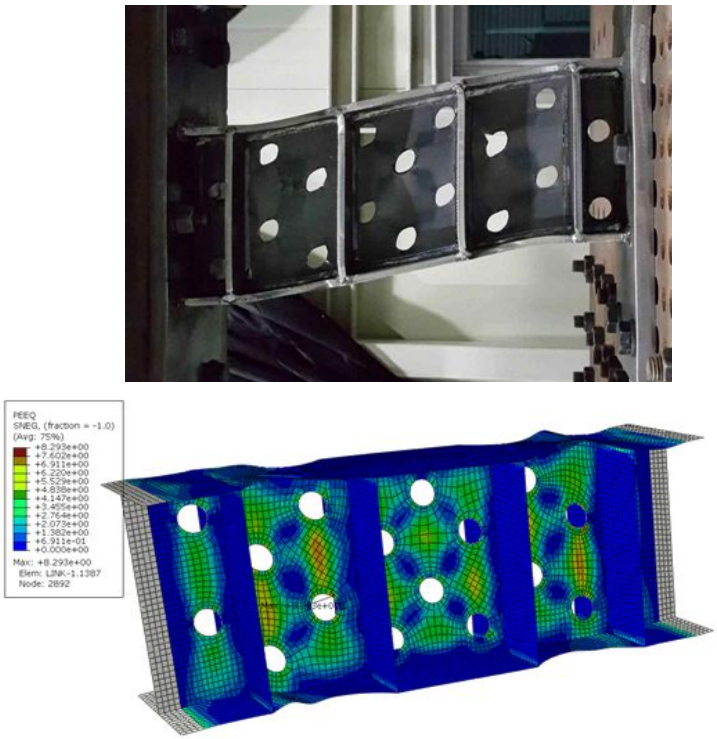

(c) Comparison of deformed shape of RLS-S10Sf2 specimen

Fig. 5.14 Comparison of deformed shape of reduced web and flange link section-500mm. *(Continued...)*

5.3.2 Comparison of Initial Stiffness

The initial stiffness is an important variable in the design of links including for calculating the plastic deformation capacity of links. In order to calculate the initial stiffness from the experimental and analysis results, the skeleton curves at least for elastic ranges should be drawn. The slope from the initial displacement (0,0) to the yield point in the skeleton curve is the initial stiffness. For each specimens of test and analysis the initial stiffness is calculated from the hysteresis reponses.

The initial stiffness (elastic stiffness) of the link might be analytically computed using basic concepts of beam elastic mechanics. The second-order axial force developing as a consequence of the shear deformation is considered negligible in the elastic range of response. The elastic stiffness can be calculated using Eq. (4.2) - Eq. (4.3).

The initial stiffness calculated from the hysteresis response of test, analysis and using Eqs. (5.8-5.9) are summarized in Table 5.2. As shown in the Table, the calculated initial stiffness is greater than the initial stiffness of test and analysis results. The comparison have been made by normalizing the test and analysis initial stiffness by the calculated values and the results are shown in the Table as well as in the Fig. 5.15(a) and Fig. 5.15(b). The value ranges from 0.82-.089 and 0.85-0.99 for test and analysis respectively.

The ratio of test and analysis result initial stiffness is also computed and presented in the Table 5.2 and Fig. 5.15 (c). As shown the plotted figure, the ratio is less than unity which indicates that the initial stiffness of analysis result is some how greater than the initial stiffness of test results. The value ranges from 0.88-0.99.

Table 5.2 Summary of Initial Stiffness of Test, Analysis and Calculated

Spe. ID	Test (K_T)	Analysis (K_A)	Calculated (K_C)	K_T/K_C	K_A/K_C	K_T/K_A	Yield Rotation Angle $\left[\frac{V}{eK_C}\right]$
RWS-S10S1	197956.3	201625.4	223048.09	0.89	0.90	0.94	0.00284
RWS-U10S1	186404.2	189560.0	223048.09	0.84	0.85	0.99	0.00284
RWS-U15S1	170059.7	175541.2	203639.08	0.85	0.86	0.99	0.00281
RWS-U10Sf1	99073.00	109563.7	118549.14	0.84	0.92	0.90	0.00341
RWS-S10Sf1	90012.32	110001.0	118549.14	0.82	0.93	0.88	0.00341
RWS-S10Sf2	90125.41	100412.4	101753.92	0.84	0.89	0.90	0.00348
RLS-U10Sf1	98021.23	109577.2	112235.92	0.87	0.98	0.98	0.00349
RLS-S10Sf1	98259.71	103059.7	112235.92	0.87	0.92	0.92	0.00349
RLS-S10Sf2	90525.01	100412.6	107136.29	0.89	0.99	0.89	0.00330

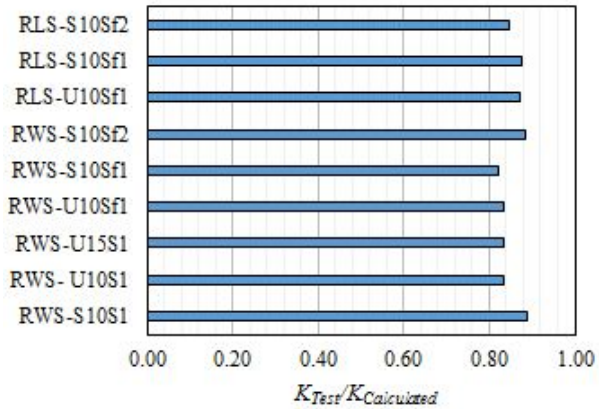

(a) Comparison of normalized initial stiffness of test results by calculated elastic stiffness

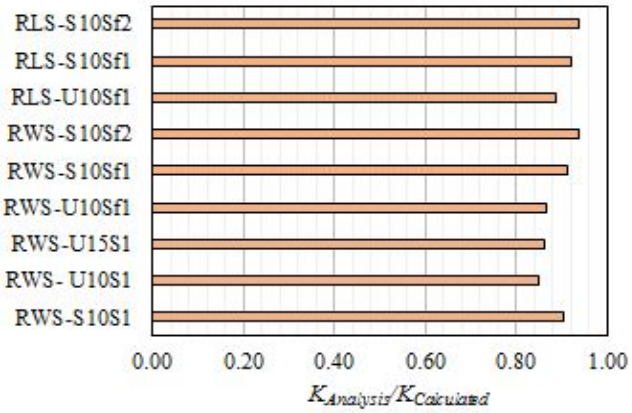

(b) Comparison of normalized initial stiffness of analysis results by calculated elastic stiffness

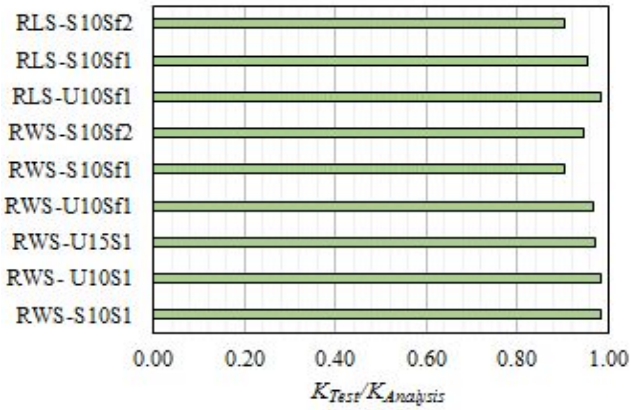

(c) Comparison of initial stiffness of test results and analysis results

Fig. 5.15 Comparison of initial stiffness

5.3.3 Comparison of Plastic Rotations

The plastic rotation capacity is the main requirements in the design of links in eccentrically braced frames. The AISC Seismic Provisions evaluate the performance of the link in terms of the inelastic component of the plastic rotation angle, γ_p. Link plastic rotation is the link total rotation minus the elastic link rotation, which is the link shear force at a given total rotation divided by the elastic link stiffness as expressed in Eq. (4.1). In equations (4.2) and (4.3), the formulas used to calculate the elastic rotation was also defined.

The other question is how the total link rotation is decided in the first place. For experimental results, the total link rotation is taken at the point where the strength degrades and becomes less than the nominal shear strength or yield strength. The same approaches can be used for finite element analysis as well. However, in some cases the hysteresis response of analysis results keeps increase even at large displacement. In this case the method stated above can't be applied to limit the total shear rotation. Thus, another method should be used. Therefore, a number of different stress, strain and combined stress/strain indices are computed. These indices includes: stress triaxial ratio, PEEQ index, rupture index and failure index. These indexes are also used to evaluate the crack susceptibility i. e fracture in steel components correlates with the triaxial stress state and the plastic strain. Hence, the point at which the cracks started in analysis model will be taken as a total link rotation (γ). Recent analytical studies of steel frame components have used a low cycle fatigue failure index based on a stress modified critical strain criterion. The failure in numerical simulation can also be predicted by the failure index in addition to the strength reduction in hysteresis response. *A. M. Kanvinde et al., 2004, 2006, 2007, 2008* established an equation to predict fracture based on microscopic triaxial stress and plastic strain values. Further, *El-Tawil et al. 1999, 2000* propose a rupture index that is a function of the triaxial stress and plastic strain to investigate fracture in steel beam-to-column connections. In this study this concept was implemented for links.

5.3.3.1 Failure Index (FI)

The failure index is defined by the triaxiality of the stress field and the accumulated plastic strain in tension and compression (*Hancock J.W. et al., 1976, McClintock F. A. et al., 1968*). The objective function is the dissipated energy before failure of the developed links. The ductility capacity of the reduced link is defined using failure index as follows.

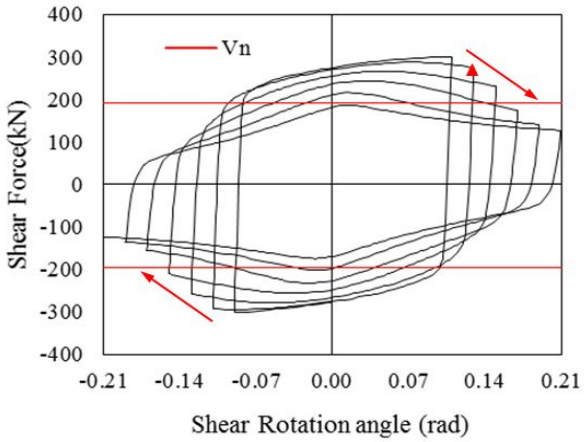

Fig. 5.16 Examples of total shear rotation calculation for RWS-U10S1 analysis specimen

The variables, which are functions of pseudo-time, such as stresses and strains are evaluated at integrated maximum possible point. Let εp(t) denote the equivalent plastic strain defined as:

$$\varepsilon_p(t) = \int_0^t \dot{\varepsilon}_{ij}^p(t)\dot{\varepsilon}_{ij}^p(t)dt \qquad \text{.....(5.8)}$$

where $\varepsilon_{ij}^p(t)$ is the plastic strain tensor, ($\dot{}$) is the derivative with respect to time, and the summation convention is used. The equivalent plastic strain represents amount of plastic deformation in material level, and is evaluated at each integration point. Many fracture criteria have been presented using εp(t). We use an extended version of the SMCS criterion that was developed for simulating ductile fracture of metals due to void growth. The critical plastic strain εcr is first defined as:

$$\varepsilon^{cr} = \alpha \exp -1.5\frac{\sigma_m}{\sigma_{eq}} \qquad \text{.....(5.9)}$$

where σm is the mean stress, and σe is the vonMises equivalent stress given by equation (5.10) and (5.11), respectively. The parameter α is dependent on material. Equation (5.9) indicates that the critical plastic strain for ductile fracture depends on the stress triaxiality σm/σe which is taken Then the failure index for monotonic loading is defined as in equation (5.12) (C.S. Oh et al., 2011).

$$\sigma_m = \frac{\sigma_1 + \sigma_2 + \sigma_3}{3} \quad \text{.....(5.10)}$$

$$\sigma_e = \sqrt{\frac{1}{2}\left[(\sigma_1 - \sigma_2)^2 + (\sigma_1 - \sigma_3)^2 + (\sigma_3 - \sigma_2)^2\right]} \quad \text{.....(5.11)}$$

$$I_f = \frac{\varepsilon_p}{\varepsilon^{cr}} \quad \text{.....(5.12)}$$

The material is assumed to fracture when If reaches 1.0. The equation (5.9) and (5.12) are based on the ductile fracture due to void growth under monotonic tensile deformation. However, we need the effect under cyclic loading, where the void shrinks due to compressive plastic loading. Therefore, the following formulation by Kanvinde and Deierlein is used [Chi W.M. et al., 2006, Mackenzie A. et al., 1977). The equivalent plastic strain εp is divided into tensile plastic loading states εt(>0) and compressive plastic loading states εc(>0), which are identified by the sign of σm. The critical plastic strain ε*, which represents the amount of void growth, is defined as (M. Ohsaki et al., 2012):

$$\varepsilon^* = \varepsilon_t - \varepsilon_c \quad \text{.....(5.13)}$$

The critical value εcr* for ε* is given as:

$$\varepsilon^{cr*} = \exp(-\lambda\varepsilon_p)\varepsilon^{cr} \quad \text{.....(5.14)}$$

where λ is a positive material parameter and according to Kanvinde and Deierlein the parameter λ for the failure index may vary between 2.5 and 8.0. In the following, an intermediate value 4.3 is used for λ. Ductile fracture is assumed to occur when the cyclic failure index If* defined as follows reaches1.0:

$$I_f^* = \frac{\varepsilon^*}{\varepsilon^{cr*}} \quad \text{.....(5.15)}$$

Taking the stable hysteresis curve among the finite element simulation results obtained above, which is RWS-S10S1, the failure index calculated is plotted as in Fig. 5.17(a). The failure index reaches one at 41st cycle. The corresponding shear rotation can be found from the loading history input as shown in Fig. 5.17 (b). Thus the shear rotation at the 41st cycle is approximately 0.1602 rad. The point at which the shear rotation reaches in hysteresis curve of RWS-S10S1 specimen is shown in Fig. 5.17 (c). Hence, even though the hysteresis curve remain stable the specimen is assumed to be failed at 0.1602 rad and the total shear rotation was taken as 0.1602 rad for this specific analysis specimen.

The calculated plastic shear rotation of test and analysis is summarized in Table 5.3. The plastic shear rotation summarized in Table 5.3 is plotted in Fig. 5.18. As shown in the Fig. 5.18, the plastic shear rotation of analysis and test results well matched for both stiffened and unstiffened specimens.

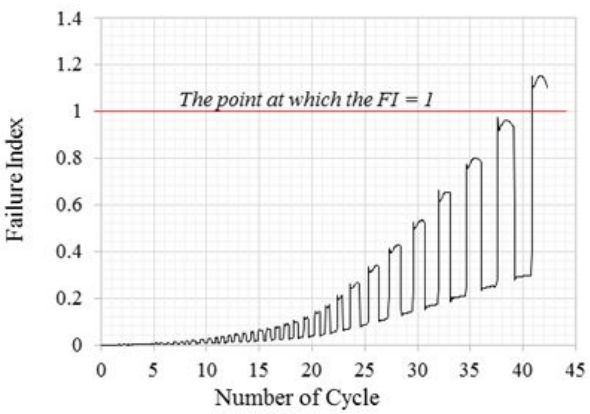

(a) the failure index and number of cycle relationship for RWS-S10S1 analysis specimen

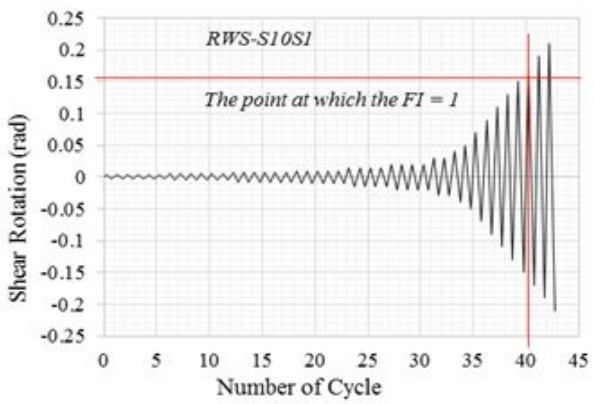

(b) the loading history input of analysis

Fig. 5.17 Failure index of analysis specimen RWS-S10S1

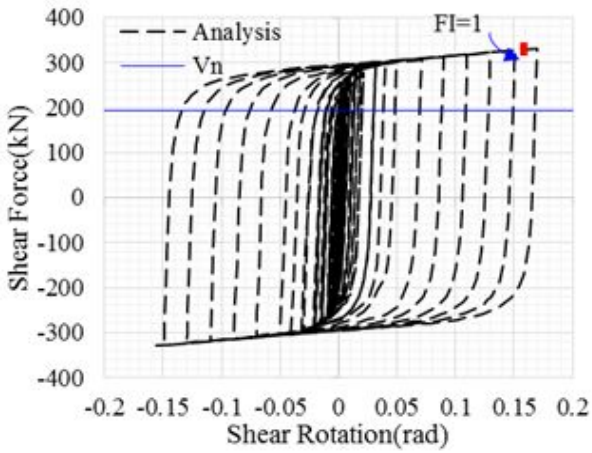

(c) the point at which the failure index reached one in the hysteresis response

Fig. 5.17 Failure index of analysis specimen RWS-S10S1 *(continue...)*

Table 5.3 Summary of analysis and test plastic rotation capacity

Section ID	ρ	γ_T	γ_y	Test			Analysis		
				Recorded Rotation	plastic rotation		Rotation @ FI=1 and/or at strength degradation	plastic rotation	
					Stiffened	Un-stiffened		Stiffened	Unstiffened
RWS-S10S1	1.1	0.08	.00284	0.1503	0.1474		0.15652	0.154	
RWS-U10S1	1.1	0.08	.00284	0.1296		0.1268	0.1250		0.1222
RWS-U15S1	1	0.08	.00281	0.1274		0.1246	0.1230		0.1202
RWS-U10Sf1	1.5	0.08	.00341	0.1075		0.1002	0.1192		0.1166
RWS-S10Sf1	1.5	0.08	.00341	0.1500	0.1466		0.1450	0.142	
RWS-S10Sf2	1.3	0.08	.00348	0.1260	0.1225		0.1326	0.129	
RLS-U10Sf1	2.3	0.038	.00349	0.1247		0.1212	0.1260		0.1225
RLS-S10Sf1	2.3	0.038	.00349	0.1523	0.1488		0.1506	0.147	
RLS-S10Sf2	2	0.056	.00330	0.1508	0.1475		0.1485	0.145	

N.B. γ_T *and* γ_y *are stands for target plastic rotation and yield (elastic) rotation respectively.*

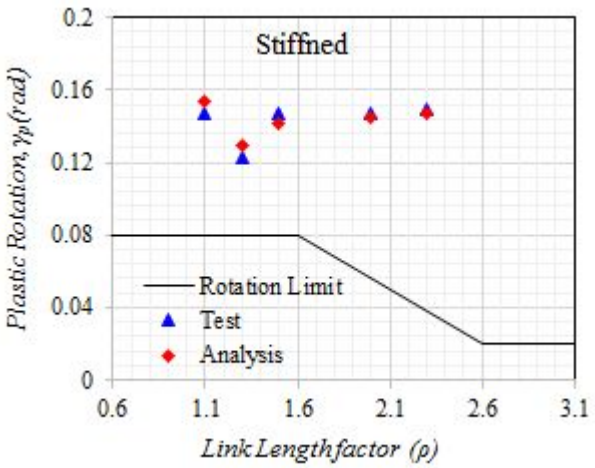

(a) Comparison of plastic rotation of stiffened test and analysis results

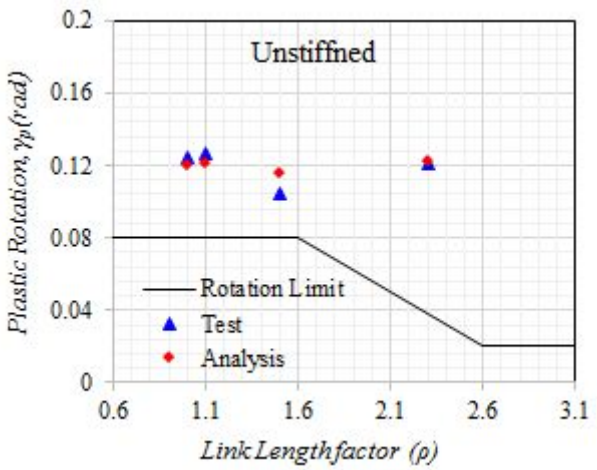

(b) Comparison of plastic rotation of unstiffened test and analysis results

Fig. 5.18 Plastic rotation capacity versus link length factors

5.3.4 Overstrength Factor (Ω)

The overstrength factor has been discussed in section 4.4.2 that it is an important variable to realize the capacity design approach in which a strength hierarchy is established within a structure so that some ductile "primary" "protected" elements are discouraged from yielding. The overstrength (Ω) factor is also called the strain hardening by some researcher because it is primarily due to stain hardening. A yielding points of links exhibited during the first to third displacement amplitude of cyclic loading and the shear resistance during the final cycle is very greater than the yield value due to strain hardening. The difference in strength at yielding and at maximum shear force is the overstrength factor or It is the ratio of maximum shear force to plastic shear strength as defined in Eq. (4.4).

The calculated overstrength factor for analysis and test results are presented in Table 5.4 for both stiffened and unstiffened specimens. As it has been discussed in Section 4, sub-section 4.4.2, different test data for link shows different values for overstrength factor. The values presented in Table 5.4, was plotted and compared with the overstrength factor defined by Richard and Uang and presented in Fig. 5.19. As shown in the plotted Fig. 5.19, the overstrength factor of analysis and test agrees well and the values are all greater than 1.5 and greater than the overstrength factor recommended by Richard and Uang.

The equations of overstrength factor by Richard and Uang can be applied for the overstrength factor of test result presented in Section 4. Here the overstrength factor test and analysis was compared along with the curves drawn by the equation suggested by Richard and Uang as shown in Fig. 5.19. As shown in the figure, the overstrength factor of stiffened section is greater than the overstrength factor of unstiffened link sections. The oversterngth factor of both analysis and test results of both stiffened and unstiffened links are bigger than the overstregth factor recommended by Richard and Uang defined in Eq (4.5).

The question that "why the value of overstrength is large?" has been raised by researchers. It was suspected that the substantially larger overstrength in very short shear links had two causes. The first cause is the shear resistance of flanges (*Itani et al. 2002 Richards et al. 2004*). The second is the cyclic hardening effect of web steel under large inelastic strains (*Kasai et al. 2004*). Yielding and energy dissipation occur primarily in the links and the hysteric energy is absorbed through the process of strain hardening. Strain-hardened links have higher capacity and thus develop higher forces. The forces developed in links that strain-hardened can vary significantly (*J. P. Vemuri 2015*)

Table 5.4 Comparison on overstrength factor of Analysis and Test results

Spe. ID	ρ	V_p (kN)	Test			Analysis		
			V_{max} (kN)	$\Omega = \frac{V_{max}}{V_p}$		V_{max} (kN)	$\Omega = \frac{V_{max}}{V_p}$	
				Stiffened	Unstiffened		Stiffened	Unstiffened
RWS-S10S1	1.1	193.4	332.91	1.722		351.06	1.815	
RWS-U10S1	1.1	193.4	317.67		1.643	302.24		1.563
RWS-U15S1	1	174.7	282.81		1.619	284.53		1.63
RWS-U10Sf1	1.5	205.9	300.46		1.46	302.24		1.468
RWS-S10Sf1	1.5	205.9	342.80	1.665		341.9	1.661	
RWS-S10Sf2	1.3	180.2	276.03	1.532		267.03	1.482	
RLS-U10Sf1	2.3	205.9	311.1		1.511	307.44		1.493
RLS-S10Sf1	2.3	205.9	346.1	1.681		340.43	1.653	
RLS-S10Sf2	2	180.2	285.9	1.587		291.94	1.620	

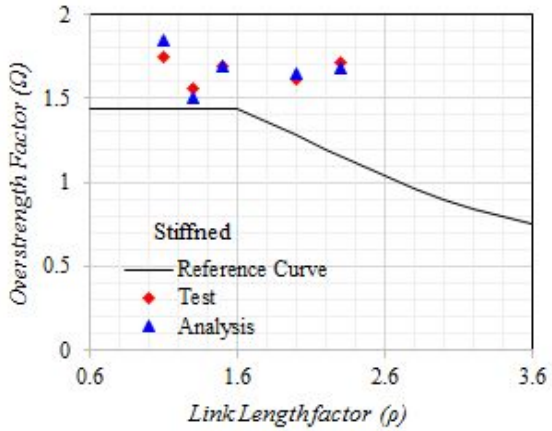

(a) comparison of overstrength factor versus link length factor for stiffened links

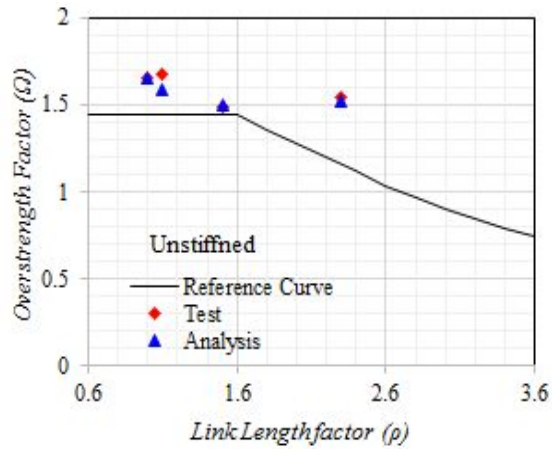

(b) comparison of overstrength factor versus link length factor for unstiffened links

Fig. 5.19 Comparison of test and analysis result of overstrength factor versus link length factor

5.4 Summary

Non-linear finite element simulation model was created using Abaqus software. The results were compared with the test results for verification and calibration purpose. From the obtained result, the following summaries were drawn.

Both the hysteresis response and the deformed shape of analysis and test results were compared. From the hysteresis response, it is noted that the experimental results shows an expansion as the amplitude increases compared to analysis results. However, the maximum shear force resisting capacity of both results well agreed even though some mis matching was noticed expecially at the bouncing. This might be one, the errors during loading test and second it needs to conduct cyclic coupon test and use for analysis material modeling in order to address the limitation observed.

From the comparison of deformed shape of test and analysis results with equivalent plastic strain distribution, the strain concentration as well as the maximum strain was created at the edge of holes on the web. which is actually an indication of the cracks and finally the fracture is occurred at the location where the maximum equivalent plastic strain was created. For specimens that the failure index was calculated, failure index reached one early when the index is considered at the edge of the holes where the equivalent plastic strain is maximum. Even though the hysteresis response shows some mismatching, the plastic shear rotation capacity of test and analysis agreed well.

The initial stiffness of test and analysis were also compared and the ratio is found to be between 0.89-0.99 which is quit satisfactory. However the calculated initial (elastic) stiffness is higher than both test and analysis initial stiffness where the ratio initial stiffness of test to calculated ranges from 0.82-0.89 and the ratio initial stiffness of analysis to calculated ranges from 0.85-0.99. The overstrength calculated for stiffened and unstiffened specimens for both test and analysis well agreed because the maximum shear resisting capacity of analysis and test is equal.

6. Parametric Study on Reduced Link Section

6.1 General

After verifying the analysis results through experimental investigation, parametric studies were conducted. The objectives of parametric study were to investigate the effects of other variables which were not considered in the experimental program and to aid in the development of further investigation and advantage of the proposed reduced link section.

The variables considered in evaluation of links in eccentrically braced frames includes: the section compactness, link length, loading condition (loading protocol), stiffeners and connection types (Jeffrey W. Berman et al., 2006, Richards P. et al., 2003, 2006). For reduced link section there are extra parameters which needs to be considered such as percent of open area or percent of reduced section, the arrangements of the perforations on the web and the type of flange reductions. Therefore, in this study the following parameters were considered.

1. Link length factor
2. Percent of reduced web area
3. Stiffeners
4. Un equal end moment (link-to-column connection)

In this chapter the effect of the above variables on reduced link section were presented. Nonlinear finite element analysis were conducted in order to evaluate these variables. The effects are presented in terms of hysteresis characteristics, plastic deformation capacity and stress and strain distribution.

6.2 Link length Factor

Literatures and available standards state that the behavior of link beam can be classified in to three depending on the link length or link length factor. Short link beams with link length factor of $\rho \leq 1.6$, intermediate link beam with link length factor between $1.6 < \rho < 2.6$ and long link beams with link length factor $\rho \geq 2.6$. The link length factor is the dimensionless value defined as: $\rho = \frac{e}{M_p / V_p}$ where e: is the link length, M_p: is the bending moment, V_p: is nominal shear strength. The plastic rotation capacity depending on the link length factor according to AISC seismic provision and the relationship of link length factor and plastic rotation capacity is summarized in Fig. 6.1.

For parametric study link length factor of all type was considered. The analysis specimen detail for parametric study is shown in Table 6.1. The length factors considered are: for shear link ρ = 0.8, 1.0, 1.2, 1.6 are used and for intermediate link, ρ = 2.0, 2.3 and for flexural yielding type ρ = 2.6, 3.0. Codes have been given for each link type used. For shear links with link length factor of ρ = 0.8, 1.0, 1.2, 1.6, the specimen code is S1, S2, S3 and S4 respectively. For intermediate links with ρ = 2.6, 3.0, the specimen code is Sf1 and Sf2 respectively. Similarly for flexural links with ρ = 2.0, 2.3, the specimen code is F1 and F2 respectively. Researches shows that the inelastic behavior of a link is significantly influenced by its length. The shorter the link length, the greater the influence of shear forces on the inelastic performance. Shear yielding tends to happen uniformly along the link. Shear yielding is very ductile with an inelastic capacity considerably in excess of that predicted by the web shear area, provided the web is adequately braced against buckling.

The same analysis procedures used in the previous chapter 5 were followed for investigating the parameters except the link-to-column connections. Where shell model was used for all components of links. However to take in to account the effect of connection type, mainly the link-to-column connection, the modeling and boundary conditions are different.

The detail of analysis specimens are presented in Table 6.1, including the section property and section compact of flange and web used for the parametric study was $\frac{b}{t_f}$=9, $\frac{d}{t_w}$=23. The plastic shear strength and plastic end moment calculated using the derived equations are also presented in the table.

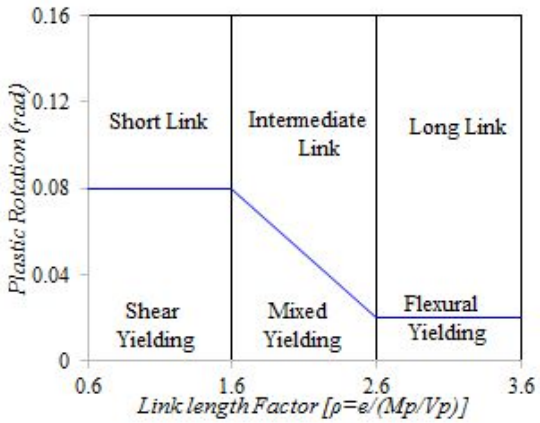

Fig. 6.1 Plastic Rotation Limit of Links in EBFs (AISC Recommendation)

Table 6.1 Analysis specimen section and link type detail for parametric study

Link Section Behavior					ρ							
Flange	Web	Section Capacity			0.8	1	1.2	1.6	2	2.3	2.6	3
$\frac{b}{t_f}$	$\frac{d}{t_w}$	V_p (kN)	M_p (kNm)	$\frac{M_p}{V_p}$(m)	Link length e (mm)							
9	23	206	60	0.38	306	382	458	611	764	878	988	1146
Link ID					S1	S2	S3	S4	Sf1	Sf2	F1	F2

N. B. the symbols used in the tables are: S: shear yielding, Sf: shear and flexural yielding and F: flexural yielding link

Table 6.2 Analysis specimen detail reduced link length amount of diameter of reduction for parametric study

% reduced web area	ρ	0.8	1	1.2	1.6	2	2.3	2.6	3.0	ID	
	ϕ (mm)	link length (mm)								Stiffened	Unstiffened
0	0	306	382	458	611	764	878	988	1064	Ss	Us
5%	19	342	427	511	682	853	980	1103	1188	S5	U5
10%	25	422	527	631	842	1053	1211	1362	1467	S10	U10
15%	34	489	610	731	975	1220	1402	1577	1699	S15	U15
20%	38	525	656	786	1049	1312	1508	1696	1827	S20	U20
25%	42	568	709	851	1135	1419	1631	1835	1976	S25	U25
		S1	S2	S3	S4	Sf1	Sf2	F1	F2		

N. B. the symbols used in the tables are: Ss, S5, S10, S15, S20, S25 and Un, U5, U10, U15, U20, U25: stiffened and unstiffened links with unreduced, 5%, 10%, 15%, 20% and 25% reduced link

6.2.1 Hysteresis response of FE analysis result on the effect of link length factor (ρ)

The hysteresis response on link length factor is shown in Fig. 6.2. In order to capture only the effect of link length factor, the reduced web area were taken constant which is 10% for both stiffened and unstiffened links. The hysteresis responses presented in Fig. 6.2 for all link length factors considered for both stiffened and unstiffened sections. As shown in the Fig. 6.2, pretty clear hysteresis response was obtained that states the effect of link length on the plastic deformation capacity of perforated links. The shear resistance decreases as the link length factor increases at large link rotation increases.

Compared to unstiffened link section, the hysteresis response of stiffened links shows stable for shear links. As the link length increase stiffeners have no significant effect. The shear resisting capacity of ustiffened links degrade earlier than stiffened links and forms a kind of pinching at initial rotation (deformation). This phenomenon is usually due to an out-of-plane buckling of web and local buckling of flanges. The stiffeners keeps the web from out-of-plane buckling. Local buckling of flanges was observed at both ends of links which is usually the compressive forces occurred due to the bending moments while the links deforms at large in the shear forces applied on the analysis specimens. The stiffeners had almost no effect on the elastic or inelastic prebuckling behaviour of all link types.

The pinching was occurred in both stiffened and unstiffened links but the severity is high in unstiffened links and as link length factor increase the pinching effect is also increases. The shear force resistance of flexural links decreases quite early compared to shear links. The rate at which the strength degradation occurred increases with an increase of link length factor.

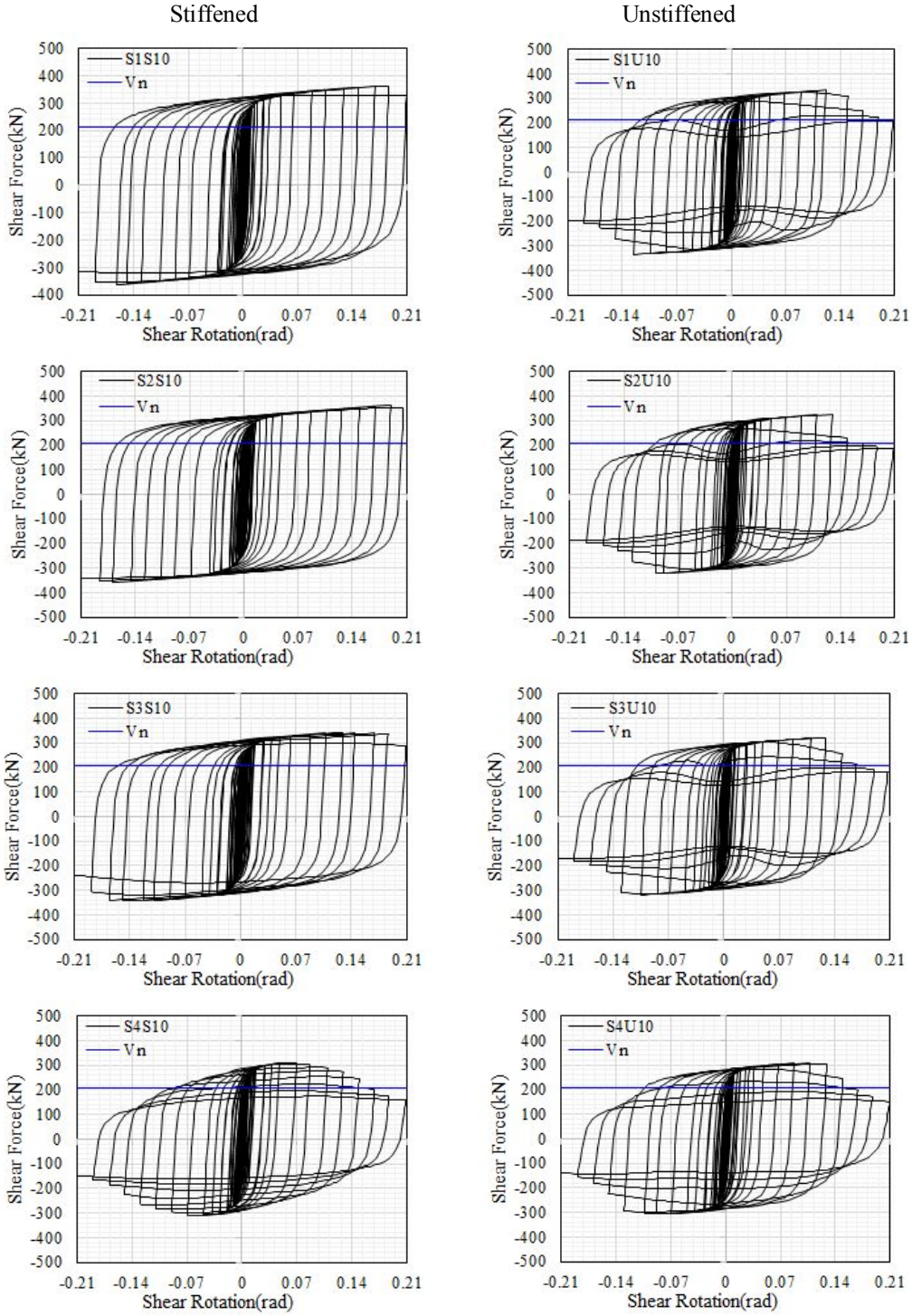

Fig. 6.2 Hysteresis response of parametric study on the effect of link length factor

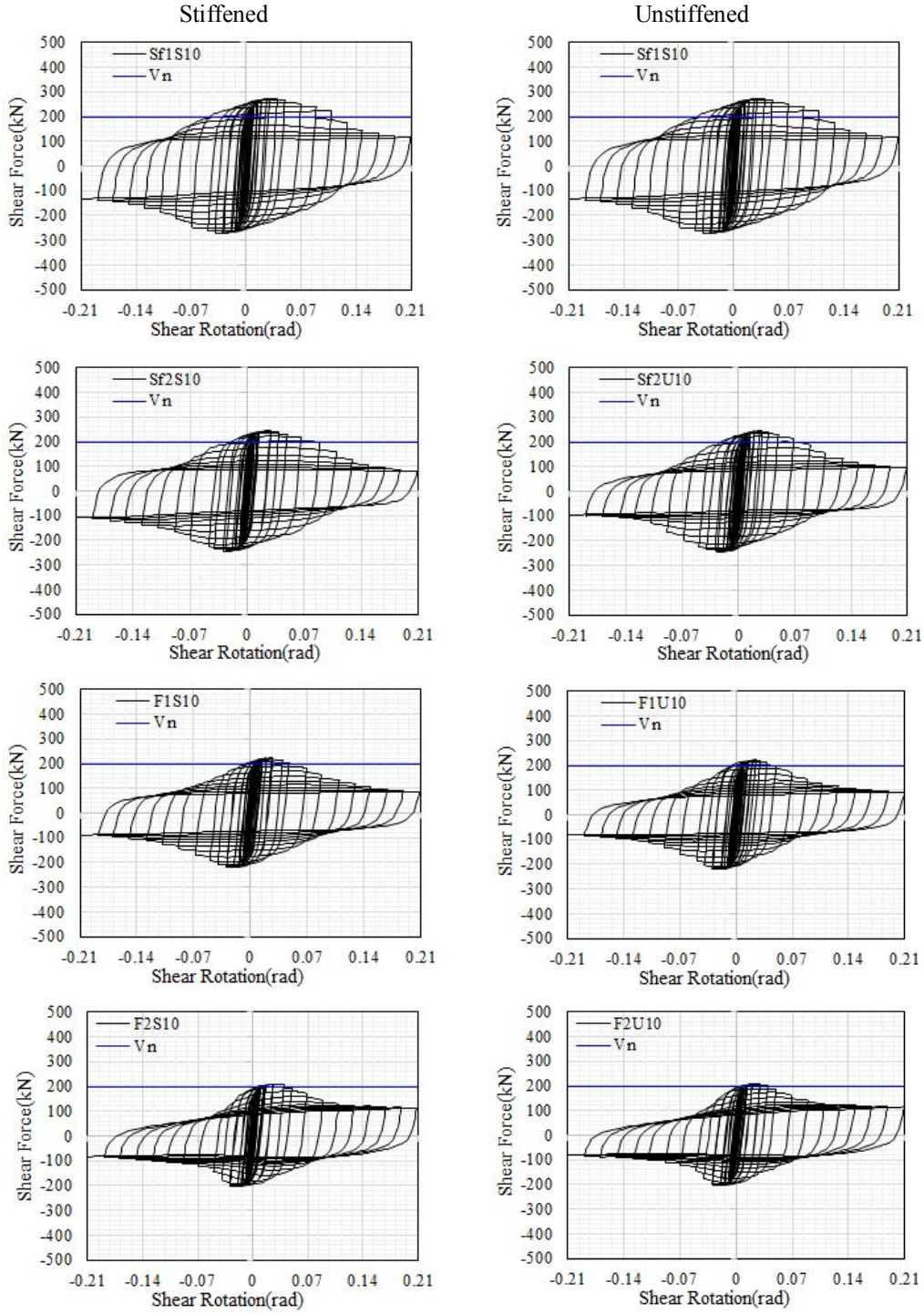

Fig. 6.2 Hysteresis response of parametric study on the effect of link length factor *(Continued)*

6.2.2 Plastic rotation capacity, Overstrength factor and Initial stiffness of FE analysis result considering link length factor (ρ)

The plastic rotation capacity (γ_p) of analysis specimen for 10% reduced web area considering link length factor is shown in Fig. 6.3 calculated using $\gamma_p = \gamma - \frac{V}{eK_e}$, where γ: is the total shear rotation, V: plastic shear strength, K_e: elastic stiffness calculated using *Eqs. [(4.1)-(4.3)]* and e: link length (both reduced and unreduced link length). The total link rotation for the parametric study was decided by the same procedure used in Chapter 5 where the point at which the shear resisting capacity degrades and/or for analyses specimens that were stable even at large displacement failure indexes were calculated and the total link rotation is taken at the point where the failure index reached unity. The plastic rotation calculated for the hysteresis response presented in Fig. 6.2 is presented in Fig. 6.7 (c). As shown in the figure, the plastic rotation of shear links of both stiffened and unstiffened links satisfy the rotation limit recommended in the AISC provision-2010. Stiffened link section shows bigger plastic rotation capacity compared to unstiffened links. The plastic rotation limit of an intermediate links with 10% reduced web area are also satisfied the rotation limit recommended in the AISC provision-2010 for both stiffened and unstiffened links. However, flexural links fail to satisfy the plastic rotation limit recommended in the AISC provision-2010 as shown in the figure.

The overstrength factor calculated for the hysteresis responses presented in Fig. 6.2 is shown in Fig. 6.8 (c) for stiffened and unstiffened link section. The calculated overstrength factor calculated was compared with the overstrength factor equation suggested by Richard and Uang in 2009 expressed in Eq. (4.5). As shown in the Fig. 6.8 (c), the overstrength factor varies with link length factor and the values ranges from 1.57-1.12.

Fig. 6.3 shows the initial stiffness of analysis specimens for stiffened, unstiffened and calculated with respect to link length factor for 10% reduced web area presented in Fig. 6.2. As shown in the figure, the initial stiffness decreases as the link length increases for all cases, stiffened, unstiffened and for calculated initial stiffness. Initial stiffness decreases with respect to link length factor and the rate at which the initial stiffness decreases is exponentially.

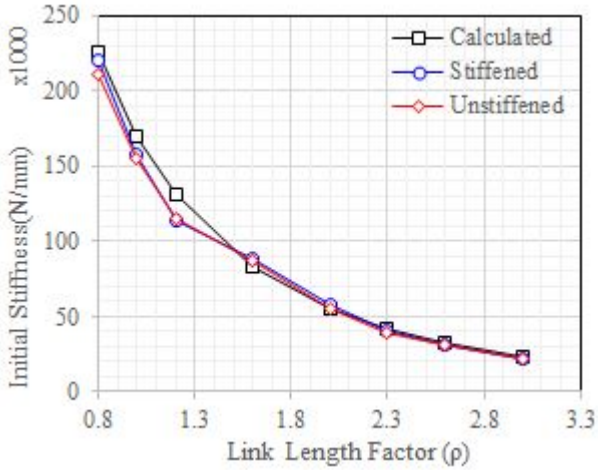

(a) Comparison of initial stiffness of stiffnned and unstiffened links with 10% reduced web area

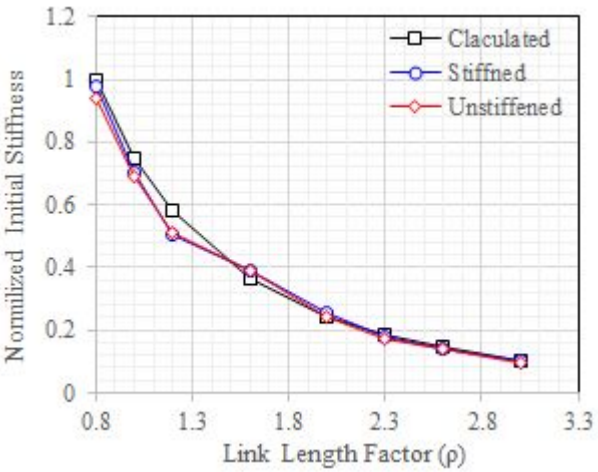

(b) Comparison of normalized initial stiffness by calculated initial stiffness of S1

Fig. 6.3 Comparison of initial stiffness of 10% reduced web area

6.3 Percent of reduced web area

The diameter of openings on the web significantly affects the shear strength of link. The plastic rotation angle can also be affected some how by the percent of open areas on the web. In order to evaluate the effect of percent of reduced web area, 0%-25% reduced web area on all types of links were considered for the analysis specimens details presented in Table 6.1 and 6.2. The percent of reduced web area is calculated using Eq. (6.1) in terms of diameter of holes and number of holes.

Six different percent of reduced web sections have been used (0%, 5%, 10%, 15%, 20% and 25%). The effects of each of the % of reduced web area are discussed here under.

$$\%\, of\, reduced\, web\, area = \frac{n\pi\phi^2}{4e_{rw}.d} \qquad \text{.....(6.1)}$$

where n: is total number of holes (perforations), ϕ: is the diameter of holes, e_{rw}: is the length of reduced web and d: is the depth of link.

6.3.1 Results on the effect of percent of reduced web area

6.3.1.1 Effect of percent of reduced web area on hysteresis response and initial stiffness

In order to identify the effect of percent of reduced web area on the hysteresis response, the hysteresis response of analysis specimen S2 was presented here for illustration. The hysteresis response of S2 analysis specimen, the hysteresis curve is presented in Fig. 6.4 for 0% to 25% reduced web area for stiffened and unstiffened links. As shown in Fig. 6.4, the hysteresis response of stiffened links shows stable compared to unstiffened link. Comparing stiffened unreduced and reduced link, the hysteresis response of reduced link is stable at large deformation. For unstiffened link, the hysteresis response is the similar for unreduced and reduced links. In both stiffened and unstiffened links, the second stiffness is less compared reduced link sections.

The maximum shear forces of the corresponding unstiffened and stiffened links of S2 analysis specimen is presented in Fig. 6.5 (a, b). As shown in the Fig. 6.5 (a, b), the maximum shear forces decreases as the percent of reduced web area increases. The maximum shear forces were normalized by the maximum shear forces of unreduced links of stiffened and unstiffened and presented in Fig. 6.5 (c, d) in order to see the rate at which the maximum shear forces are decreased. As shown in the Fig. 6.6 (c, d), the maximum shear forces decreases in high rate compared to flexural links for both stiffened and unstiffened.

The effect of percent of reduced web area on the initial stiffness of all types of specimens has been calculated and presented in Fig. 6.6 (a). As shown in the Fig. 6.6 (a), the initial stiffness decreases as the link length factor and the percent of reduced web area increases. The rate at which the initial stiffness decreases as the percent of reduced web area increases is low as the link length factor increases i.e the initial stiffness of S1 decreases rapidly as the percent of reduced web area increase compared to initial stiffness of S2, S3 and other specimen as shown the normalized initial stiffness presented in Fig. 6.6(b). The rate at which the initial stiffness of F2 decreases as the percent of reduced web area increase is smaller compared to other analysis specimens. The initial stiffness was normalized by the calculated initial stiffness of unreduced links.

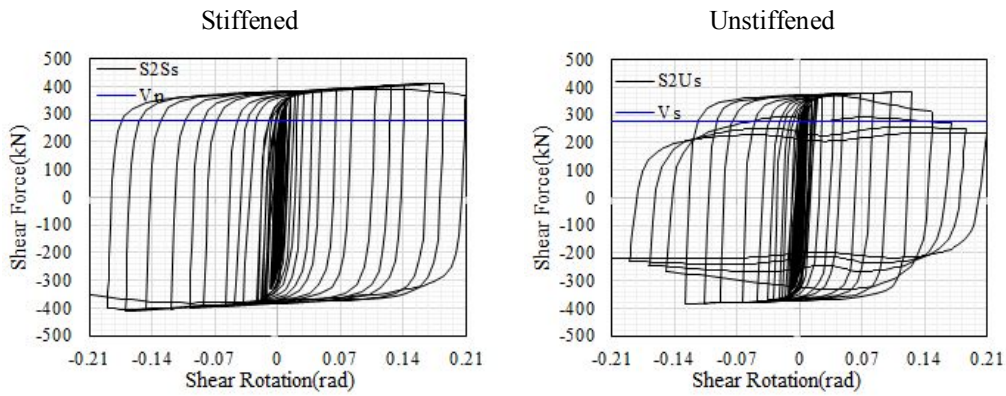

Fig. 6.4 Hysteresis response of S2 analysis specimen with different percent of reduced web area

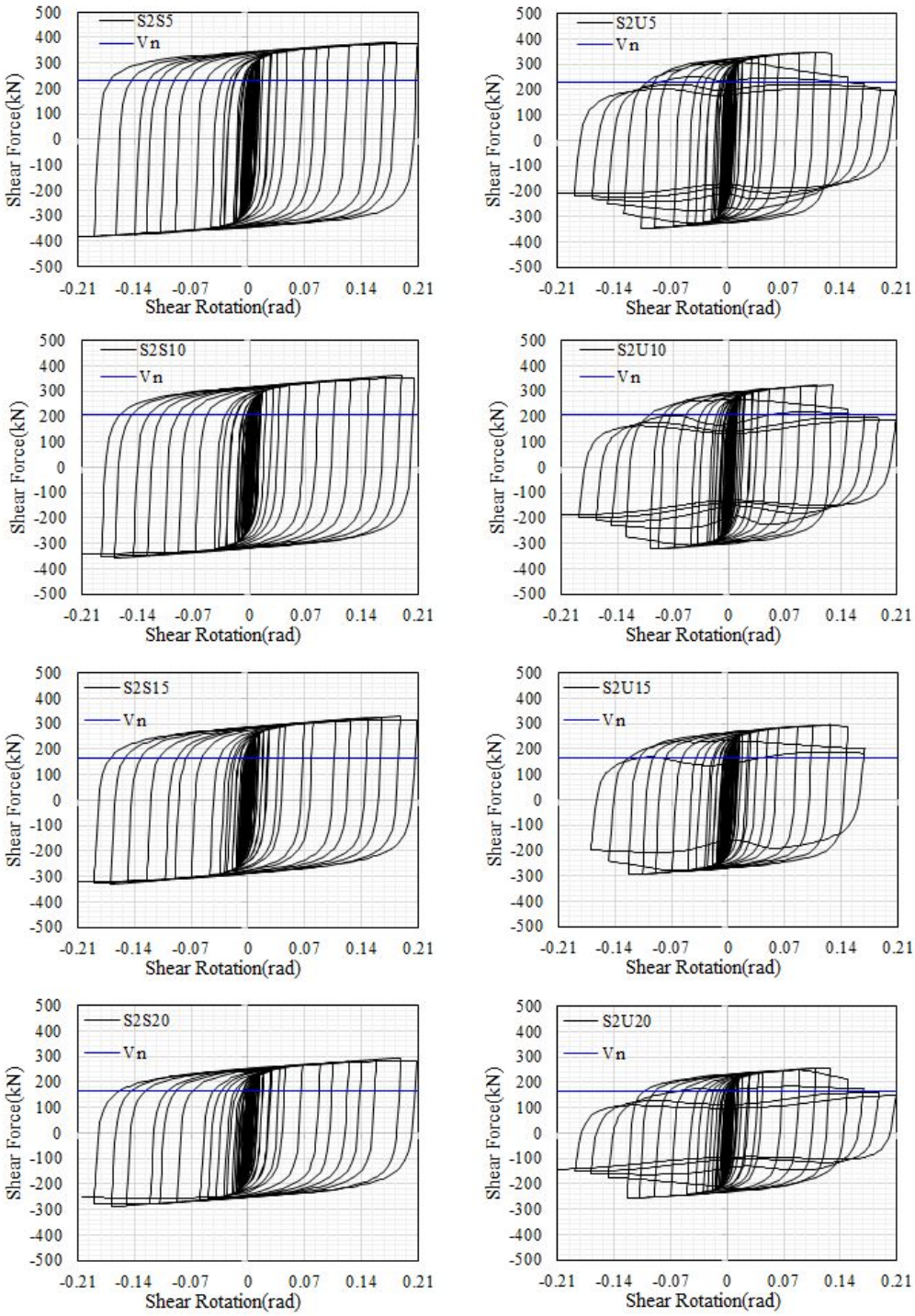

Fig. 6.4 Hysteresis response of S2 analysis specimen with different percent of reduced web area *(Continued...)*

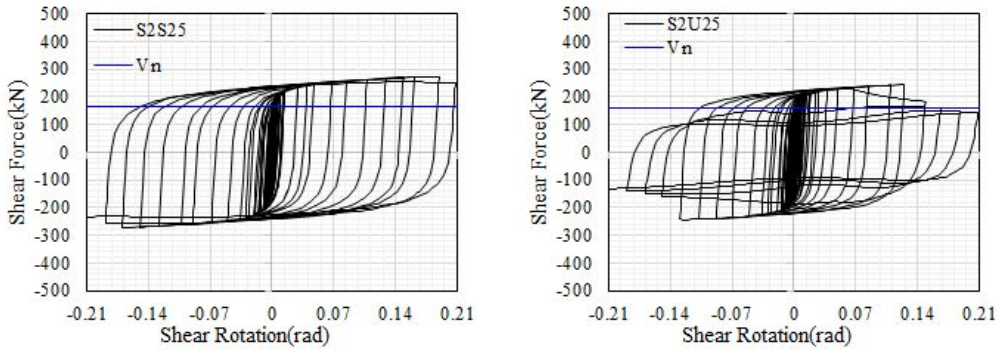

Fig. 6.4 Hysteresis response of S2 analysis specimen with different percent of reduced web area *(Continued...)*

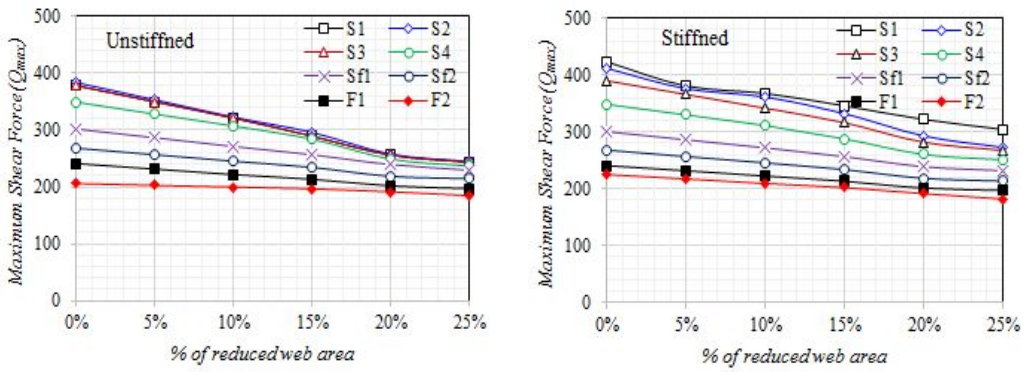

(a) maximum shear forces measured of unstiffened link

(b) maximum shear forces measured for stiffened links

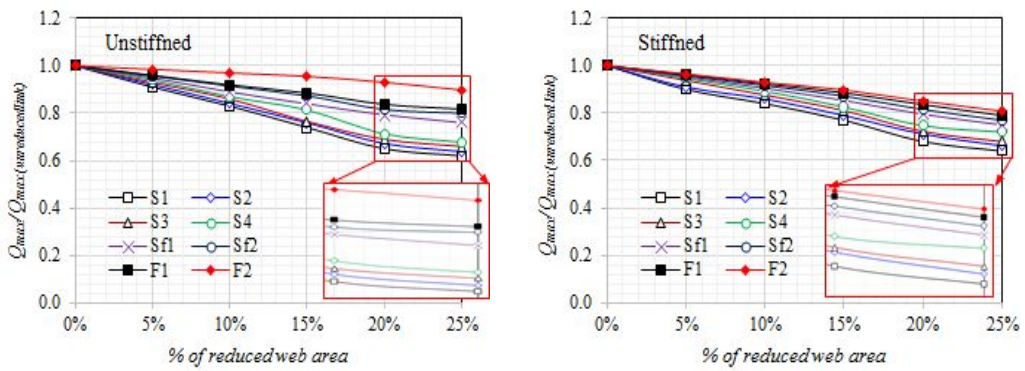

(c) normalized maximum shear by the maximum shear force of normal links for unstiffened links

(d) normalized maximum shear by the maximum shear force of normal links for stiffened links

Fig. 6.5 Measured maximum shear force versus percent of reduced web area

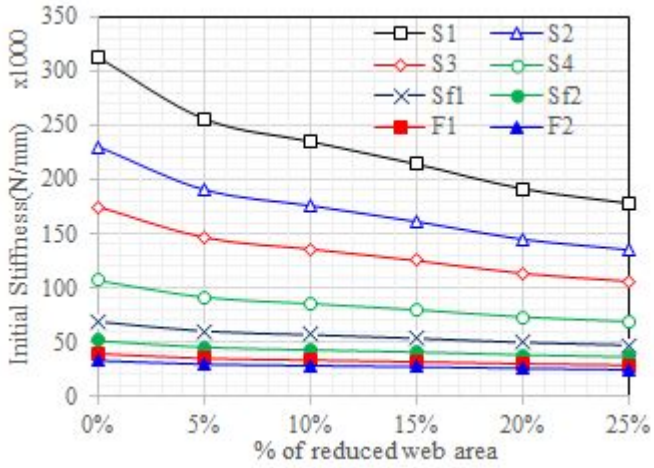

(a) Comparison of initial stiffness of unstiffened analysis specimens with different percent of reduced web area

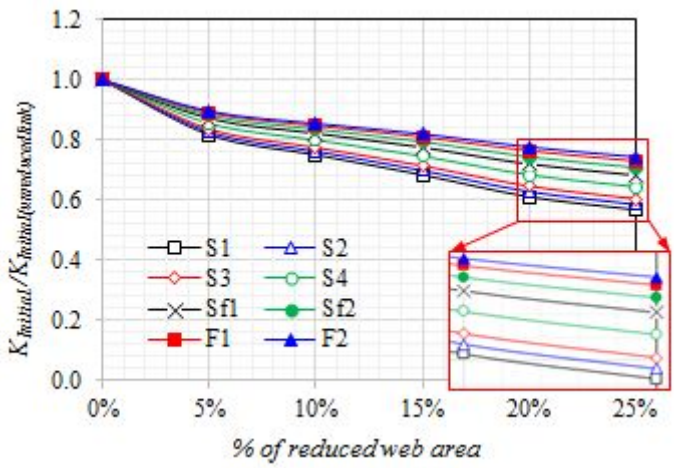

(b) Comparison of normalized initial stiffness of analysis specimens by calculated initial stiffness of normal web area of the respective specimens

Fig. 6.6 Initial stiffness versus percent of reduced web area relationship

6.3.1.2 Effect of percent of reduced web area on plastic rotation and overstrength factors

The plastic rotation which is given by $\gamma_p = \gamma - \frac{V}{eK_e}$, where γ: is the link rotation, V: is shear force, e: link length and K_e is the elastic stiffness, is calculated for all specimens considered for parametric study and presented in Fig. 6.7. The plastic rotation of stiffened link is bigger compared unstiffened links. Generally, the plastic rotation slightly decreases as the percent reduced web area increases. he effect of reduced web area on plastic rotation capacity is shown in Fig. 6.9. As shown in the Fig. 6.9, the plastic rotation of analysis specimens generally decreases as the percent of reduced web area increases. Even though the hysteresis response of specimens having high reduced web area, the calculated failure index reached unity earlier compared to unreduced and with reduced web of small percentage, 5% and 10%. Generally the plastic rotation of reduced web links of shear link and intermediate link satisfy the plastic rotation limit recommended in AISC-341-10. While flexural link failed to satisfy for both stiffened and unstiffened links including unreduced links as shown figure.

The overstrength factor which is given by the ratio of maximum shear force recorded from the analysis result and the plastic shear strength calculated by the equation, is presented in Fig. 6.8 for all analysis specimens along with the plots using the overstrength factor recommended by Richard et al. 2006 in terms of link length factor. As shown in the figure, the overstregth factor increases as the percent of reduced web area increases expecially for stiffened analysis specimens. Which indicates that some limitation of the suggested design equation of plastic shear strength. Considering the overstrength factor, the maximum reduced web diameter in a vertical alignment should be limited. It has been discussed in chapter 3 presented in Fig. 3.10, the maximum perforation diameter has been set. Fig. 3.10, has also repeated for initial stiffness as well and presented in Eq. (6.2). The elastic stiffness of link (K_e), which is defined in Eq. (4.6) and Eq. (4.7) in terms of elastic modulus, second moment of inertia, shear modulus and cross sectional area, has been modified for reduced link section. The plotted design curve and the results obtained from the parametric study was compared and presented in Fig. 6.10.As shown in the Fig. 6.10, the design curve is more accurate for the small diameter to depth ratio. As the ϕ/d ratio increases the accuracy of design curve decreases.

$$\frac{V_p^{rw}}{V_p} = \frac{K_e^{rw}}{K_e} = 1 - \frac{n\phi}{d} \qquad \text{.....(6.2)}$$

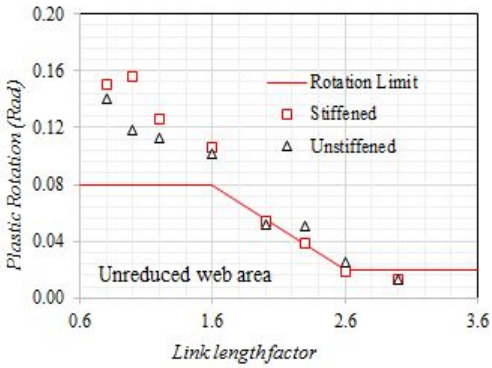

(a) plastic rotation vs link length factor for unreduced links

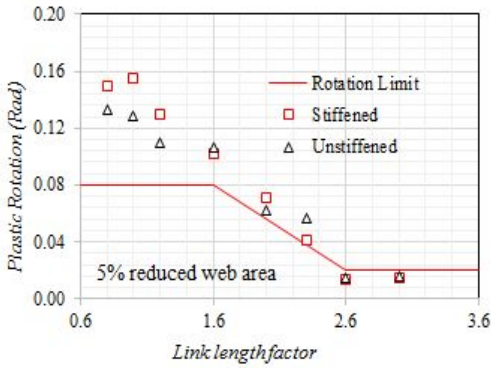

(b) plastic rotation vs link length factor for 5% reduced web area links

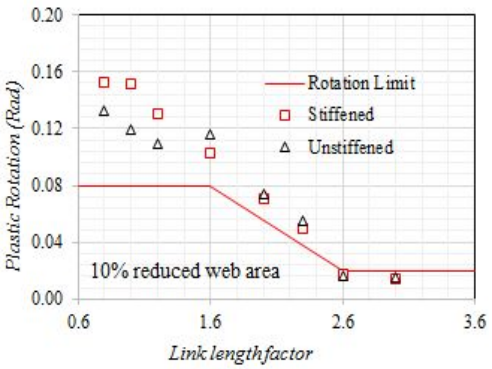

(c) plastic rotation vs link length factor for 10% reduced web area links

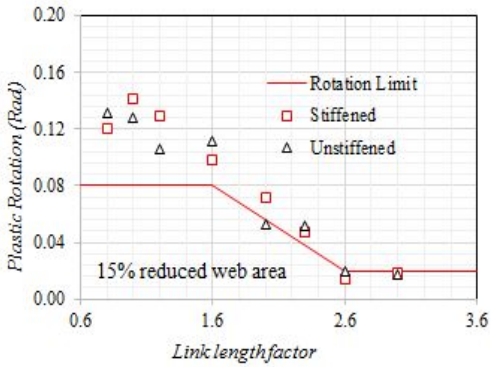

(d) plastic rotation vs link length factor for 15% reduced web area links

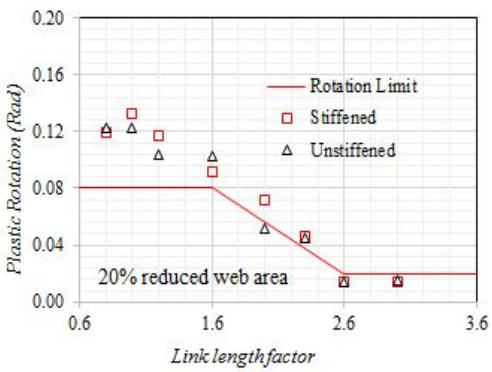

(e) plastic rotation vs link length factor for 20% reduced web area links

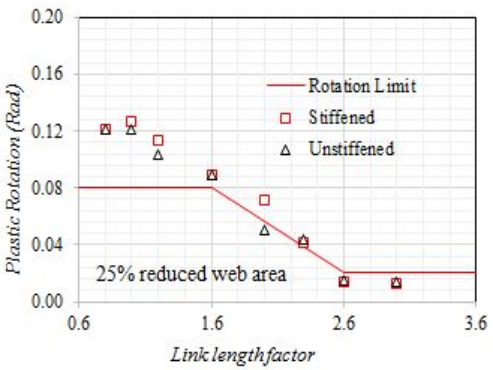

(f) plastic rotation vs link length factor for 25% reduced web area links

Fig. 6.7 Relationship of plastic rotation versus link length factor for stiffened and unstiffened links

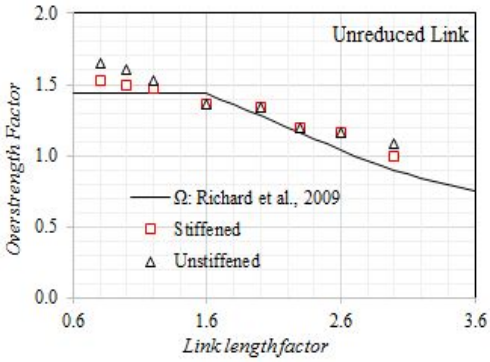

(a) Overstrength factor vs link length factor for unreduced web area links

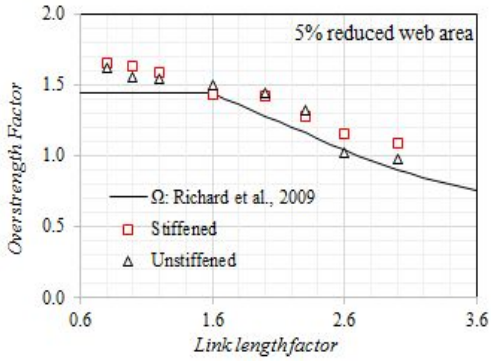

(b) Overstrength factor vs link length factor for 5% reduced web area links

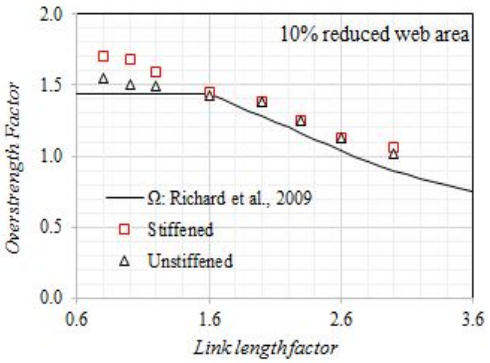

(c) Overstrength factor vs link length factor for 10% reduced web area links

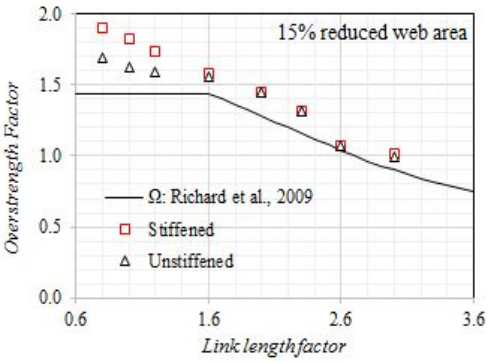

(d) Overstrength factor vs link length factor for 15% reduced web area links

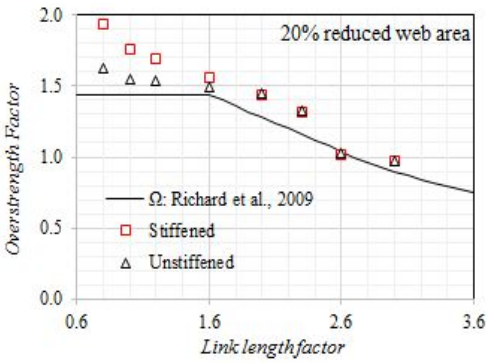

(e) Overstrength factor vs link length factor for 20% reduced web area links

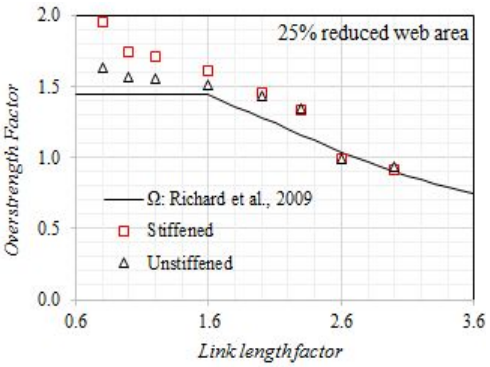

(f) Overstrength factor vs link length factor for 25% reduced web area links

Fig. 6.8 Relationship of overstrength factor versus link length factor for stiffened and unstiffened links

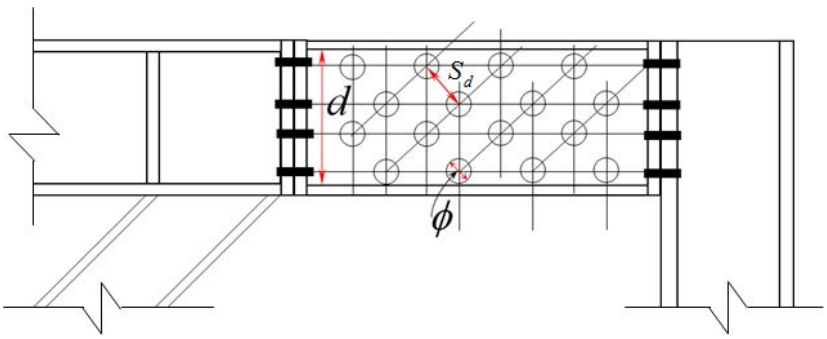

Fig. 6.9 Schematic detail of reduced web link

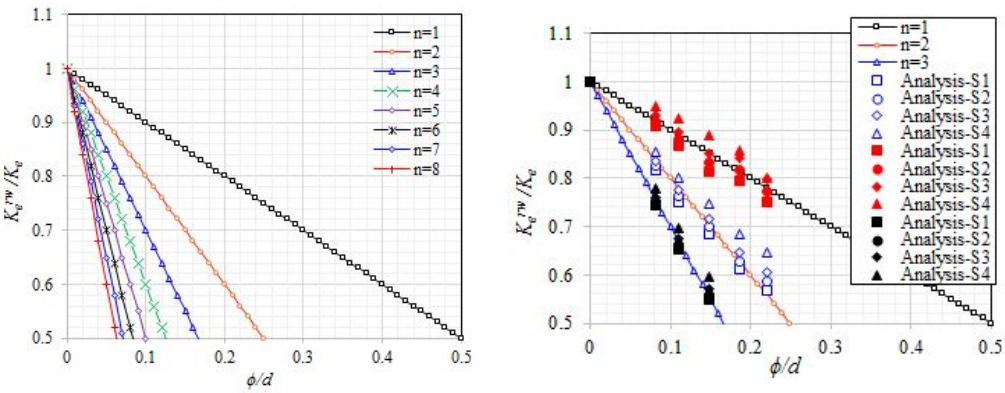

(a) stiffness reduction vs diameter of perforation to depth ratio

(b) comparison of design curve and analysis results from the parametric study

Fig. 6.10 stiffness reduction vs diameter of perforation to depth ratio

The question why the overstrength factor increases as the % of reduced web area increase is still not addressed. In the researches done on shear strength of perforated steel panel shear wall (SPSW) and un-perforated steel panel shear wall studied by Roberts and Sabouri-Ghomi, 1992, Darren Vian et al., 2005, 2009. The ratio of shear strength of perforated SPSW and un-perforated SPSW is 0.58 (Vian et al., 2005 and A. K. Bhowmick et al. 2012). Even though the design procedure of perforated SPSW and reduced web link is a bit different, in order to limit the ratio of S_{dia}/ϕ, the values suggested for perforated SPSW was used 0.42.

6.4 Stiffeners

AISC-2010 recommends the size as well as installations of stiffeners in the link beam. This recommendations are used. Full-depth web stiffeners shall be provided on both sides of the link web at the diagonal brace ends of the link. These stiffeners shall have a combined width not less than $(b_f - 2t_w)$ and a thickness not less than the larger of $0.75t_w$ or 10mm, where b_f and t_w are the link flange width and link web thickness, respectively.

Links shall be provided with intermediate web stiffeners as follows:

Links of lengths $1.6M_p/V_p$ or less shall be provided with intermediate web stiffeners spaced at intervals not exceeding $(30t_w - d/5)$ for a link rotation angle of 0.08 rad or $(52t_w - d/5)$ for link rotation angles of 0.02 rad or less. Linear interpolation shall be used for values bet ween 0.08 and 0.02 rad.

Links of length greater than or equal to $2.6M_p/V_p$ and less than $5M_p/V_p$ shall be provided with intermediate web stiffeners placed at a distance of 1.5 times b_f from each end of the link.

Links of length between $1.6M_p/V_p$ and $2.6M_p/V_p$ shall be provided with intermediate web stiffeners meeting the requirements of (a) and (b) above. Intermediate web stiffeners are not required in links of length greater than $5M_p/V_p$.

6.4.1 Results on the effect of stiffeners

The effect of stiffener is the most sensitive parameter in link evaluation. The hysteresis characteristics has quite dependent on the stiffeners. As shown in figures presented above in comparison of unstiffened and stiffened link, the hysteresis curve is stable for most of stiffened specimens considered. The main instability of hysteresis curves of unstiffened link is due to out-of-plane buckling of the web. Out-of-plane buckling causes not only decrease the cyclic shear force resisting capacity but also it decreases the plastic rotation capacity as well.

The difference between the out-of-plane buckling of stiffened and unstiffened link is bigger than the out-of-plane buckling of stiffened link. Fig. 6.11 shows the out-of-plane buckling of stiffened and unstiffened link with respect to % of open area. As shown in the figure, the out-of-plane buckling of unstiffened link is 60% more than stiffened link for almost all % of reduced web areas considered.

The effect of stiffener on the plastic rotation was also presented in Fig. 6.7. As shown in this figure, both stiffened and unstiffened links satisfy the plastic rotation level recommended by the standards with out flexural links. However, stiffened links has a plastic rotation capacity greater than unstiffened links. This due to the fact that unstiffened links yields early because of an out-of-plane buckling of web and local buckling of flanges. The overstrength factor of stiffened links are bigger than unstiffened links for reduced web shear links as shown in Fig. 6.8. However the overstrength factor of unstiffened unreduced link is bigger for shear link compared to stiffened analysis specimens.

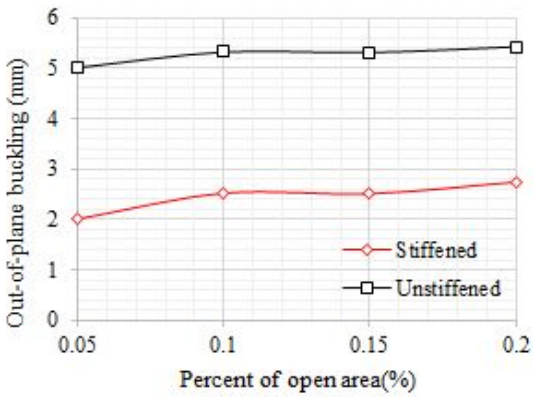

(a) Out-of-plane buckling vs percent of open area of analysis specimen S2

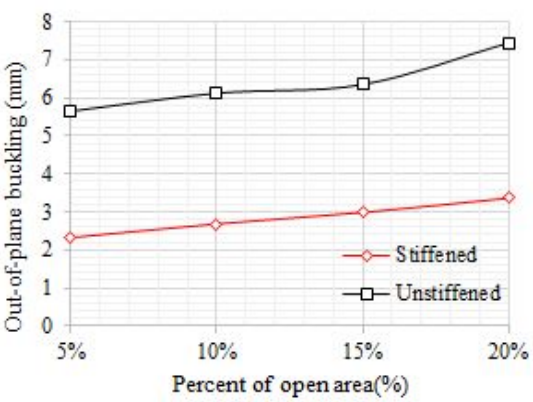

(b) Out-of-plane buckling vs percent of open area of analysis specimen Sf1

Fig. 6.11 Effect of stiffeners on out-of-plane buckling of analysis specimen

6.5 Unequal end-moment (Link-to-column connections)

6.5.1 General

Both analysis and experimental investigations conducted in this study have been for eccentrically braced frame V-brace that means considering equal end moment. In this study FE analysis for unreduced links and reduced links for link-to-column connection in EBFs is carried out and the results were compared to show the advantage of the developed links. Link-to-column connection tend to fracture at flange-to-column connection prior to large plastic rotation.

The most influential research works on link-to-column connection was the research done by Okasaki in 2004, Okasaki et al., 2004. Taking the loading test set-up considered by Okasaki et. al., 2004. Assuming the boundary condition of link-to-column connection in eccentrically braced frame as shown in Fig. 6.12 (a), the reaction forces at the A, B, D, E will be developed when the forces are applied in longitudinal direction of column. The free body diagram of the whole system is shown in Fig. 6.12 (b). From the free body diagram shown in Fig. 6.12 (c), the force and the moment using equilibrium equation can be:

$$V = R_A + R_B \quad \text{.....(6.3)}$$

$$M_B = - R_A L - R_B x \quad \text{.....(6.4)}$$

The value of x in equation (6.5) varies with the type of link used. For reduced web link the value of x will be approximately the thickness of end plate. Whereas for reduced flange and web link section the value of x can be the sum end plate thickness and the length from the end to the start of section reduction (a) and half of chord length of cutoff section (b/2). Where the dimension of a expressed in section 3, Eq. (3.23)- (3.26).

$x = t_e$ [for reduced web link]

$x = t_e + a + \frac{b}{2}$ [for reduced web and flange link] .....(6.5)

From the Fig. 6.12 (d), the moment Mc from equilibrium equation can be:

$$M_C = Ve - M_B \quad \text{.....(6.6)}$$

where e is the link length. From the Fig. 6.12 (e), the moment Mc from equilibrium equation can be:

$$V = P \quad \text{.....(6.7)}$$

$$M_C = -Px' + (R_E - R_D)\frac{h}{2} \quad \text{.....(6.8)}$$

The x' in Equation 6.9 can be the sum of half of column depth and thickness of end plate for reduced web link section x'and the sum of half of column depth and thickness of end plate and the lengthfor reduced web from the end to the start of section reduction (a) and half of chord length of cutoff section (b/2).

$$x' = \frac{d_1}{2} + t_e \text{ [for reduced web link]}$$
$$x = \frac{d_1}{2} + t_e + a + \frac{b}{2} \text{ [for reduced web and flange link]} \quad \text{.....(6.9)}$$

where d_1: is the column depth, a the length from end plate to the start of section reduction expressed in section 3, Eq. (3.23, 3.26).

To take into account the link-to-column connection in EBFs analysis model shown in Fig. 6.12 which is similar to the loading test set-up and analysis modeled by Okazaki et al., 2004, were created. Where two constraints were created on the beam at the joint of column and brace.

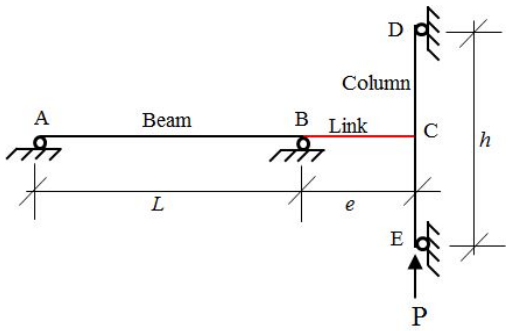

(a) Test set-up model of link-to-column connection (Okasaki et al., 2004)

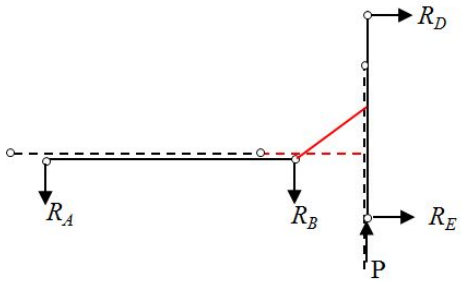

(b) The free body diagram of deformed shape

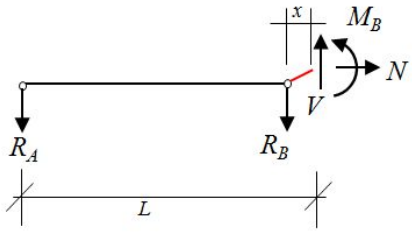

(c) The free body diagram of deformed shape

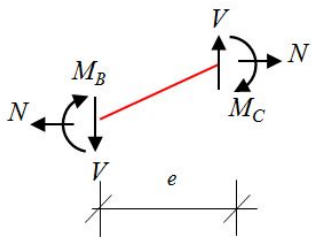

(d) The free body diagram of deformed shape

Fig. 6.12 Link-to-column connection model

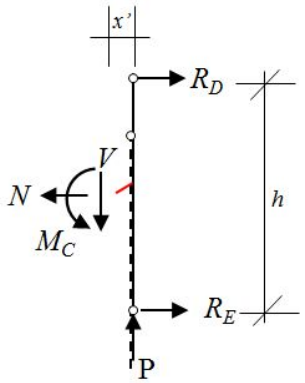

(e) The free body diagram of deformed shape

Fig. 6.12 Link-to-column connection model *(Continued...)*

6.5.2 FE Analysis on link-to-column connection

6.5.2.1 Material Modeling

The FE analysis conducted to evaluate the effect of link-to-column connection in EBFs and the 3D meshed analysis model for reduced web link section is shown in Fig. 6.13. Solid model was used to evaluate the behavior of link-to-column connection using reduced link section and unreduced links. The model is meshed with C3D8R. The link is tied to the end plates both sides. The beam is also tied to the end plate. The contacts between the two end plates are modelled as hard contacts and the column flanges and the end plate in the column face also modeled as hard contacts. The constitutive model of a "hard contact" is shown in Fig. 6.14. Normal contact pressure is generated when the two surfaces touch, whereas no pressure exists when they separate. Normal contact pressure is generated when the two surfaces touch, whereas no pressure exists when they separate. Coulomb friction was employed to simulate the behavior between the contacted surfaces in the tangential direction. The friction coefficient was 0.3 in this study. The contact model with hard contacts was used between the six bolts used to connect the two end plates in the beam face and end plate and column flanges in the column face. However, the evaluation was unable to proceed. Therefore the heads of the bolts were tied to the corresponding surfaces.

The beam, column out side the panel zone, the beam and the rigid body (end plates) are modeled as elastic with young's modulus and poison's ratio of 205000MPa and 0.3 respectively. The panel zone of column, the link and stiffeners are modeled as inelastic (plastic). The detail of material inputs used are shown in the table below.

Table 6.3 Material properties used for link-to-column connection

*Material, name=Column *Elastic 205000, 0.3 *Plastic 312.2, 0.0 365.02, 0.04808 426.32, 0.2508	Panel zone of column
*Material, name=Linear *Elastic 205000, 0.3	Column out side panel zone
*Material, name=Link *Elastic 205000, 0.3 *Plastic 316.02, 0.0 368.23, 0.0621 426.36, 0.2908	links
*Material, name=End Plate *Elastic 205000, 0.3	End plate
*Material, name=Stifferes *Elastic 205000, 0.3 *Plastic 312.2, 0.0 425.36, 0.27	Stiffeners

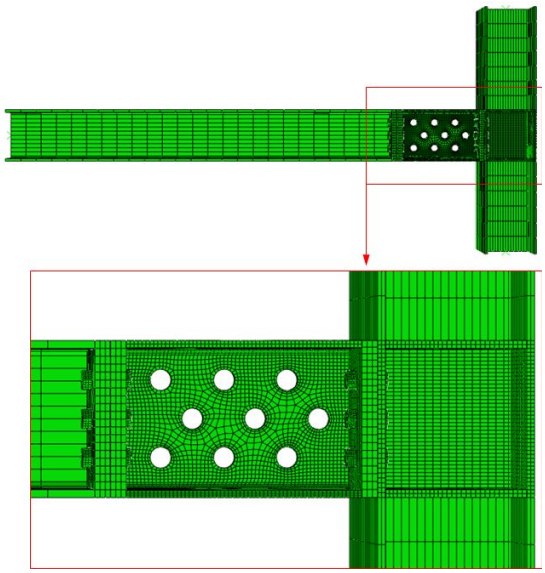

Fig. 6.13 3D meshed analysis model of link-to-column connection

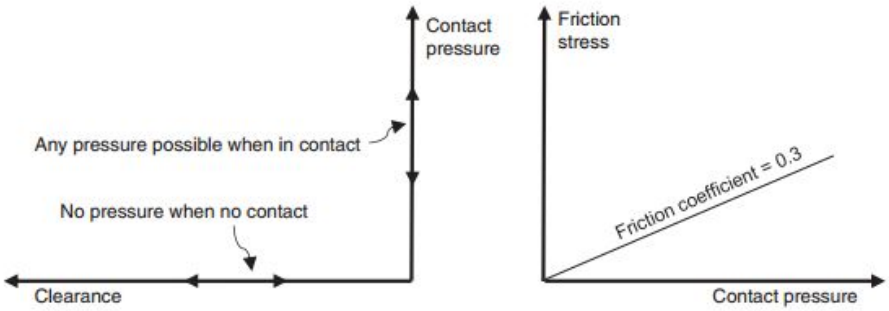

Normal Behaviour Tangential Behaviour

Fig. 6.14 Constitutive model of "hard contact"

Table 6.4 Analysis specimen detail of reduced link length amount of diameter of reduction for parametric study

% reduced web area	ρ	1	1.3	1.5	1.65	2.3
	Section property	link length (mm)				
	t_w(mm)	*D (mm)*	*B (mm)*	*tf (mm)*		
0	8	200	120	10	316	362	419	601	764
10%	8	200	120	10	348	437	521	672	843

For unequal end moment or link-to-column connection, a parametric study was conducted on shear and intermediate links for both reduced and unreduced link section. Table 6.4 summarizes the detail of analysis specimen details.

6.5.2.2 Loading and boundary condition

The boundary condition and loading condition is shown in Fig. 6.15. As shown in the figure, the at point A and B, the translation is free in Z-direction and fixed in X and Y-direction. The translation is free at point D and E in the loading direction Y-direction and fixed in X and Z-direction. The loading is applied at point D or E by controling the displacement in Y-axis. This boundary and loading condition was adapted from the test setup of link-to-column connection at University of Texas, Austin by Arce 2002 and Galvez 2004.

The loading protocol used to evaluate the link-to-column connection is the same as the loading protocol used in the experimental and parametric studies used, which is the revised protocol.

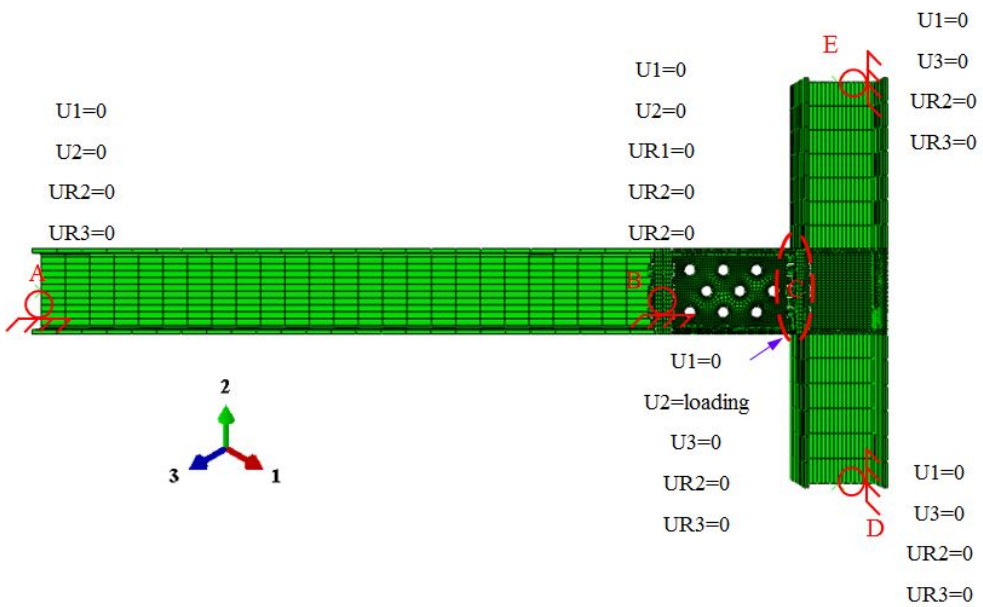

Fig. 6.15 Boundary Conditions of link-to-column connection

6.5.3 FE Results of link-to-column connection

6.5.3.1 Hysteresis Response and Plastic Rotation Capacity

The hysteresis response of analysis result of link-to-column connection is shown in the Fig. 6.16 for shear link with link length factor of one (ρ=1). As shown in the comparison of 10% reduced web link section and unreduced link section, the hysteresis response of reduced link section of link-to-column connection shows stable hysteresis characteristics compared to unreduced link section. For intermediate link with link length factor 1.65 (ρ = 1.65), the comparison of hysteresis response of 10% reduced web area link and unreduced link are shown in Fig. 6.17. Similar results were obtained with shear link but for intermediate link the second stiffness is some how is bigger for both reduced and unreduced link section compared shear links. As shown in the figure, reduced link section shows stable hysteresis response compared unreduced link.

The maximum shear resisting capacity of unreduced link section is bigger than reduced link section. That is one of the advantages of reduced link section because in order to control the plastic deformation at the links in eccentrically braced frame keeping the remaining structural elements in elastic range, the link should have weaker in strength compared to the collector beam. Hence, the reduced web section of link have a dual advantage. First, it keeps stable hysteresis response even at large displacement and second the shear resisting capacity lesser or weaker in strength compared to collector beam.

The plastic rotation capacity of reduced web link section and unreduced link section is also calculated. The total shear rotation in both cases were decided by calculating the failure index i.e the total shear rotation is taken at the point where the failure index reaches one. The calculated failure index for shear links (ρ=1) of reduced and unreduced link section with respect to number cycle is presented in Fig. 6.18 (a) and (c) respectively. In order to know the exact points where the failure index reached one, the loading protocol with the corresponding number of cycle is plotted for both reduced and unreduced link section and shown in Fig. 6.18 (b) and (d) respectively. Looking at the loading protocol with the corresponding number of cycle at which the failure index reached one, the total shear rotation of reduced and unreduced link section is 0.16 rad and 0.07 rad respectively. Therefore the plastic rotation can be the 0.1502 rad and 0.0602 rad for reduced and unreduced link section respectively.

Similarly, the plastic rotation of intermediate links (ρ=1.65) of both reduced and unreduced link section was calculated where the total shear rotation is decided by the failure index. The calculated failure index was plotted for both reduced and unreduced link section with respect to number of cycle as shown in Fig 6.19 (a) and (c) respectively. The loading protocol used to specify the shear rotation that corresponds the number of cycle founded in the failure index is plotted and shown in Fig 6.19 (b) and (d) for reduced and unreduced link sections respectively. For the loading protocol, the total shear rotation is 0.125 rad and 0.035 rad for reduced and unreduced link sections respectively. Thus, the plastic rotation of reduced and unreduced link section is 0.1204 rad and 0.0302 rad respectively.

From the results obtained in this study, it fair to say that the reduced link section satisfies the plastic rotation limit recommended in AISC provision for shear and intermediate links in link-to-column connection in eccentrically braced frames even though further researches needs to be done. The limitation of link-to-column connections of eccentrically braced frame according to many researches and AISC provision is fracture of flanges welds at flange-to-column connection prior to the target plastic rotation.

The plastic rotation of parametric study for link-to-column connection is presented in Table 6.5. The analysis results were compared with test results grasped from Okazaki et., el. 2004 and presented in Fig. 6.20(a). As shown in the Fig. 6.20(a), the plastic rotation capacity of reduced web link section satisfied the plastic rotation limit while unreduced links and the test results from the Okasaki et., el failed to satisfy the plastic rotation limit recommended in AISC seismic provision (AISC-341-10).

The corresponding overstrength factor of unreduced and reduced link section has also been calculated and presenetd in Fig. 6.20 (b). As shown in the Fig. 6.20 (b), the overstrength factor of unreduced and reduced link well matches with the overstrength factor recommended by Richard et al. 2009.

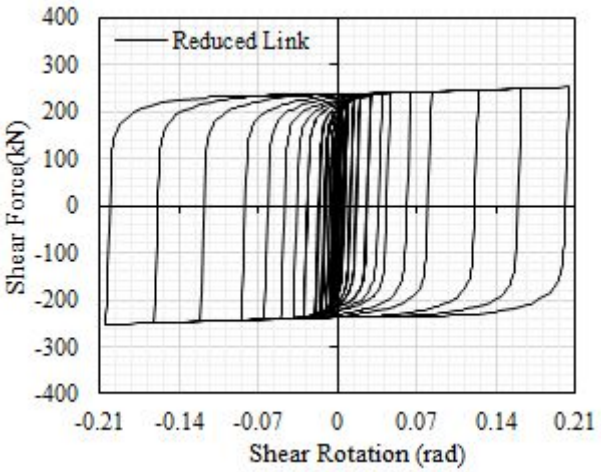

(a) 10% reduced web area link section with ρ=1

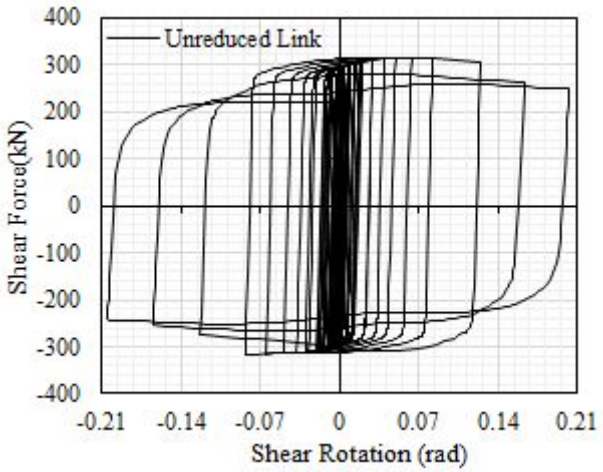

(b) Unreduced link section with ρ=1

Fig. 6.16 Hysteresis response of reduced and unreduced link section (ρ = 1)

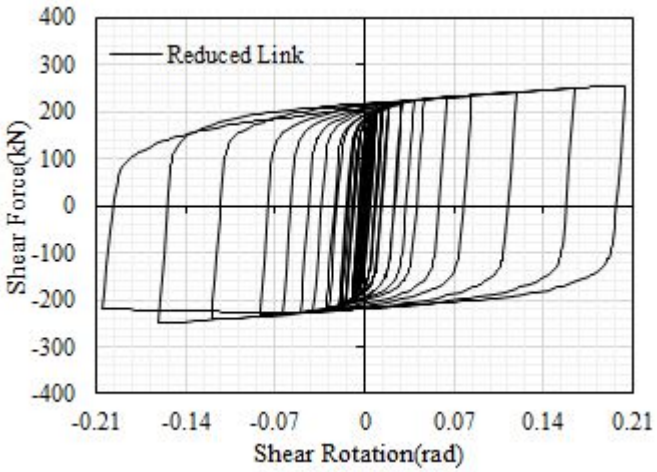

(a) Reduced web link section

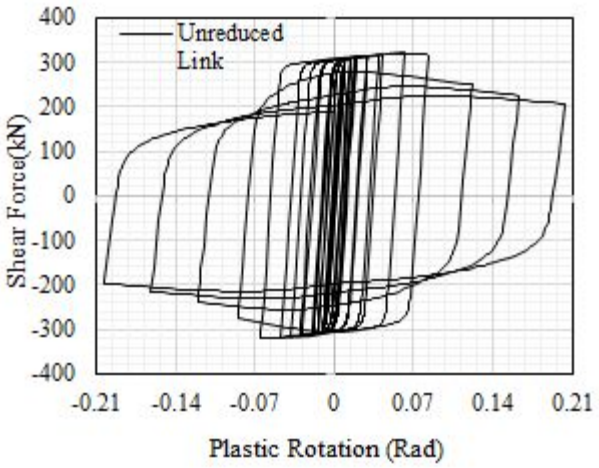

(b) Unreduced web link section

Fig. 6.17 Hysteresis response of reduced and unreduced link section of intermediate link (ρ = 1.65)

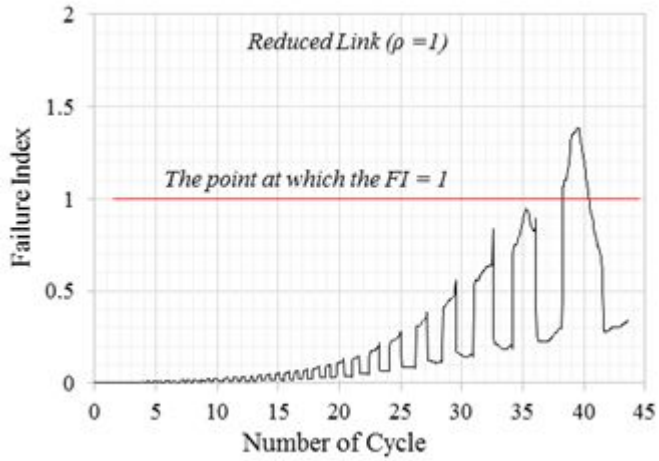

(a) Failure Index versus number of cycle for reduced web link section (ρ = 1)

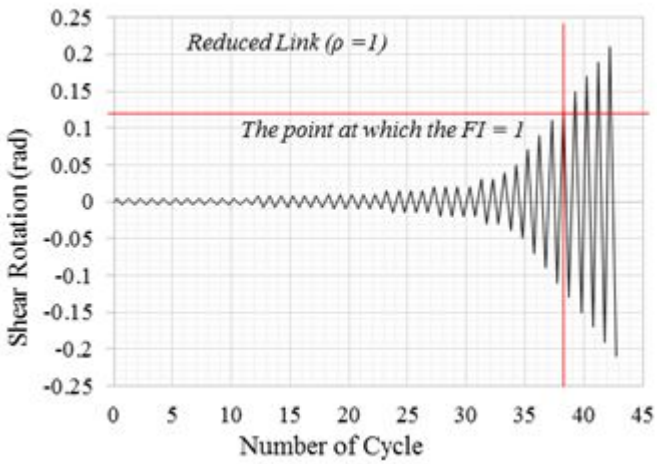

(b) The point at which FI is one on the loading prtocol for reduced web link section (ρ = 1)

Fig. 6.18 Comparison of Failure index of Reduced web section and unreduced web link section of ρ = 1

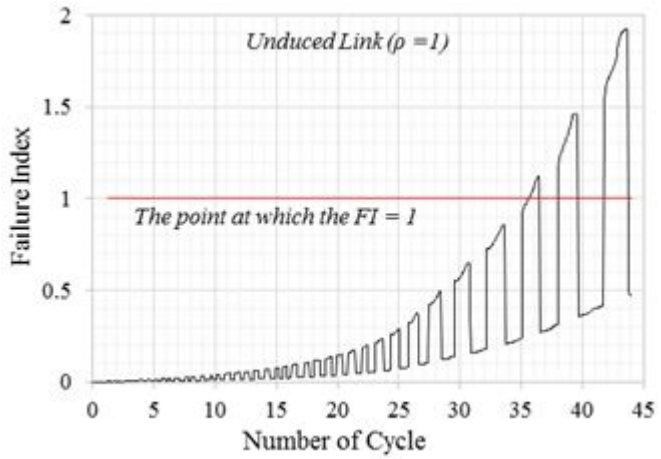

(c) Failure Index versus number of cycle for unreduced web link section (ρ = 1)

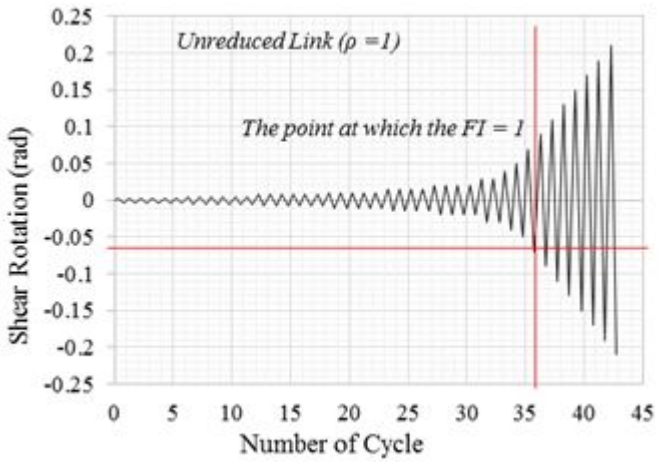

(d) The point at which FI is one on the loading protocol for unreduced web link section (ρ = 1)

Fig. 6.18 Comparison of Failure index of Reduced web section and unreduced web link section of ρ = 1. *continued...*

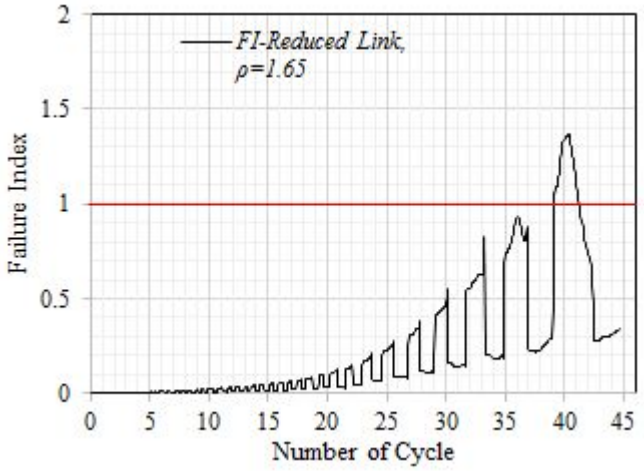

(a) Failure Index versus number of cycle for reduced web link section (ρ = 1.65)

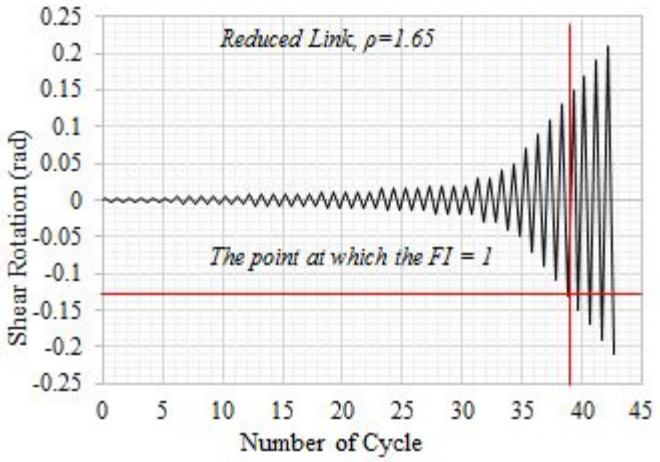

(b) The point at which FI is one on the loading protocol for reduced web link section (ρ = 1.65)

Fig. 6.19 Comparison of Failure index of Reduced web section and unreduced web link section of ρ = 1.65

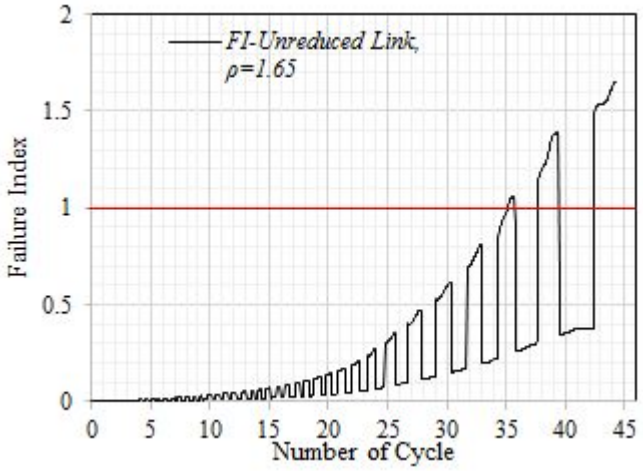

(c) Failure Index versus number of cycle for unreduced web link section (ρ = 1.65)

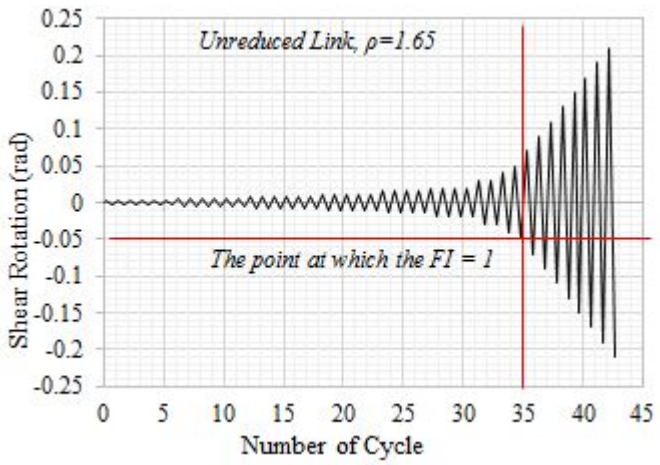

(d) The point at which FI is one on the loading protocol for unreduced web link section (ρ = 1.65)

Fig. 6.19 Comparison of Failure index of Reduced web section and unreduced web link section of ρ = 1.65. *continued...*

Table 6.5 Summary of plastic rotation of analysis specimen for link-to-column connection

Specimen Type	ρ/ρ_{rw}	V_p (kN)		Initial Stiffness (N/mm)		Yield rotation angle $= \frac{V}{eK_e}$		Shear Rotation @FI=1		Plastic Rotation (rad)	
		Reduced	Unreduced	Reduced	Unreduced	Reduced	Unreduced	Reduced	Unreduced	Reduced	Unreduced
Shear Link	1.0	206.7	310.1	258945	377089	.00313	.0047	.11334	.0602	.1102	.0555
	1.4	206.7	310.	215885	311441	.00373	.0056	.0944	.0579	.091	.0523
	1.5	206.7	310.1	172101	244743	.00432	.0065	.13388	.0824	.129	.0759
Intermediate Link	1.65	193.6	286.4	102120	138243	.00383	.0057	.09644	.082	.093	.0763
	2.3	185.75	277.6	82454	110279	.00512	.0077	.07574	.0437	.071	.036

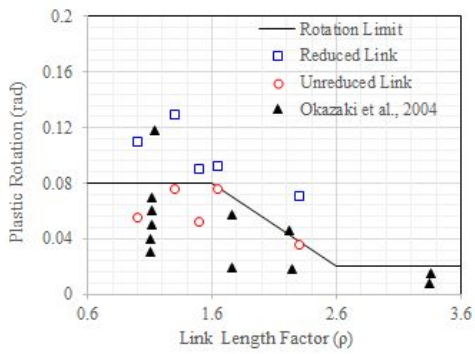

(a) Comparison of plastic rotation of reduced and unreduced links

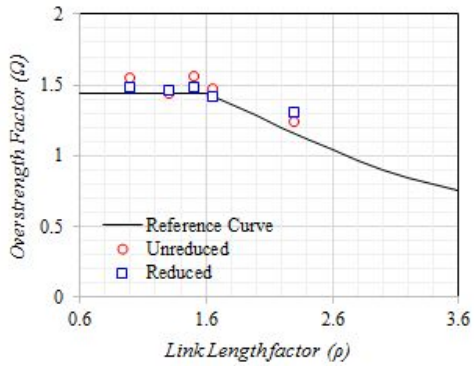

(b) Comparison of overstrength factor of reduced and unreduced links

Fig. 6.20 Comparison of Reduced and Unreduced Links

6.5.3.2 Comparison of Deformed shape

The deformed shape of reduced link section and unreduced link section with distribution of strain, stress and with out-of-plane buckling is presented in Fig 6.21. The comparison of deformed shape with the equivalent plastic strain of reduced and unreduced link is presented in Fig. 6.21 (a) and (b). As shown in the Fig. 6.21 (a) and (b), the equivalent plastic strain for reduced link concentrated at the edge and along the line of hole introduced on the web whereas for unreduced link, the equivalent plastic strain is distributed all over the web and at the flanges on the column face as well.

The comparison of out-of-plane buckling of reduced and unreduced link is presented in Fig. 6.21 (c) and (d). As shown in the figure, the maximum and minimum out-of-plane buckling reduced and unreduced link is 1.559 and –2.544 and 27.08 and –24.64 respectively. The out-of-plane buckling of unreduced link is more than ten times bigger than reduced link section. The deformed shape with von mises stress distribution of reduced and unreduced link is also presented in Fig. 6.21 (e) and (f). The crack susceptibility of links can be calculated using the stress striaxiality ratio, PEEQ index, and rupture index and defined and discussed below.

6.5.3.2.1 Stress Triaxiality ratio (τ)

Stress triaxiality ratio is known to greatly influence the amount of plastic strain which a material may undergo before ductile failure occurs. A number researcher take this fracture criteria effect into consideration in to predict failure. It is defined mathematically as the ratio of hydrostatic pressure, or mean stress, to the von Mises equivalent stress as shown in Eq. (6.10). This ratio is an important quantity when considering ductile rupture of steel material. High triaxiality ($0.75 < \sigma_m/\sigma_e < 1.5$) can cause a large reduction in the rupture strain of metals. Very high triaxiality ($\sigma_m/\sigma_e > 1.5$) can result in brittle behavior (LeMaitre, 1996).

$$\tau = \frac{\sigma_m}{\sigma_e} = \frac{\frac{1}{3}(\sigma_1 + \sigma_2 + \sigma_3)}{\sqrt{\frac{1}{2}(\sigma_1 - \sigma_2)^2 + (\sigma_2 - \sigma_3)^2 + (\sigma_3 - \sigma_1)^2}} \quad \text{.....(6.10)}$$

where σ_1, σ_2, and σ_3: normal stresses in x, y and z direction respectively.

6.5.3.2.2 PEEQ Index

PEEQ index is used to measure the local ductility which is defined as the plastic equivalent strain divided by the yield strain.

$$PEEQIndex = \frac{\varepsilon_e^p}{\varepsilon_y} \quad \text{.....(6.11)}$$

where ε_e^p is plastic equivalent strain which is given the plastic strain components (ε_{ij}) in directions i and j as in Eq. (6.12) and ε_y: is the strain at yield.

$$\varepsilon_e^p = \sqrt{\frac{2}{3}\varepsilon_{ij}\varepsilon_{ij}} \quad \text{.....(6.12)}$$

6.5.3.2.3 Rupture Index (RI)

The ratio between the hydrostatic stress and the Mises stress (σ_m/σ_e) is known as the stress triaxiality ratio. This ratio is an important quantity when considering ductile rupture of metals. High triaxiality (0.75 < s m /s < 1.5) can cause a large reduction in the rupture strain of metals. Very high triaxiality (s m /s > 1.5) can result in brittle behavior (LeMaitre 1996 and Barsom and Rolfe 1988). A crude, albeit effective, criterion for calculating the strain at ductile fracture is given by Hancock and Mackenzie (1976) as the ratio of PEEQ index to Stress triaxiality ratio. RI can be used to compare between the potential for ductile fracture of different critical points.

$$RI = \frac{PEEQIndex}{\exp(-1.5\tau)} \quad \text{.....(6.13)}$$

In order to identify the effect of reduced webs on the stress concentration in the flanges, the stress and strains including stress triaxiality was calculated for both reduced and unreduced link length. The measurement locations is shown in Fig. 6.22 (a) for reduced and Fig. 6.22 (b) for unreduced link section. The comparison of the measured and calculated triaxial stress and equivalent plastic strain for reduced and unreduced link is presenetd in Fig. 6.23 (a) and (b) respectively. As shown in the figure, the stress triaxial stress and equivalent plastic strain of flange in column face decreases as the reduced web area increases and for the web triaxial stress and equivalent plastic strain increases as the reduced web area increases.

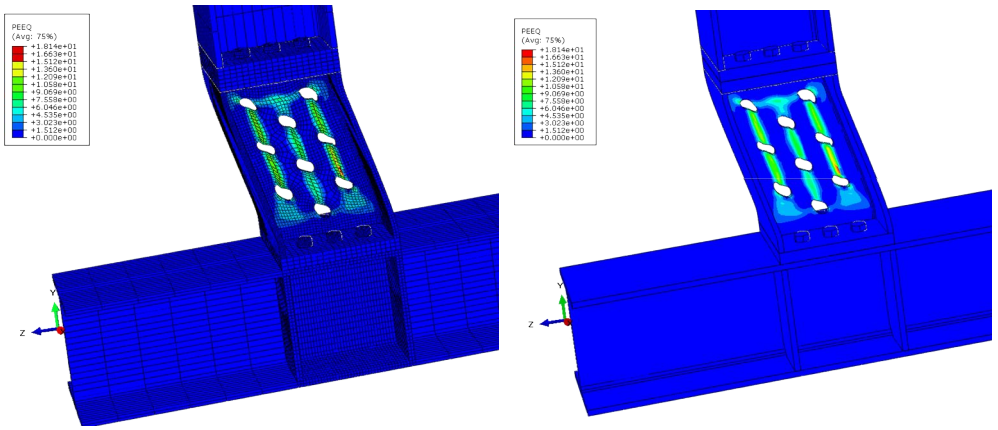

(a) equivalent plastic strain distribution of reduced link section

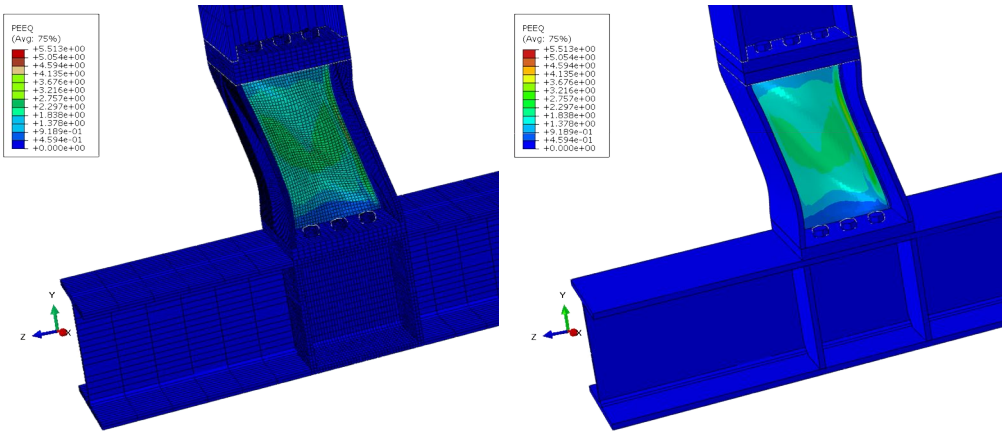

(b) equivalent plastic strain distribution of unreduced link section

Fig. 6.21 Buckling shape of analysis results of reduced and unreduced link section for ρ=1

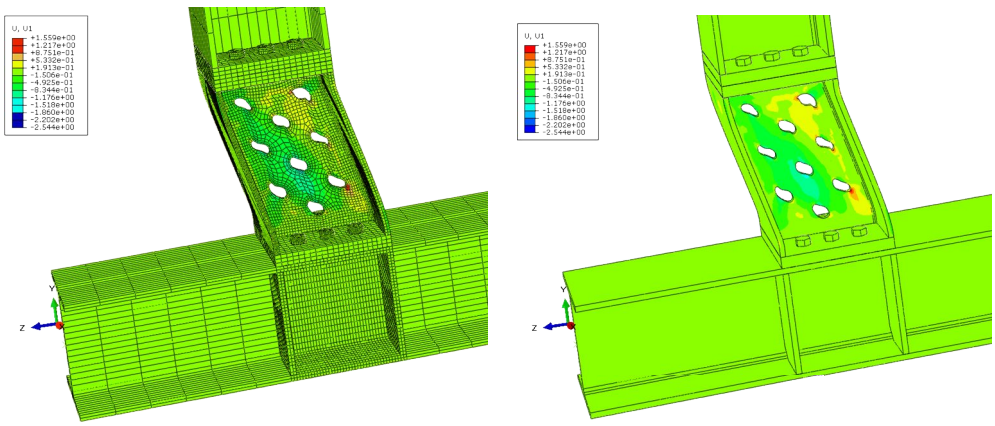

(c) out-of-plane buckling of reduced link section

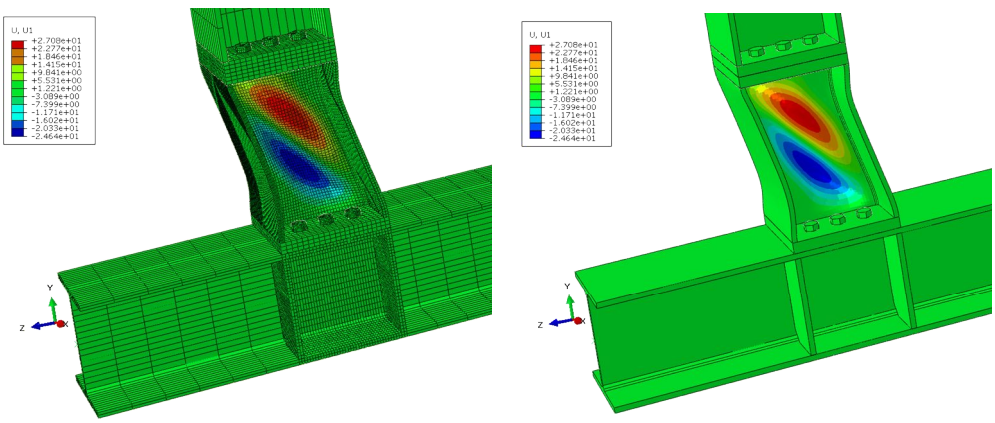

(d) out-of-plane buckling of unreduced link section

Fig. 6.21 Buckling shape of analysis results of reduced and unreduced link section for ρ=1. *continued...*

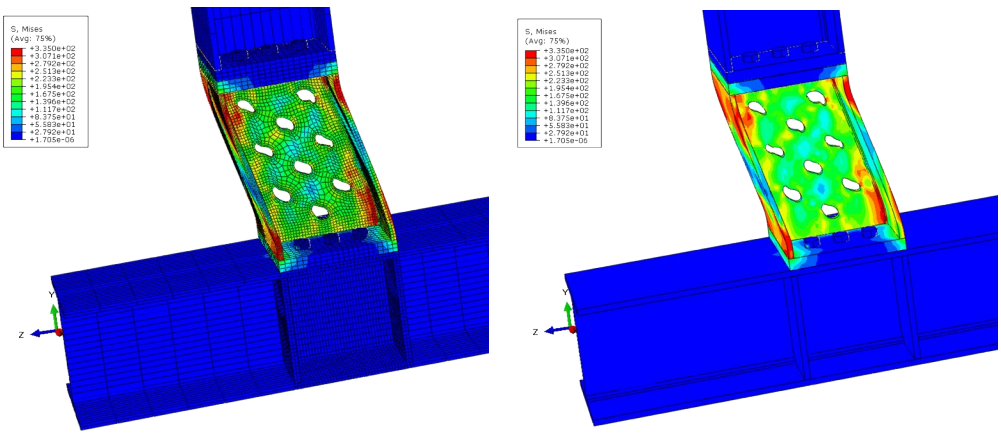

(e) von Mises stress distribution of reduced link section

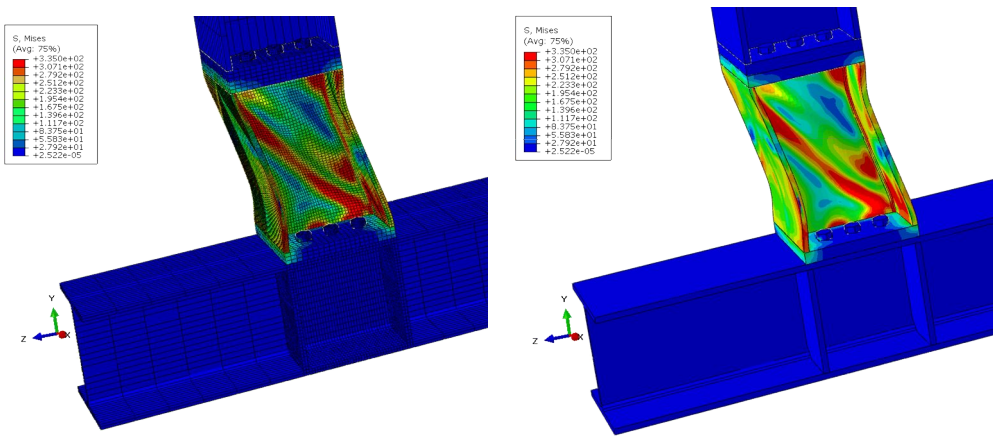

(f) von Mises stress distribution of unreduced link section

Fig. 6.21 Buckling shape of analysis results of reduced and unreduced link section for ρ=1. *continued...*

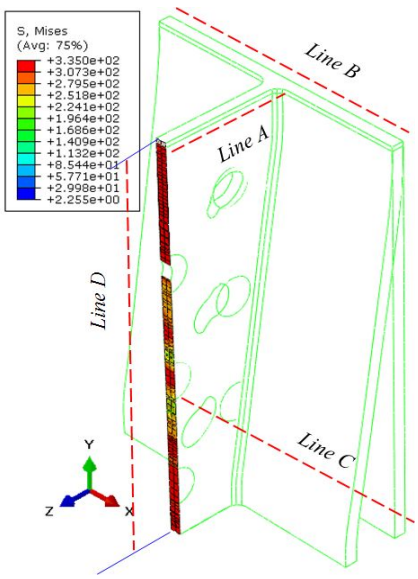

(a) stress and strain measurement lines of reduced link section

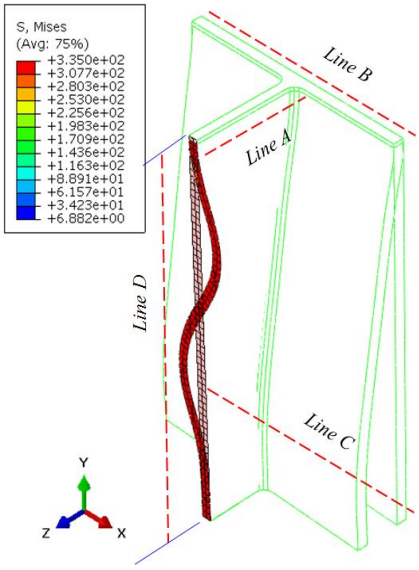

(b) stress and strain measurement lines of unreduced link section

Fig. 6.22 Measurement of lines of stress and strain ρ = 1

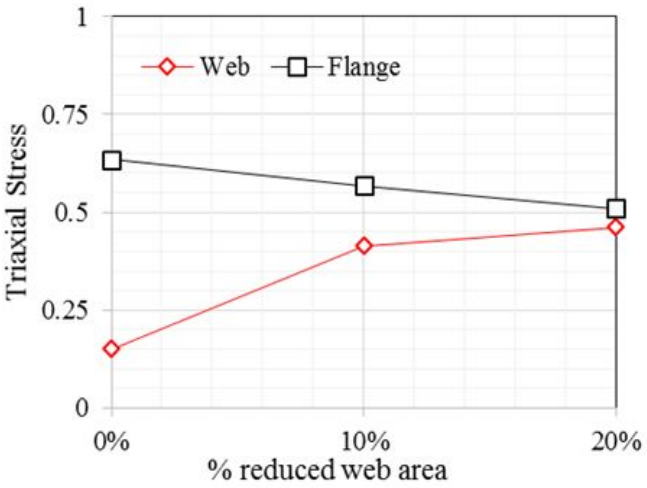

(a) effect of reduced web area on triaxial stress

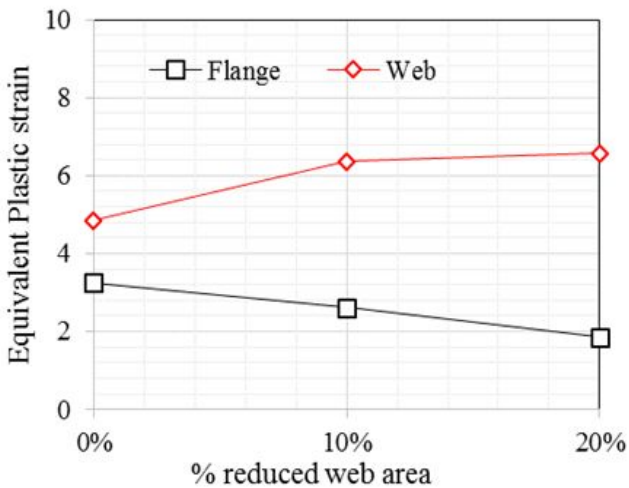

(b) effect of reduced web area on equivalent plastic strain

Fig. 6.23 Effect of reduced web area on link-to-column connection

6.5.3.3 End Moments Rations in Link-to-column Connections

In order to measure the moments directly from the finite element analysis monotonic loading analysis were conducted on link-to-column connection in a analysis model shown in Fig. 6.13 and with the boundary condition shown in Fig. 6.15. The end-moments were measured both beam and column faces. ed as in From the analysis results, moments were measured directly at the ends of link in the column face and beam face. In link-to-column connection of eccentrically braced frame, the moment in column face and beam face is not equal. The end moments in column face is greater than the moments in beam face.

The ratios of measured end moments directly from the monotonic loading of finite element analysis were calculated for reduced and unreduced link section. In addition the end moments using equations derived in section 6.6.1 of Eqs (6.3) - (6.9) are also calculated and the results were plotted in Fig. 6.24 along with the results collected from the research work of Richard and Uang (2003) and Okazaki (2004).

Richard and Uang (2003) conducted a series of 2-D elastic frame analyses to identify the realistic end moment rations. The end moment rations of their analyses are shown in Fig 6.24, the notation 3L, 3T and 10 in the plotted figure correspond to three frames, two three-story frames and one ten-story frame according to Richard and Uang. The other results considered for comparison is the test set-up of Okazaki et al., 2004, where the end moment ratios are decrease exponentially with an increase of link length factor.

Looking at the plots of analysis results, the measured end-moment ratios of reduced link section less than the calculated end moment ratios and the ratios presented by Okazaki and Richard as shown in Fig. 6.24 (a). Compared to reduced link section, unreduced link section has relatively similar end moment ratios as shown in Fig. 6.24 (b). The comparison of end moment ratios of reduced link section and unreduced link section is presented in Fig. 6.24 (c). In both cases calculated end moment ratios are greater than the measured values. Thus, it is difficult to conclude the end moment ratios for link-column connection. Further research needs to be conducted regarding this issue both experimentally and analytically to come up with a clear end moment ratios.

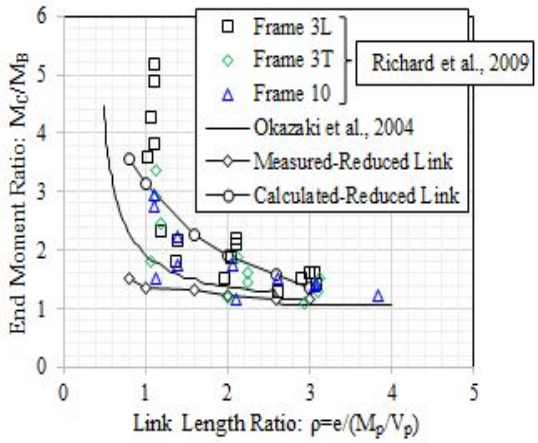

(a) Comparison of end-moment ratio of reduced link section with existing research results

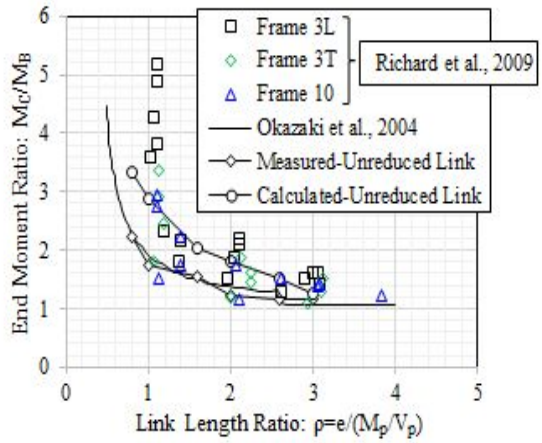

(b) Comparison of end-moment ratio of unreduced link section with existing research results

Fig. 6.24 Comparison of End-moment ratios

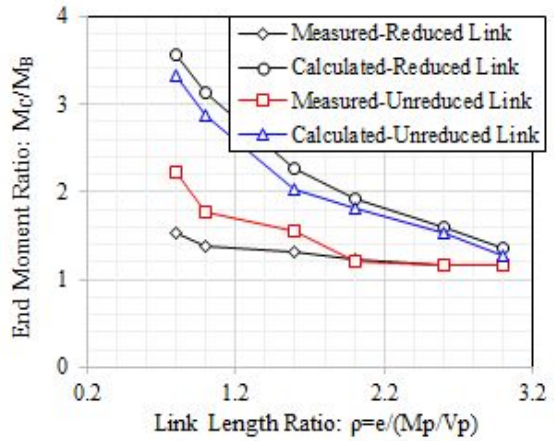

(c) Comparison of end-moment ratio of reduced link section and unreduced link section

Fig. 6.24 Comparison of End-moment ratios (*Continued...)*

6.5.3.4 Equivalent Viscous Damping (ξ) and effective stiffness

The effect of reduced web on equivalent viscous damping (damping ratio) and effective stiffness of link-to-column connection is presented in this section. The calculation process and the necessity of damping ratio and effective stiffness has been explained in Section 4.4. The same procedure was used for link-to-column connections. Fig. 6.25 (a) shows the comparison of damping ratio and effective stiffness of reduced web shear link and unreduced shear link. In this relationship, the damping ratio and effective stiffness of unreduced shear link is generally higher than the damping ratio and effective stiffness of reduced web shear link. However, when we look at the relationship between damping ratio versus number cycle of reduced web and unreduced shear links as shown in Fig. 6.25 (b), the damping ratio of reduced web shear link is relatively higher compared to the damping ratio of unreduced shear link.

Looking at the relationship between the effective stiffness versus number cycle of reduced web and unreduced shear links shown in Fig. 6.25 (c), the effective stiffness of unreduced shear link is by far higher than the reduced web shear link at early cycle and as the number of cycle increase the effective stiffness converged and lastly became equal. The damping ratio and effective stiffness of reduced web shear link ranges from 10.72%-58.5% and 4.13kN/mm-180.33kN/mm respectively. And for unreduced shear link the damping ratio and effective stiffness are 5.73%-54.75% and 4.17kN/mm-257.91kN/mm respectively.

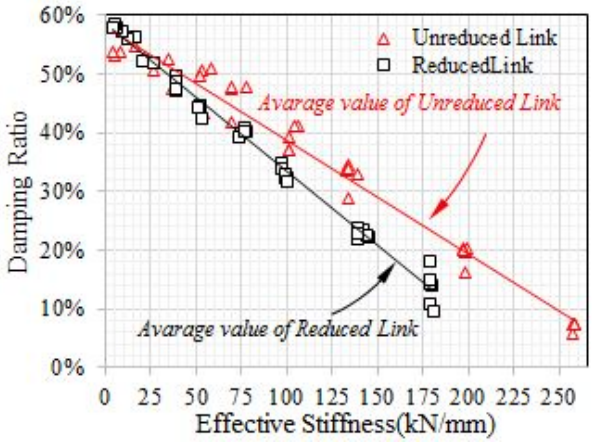

(a) Comparison of damping ratio and effective stiffness of reduced web and unreduced shear links

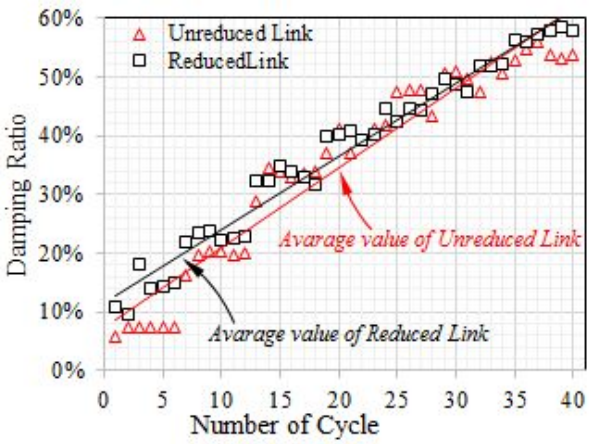

(b) Comparison of damping ratio versus number cycle of reduced web and unreduced shear links

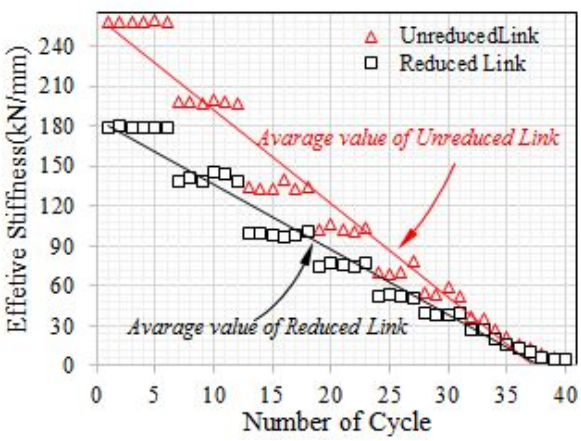

(c) Comparison of effective stiffness versus number cycle of reduced web and unreduced shear links

Fig. 6.25 Effect of reduced web on damping ratio and effective stiffness

6.6 Summary

The reduced link sections in eccentrically braced frames according to Hauksdottir recommendation is effective in reducing flange strains at the ends of all link types, though more effective for intermediate and flexural links than shear links. The design recommendations and non-linear finite element analysis was conducted to check the applicability of the design recommendations for both reduced web link section and reduced web and flange link section. The design considerations of reduced web link section and reduced web and flange link section is different. The main difference is the assumptions i.e. for reduced web link section, the changes in the plastic moment is slight and so it is ignored for simplicity and for the reduced web and flange link section the effect of plastic moment is considered.

The link length factor (link length) is among the parameters considered in preliminary studies. The effect of design considerations made are seen mainly on this parameter called link length factor. The analysis result shows that, reduced web link section is effective mainly for shear link and for intermediate link as well. Where as the reduced web and flange link section is effective mainly for intermediate links. This is not only because of the shear rotation capacity but also the hysteresis characteristics and failure mode. For the same link length measured, the link length factor for reduced web and reduced web and flange section is different because of the difference in plastic moment.

7. Design Recommendations

7.1 General

In this chapter, design recommendations was made from the non-linear finite element analysis, experimental investigations, material mechanics and geometrical effect of the developed links considering overstrength factor and effect of flanges. The plastic shear strength and plastic end moment of links for the developed links have been discussed in Chapter 3 of section 3.2. which can be taken as modified AISC design procedure. In previous sections the effect of flanges wasn't considered. The general design procedure of EBFs with reduced link sections is the same as the design procedure of existing EBFs (unreduced link sections).

Once the link overstrength was calculated from the results of non-linear finite element analysis and experimental investigation, the governing equations have been drawn. The overstrength factor of reduced link section calculated from the experimental and analytical investigation, it has been noted that the overstrength factor proposed by other researcher in terms of link length ratio for unreduced link can be applied for the reduced link section. Thus taking in to account the effect of reduced sections of link during calculation of link length factor, the overstrength factor can be calculated simply by the equations suggested by Richard and Uang. In this chapter the plastic shear strength and ultimate shear strength (considering the overstrength factor) is presented. The developed equations was verified through the experimental and analytical results. In addition, the errors of the equations was calculated in terms of the experiment and analysis results.

From the research works available on the conventional eccentrically braced frames, different equations including initial stiffness and displacement of the total frame has been recommended. The recommended design equations have been verified through experimental and analytical results for both reduced web link and reduced web and flange links.

7.2 Design Strength and Link Length of Reduced Link Section

The plastic shear, V_p, moment, M_p, capacities and the link length factor of reduced link section have been recommended in chapter 3. In this section, it is tried to review the recommendations done in Chapter 3 and comparing the recommended design equations with experimental and analytical results considering the effect of all possible elements. Thus, the reduced web link section and reduced web and flange link section are treated separately for ease of understanding.

7.2.1 Reduced web link section

7.2.1.1 Plastic shear strength

The plastic shear force of links with reduced web section can be calculated using the design recommendation suggested in AISC but with the cross-sectional area of web being modified and the equation is expressed in Eq. (7.1):

$$V_p^{rw} = \frac{\sigma_y A_w^*}{\sqrt{3}} \quad \text{for shear yielding}$$
$$= 2M_p^{rw}/e_{rw} \quad \text{for flexural yielding} \qquad \text{.....(7.1)}$$

where σ_y: yield strength and A_w^*: the area of reduced web given in Equation (7.2) in terms of ϕ: is the diameter of perforation, n: number of perforation in a vertical alignment, e_{rw}: is the reduced web link length given by Eq (7.3) in terms of unreduced link length, M_p^{rw}: is the plastic end-moment of reduced web link section and given by Eq. (7.4).

$$A_w^* = (D - 2t_f - n\phi)t_w \qquad \text{.....(7.2)}$$

where D: the over all depth of link, t_f: flange thickness, ϕ: is the diameter of perforation, n: number of perforation in a vertical alignment, t_w: web thickness.

$$e_{rw} = \frac{de}{1 - n\phi} = \left(\frac{1}{1 - \frac{n\phi}{d}}\right).e \qquad \text{.....(7.3)}$$

where d: the depth of link, ϕ: is the diameter of perforation, n: number of perforation in a vertical alignment and e: is the unreduced link length.

$$M_p^{rw} = V_p^{rw} e_{rw}/2 \quad \text{for shear yielding}$$
$$= Z_p^{rw} \sigma_y \quad \text{for flexural yielding} \qquad \text{.....(7.4)}$$

where M_p^{rw}: plastic end moment of reduced web link, V_p^{rw}: plastic shear strength of reduced link web link. e_{rw}: reduced web link length, the depth of link, Z_p^{rw}: plastic section modulus of reduced web link, σ_y: yield strength. Web reduction has a slight effect of the plastic section modulus, hence it is ignored for simplicity.

The plastic shear strength expressed in Eq. (7.1) do not consider the effect of flanges. Thus, the plastic shear considering the effect of flange can be given by Eq. (7.5).

$$V_p^{rw\prime} = V_p^{rw} + V_f \qquad \text{.....(7.5)}$$

where $V_p^{rw\prime}$: the plastic shear strength considering the effect of flanges, V_p^{rw}: the plastic shear strength defined in Eq. (7.1) and V_f: shear carried by the flanges. The plastic shear strength including the effect of flanges have been derived by Richard and Uang, 2002. Since the equation suggested by Richard and Uang is for unreduced link, for reduced link section the link length and cross-sectional area of web can be modified, thus Eq. (7.6) can be called modified Richard and Uang equation.

$$V_p^{rw\prime} = \frac{\sigma_{yw} A_w^*}{\sqrt{3}} + \left(\frac{\sigma_{yf} b t_f^2}{2 e_{rw}} - \frac{\sigma_{yf} t_w^2 . e_{rw}}{8b} \right) \qquad \text{.....(7.6)}$$

where $V_p^{rw\prime}$: the plastic shear strength considering the effect of flanges, σ_{yw}: yield strength of web, A_w^*: the area of reduced web given in Eq. (7.2), σ_{yf}: yield strength of flange, b: is width of flange, t_f: flange thickness, t_w: web thickness.

From the geometry and material properties the plastic shear strength considering the effect of flanges can be expressed as in Eq. (7.7) which can also be called design equation suggested in this study.

$$V_p^{rw\prime} = \frac{\sigma_{yw} A_w^*}{\sqrt{3}} + \frac{\sigma_{yf} b t_f^2}{d} \qquad \text{.....(7.7)}$$

where d: depth, σ_{yw}: yield strength of web, A_w^*: the area of reduced web given in Eq. (7.2), σ_{yf}: yield strength of flange, b: is width of flange, t_f: flange thickness, t_w: web thickness. In Eq. (6.4), the first expression is the web and the second term is for flanges.

7.2.1.2 Ultimate shear strength

The maximum shear force of reduced web link (V_{ult}^{rw}) can be taken as the product of the plastic shear strength, the cyclic hardening factor (overstrength factor, Ω) and the ratio of mean to nominal material yield stress (R_y). The ultimate shear force with out considering the effect of flanges is given by Eq (7.8)

$$V_{ult}^{rw} = \Omega R_y V_p^{rw} = \Omega R_y \frac{\sigma_y A_w^*}{\sqrt{3}} \quad \text{for shear link}$$
$$= \frac{\Omega R_y M_p^{rw}}{e} \quad \text{for flexural link} \qquad \text{.....(7.8)}$$

where Ω: is the cyclic hardening factor (overstrength factor) given by Eq. (7.9) in terms of link length factor.

$$\Omega = \begin{cases} 1.44 & \rho \le 1.6 \\ 1.44 - 0.4(\rho - 1.6) & 1.6 < \rho < 2.6 \\ 2.7/\rho & \rho \ge 2.6 \end{cases} \qquad \text{.....(7.9)}$$

The ultimate shear force considering the effect of flanges called modified Richards and Uang design equation and design equation suggested in study are presented in Eq. (7.10) and Eq. (7.11) respectively.

$$V_{ult}^{rw\prime} = \Omega R_y \left[\frac{\sigma_{yw} A_w^*}{\sqrt{3}} + \left(\frac{\sigma_{yf} b t_f^2}{2 e_{rw}} - \frac{\sigma_{yf} t_w^2 . e_{rw}}{8b} \right) \right] \qquad \text{.....(7.10)}$$

$$V_{ult}^{rw\prime} = \Omega R_y \left[\frac{\sigma_{yw} A_w^*}{\sqrt{3}} + \frac{\sigma_{yf} b t_f^2}{d} \right] \qquad \text{.....(7.11)}$$

where all the variables are stated above.

The ultimate shear forces suggested above have been verified through the test and analytical results. Fig. 7.1 (a, b and c) shows the modified AISC, modified Richard and Uand and design equation suggested in this study respectively. The comparison of all equations are presented in Fig. 7.1 (c). As shown in the Fig. 7.1 (a), the ultimate shear force calculated modified AISC is less than the recorded maximum shear force of test and

analysis. The ratio $V_{\max}/V_{ult}^{rw}$ is greater than 1. Compared to modified AISC, modified Richard and Uang is better define the ultimate shear force as shown in Fig. 7.1 (b). Among all, the design equations suggested in this study is more better define the ultimate shear forced of reduced web link as shown in Fig. 7.1 (c).

The errors between the recorded maximum shear forces from test and analysis results and calculated by the modified AISC, modified Richard and Uang and the design equation suggested in this study was calculated using Eq,. (7.12).

$$\%of\,error=\left(\frac{V_{\max}-V_{ult}}{V_{\max}}\right)*100 \qquad \text{.....(7.12)}$$

where $V_{\max}$: is the recorded maximum shear force of either experiment result or the corresponding analysis result, V_{ult}: is the calculated ultimated shear force using modified AISC, modified Richards and Uang and design equations suggested in this study.

The errors expressed in terms of the calculated ultimate shear force and the maximum recorded test and analysis results were presented in Fig. 7.2. As shown in the figure, the errors calculated for modified AISC, the average error calculated in terms of test and analysis results are 8.33% and 8.88% respectively as shown in Fig. 7.2 (a). The average error calculated for modified Richard and Uang is 5.44% and 6.01% for test and analysis respectively as shown in Fig. 7.2 (b). For the design equations suggested in this study, the average errors calculated is –0.38% and 0.24% respectively for test and analysis results as shown in Fig. 7.2 (c).

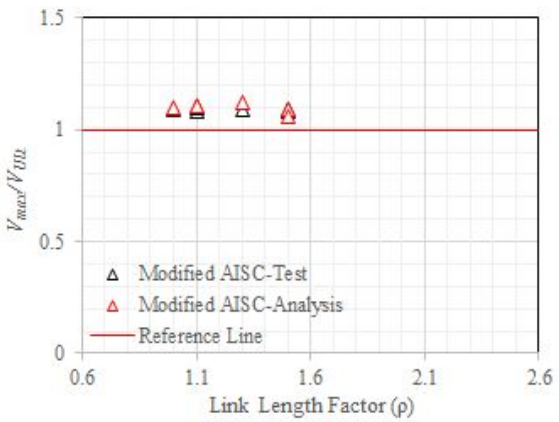

(a) Modified AISC

Fig. 7.1 Verification of suggested design equations for reduced web link section

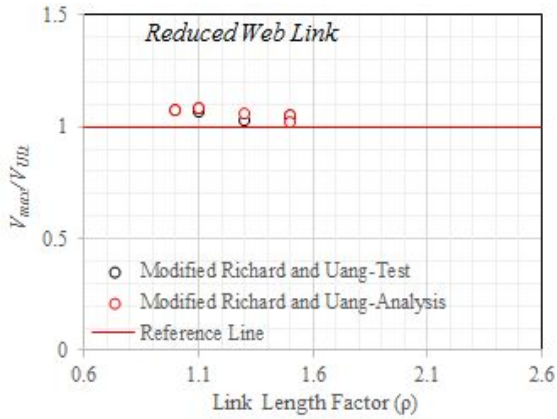

(b) Modified Richards and Uang

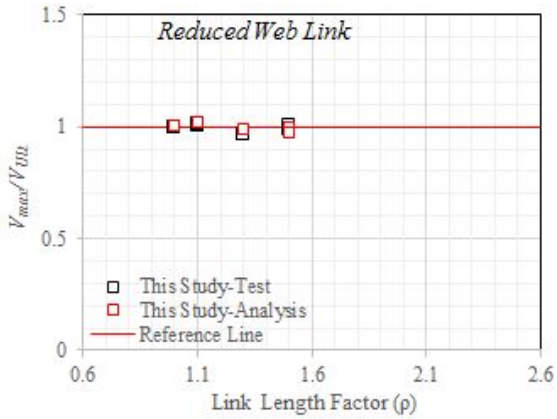

(c) Suggested in this study

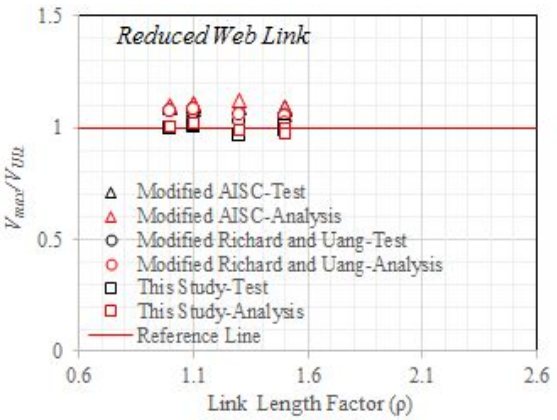

(d) Comparison of suggested equations

Fig. 7.1 Verification of suggested design equations for reduced web link section

(continue...)

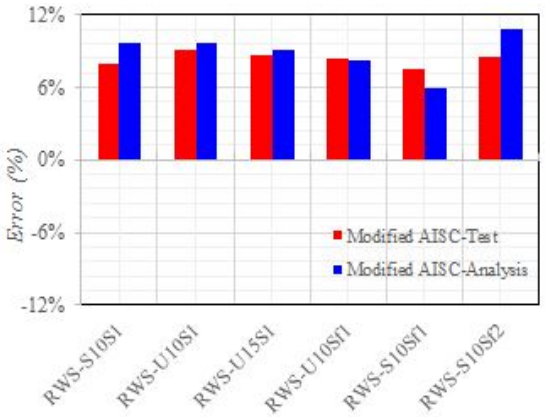

(a) Modified AISC

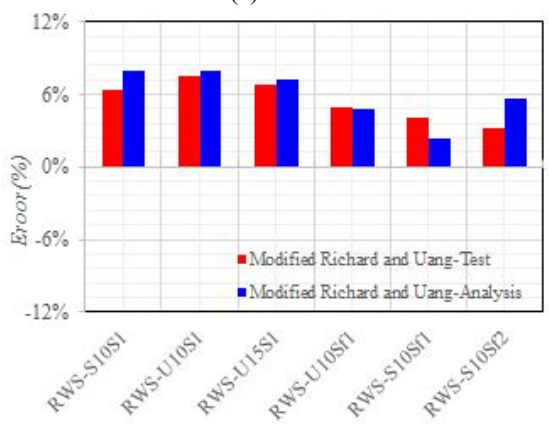

(b) Modified Richards and Uang

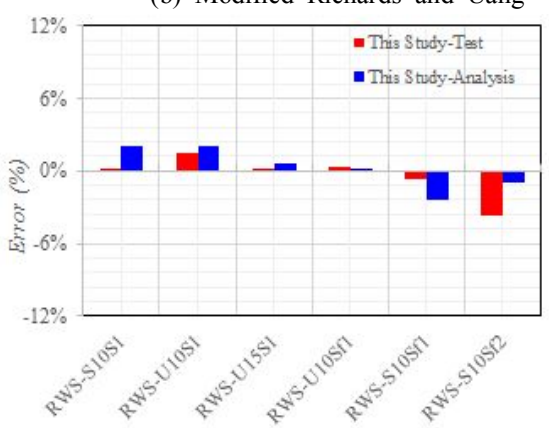

(c) Suggested in this study

Fig. 7.2 Calculated errors for suggested design equations for reduced web links

7.2.2 Reduced web and flange link section

7.2.2.1 Plastic shear strength

The plastic shear force of links with reduced web and flange section can be calculated using the design recommendation suggested in AISC but with the cross-sectional area of web being modified. The equation is expressed in Eq. (7.1) for reduced web link can be applied for reduced web and flange section for the case without flange effect. However, the shear carried by the flanges is assumed to be less compared to links with reduced web section. All the equations given above will be applicable for links with reduced web and flange section by only substituting the link flange width by: b' = b – c, where b' is the reduced link flange width, c: is the depth of reduced link flange and b: is the width of link flange. The plastic shear strength considering the effect of flanges then expressed by the modified Richard and Uang and the design equation suggested in this study as presented in Eq. (7.13) and Eq. (7.14) respectively.

$$V_p^{rl\prime} = \frac{\sigma_{yw} A_w^*}{\sqrt{3}} + \left(\frac{\sigma_{yf} b' t_f^2}{2 e_{rl}} - \frac{\sigma_{yf} t_w^2 . e_{rl}}{8b} \right) \quad \text{.....(7.13)}$$

$$V_p^{rl\prime} = \frac{\sigma_{yw} A_w^*}{\sqrt{3}} + \frac{\sigma_{yf} b' t_f^2}{d} \quad \text{.....(7.14)}$$

where $V_p^{rl\prime}$: is the plastic shear strength considering the effect of flanges, d: link depth, A_w^*: reduced web area given by Eq. (7.2), $b' = b - c$: width of reduced link flange, t_f: the thickness of flange, σ_{yw} and σ_{yf}: yield strength of web and flange respectively, e_{rl}: reduced web and flange link section length defined derived and given as in Eq. (7.15) in terms of unreduced section:

$$e_{rl} = \left(\frac{1}{1 - \frac{n\phi}{d}} \right) . \left(\frac{Z_p^{rl}}{Z_p} \right) . e \quad \text{.....(7.15)}$$

where e_{rl}: link length of reduced web section, n: number of perforation in a vertical alignment, ϕ: the opening diameters, d: depth and e: unreduced link length.

7.2.2.2 Ultimate shear strength

The maximum shear force of reduced web and flange link (V_{ult}^{rl}) can be taken as the product of the plastic shear strength, the cyclic hardening factor (Ω) and the ratio of mean to normal material yield stress (R_y). The ultimate shear force using modified AISC, modified Richard and Uang and using the design equations suggested by this study is given by Eq. (7.16), Eq. (7.17) and Eq. (7.18) respectively.

$$V_{ult}^{rl} = \Omega R_y \frac{\sigma_y A_w^*}{\sqrt{3}} \quad \text{.....(7.16)}$$

$$V_{ult}^{rl'} = \Omega R_y \left(\frac{\sigma_{yw} A_w^*}{\sqrt{3}} + \frac{\sigma_{yf} b' t_f^2}{d} \right) \quad \text{.....(7.17)}$$

$$V_{ult}^{rl'} = \Omega R_y \left[0.6\sigma_{yw} A_w^* + \left(\frac{\sigma_{yf} b' t_f^2}{2e_{rl}} - \frac{\sigma_{yf} t_w^2 . e_{rl}}{8b} \right) \right] \quad \text{.....(7.18)}$$

where the variables used in the equations are explained in above.

In order to verify the design equations expressed above, the calculated ultimate shear force and the recorded maximum shear forces of test and analysis results. Fig. 7.3 (a, b and c) is a comparison of test and analysis and the calculated ultimate shear forces using modified AISC, modified Richard and Uang and the design equation suggested by this study respectively. Link reduced web link section, the ratio of maximum shear to ultimate shear forces using the modified AISC is greater than one. That means the maximum recorded shear forces are greater than the calculated shear forces calculated using modified AISC as shown in Fig. 7.3(a). The ratio of $V_{\max}/V_{ult}$ is also greater than one for the ultimate shear forces calculated using modified Richard and Uang as shown in Fig. 7.3(b). However, compared to modified AISC, the modified Richard and Uang is better define the maximum shear forces of reduced web and flanges links. Looking at the Fig. 7.3(c), the ratio of $V_{\max}/V_{ult}$ is approximately one which indicates that the design equation suggested in this study including the effect of flange is better define the maximum shear forces of reduced web and flange links compared to modified AISC and modified Richard and Uang.

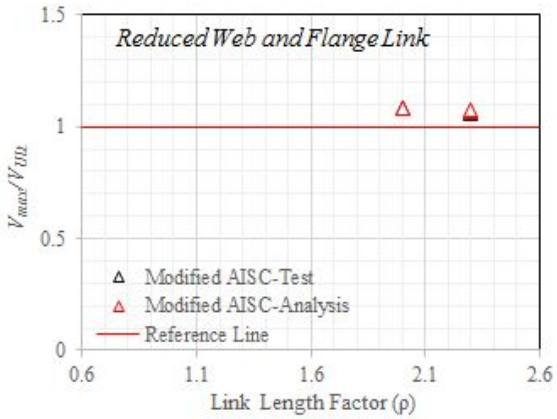

(a) Modified AISC

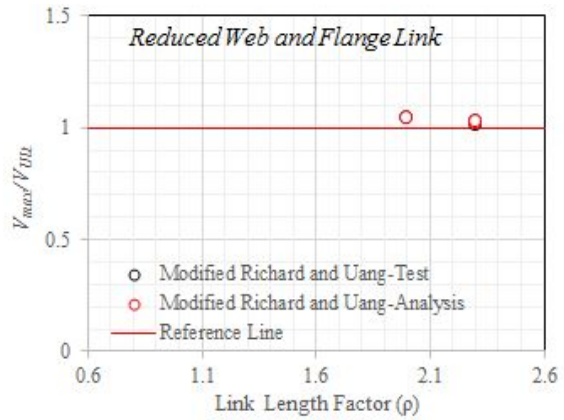

(b) Modified Richards and Uang

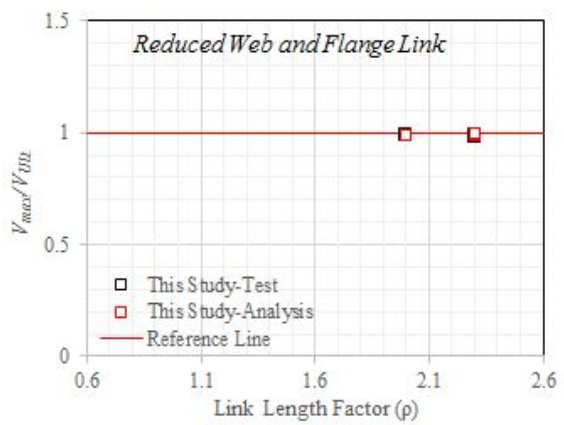

(c) Suggested in this study

Fig. 7.3 Verification of design equations for reduced web and flange link section

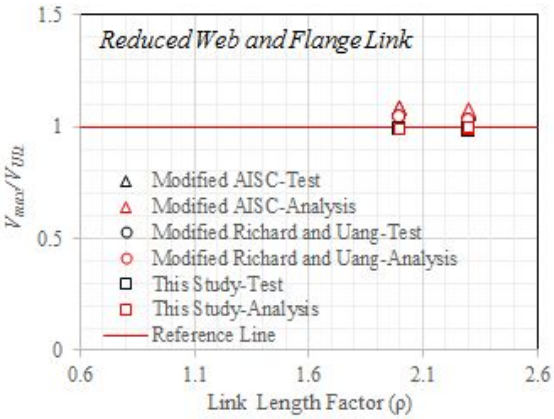

(d) Comparison of suggested equations

Fig. 7.3 Verification of design equations for reduced web and flange link section *(continue...)*

The error of design equation for reduced web and flange link section has also been calculated in the same way it was done for reduced web link section. The errors was calculated using Eq. (7.12). The calculated errors are presented in Fig. 7.4 (a, b and c) for modified AISC, modified Richard and Uang and design equation suggested in this study respectively. The errors for modified AISC for test and analysis is 6.57% and 6.9% respectively as shown in Fig. 7.4(a). The average error for modified Richard and Uang using test and analysis is 2.72% and 3.06% respectively as in Fig. 7.4(b). Similarly for the design equations suggested in this study, the average error using test and analysis result is –1.17% and –0.815% respectively. From the calculated errors, it can be noted that the design equations suggested in this study is less than the errors calculated for modified AISC and modified Richard and Uang design equations.

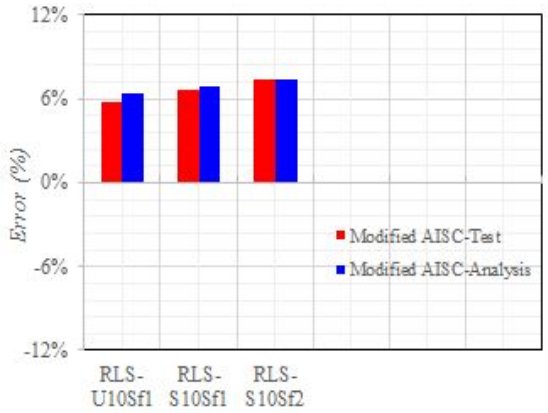

(a) Modified AISC

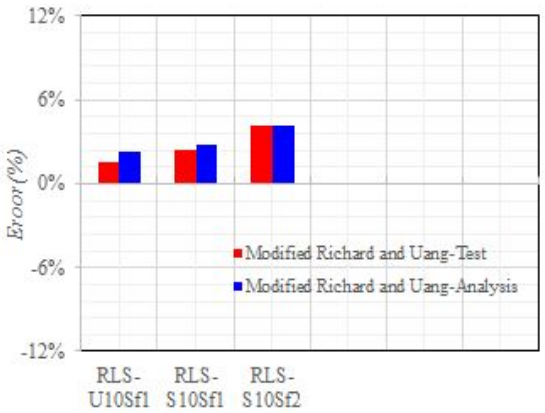

(b) Modified Richards and Uang

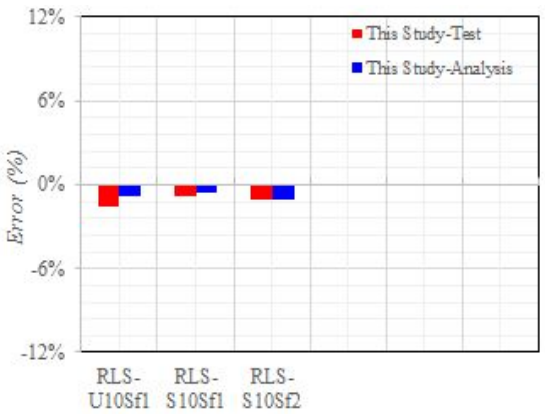

(c) Suggested in this study

Fig. 7.4 Calculated errors for suggested design equations for reduced web and flange link sections

7.3 Summary

The design equations are important to predict the general behaviour of any structures. For the developed links called reduced web link and reduced web abd flange link section, the suggested design equations have been verified through experimental and analytical results. Three different design equations have been suggested. Namely: modified AISC, modified Richard and Uang and the equation developed in this study for both nominal shear strength and ultimate shear strength. The ultimate shear strength can be calculated considering the overstrength factor which is the ratio of maximum shear force to the nominal shear strength.

8. Summary and Recommendations

8.1 Introduction

The structural performance of reduced link section used in eccentrically braced frames including the plastic deformation capacity, buckling and failure mode. The proposed links addresses the limitations of existing eccentrically braced frames including EBFs with replaceable links. The investigations was made to identify the characteristics of proposed links both analytically and experimentally. In this section, the summary of analytical and experimental studies and recommendations including the future works to be done is presented.

8.2 Summary

Before the start of evaluations using analysis and experiment, a design procedures for links with reduced web section and links with reduced web and flange section was made. The design was made considering: equal end moments developed in the links, engineering mechanics of material, geometry and existing design recommendation from the available standards and literatures. The ultimate shear forces for the design of reduced link web suggested considering the overstrength factors. The recommended design equation have been cross-checked with both loading test results and finite element analysis results. From the comparison, it can be noted that, the design equations suggested can be used to estimate the basic strengths of reduced link section.

From the design the possible geometrical variables such as section compactness, the percent of open area (the diameter of perforations), link length factor, arrangement of perforations (inclination angle of perforations) and effect of stiffeners. Then the preliminary analysis was conducted in order to understand the general behavior and identify the sensitive parameters in the design of reduced link section. The link-to-column connection in eccentrically braced frames lacks the desired plastic rotation recommended in AISC provision. Okazaki et el. conducted a series of experimental investigation and concluded that link-to-column connections should be avoided because of their limited ductility resulting from flange fracture which was found to be a major concern for links of all practical lengths.

The proposed links addresses the limitations of existing eccentrically braced frames listed in statements of problems including link-to-column connections. From the general perspective of design procedures, experimental investigation and FE analysis the following conclusions was drawn.

1. the design and detail of proposed links are isolated from the other structural components such as the collector beam, from column in link-to-column connections of eccentrically braced frames. Therefore, it helps to simplify and make easy to maintain, repair or replace the active portion of frame which is the link beam with out disturbing the functionality as well as serviceability of the building. This will address the limitations observed in conventional eccentrically braced frames.

2. researcher come-up with the concept of replaceable links concepts. Literatures suggested that, in order to control the plastic deformation only at the link, the link should have weaker in strength or less cross-sectional area. In case difference in cross-sectional area, the slab may need a deck support the replaceable link according to New Zealand Steel Constitution. This phenomenon has been one of the limitations of replaceable links. Since the detail of the proposed link section is reduced the web section, the strength significantly decreases and this will help to control the plastic deformation at the link easily with out decreasing the depth of link i. e with equal cross-section with the collector beam. Thus, the web reduction makes the proposed link weaker in strength so that the plastic deformation can be easily controlled only at the links with an equal cross-section of link with collector beam, hence no deck support is needed as in EBFs with replaceable links.

3. link-to-column connections in EBFs have been a critical problem. AISC also warns the designer in during the designing and detailing of link-to-column connection. Experimental loading test results and FE analysis, it was known that in link-to-column connection, the of link-to-column connection in eccentrically braced frames was fracture of the link flange initiating near the groove weld which connects the link to the column flange because of the fracture is concentrated at the web of reduced area prior to the required plastic rotation. This is due to column connection attracts greater moments because the axial stiffness of column is stiffer than the flexural stiffness of the collector beam.

Putting holes in the shear plate increases the plastic strain and stress triaxiality at the edge of holes. In return the plastic strain and stress concentration at the flanges decreases. Thus, the failure supposed to occur at the flange moves to the web. This will address the limitations in link-to-column connection as the failure supposed to be occurred at link flanges in the column face before reached at the plastic rotation is controlled.

4. design procedure for reduced web link was presented in terms of flow chart. The minimum ϕ/d ratio was set in terms of plastic shear strength ratio of reduced web link and unreduced links. The minimum plastic shear strength is assumed to be greater than 0.5 in order to allow the link absorb seismic energy. Thus, the minimum ϕ/d ratio will be determined from the relationship with striction of plastic shear strength ratio of reduced web link and unreduced links.

5. quasi static loading test have been carried out in order to examine the plastic deformation and the failure mode of reduced link section. two types of links was considered: shear links and intermediate links. For intermediate link, both reduced web and reduced web and flange links were considered. The loading protocol used to evaluate the test specimens were the revised protocol of AISC. The test results shows that both reduced web and flange links satisfied the rotation limit recommended in AISC seismic provision. All test specimens shows a crack at the edge of holes introduced on the web before final fracture and proves the assumed behavior of reduced web links.

6. compared to unstiffened reduced links, stiffened links show stable hysteresis response at large displacement. This is due to the fact that out-of-plane buckling is formed in unstiffened links compared to stiffened specimens. Stiffeners have no effect on the initial stiffness. The maximum shear force resisting capacity of unstiffened link is less compared to stiffened specimens and therefore the ratio of maximum shear force and nominal plastic shear strength (overstrength factor) of stiffened link is bigger compared to unstiffened links. The cumulative plastic rotation of stiffened links was bigger than the cumulative plastic rotation of unstiffened links.

7. link section reduction type i.e reduced web and reduced web and flange has no effect on the hysteresis response, plastic rotation as well as shear resisting capacity. In unstiffened links the failure mode of reduced web and reduced web and flange section is the same. However, the for stiffened reduced web and flange link section, a plastic hinge is formed at reduced flange section. Thus, for stiffened web and flange link section has a dual advantage. These are: 1. the strength is reduced because of the reduced web section and 2. because of the reduced flange the plastic hinge is formed at the reduced flange section.

8. a calibrated finite element simulation model was created from the experimental investigations. A combined harding model with parametric material modeling was used and the hysteresis response as well as the deformed shape with equivalent plastic strain distribution of analysis model was compared with the test results. From the comparison of hysteresis response the maximum shear resistance of test and analysis agreed well. However, there is some mis matching in the bouncing effect. This might be due to the errors arise during experiment and it might also be the limitations of finite element simulation. The plastic rotation (γ_p) which is given by: $\gamma_p = \gamma - \frac{V}{eK_e}$ where γ: is the total link rotation, V: plastic shear strength, e: link length and K_e: is the elastic stiffness, of analysis and experimental results were also compared. The total link rotation for test specimen is taken at the point where the strength degrades. For analysis simulation, the link rotation is taken at the point where the strength degrades and/or at the point where the failure index reached unity. The indexes are maximum at the edge of perforations of link in most of analysis specimens considered. The plastic rotation capacity of test and analysis results were well agreed.

9. once the FE simulation is verified through experimental results, parametric study was conducted to consider unconsidered parameters during experiment. Which includes link length, percent of reduced web area, and link-to-column connection (unequal end moment). As the link length increase, the plastic rotation capacity decreases and most of flexural links fails to achieve the rotation level recommended in AISC provision. The effect of percent of reduced web area was also discussed. The percent of reduced web area affects both shear resisting capacity and initial stiffness where the percent of reduced web area increases the shear force resisting capacity and initial stiffness decreases. The reduced web

amount has a mixed effect on the plastic rotation capacity but in most cases as the percent of reduced web area increase the plastic rotation limit decreases and when it exceeds 25%, the plastic rotation failed to satisfy the level recommended in AISC seismic provision. Initial stiffness decreases as the percent of reduced web area increases. The rate at which the initial stiffness decreases as the amount of reduced web area increases is bigger as the link length factor decreases. The rate at which the initial stiffness decrease for shear link is bigger compared to intermediate and flexural links.

10. the effect of reduced web on the link-to-column connection has also been evaluated analytically considering reduced web link and unreduced links as well as link length as a parameter. The hysteresis response and deformed shape was compared. The hysteresis response shows that the hysteresis curve of unreduced link is unstable compared to reduced web link for shear and intermediate links. The total link rotation is decided by calculating the failure index for both reduced and unreduced links. The plastic rotation was compared and unreduced links failed to satisfy the rotation level where as reduced link satisfied the rotation limit for both shear and intermediate links. The stress and equivalent plastic strain concentration of reduced and unreduced web link was measured and for shear links. The triaxial stress and equivalent plastic strain of flanges at connection decreases as the percent of reduced web area increases. For the web, the triaxial stress and equivalent plastic strain increases as the reduced web area increases. Which shows the advantage of reduced web link section in link-to-column connection.

11. the damping ratio and effective stiffness of reduced shear link and unreduced shear link was calculated and compared. The damping ratio of reduced shear link decreases as the effective stiffness increased rapidly compared to the damping ratio of unreduced link shear section. From the comparison of damping ratio versus number of cycle, the average value of damping ratio of reduced link is bigger compared to unreduced links. From the comparison of effective stiffness, unreduced link section has high effective stiffness at low cycle and the average value of effective stiffness of unreduced link section also bigger compared to reduced shear link.

12. Design equations for both nominal shear strength and ultimate shear strength were recommended which includes the modified AISC, modified Richard and Uang. The recommended equations have been verified through the experimental and analytical data. For each of the recommended design equations the errors has also been calculated and the design equations suggested in this study considering the effect of flanges has shown less error compared to the design equation of modified AISC and modified Richard and Uang. Web section reduction has a significant effect on the shear strength and flange section reduction has sensitive towards the plastic bending moment.

8.3 Recommendations

This dissertation can be taken as pilot work for further investigation including full scale experimental investigations. The effect of the parameters included in this research work also needs to be researched further. The most important things to be considered is the arrangements of perforations in web.

1) both experimental and analytical on investigations on different configurations of EBF links with reduced link sections are recommended, for links of various cross-sections and link lengths. Optimization of reduced web area needs to be done in order to come-up with the maximum possible web reduction that satisfy the target plastic rotation limit. The optimization will also helps to identify no only the maximum possible allowable reduced web area but also to find out the reduced amount area with maximum plastic deformation capacity. This is usually because in some cases of as the percent of reduced web area increases the plastic rotation capacity is bigger even for links equal end moments.

2) different types web area reduction geometry is also recommended. For instance: vertical ellipse, horizontal ellipse and diagonal ellipse. The effectiveness of each of these reduction geometries needs also evaluated to understand the performance of links such as the plastic deformation capacity and a clear failure mode. It is assumed that links with web area reduced with elliptical shape will have different response than circular hole because researches shows that plates with circular hole and elliptical hole behaves differently.

3) web area reduction arrangements other than the possible arrangements used in this study. The effects of web area arrangements needs to evaluated for studies. The arrangements may vary for stiffened and unstiffened links because it is difficult to keep the hole arrangements and stiffeners spacing at the same time as stiffeners sometimes restricts the hole arrangements.

4) the stiffeners requirements of the provisions needs to be revised or altered because of the reduced link section geometry. The spacing also needs to be revised depending on the reduced areas.

5) full scale experimental investigation is highly recommended especially for link-to-column connection of eccentrically braced frames considering different connection types, loading history, cross-section and link length..

6) Application of the proposed links needs to be evaluated using time history or other evaluation mechanism.

References

[1] ABAQUS. Analysis user's manual IV. Version 6.10. USA: ABAQUS, Inc., Dassault Systèmes; 2007.

[2] ABAQUS. Analysis user's manual IV. Version 6.14. USA: ABAQUS, Inc., Dassault Systèmes; 2011.

[3] ABAQUS, Inc. ABAQUS Analysis Reference Manual 2010 3. ABAQUS, Inc. ABAQUS Analysis User's Manual 2010.

[4] AISC. 2005. Seismic Provisions for Structural Steel Buildings, ANSI/AISC 341-05. *American Institute of Steel Construction, Chicago, Illinois, 309.*

[5] AISC. 2010. Seismic Provisions for Structural Steel Buildings, ANSI/AISC 341-10. *American Institute of Steel Construction, Chicago, Illinois, 309.*

[6] Arce, G., Okazaki, T., & Engelhardt, M. D. (2001). Experiments on the Impact of Higher Strength Steel on Local Buckling and Overstrength of Links in EBFs. Chicago: *American Institute of Steel Construction.*

[7] Arce, G., & Engelhardt, M. D. (2003). Experiments behavior of shear and flexural yielding links of ASTM 992 steel. In: STESSA 2003: *proceedings of the conference on behaviour of steel structure, pp 107-114*

[8] Amin M., Behrouz C., (2014). Overstrength and rotation capacity for EBF links made of European IPE sections. *Thin-Walled Structures (74) pp255–260*

[9] Anil K. Chopra. Dynamics of Structures: Theory and application to earthquake engineering. Prentice Hall, 1995, USA.

[10] Australian Standards(1998). AS 4100-1998, Steel Structures , Sydney, Australia.

[11] Balut N. and Gioncu V. (2003). Suggestion for an improved 'dog-bone' solution. *In STESSA 2003. Proceedings of the Conference on Behaviour of Steel Structures in Seismic Areas, 9–12 June, Naples, Italy, Mazzolani FM (ed.). A.A. Balkema Publishers: Rotterdam, 129–134.*

[12] Bhowmick A. K., Grondin G.Y. & Driver R.G. Nonlinear Seismic Analysis of Perforated Steel Plate Shear Walls. *Proceeding of 15th world congress on earthquake engineering, 2012, Lispon , Portugal.*

[13] Brian K. and Iyad H. A., (1992). Steel Structures Design Manual To As 4100. *Thin-Walled Struct., 14, 139–151.*

[14] Chaboche J.L (1986). Time independent constitutive theories for cyclic plasticity. *International Journal of Plasticity;2(2):149–188.*

[15] Chao Shih-Ho, Khandelwal Kapil, El-Tawil Sherif. Ductile web fracture initiation in steel shear links. *J Struct Eng 2006;132(8):1192-1200.*

[16] Chi. W-M. (2000), "Prediction of steel connection failure using computational fracture mechanics," Ph.D. Thesis submitted to Stanford University, Stanford, CA

[17] Chi. W-M, Kanvinde, A.M., and Deierlein, G.G., (2006). "Prediction of Ductile Fracture In Welded Connections Using the SMCS Criterion," *Journal of Structural Engineering, ASCE, 132(2), 171-181.*

[18] Clifton G.C., Nashid H., Ferguson G, Hodgson M., Seal C., Bruneau M., MacRae G.A., Gardiner S., (2013). Performance of Eccentrically Braced Framed Buildings In The Christchurch Earthquake Series of 2010/2011. *proceeding of 15WCEE, Lisbon.*

[19] Dam Safety Office, Nonlinear Response of Steel Beams. *Report No. DSO-00-01, Department of the interior Bereau of Reclamation, December, 2000.*

[20] Daniel Y. Abebe *and* Jaehyouk Choi (2015). Finite element Imvestigation on Removable Shear Link with Perforated Web. *Proc. of the 2nd Australian Conference on Computational Mechanics, 30 Nov-1 December, Brisbane, Australia.*

[21] Daniel Y. Abebe, *Gyumyong Gwak, Meron W. Lemma*, Jaehyouk Choi (2015). Development and Analytical Evaluation of Removable Shear Link with Perforated Web. *Proc. of International Conference on Mechanical Engineering and Advanced Material 2015,3-4 December, 2015, Kota Kinabalu, Sabah, Malaysia (Invited Paper)*

[22] Daniel Y. Abebe, G.Y. Gwak, S.J.Jeong and Jaehyouk Choi (2016). Analytical Investigation on removable reduced link sections for EBFs. *Proc of the 7th International Conference on Computational Methods, August 1-4, Berkeley, CA, USA.*

[23] Daniel Y. Abebe**,** G.Y. Gwak and Jaehyouk Choi (2016). Design of removable link beams with perforated web used in EBFs. *Proc. of 2016 International Conference on Advances in Structural Monitoring and Maintenance, August 28-September1, Jeju, KOREA.*

[24] Daniel Y. Abebe**,** G.Y. Gwak and Jaehyouk Choi (2016). Reduced Web and Flange Link Sections to Enhance the Ductility of Link-to-column Connections in EBFs. *Proc. of 2nd World Congress and Exhibition on Construction and Steel Structure, September 22-24, Las Vegas, Nevada, USA.*

[25] Daniel Y. Abebe**,** G.Y. Gwak and Jaehyouk Choi (2016). Replaceable reduced web link section for link-to-column connections in EBFs. *Proceeding of Australian Earthquake Engineering Society Annual Conference, Nov 25-27, 2016 Melbourne, AUSTRALIA.*

[26] Della Corte G., D'Aniello M., Landolfo R., (2013). Analytical and numerical study of plastic overstrength of shear links. *Journal of Constructional Steel Research (82) 19–32.*

[27] Deng K, Pan P., Li W., Xue Y., (2015). Development of a buckling restrained shear panel damper. *Journal of Constructional Steel Research 106, pp 311–321.*

[28] Dusicka, P. and Iwai, R. (2007). Development of linked column frame system for seismic lateral loads. *Proceedings of the SEI Structures Congress, Vancouver, B.C. American Society of Civil Engineers.*

[29] Dusicka, P. and Lewis, G. (2010). Investigation of replaceable sacrificial steel links. *Proceedings of the 9th U.S. National and 10th Canadian Conference on Earthquake Engineering, number 1659. EERI.*

[30] El-Tawil, S., Vidarsson, E., Mikesell, T., and Kunnath, K. (1999). Inelastic behavior and design of steel panel zones. *Journal of Structural Engineering, ASCE,125(2), 183-193.*

[31] El-Tawil S., Mikesell, T., and Kunnath, S. K. (2000). Inelastic behavior and design of steel panel zones. *Journal of Structural Engineering, ASCE,126(1), 79-87.*

[32] El-Tawil, S., Vidarsson, E., Mikesell, T., and Kunnath, K. (2000). Inelastic behavior and design of steel panel zones. *Journal of Structural Engineering, ASCE,126(2), 274-276.*

[33] Engelhardt, M.D. and Popov, E.P. (1989b). "On design of eccentrically braced frames." *Earthquake Spectra*, 5(3).

[34] Engelhardt, M.D. and Popov, E.P. (1992). "Experimental performance of long links in eccentrically braced frames." *Journal of Structural Engineering*, American Society of Civil Engineers, 118(11), 3067-3088.

[35] Engelhardt, M.D. and Husain, A.S. (1993). "Cyclic-loading performance of welded flange-bolted web connections." *Journal of Structural Engineering*, 119(12), 3537-3550.

[36] Engelhardt, M.D. and Sabol, T.A. (1994). "Testing of welded steel moment connections in response to the Northridge earthquake." *Progress report to the AISC advisory Subcommittee on Special Moment Resisting Frame Research*.

[37] Engelhardt, M.D. and Sabol, T.A. (1997). "Seismic-resistant steel moment connections: developments since the 1994 Northridge earthquake." *Progress in Structural Engineering and Materials*, 1(1), 68-77.

[38] Engelhardt, M.D., Winneberger, T. Zekany, A.J., and Potyraj, T.J. (1998a). Experimental investigation of dog-bone moment connections. *Engineering Journal*, AISC, 35(4), 128-139.

[39] Engelhardt, M.D. and Sabol, T.A. (1998). "Reinforcing of steel moment connections with cover plates: benefits and limitations." *Engineering Structures*, 20(4-6), 510-520.

[40] Engelhardt, M.D. (1999) "The 1999 T. R. Higgins Lecture: Design of Reduced Beam Section Moment Connections," *Proceedings: 1999 North American Steel Construction Conference*, American Institute of Steel Construction, Toronto, Canada, pp. 1-1 to 1-29.

[41] Englekirk, R. 1994. Steel structures: Controlling behavior through design, *Wiley, New York, 481–484.*

[42] Esin A. (1968). The microplastic strain energy criterion applied to fatigue. *Journal of Basic Engineering, ASME 90(1):28-36.*

[43] Fell BV, Myers AT, Deierlein GG, Kanvinde AM (2006). Testing and simulation of ultra-low cycle fatigue and fracture in steel braces. I*n: Proc. 8th US national conference on earthquake engineering. Paper no. 587.*

[44] Fussell A.J., Cowie K.A., Clifton G.C. and Mago N., Development and research of eccentrically braced frames with replaceable active links. *proceeding of 2014 NZSEE.*

[45] Ghobarah A. and Ramadan T. (1994). Bolted link-column joints in eccentrically braced frames. *Engineering Structures, 16(1): 33–41.*

[46] Heidrun Osp Hauksdottir (2008). Application of the Reduced Beam Section Concept for Improving the Ductility of Certain Eccentrically Braced Frames. *Master thesis, University of Washington.*

[47] Hjelmstad, K.D. and Popov, E.P. 19 83a. Seismic behaviour of active beam links in eccentrically braced frames. *Report No. UCB/EERC-83/15. University of California, Berkeley, California*.

[48] Hjelmstad, K.D. and Popov, E.P. 19 83b. Cyclic behaviour and design of link beams. *Journal of Structural Engineering, ASCE 109(10) 2387-2403.*

[49] Gardiner S., Clifton G. C. and MacRae G. A., (2013). Performance, damage assesment and repair of a multistorey eccentrically braced framed building following the Christchurch earthquake series. *Steel Innovations Conference, Christchurch, New Zealand 21-22 Febr.*

[50] Hancock J.W. and Mackenzie A.C. (1976). On the mechanics of ductile failure in high-strength steel subjected to multi-axial stress-states. *J Mech. Phys Solids; 24: 147-169.*

[51] Hanson R. D., Xia C. and Su Y. F. (1992). Design of supplemental steel damping devices for buildings. *Proc. 10th world congress on earthquake engineering. Balkema, Rotterdam*.

[52] Hancock J.W. and Mackenzie A.C. (1976). On the mechanics of ductile failure in high-strength steel subjected to multi-axial stress-states. *J Mech. Phys Solids; 24: 147-60.*

[53] Hanson R. D., Xia C. and Su Y. F. (1992). Design of supplemental steel damping devices for buildings. *Proc. 10th world congress on earthquake engineering. Balkema, Rotterdam.*

[54] Hjelmstad, K. D., and Popov, E. P. (1983). “Seismic behavior of active beam link in eccentrically braced frames.” Rep. No. UCB/EERC-83/ 15, Earthquake Engineering Research Center, Univ. of California, Berkeley, CA.

[55] Horne, J. P., Rubbo, A., and Malley, J. O. (2001). AISC-LRFD design and optimization of steel eccentrically braced frames. *Proc. 70th Annual SEAOC Meeting, San Diego.*

[56] Housner G. W. (1961). Vibration of structures Induced by Seismic Waves-Part I Earthquake. *Shock and Vibration Handbook (Harris, C.M., and Crede C. E eds.) McGraw-Hill Book Co., Inc., N.Y.*

[57] Housner G. W. and Jennings P. C., (1964). Generation of Artificial Earthquake. *Jour. Eng. Mech. Div., Procedings ASCE Feb.*

[58] Itani, A. M. (2002). “Cyclic behavior of shear links and tower shaft assembly of San Francisco–Oakland bay bridge tower.” Rep. No. CCEER 02-06, Center for Civil Engineering Earthquake Research, Univ. of Nevada at Reno, Reno, NV.

[59] Jacobsen L.S. (1930). Steady Forced Vibration as Influenced by Damping. *Trans ASME Vol. 51, p 227.*

[60] *Jeffrey W. Berman and Michel Bruneau (2006).* Further Development of Tubular Eccentrically Braced Frame Links for the Seismic Retrofit of Braced Steel Truss Bridge Piers. *Technical Report MCEER-06-0006, University at Buffalo, State University of New York*

[61] Jeffrey W. Berman, Taichiro Okazaki, and Heidrun O. Hauksdottir (2010). Reduced Link Sections for Improving the Ductility of Eccentrically Braced Frame Link-to-Column Connections. *J. Struct. Engineering, 136(5): 543-553*

[62] Ji X., Wang Y., Ma Q. and Okazaki T. (2016). Cyclic behavior of very short steel shear links. J. Struct. Eng. 142(2) 04015114-1-10

[63] Jin J. and El-Tawil S. (2003). Inelastic Cyclic Model for Steel Braces. *Journal Engineering Mechanics, 129(5), 548-557.*

[64] Jin J. and El-Tawil S. (2005). Evaluation of FEMA-350 Seismic Provisions for Steel Panel Zones. *J. Struct. Eng., 131(2), 250-258.*

[66] Jones, S. L., Fry, G. T., and Engelhardt, M. D. (2002). Experimental evaluation of cyclically loaded reduced beam section moment connections. *J. Struct. Eng., 1284, 441–451*

[67] Kasai K. and Popov E. P. (1986). Cyclic web buckling control for shear link beams. *J. Struct. Eng., 10.1061/(ASCE)0733-9445(1986)112:3 (505), 505–523.*

[68] Kailai Deng, Peng Pan, Chaoyi Wang (2013). Development of crawler steel damper for bridges. *Journal of Constructional Steel Research (85) 140–150.*

[69] Kailai Deng, Peng Pan, Jiangbo Sun, Jixin Liu, Yantao Xue (2014). Shape optimization design of steel shear panel dampers. *Journal of Constructional Steel Research (99) 187–193.*

[70] Kailai Deng, Peng Pan, JWei Li, Yantao Xue (2015). Development of a buckling restrained shear panel damper. *Journal of Constructional Steel Research (106) 311-321.*

[71] Kanvinde, A.M. and Deierlein, G.G. (2004). Micro mechanical simulation of earthquake-induced fracture in steel structures. *Stanford University.*

[72] Kanvinde, A.M. and Deierlein, G.G. (2006). Void growth model and stress modified critical strain model to predict ductile fracture in structural steels. *Journal of Structural Engineering ASCE. 132: 12, 1907-1918.*

[73] Kanvinde, AM. and Deierlein, GG. (2007). Finite-element simulation of ductile fracture in reduced section pull plates using micromechanics fracture models. *J. Struct. Eng. 133:5, 656–664.*

[74] Kanvinde, A.M. and Deierlein, G.G. (2007). Cyclic void growth model to assess ductile fracture initiation in structural steels due to ultra low cycle fatigue. *Journal of Engineering Mechanics. 133: 6, 701-712.*

[75] Kanvinde, A.M. and Deierlein, G.G. (2008). Validation of cyclic void growth model for fracture initiation inblunt notch and dogbone steel specimens. *Journal of Structural Engineering ASCE. 134: 9, 1528-1537.*

[76] Karami Mohammadi R., Moussavi Nadoushani Z. S., (2012). Optimum Design of Eccentrically Braced Frames Using Endurance Time Method. *Proceeding of WCEE, Lisbon.*

[77] Kaufmann EJ, Metrovich BR, Pense AW (2001). Characterization of cyclic inelastic strain behavior on properties of A572 Gr. 50 and A913 Gr. 50 rolled sections. *ATLSS Rep. No. 01-13. Bethlehem (Pa): National Center for Engineering Research on Advanced Technology for Large Structural Systems, Lehigh Univ.*

[78] Kerem Gulec C., Bruce Gibbons, Albert Chen, Andrew S. Whittaker (2011). Damage states and fragility functions for link beams in eccentrically braced frames. *Journal of Constructional Steel Research (67) 1299–1309*

[79] KBC (2011). Korean Building Code. *Korea Construction Standard Center (KCSC)*

[80] Koboevic S., Rozon J. and Tremblay R. (2012). Seismic Performance of Low-to-Moderate Height Eccentrically Braced Steel Frames Designed for North American Seismic Conditions. *Journal of Structural Engineering, 138(12) 1465-1476.*

[81] Krawinkler, H., Gupta, A., Medina, R., and Luco, N. (2000). Loading histories for seismic performance of testing of SMRF components and assemblies. *Report No. SAC/BD-00/10*, SAC Joint Venture, Sacramento, CA.

[82] Mackenzie A., Hancock J., Brown D., 1977. On the influence of state of stress on ductile failure initiation in high strength steels. *Engineering Fracture Mechanics, Vol.9:167–88.*

[83] Mahmoudi M, Zaree M., (2011). Evaluating the overstrength of concentrically braced steel frame systems considering members post-buckling strength. *International Journal of Civil Engineering 9(1):57-62.*

[84] Malley JO, Popov EP (1983). Design considerations for shear links in eccentrically braced frames. *Report no. UCB/EERC-83/24. Berkeley (CA): Earthquake Engineering Research Institute.*

[85] Manheim D. N., (1982). On the Design of Eccentrically Braced Frames, *Thesis, D. Eng, Department of Civil Engineering, University of California at Berkeley.*

[86] McClintock F. A., 1968. A criterion of ductile fracture by the growth of holes. *Journal of Applied Mechanics, vol. 35, issue 2, p. 363.*

[87] McDaniel, C. C., Uang, C. M., and Seible, F. (2003). "Cyclic testing of built-up steel shear links for the new bay bridge." J. Struct. Eng., 129:6(801), 801–809.

[88] Myers, A.T. (2010). Testing and probabilistic simulation of ductile fracture initiation in structural steel components and weldments. *Ph.D. thesis, Stanford University*.

[89] Myers, A.T., Deierlein, G.G. and Kanvinde, A. (2009). Testing and probabilistic simulation of ductile fracture initiation in structural steel components and weldments. *Stanford University.*

[90] Myers, A.T., Kanvinde, A.M., Deierlein, G.G. and Fell, B.V. (2009). Effect of weld details on the ductility ofsteel column baseplate connections. *Journal of Constructional Steel Research. 65: 6, 1366-1373.*

[91] Nabil Mansour (2010). Development of the design of eccentrically braced frames with replaceable shear links. *Doctoral thesis, University of Toronto.*

[92] Nabil M., Constantin C. and Robert T. (2010). Experimental Validation of Replaceable Shear Links for Eccentrically Braced Steel Frames. *Journal of Structural Engineering V(137) 10, p1141–1152.*

[92] Needleman, A. and Tvergaard, V. (1984). An analysis of ductile rupture in notched bars. *Journal of the Mechanics and Physics of Solids. 32: 6, 461-490.*

[93] Nip K.H., Gardner L., Davies C.M., and Elghazouli A.Y., (2010). Extremely low cycle fatigue tests on structural carbon steel and stainless steel. *Journal of Constructional Steel Research 66 96110*

[94] Okazaki, T., (2004). Seismic performance of link-to-column connections in steel eccentrically braced frames. *PhD dissertations, University of Texas at Austin.*

[95] Okazaki, T., Arce, G., Ryu, H.C., & Engelhardt, M.D. (2005). Experimental study of local buckling, overstrength, and fracture of links in eccentrically braced frames. *Journal of Structural Engineering, 131(10), 1526-1535.*

[96] Okazaki, T., Engelhardt, M., (2006). Cyclic loading of EBF links constructed ofA STM A992 steel. *Journal of Constructional Steel Research, 63: 751-765.*

[97] Okazaki, T., Liu, D., Nakashima, M., and Engelhardt, M. (2006). Stability requirements for beams in seismic steel moment frames. *J. Struct. Eng., 132(9), 1334-1342.*

[98] Oh C. S., Kim N. H., Kim Y. J., Baek J. H., Kim Y. P., Kim W. S., (2011). A finite element ductile failure simulation method using stress-modified fracture strain model. *Engineering Fracture Mechanics (78) 124–137.*

[99] Ohsaki M. and Nakajima T. (2012). Optimization of link member of eccentrically braced frames for maximum energy dissipation. *Journal of Constructional Steel Research 75, 38–44.*

[100] *Paul W. Richards and Chia-Ming Uang (2006).* Testing Protocol for Short Links in Eccentrically Braced Frames. *J. Struct. Eng., 132(8): 1183-1191.*

[101] Paul W. Richards (2010). Estimating the Stiffness of Eccentrically Braced Frames. *Pract. Period. Struct. Des. Construction, 15(1): 91-95.*

[102] Pristley M. J. N. and Grant D. N. (2004). Equivalent Viscous Damping in Seismic Design and Analysis. *Journal of Earthquake Engineering. Imperial College Press.*

[103] Popov, E. P., and Engelhardt, M. D. (1988). "Seismic eccentrically braced frames." J. Constr. Steel Res., 10, 321–354.

[104] Purba, R. H. (2006). Design recommendations for perforated steel plate shear walls. *M.Sc. Thesis, State University of New York at Buffalo, Buffalo, N.Y, USA.*

[105] Ramadan, T. and Ghobarah, A. (1995). Analytical Model for Shear-Link Behavior. J*ournal of Structural Engineering. 121:11, 1574-1580.*

[106] Rice, J.R. (1968), Path independent Integral and the Approximate Analysis of StrainConcentration for Notches and Cracks. *Journal of Applied Mechanics, 35, 379-386.*

[107] Rice, J.R. and D. M. Tracey., (1969). On the ductile enlargement of voids in triaxial stress fields. *Journal of the Mechanics and Physics of Solids 17, 201-217.*

[108] Richards P. and Uang, C.M. (2002). Evaluation of rotation capacity and overstrength of links in eccentrically braced frames. *Report No. SSRP-2002/108, Department of Structural Engineering, University of California, San Diego, CA.*

[109] Richards P. and Uang, C.M. (2003). Development of testing protocol for short links in eccentrically braced frames. *Report No. SSRP-2003/08, Department of Structural Engineering, University of California, San Diego, CA.*

[110] Richards P. and Uang, C.M. (2002). "Evaluation of rotation capacity and overstrength of links in eccentrically braced frames." *Report No. SSRP-2002/108, Department of Structural Engineering, University of California, San Diego, CA.*

[111] Richards P. and Uang, C.M. (2003). "Development of testing protocol for short links in eccentrically braced frames." *Report No. SSRP-2003/08, Department of Structural Engineering, University of California, San Diego, CA.*

[112] Richards, P. W. (2004). "Cyclic stability and capacity design of steel eccentrically braced frames." Ph.D. dissertation, Univ. of California, San Diego.

[113] Richards P. and Uang, C.M. (2004c). "Recommended EBF link loading protocol for the AISC Seismic Provisions." *Technical Note.*

[114] Richards P. and Uang, C.M. (2005). "Effect of flange width-thickness ration on EBF link cyclic rotation capacity." *Journal of Structural Engineering, 131(10) 1546-1552.*

[115] Richards P. and Uang, C.M. (2006). "Testing protocol for short links in eccentrically braced frames." *Journal of Structural Engineering, 132(8) 1183-1191.*

[116] Richards PW, Prinz GS (2007). Nonlinear time-history analysis of refined mesh steel structures. *In: Proc. 9th Canadian conference on earthquake engineering. Paper no. 1365.*

[117] Richards P.W, (2007). Estimating the stiffness of eccentrically braced frames. *Pract. Period. Structural Engineering Des. Constr.15(1), 91-95.*

[118] Ricles, J.M. and Popov, E.P. (1987). Dynamic Analysis of Seismically Resistant Eccentrically Braced Frames, *UCB/ERCC 87/07, Berkeley (CA, USA), Earthquake Engineering Research Center, University of California.*

[119] Ricles, J.M. and Popov, E.P. (1989). Composite action in eccentrically braced steel frames. *Journal of Structural Engineering*, American Society of Civil Engineers, 115(8), 2064-2066.

[120] Ricles, J.M. and Popov, E.P. (1994). Inelastic link element for EBF seismic analysis. *Journal of Structural Engineering*, American Society of Civil Engineers, 120(2), 441-463.

[121] Ricles, J.M. and Popov, E.P. (1994). Inelastic Link Element for EBF Seismic Analysis. *Journal of Structural Engineering 120:2, 441-463.*

[122] Roberts, T.M. and Sabouri-Ghomi, S. (1992). Hysteretic characteristics of unstiffened perforated steel plate shear panels. *Thin Walled Structures 14:139-151.*

[123] Roeder, C.W. and Popov, E.P. (1977). Inelastic Behavior of Eccentrically Braced Steel Frames under Cyclic Loadings. *UCB/ERCC 77/18, Berkeley (CA, USA), Earthquake Engineering Research Center, University of California.*

[124] Rossi, PP., Lombardo, A., (2007). Influence of the link overstrength factor onthe seismic behaviour of eccentrically braced frames, *J. of Constr. Steel Research, 63(11): 1529-1545.*

[125] Rozon J., Koboevic S. and R. Tremblay (2008). Study of Global Behaviour of Eccentrically Braced Frames in Response to Seismic Loads. *Proceeding of 14WCEE, Oct. 12-17, 2008.*

[126] Sherif El-Tawil, Tameka Mikesell, Egill Vidarsson, and Sashi K. Kunnath, (1998). Strength and Ductility of FR Welded-Bolted Connections. *Report No. SAC/BD-98/01, Department of Civil and Environmental Engineering University of Central Florida, Orlando, Florida.*

[127] Souza Neto E. A. de, Perić D., Owen D. R. J. (2008). *Computational methods for plasticity: theory and applications.* John Wiley & Sons, New York.

[128] *Taichiro Okazaki, Michael D. Engelhardt (2007).* Cyclic loading behavior of EBF links constructed of ASTM A992 steel. *Journal of Constructional Steel Research 63 (2007) 751–765*

[129] Timoshenko SP, Goodier JN. Theory of elasticity. 3rd ed. New York: Mgraw Hill Book Co., Inc; 1951.

[130] Vian, D. (2005). Steel plate shear walls for seismic design and retrofit of building structures. *Ph.D dissertation, State Univ. of New York at Buffalo, Buffalo, N.Y, USA.*

[131] Vemuri, J P (2015). A Novel Statistical Model for Link Overstrength. *Advances in Structural Engineering: Mechanics. Springer, India, pp. 567-575. ISBN 978-81-322-2189-0*

[132] Zhang, X., Ricles, J.M., Fisher, J.W., and Lu, L.W. (2004). "Analytical and experimental studies on seismic behavior of deep column-to-beam welded reduced beam section steel moment connections." *The 10th World Conference on Earthquake Engineering*, Paper No. 1599, Vancouver, B.C., Canada.

APPENDIX A. Coupon Test Report

The report from DEA HO MACHINERY Co. ltd where the coupon test was carried out is shown in Fig. A. to A.4.

Tensile test report

Test Date	2016-06-14	**Test Machine**	SHIMADZU 500kN
Tested By	In-Yong.Park	**Customer**	Chosun University
Test Method	ASTM A370	**Report No**	C-16-2850
Material	SS400	**Thickness**	7mm

Name	Cross section	Tensile strength	Maximum load	Yield strength	Yield load	Elongation
Parameters		Calc. at Entire Areas	Calc. at Entire Areas	0.2 %	0.2 %	
Unit	mm2	MPa	N	MPa	N	%
7mm-1	270.535	370.485	100229	309.533	83739.7	57.5800
7mm-2	270.732	370.476	100300	310.537	84072.4	56.4200
7mm-3	270.468	370.208	100129	304.614	82388.2	54.7000

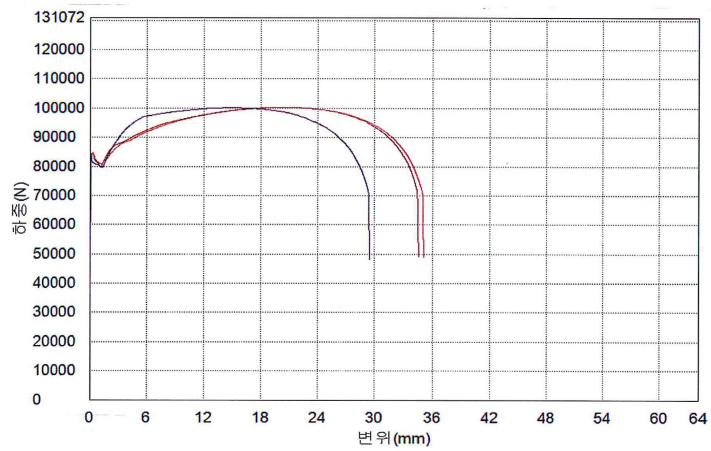

(주) 대 호 기 계
DAE HO MACHINERY co. ,ltd

Fig. A.1 Coupon test (tensile test) report for 7mm thick web

Tensile test report

Test Date	2016-06-14	**Test Machine**	SHIMADZU 500kN
Tested by	In-Young.Park	**Customer**	Chosun University
Test Method	ASTM A370	**Report No**	C-16-2851
Material	SS400	**Thickness**	8mm

Name	Cross section	Tensile strength	Maximum load	Yield strength	Yield load	Elongation
Parameters		Calc. at Entire Areas	Calc. at Entire Areas	0.2 %	0.2 %	
Unit	mm2	MPa	N	MPa	N	%
8mm-1	314.800	448.834	141293	293.184	92294.5	46.5200
8mm-2	314.079	449.367	141137	303.989	95476.6	44.2800
8mm-3	314.000	449.920	141275	301.975	94820.2	43.4800

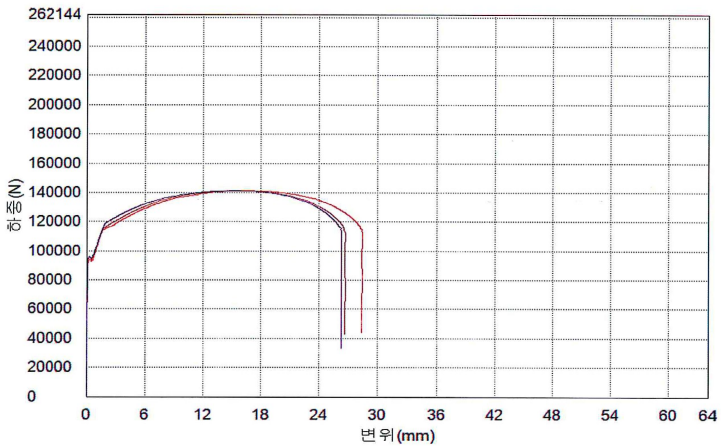

(주) 대 호 기 계
DAE HO MACHINERY co. ,ltd

Fig. A.2 Coupon test (tensile test) report for 8mm thick web

Tensile test report

Test Date	2016-06-14	**Test Machine**	SHIMADZU 500kN
Tested By	in-young.Park	**Customer**	Chosun University
Test Method	ASTM A370	**Report No**	C-16-2852
Material	SS400	**Thickness**	9mm

Name	Cross sectionn	Tensill strength	Maximum load	Yield strength	Yield load load	Elongation
Parameters		Calc. at Entire Areas	Calc. at Entire Areas	0.2 %	0.2 %	
Unit	mm2	MPa	N	MPa	N	%
9mm-1	350.400	424.014	148574	322.900	113144	41.2800
9mm-2	349.200	421.522	147196	321.549	112285	35.2000
9mm-3	349.287	425.170	148506	323.637	113042	40.1600

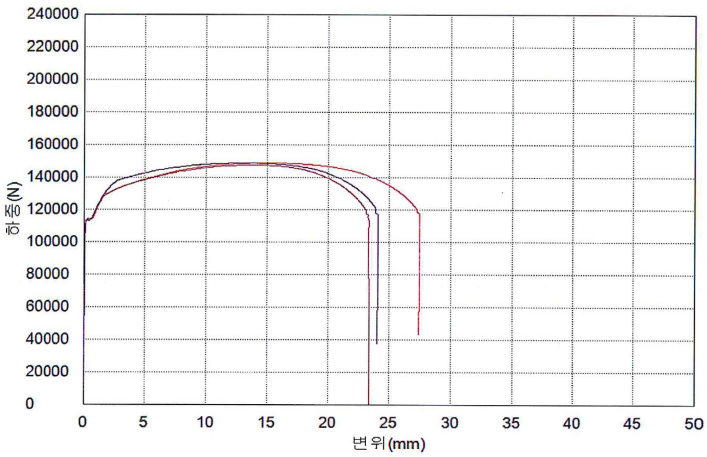

(주) 대 호 기 계
DAE HO MACHINERY co. ,ltd

이 결과서는 소송용 및 (주)대호기계 선전에 사용할 수 없음

Fig. A.3 Coupon test (tensile test) report for 9mm thick flange

Tensile test report

Test Date	2016-06-14	**Test Machine**	SHIMADZU 500kN
Tested By	In-Young.Park	**Customer**	Chosun University
Test Method	ASTM A370	**Report No**	C-16-2853
Material	SS400	**Thickness**	10mm

Name	Cross sectiong	Tensile strength	Maximum load	yield strength	yield load	Elongation
Parameters		Calc. at Entire Areas	Calc. at Entire Areas	0.2 %	0.2 %	
Unit	mm2	MPa	N	MPa	N	%
10mm-1	390.800	369.413	144366	282.052	110226	50.2400
10mm-2	391.200	368.649	144216	281.161	109990	52.2400
10mm-3	391.102	368.319	144050	277.906	108690	52.4400

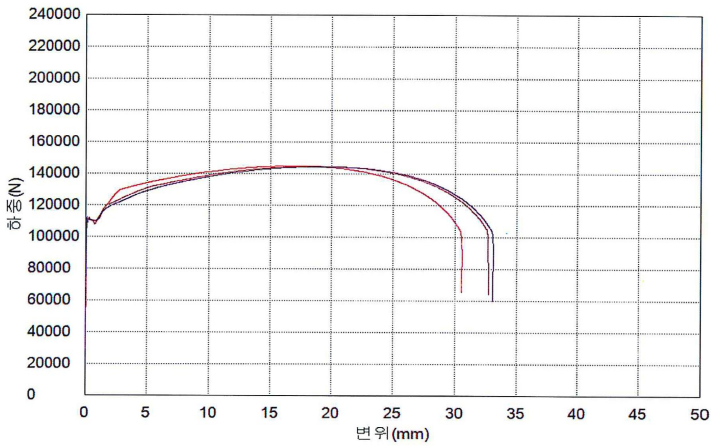

(주) 대 호 기 계
DAE HO MACHINERY co. ,ltd

Fig. A.4 Coupon test (tensile test) report for 10mm thick flange

APPENDIX B. Experimental Investigation and Different Measured Responses

B.1 Sample Welding Design

Given the electrode used: E70, $F_{EXX} = 480MPa$

Steel type SS400, Fy=320MPa and Fu=400MPa

Web thickness t_w=8mm

Flange thickness, t_f=9mm

Flange thickness, t_f=10mm

End plate thickness, tp=20mm

I. Web-to-flange weld: welding type used shielded metal arc welding (SMAW)

Minimum weld size => $a_{\min} = 8mm$ (AISC-Table J2.4) or for two line welding

$a_{\max,eff} = 0.943\frac{F_y t_w}{F_{EXX}} \Rightarrow 0.943\frac{320*8}{480} = 5.03mm$ For yielding of the base metal govers the design

$a_{\max,eff} = 0.707\frac{F_u t_w}{F_{EXX}} \Rightarrow 0.707\frac{400*8}{480} = 4.7mm$ For rupture of the base metal govers

Therefore, the minimum governs so effective fillet size a = 4.7mm~=5mm

Design shear strength weld

$$\begin{aligned}\phi R_{nw} &= 0.75(a)(0.707)(0.60F_{EXX}) \\ &= 0.75*5*.707*0.60*480 \\ &= 763kN/mm\end{aligned}$$

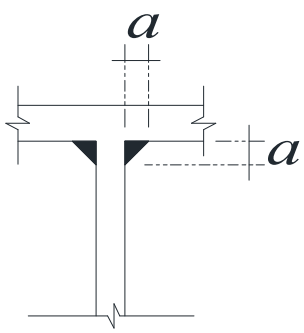

Fig. B.1 Welding detail

II. Flange-to-end plate weld: welding type used shielded metal arc welding (SMAW)

Minimum weld size => a_{min}=8mm(AISC-TableJ 2.4) or

$$a_{max,eff} = 0.943\frac{F_y t_f}{F_{EXX}} = 0.943\frac{320*10}{480} = 6.29mm$$

For yield strength:

$$a_{max,eff} = 0.707\frac{F_u t_f}{F_{EXX}} = 0.707\frac{400*10}{480} = 5.89mm$$

For rupture strength:

Therefore, the minimum governs so effective fillet size a = 5.89mm ~=6mm

Design shear strength weld ϕRnw=0.75(a)(0.707)(0.60FEXX)=0.75*6*0.707*0.6*480=916kN/mm

Stiffeners-to-flange and web weld: welding type used shielded metal arc welding (SMAW)

$$a_{max,eff} = 0.943\frac{F_y t_s}{F_{EXX}} = 0.943\frac{320*10}{480} = 6.29mm$$

For yield strength:

$$a_{max,eff} = 0.707\frac{F_u t_s}{F_{EXX}} = 0.707\frac{400*10}{480} = 5.89mm$$

For rupture strength:

Therefore, the minimum governs so effective fillet size a = 5.89mm~=6mm

Design shear strength weld ϕRnw=0.75(a)(0.707)(0.60FEXX)=0.75*6*0.707*0.6*480=916kN/mm

B.2 Quasi-static loading test

During quasi static loading test, six displacement meters have been installed at different location in order to measure the displacements at different location. These instrumentations are shown in Fig. B.2. As shown in the Fig. B.2, the shear displacement of specimen is the difference of DT1 and DT2 where the responses were presented in Chapter 4. The response of each of the remaining displacement meters installed are presented for some specimens with respect to the shear force measured from the loading cell is presented in this section. Fig. B.3, also shows the photos taken during testing to show the displacement meters installed and their respective location.

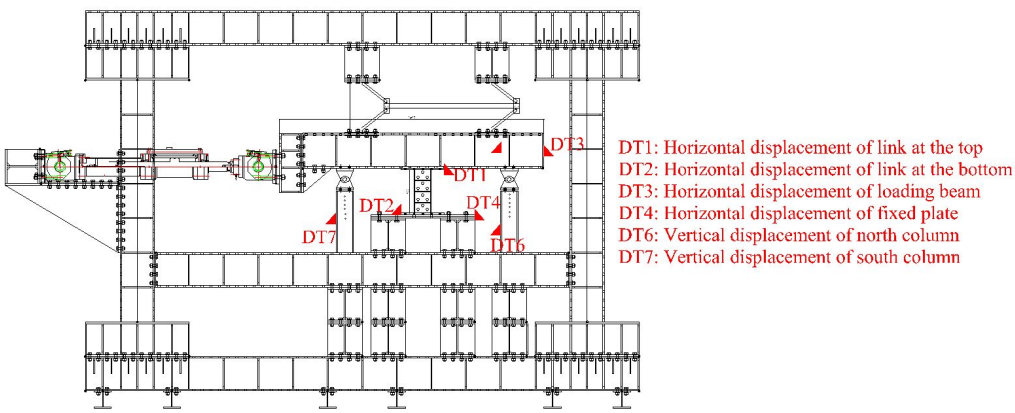

Fig. B.2 Location of Displacement meters

Fig° B° 3 Photos captured to show the location of Displacement meters

B.3 Results of Responses Measured by Different Displacement Meters

RWS-S10S1

The response of displacement from the bottom of link end plate that measure horizontal deformation (DT2) to the vertical displacement of north and south column is presented in Fig. B.4 for RWS-S10S1. The plot shows that the expected results in all displacement meters.

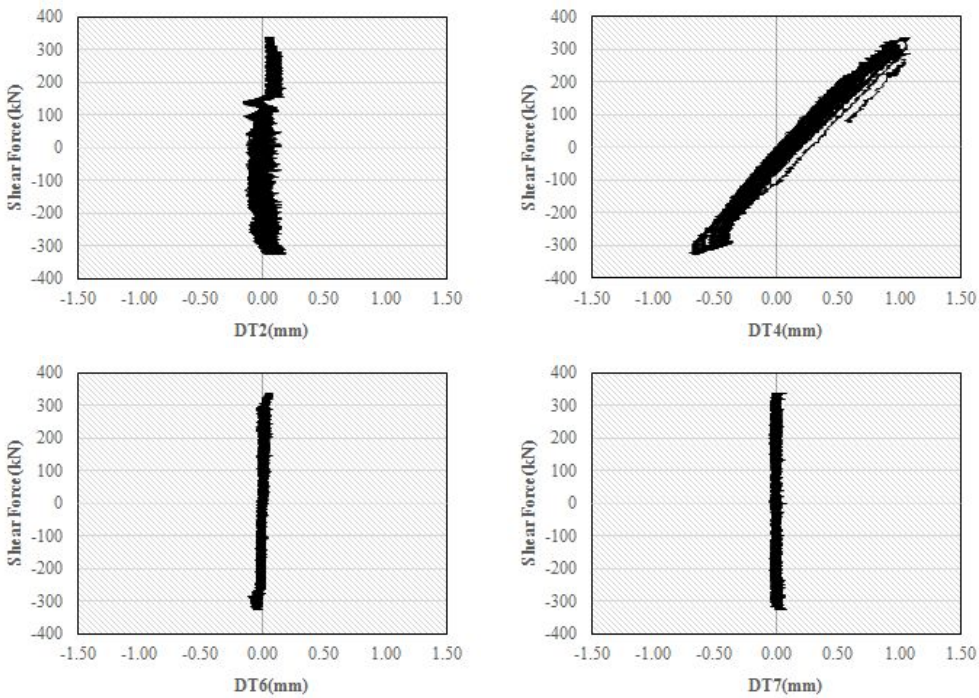

Fig. B.4 Response of RWS-S10S1

RWS-U10Sf1

The displacements measured for all shear link is the same so only the response of RWS_S10S1 is presented included here. Fig B.5 shows the response of displacement meters DT2, DT4, DT6 and DT7 respectively. As shown in the fig. B.5, the displacement smeasured by DT2, DT6 and DT7 is small. This indicates that the lower end plated is well fastened to the horizontal fixed plate and there was no slippage during loading. Vertical displacements of both south and north column is also small that means there is no axial forces applied to the test specimens while loading. However, DT4 reads about –0.5mm to 0.65mm, which indicates that the fixed horizontal plate somewhat moved while loading.

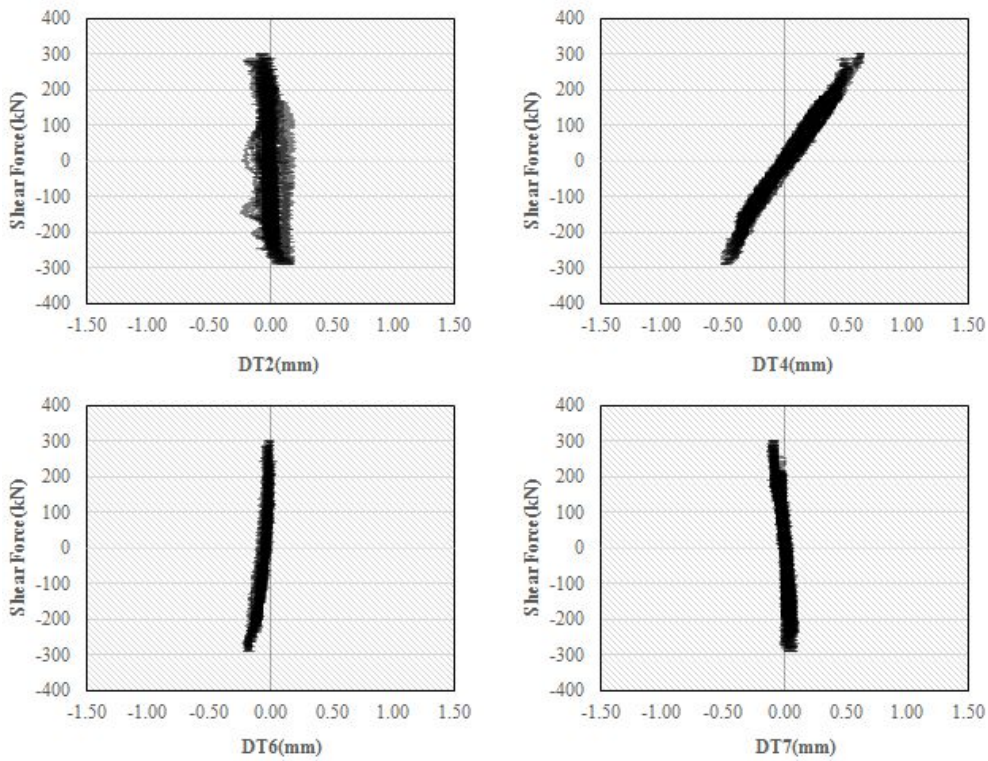

Fig. B-5 Response of RWS-U10Sf1

RWS-S10Sf1

The same response with RWS-S10S1 is obtained for test specimen RWS-S10Sf1 as shown in Fig. B.6 except some unstability is noticed in the DT2 for RWS-S10Sf1. The displacement recorded by DT4 of RWS-S10Sf1 is also in the range of –0.5mm to 0.9mm.

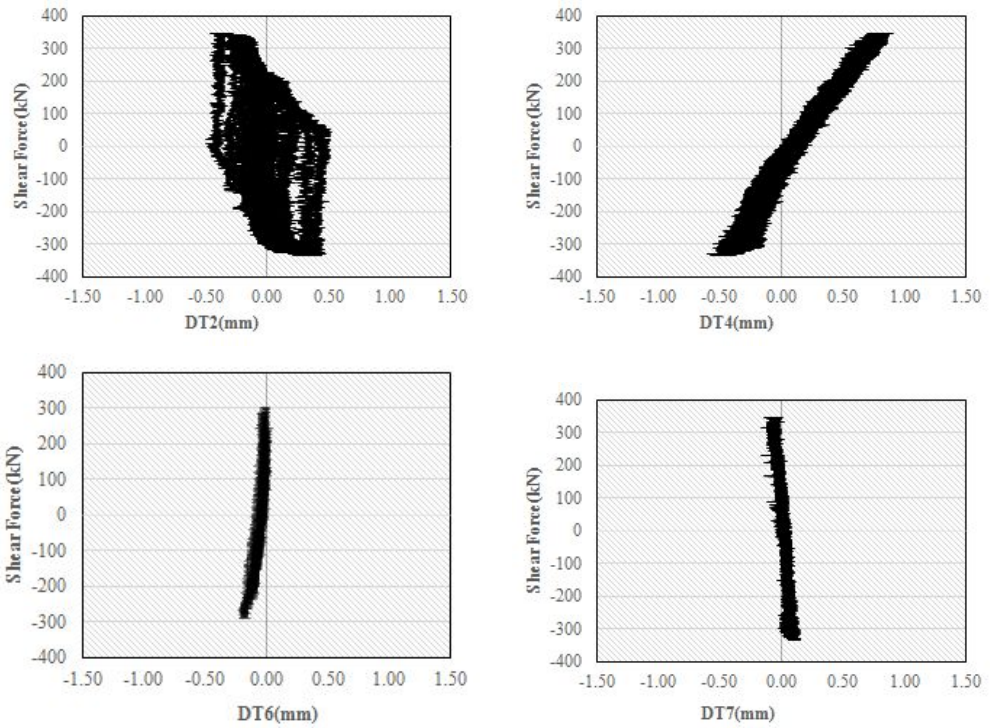

Fig. B-6 Response of RWS-S10Sf1

RWS-S10Sf2

Fig. B.7 shows the response of specimen RWS-S10Sf2 for DT2, DT4, DT6 and DT7 respectively. As shown in the figure, the response shows that sudden increment of displacements are noticed due to some shocks during experiments otherwise the same results with other test specimens are obtained.

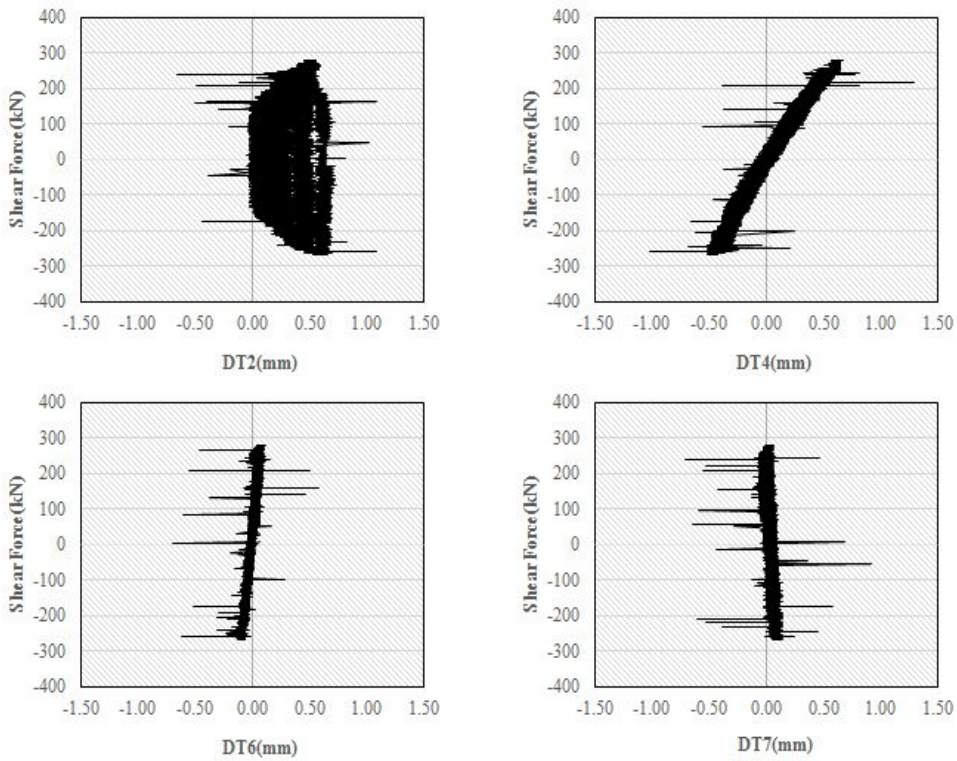

Fig. B-7 Response of RWS-S10Sf2

RLS-U10Sf1

The response of test specimen RLS-U10Sf1 for all displacement meters installed are presented in Fig. B-8. As shown in the Fig. B-8, all displacement response shows unstability during the loading process and sudden increment due to shocking like test specimen RWS-S10Sf2.

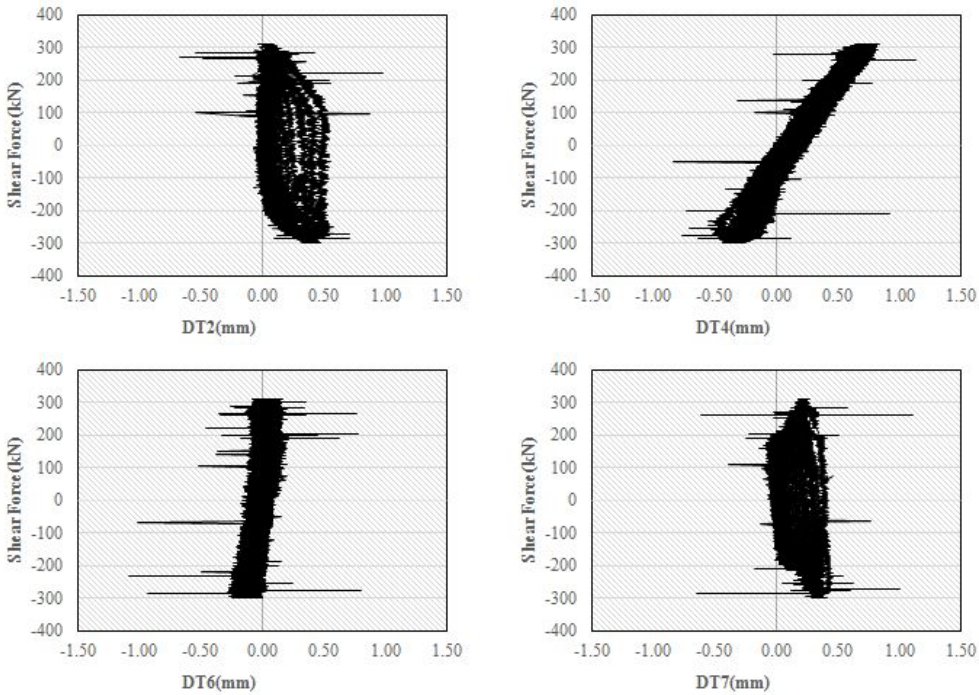

Fig. B-8 Response of RLS-U10Sf1

RLS-S10Sf2

The similar results with RLS-U10Sf1 is obtained for RLS-U10Sf2 as shon in Fig. B.9. The range at which the measured values for RLS-U10Sf2 is the same as RLS-S10Sf1 as well.

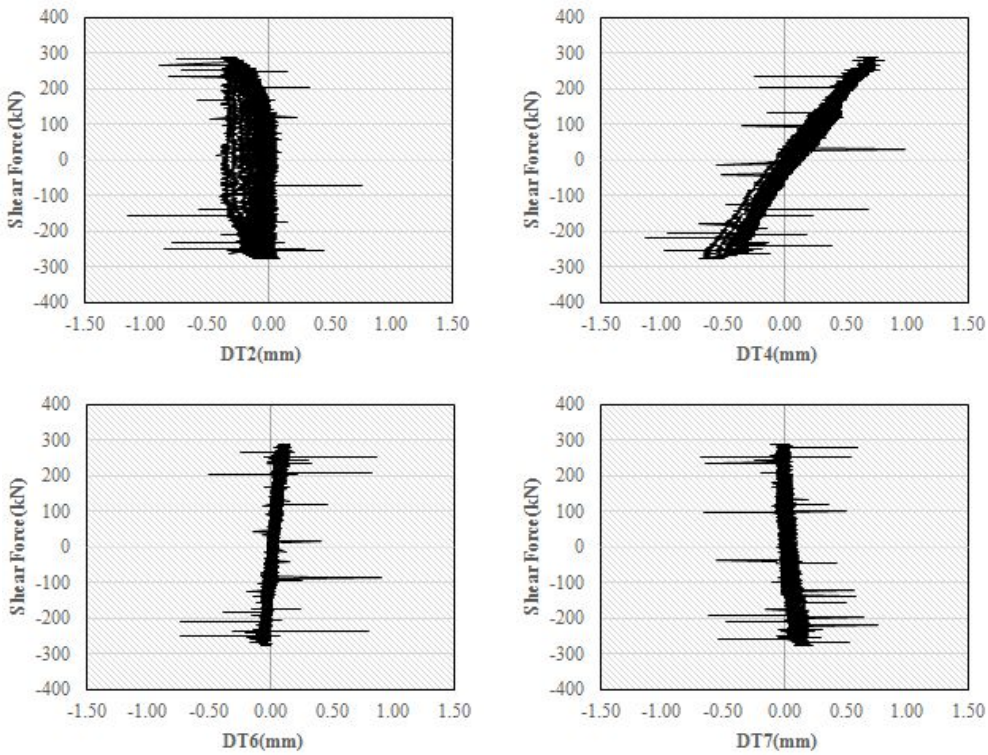

Fig. B-9 Response of RLS-S10Sf2

APPENDIX C. Results of Parametric Study

The hysteresis response of parametric study was presented here. The parameters considered were: link length factor, percent of reduced web area and effect of stiffness. In the legend the letters and numbers indicates: S1, S2, S3 and S4 are shear links with link length factor of 0.8, 1.0, 1.2, and 1.6 respectively. Sf1 and Sf2 are combined shear and flexural or intermediate links with link length factor of 2.0 and 2.3 respectively. F1 and F2 are flexural links with link length factor of 2.6 and 3 respectively.

The letters S and U stands for stiffened and Unstiffened respectively. The last small letter 'n' is for normal or unreduced links. The numbers 5, 10, 15, 20 and 25 stands for 5%, 10%, 15%, 20% and 25% of reduced web area respectively. Fig. C.1 is the hysteresis response of parametric study that were not included in Chapter 6.

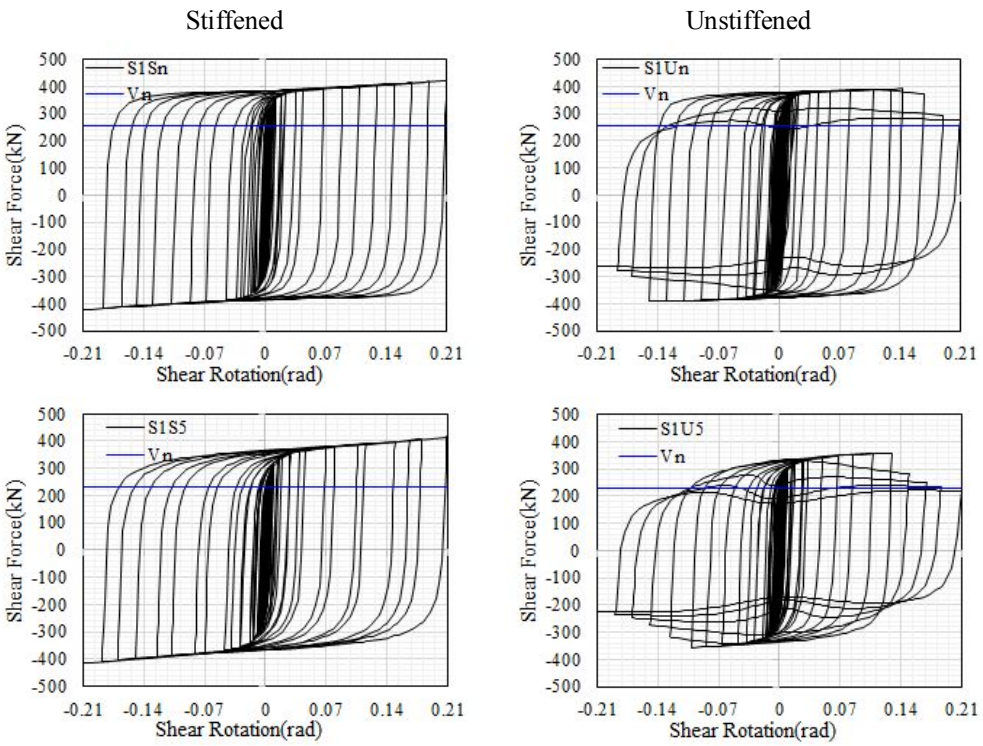

Fig. C.1 Hysteresis response of analysis specimens considered for parametric study

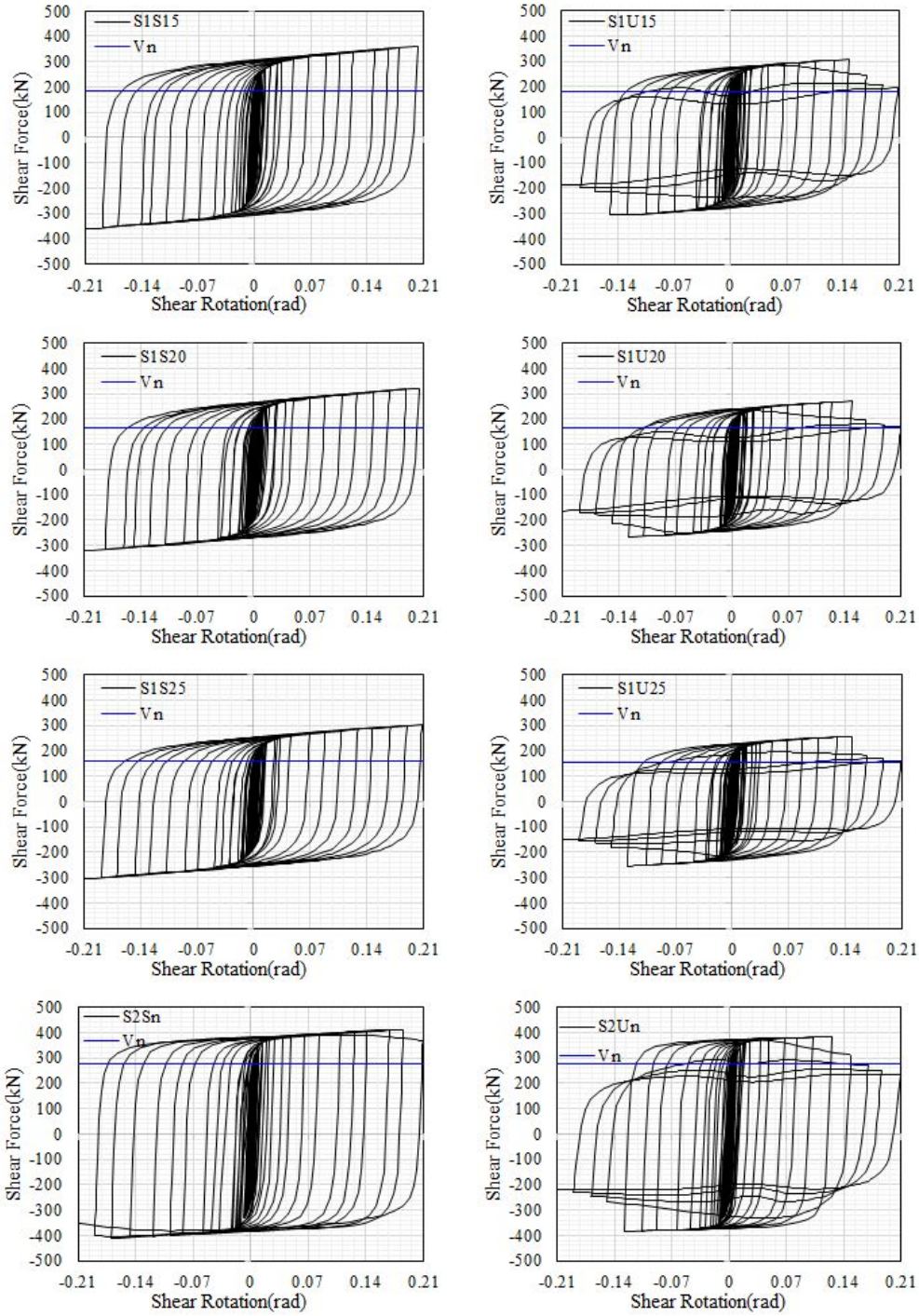

Fig. C.1 Hysteresis response of analysis specimens considered for parametric study

(Continued...)

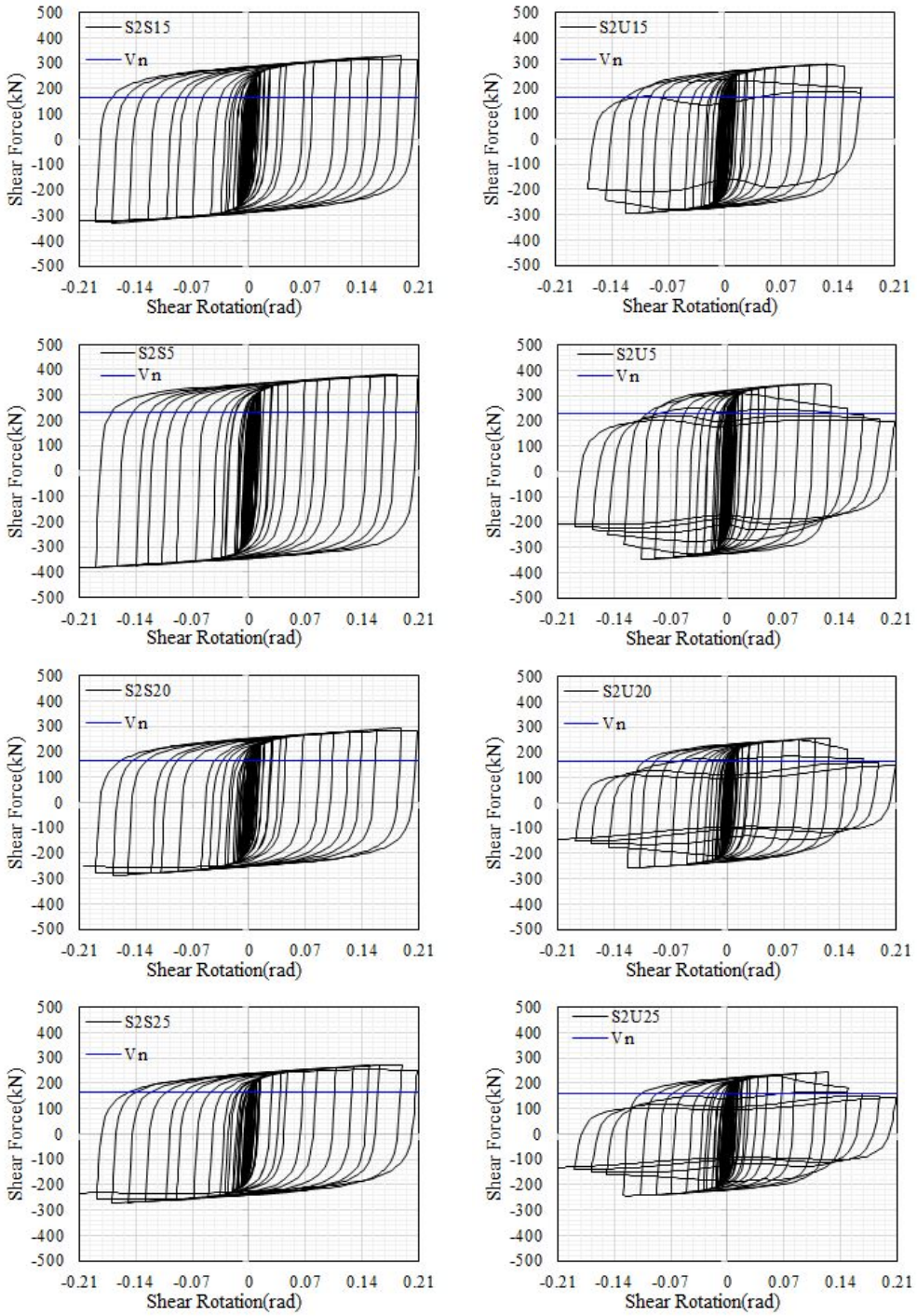

Fig. C.1 Hysteresis response of analysis specimens considered for parametric study

(Continued...)

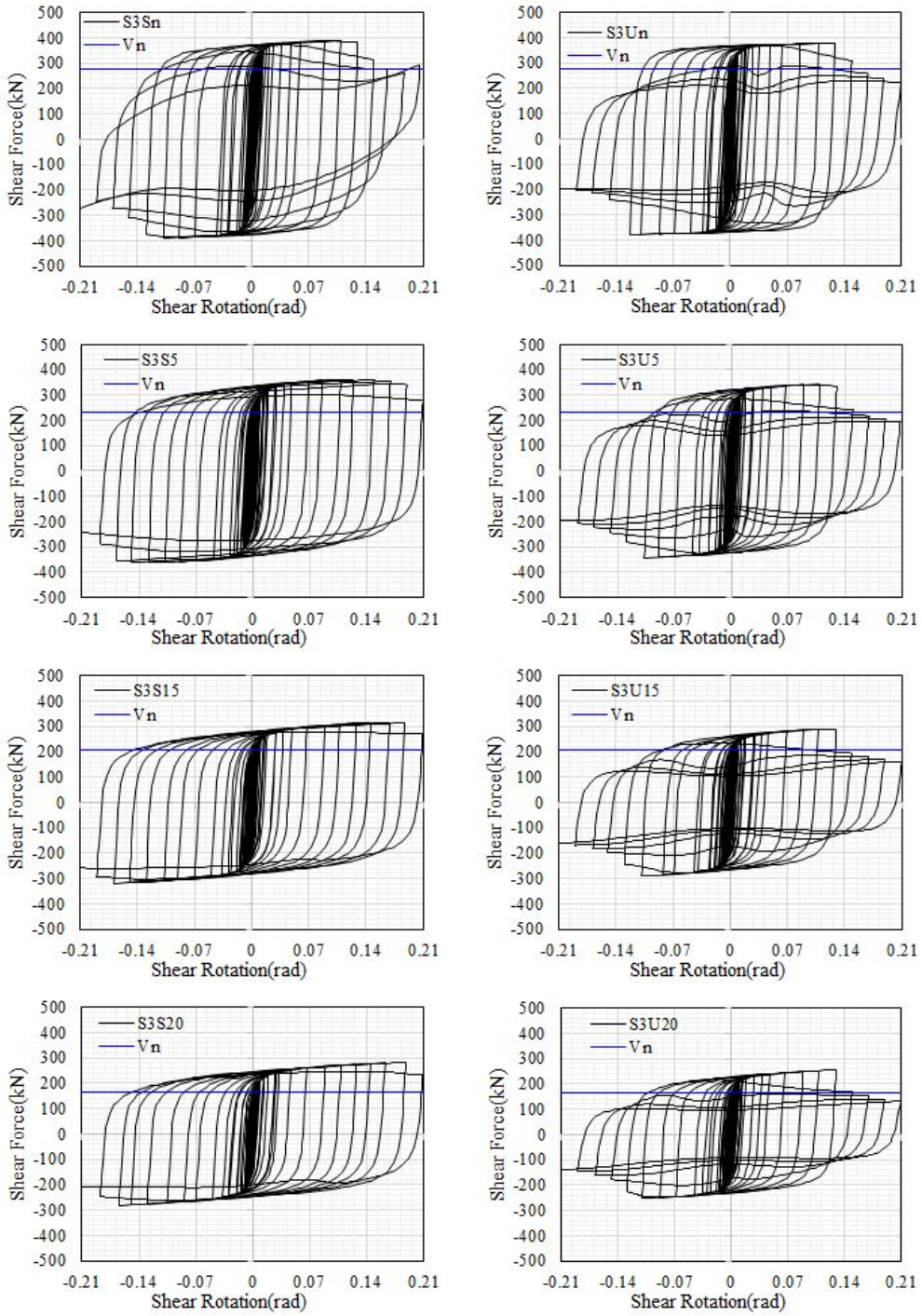

Fig. C.1 Hysteresis response of analysis specimens considered for parametric study *(Continued...)*

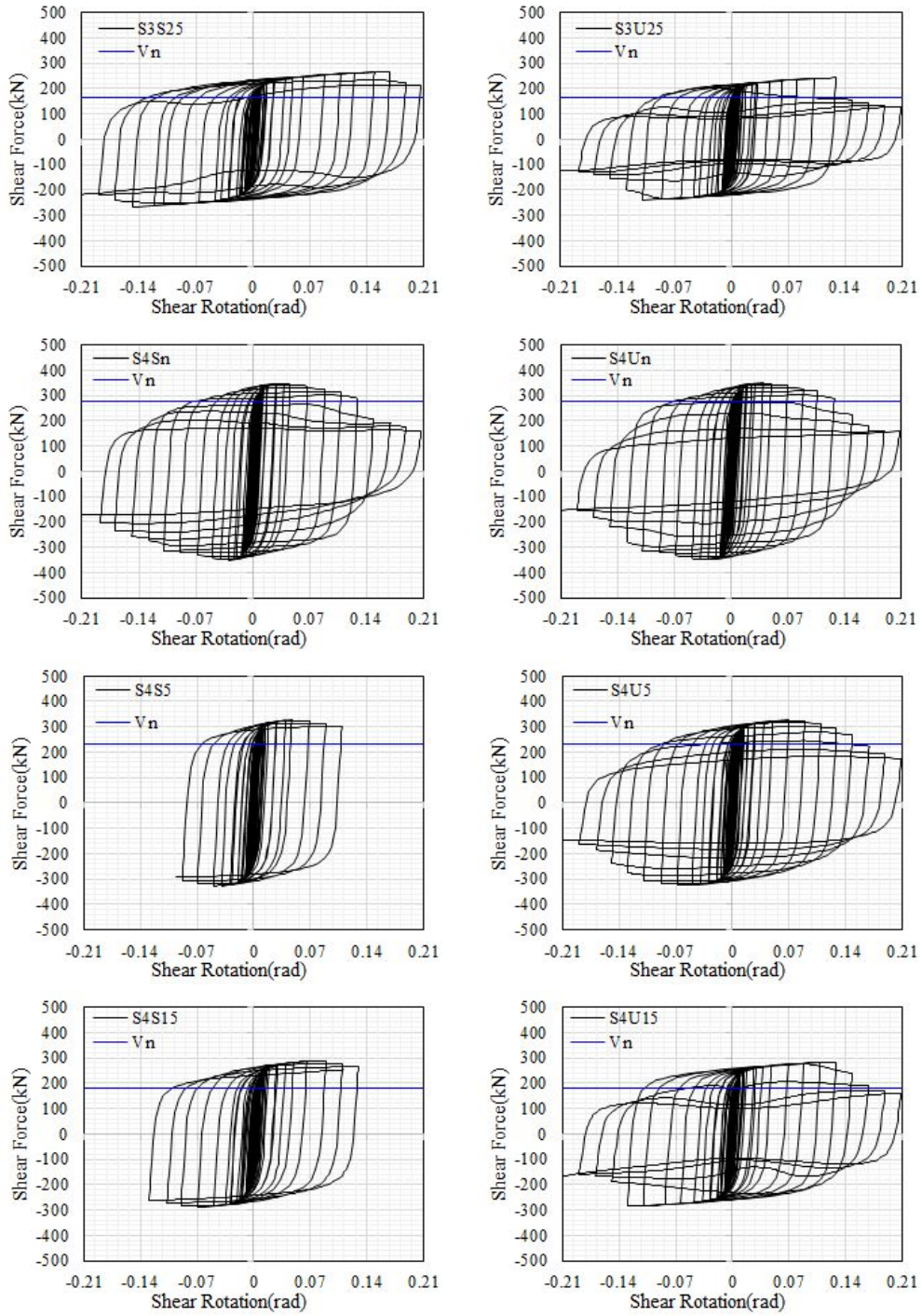

Fig. C.1 Hysteresis response of analysis specimens considered for parametric study *(Continued...)*

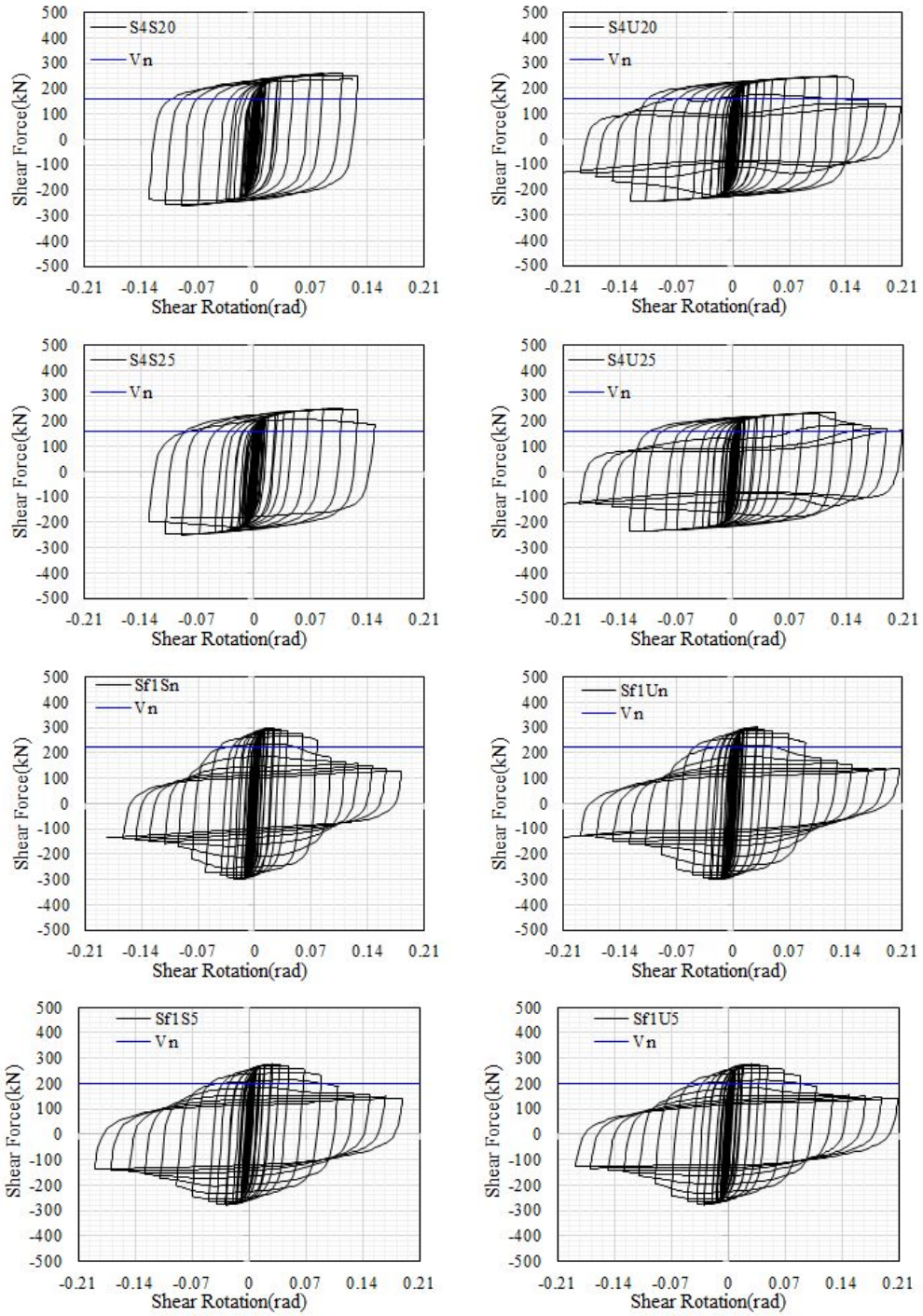

Fig. C.1 Hysteresis response of analysis specimens considered for parametric study

(Continued...)

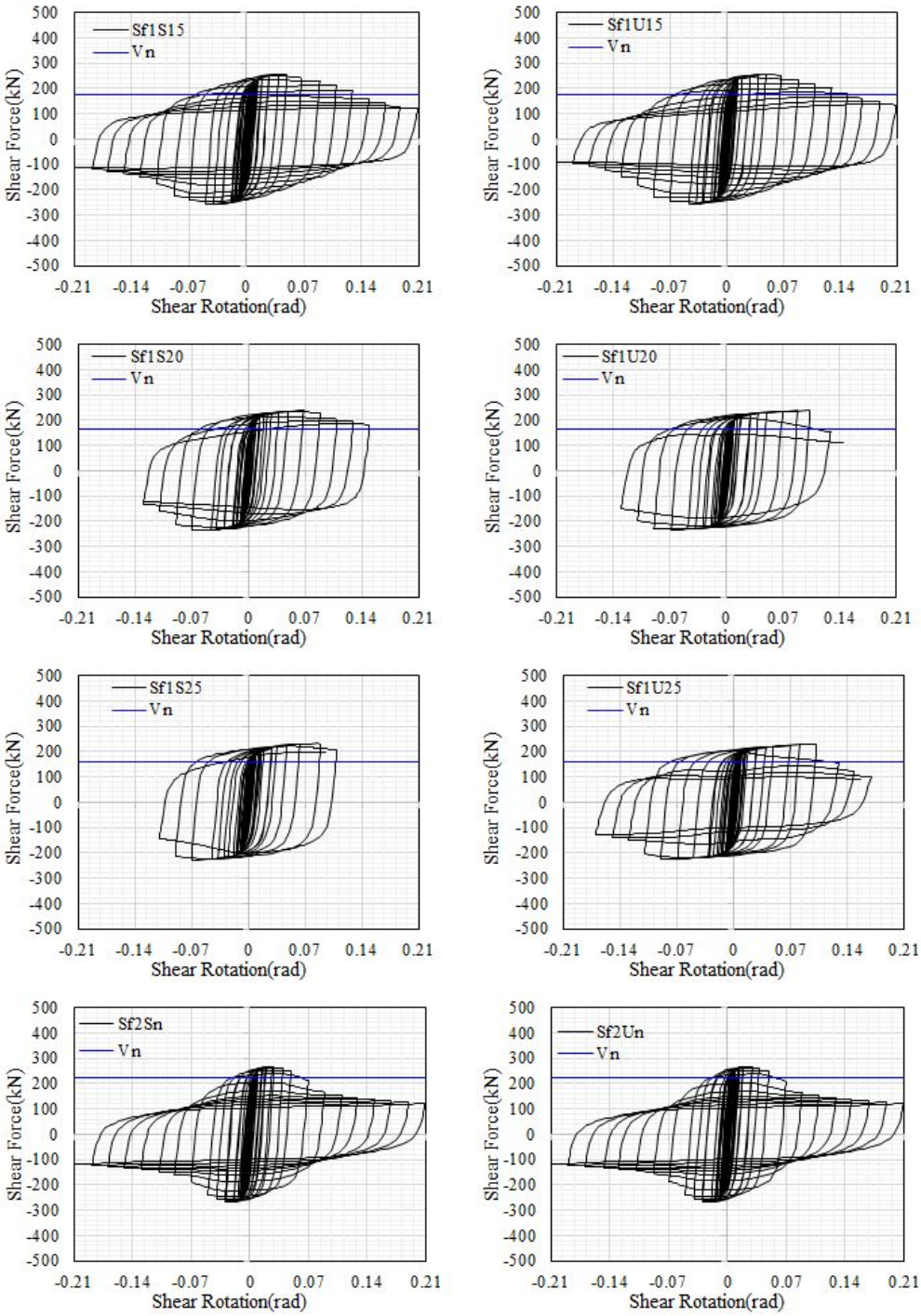

Fig. C.1 Hysteresis response of analysis specimens considered for parametric study

(Continued...)

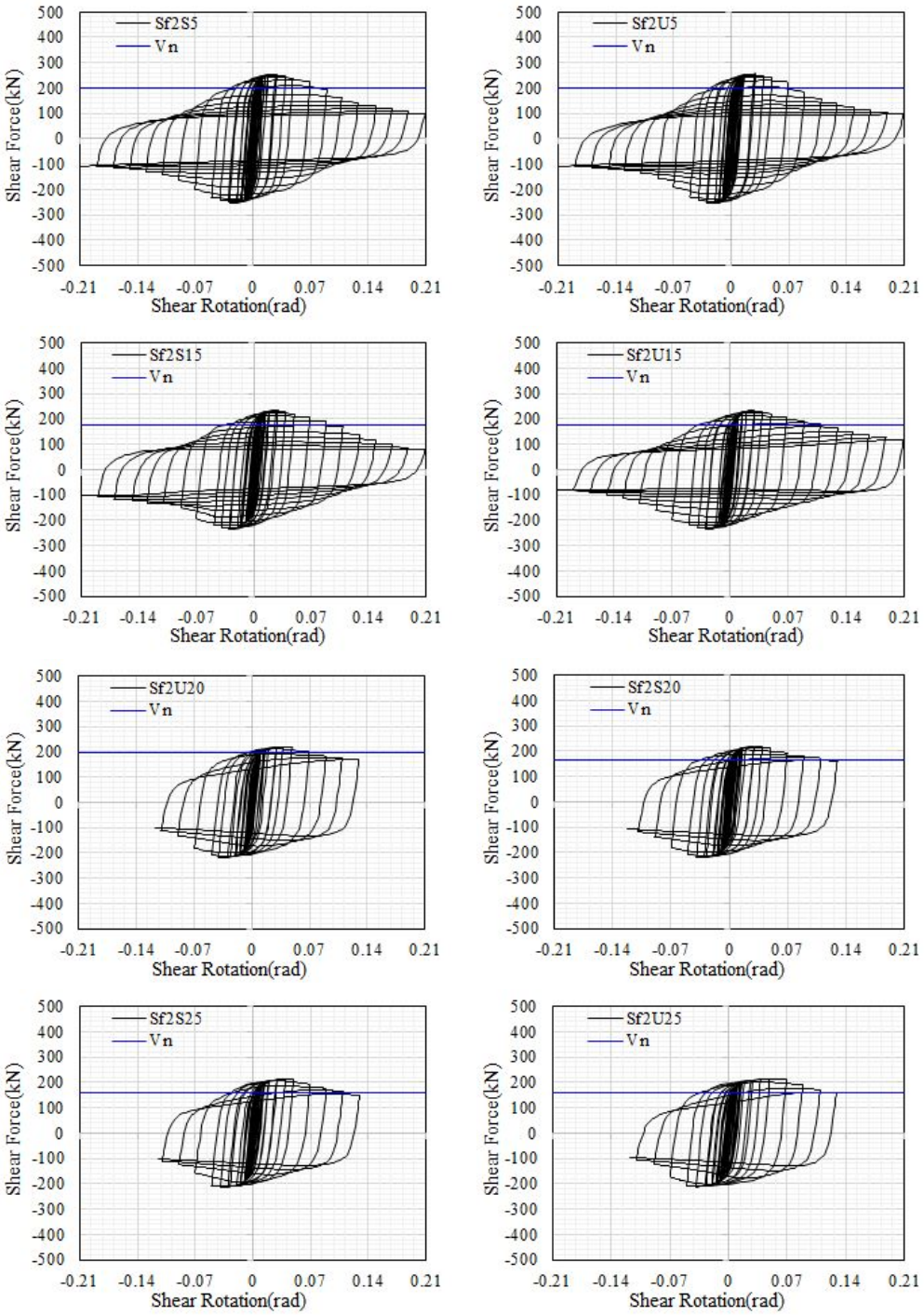

Fig. C.1 Hysteresis response of analysis specimens considered for parametric study

(Continued...)

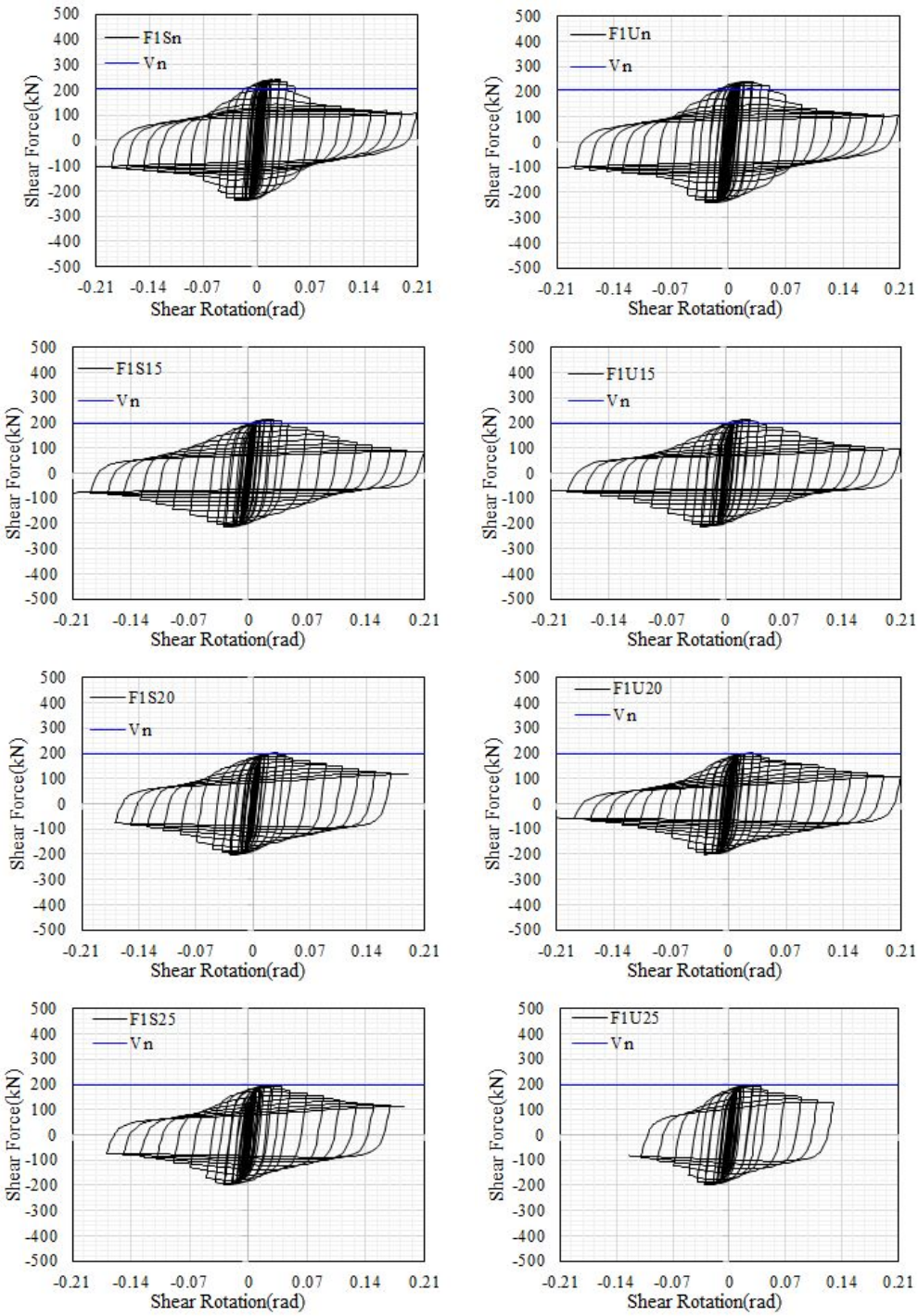

Fig. C.1 Hysteresis response of analysis specimens considered for parametric study *(Continued...)*

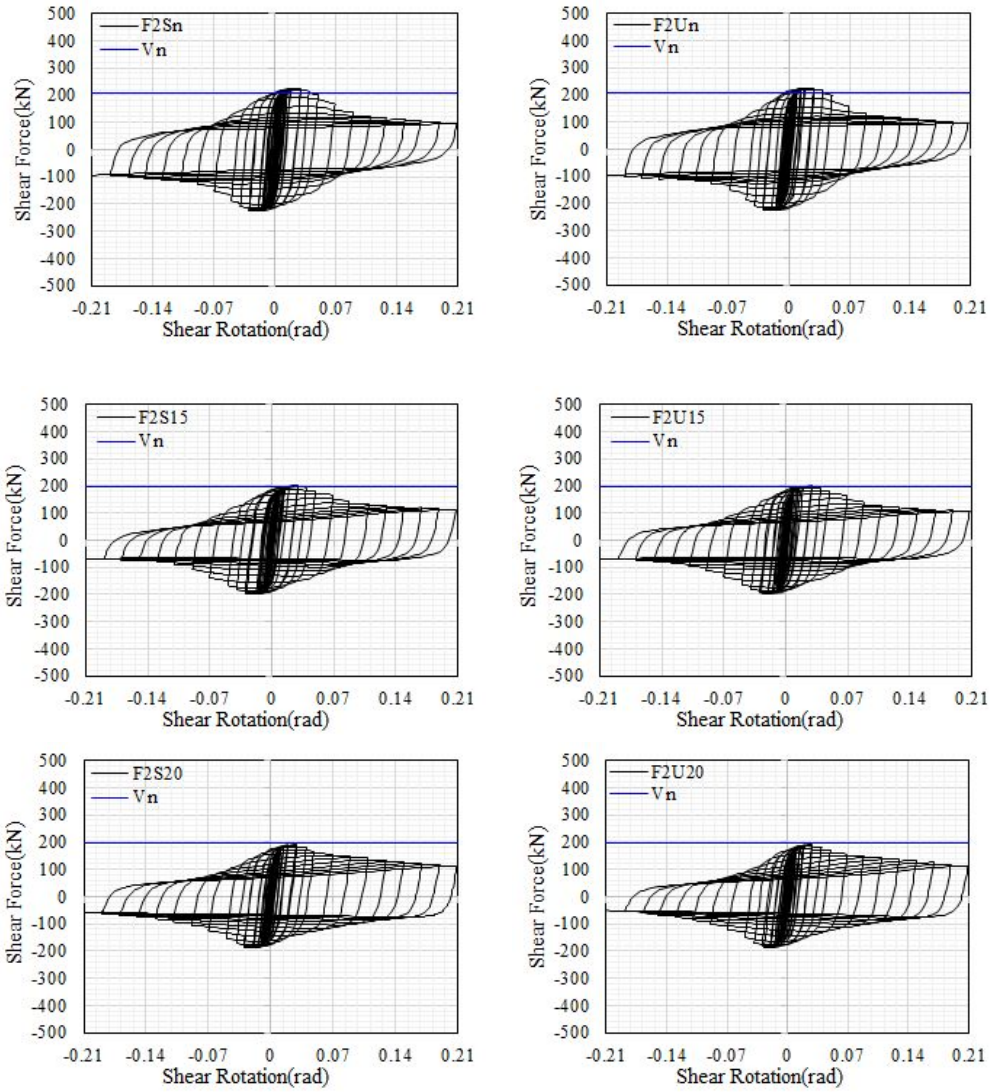

Fig. C.1 Hysteresis response of analysis specimens considered for parametric study *(Continued...)*

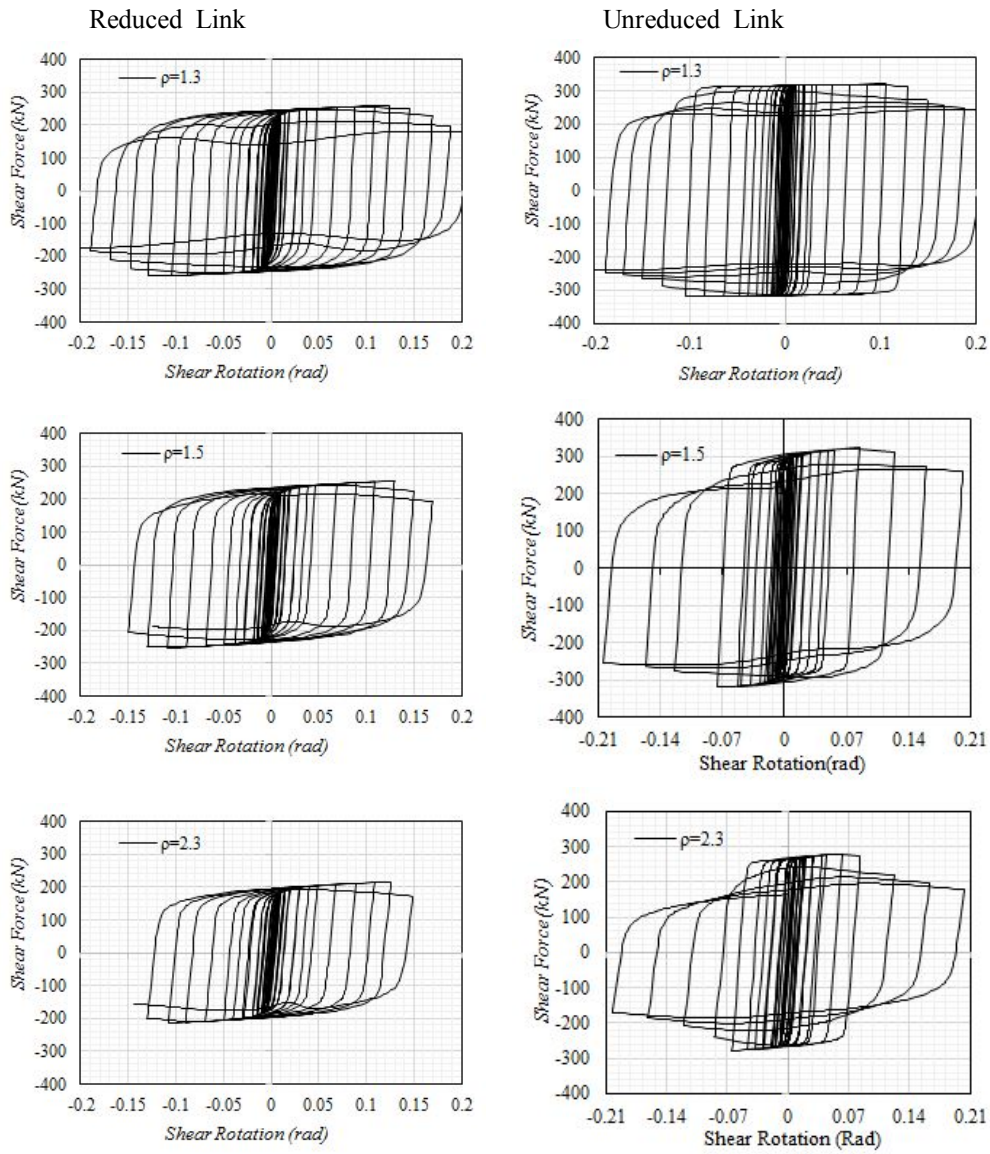

Fig. C.2 Hysteresis response of analysis specimens considered for parametric study for link-to-column connection

APPENDIX D. Initial Stiffness of EBFs

D.1 Initial Stiffness of EBFs Estimated by Richard, 2010

Richards (2010) derived the stiffness of EBFs based on Englekirk (1994) formulations. Richards (2010) assumed that the summation of horizontal displacements, caused by different frame component deformations which includes axial deformation of braces (Δ_{da}), beam axial deformation (Δ_{ba}), link shear deformation (Δ_{bv}) and beam and link flexural deformation (Δ_{bf}). The total elastic deformation of eccentrically braced frames (Δ_T) will be the sum of deformations of each components. The deformations formulated by Englekirk and extended by Richards are presented in Fig. D.1.

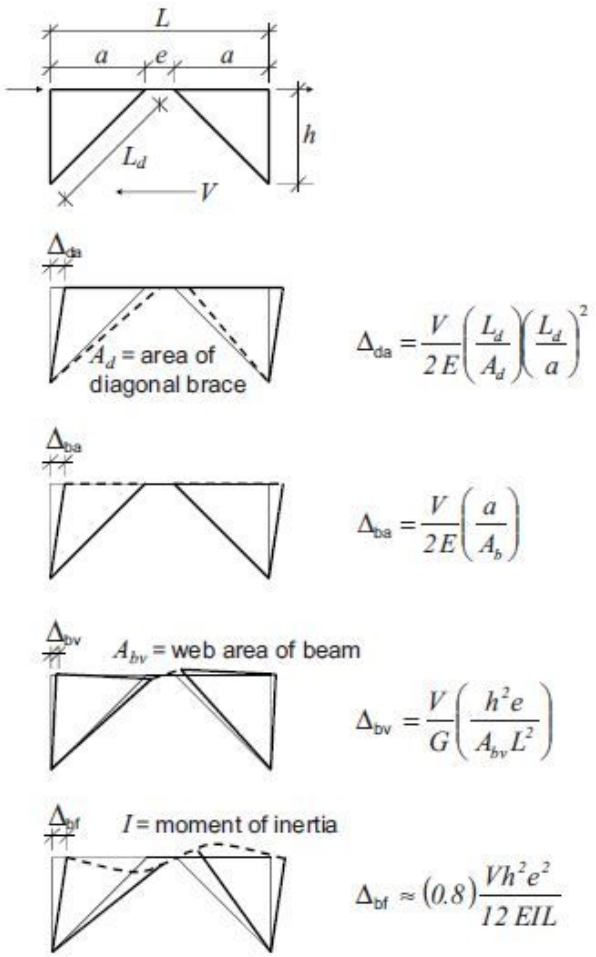

Fig. D.1 EBF dimensions and components of story drift (Richard, 2010)

Richards (2010) proposed stiffness k of an EBF story which is expressed as in Eq. (D.1).

$$k = 1.35 V_d \left(\frac{E/F_y}{[0.72(1.19 - 0.092L_{br})(L_{br}^2/a) + (0.13La/h) + (1.71he/L) + 0.21eh/d)]} \right) \quad \text{.....(D.1)}$$

where V_d = design story shear; F_y and E = beam material properties; d = beam depth; and L_{br}, a, h, and e = frame dimensions. Richard verified the derived equation by conducted pushover analysis considering three different frame story having 3-story, 9-story and 18-story with different cases. From the pushover analysis results of 12 EBFs, the initial stiffness were calculated and the errors with the one calculated by Eq. (D.1). The errors calculated using Eq. (D.2) is presented in Fig. D.2.

$$\text{percent difference} = (\text{Eq. (D.1)} - k_{analysis}) / (k_{analysis}) \quad \text{.....(D.2)}$$

As shown in Fig. D.2, the difference in estimated stiffness and stiffness calculated from the analysis, for design shear force less than 500kN, the difference gets as big as 45%for 1300kN, the difference gets smaller relative to other values. In order to prove the initisl stiffness recommended in Eq. (D.1), finite element analysis was conducted and presented here under.

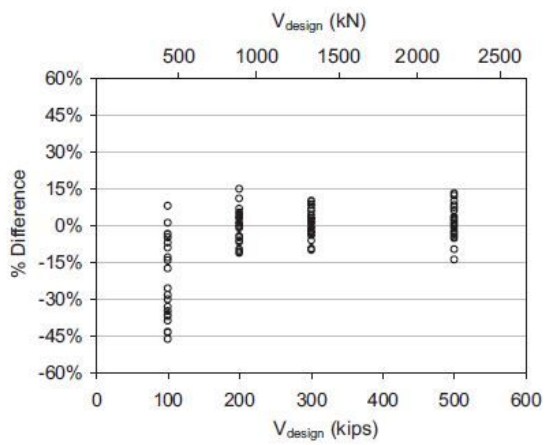

Fig. D.2 Difference in estimated stiffness and stiffness from analysis for frames (Richard 2010)

D.2 FE simulation of D-brace frames

Single story and two story diagonally braced EBFs with reduced web link section and unreduced link section were modeled using nonlinear finite element analysis in order to prove Eq. (D.1) for reduced link section. The frame was modeled solid and meshed with C3D8R as shown in Fig. D.3. The material model of analysis the same as that used in link-to-column connection of parametric study. The lower portion of the column is fixed both translation and rotation in all direction and the loading is applied at the edge of the upper beam monotonically by controlling the displacement. he parameter used for D-braced frames is frame height to length between the column (h/L = 0.5, 0.75 and 1.0). The frame was design according to AISC-341-10 provision of capacity design principles where braces and the outer beam segments were designed for forces introduced by $1.3R_y$ times the nominal shear resistance of the link V_p, where R_y is the ratio between the expected and the nominal yield stress and has a value of 1.1.

D.3 FE Analysis Results of D-brace frames

The deformed shape of diagonal braced frame with von Mises stress and equivalent plastic strain distribution is presented in Fig. D.4. As shown in the deformed shape of analysis result, both stress and equivalent plastic strain concentrated at the link for both EBFs with reduced and unreduced link sections. The stress distribution on each members for reduced links having h/L=0.75 of one story is measured at possible critical location and presented in Fig. D.3. As shown in Fig. D.5 (a), the equivalent plastic strain of brace is column and beam is zero. The von Mises stress of link is bigger compared to brace, beam and column as shown in Fig D.5 (b).

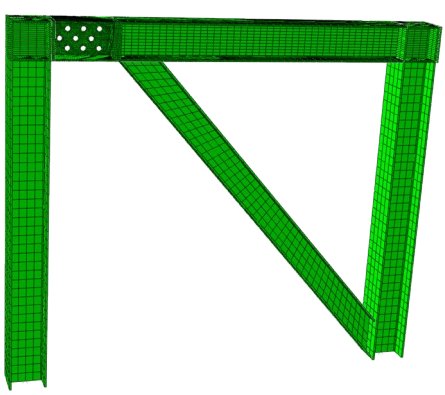

Fig. D.3 3D Analysis Model of EBFs

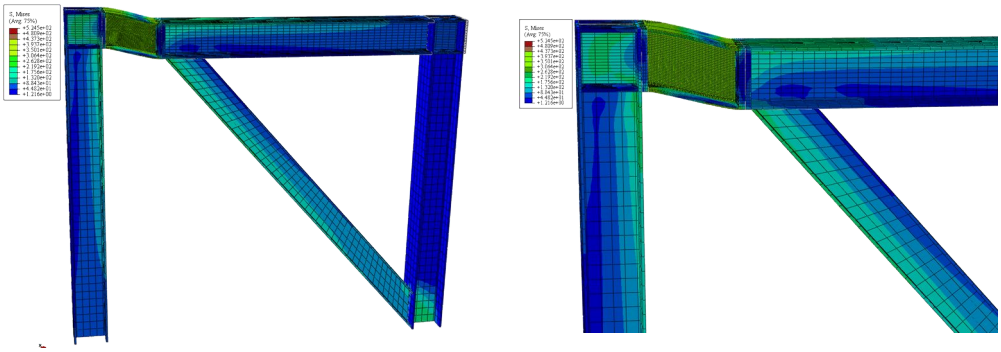

(a) Deformed shape with von Mises stress distribution of 1-story, h/L=1 EBF with unreduced link

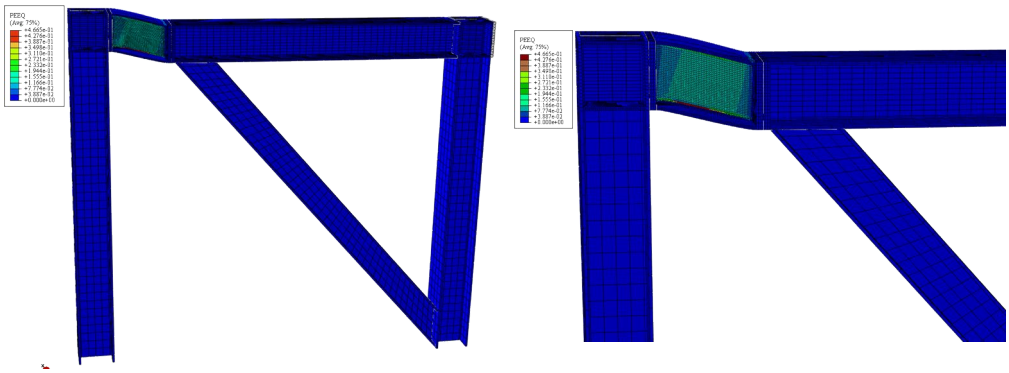

(b) Deformed shape with equivalent plastic strain distribution of 1-story, h/L=1 EBF with unreduced link

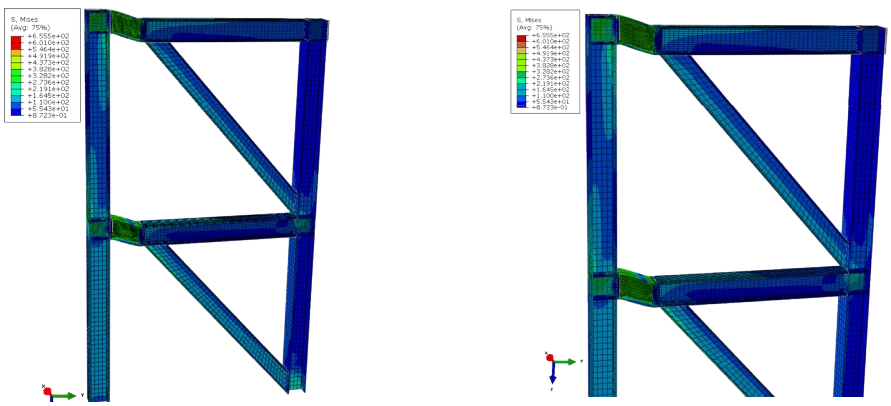

(c) Deformed shape with von Mises stress distribution of 2-story, h/L=1 EBF with unreduced link

Fig. D.4 Deformed shape of EBFs with von Mise's stress and equivalent plastic strain distribution

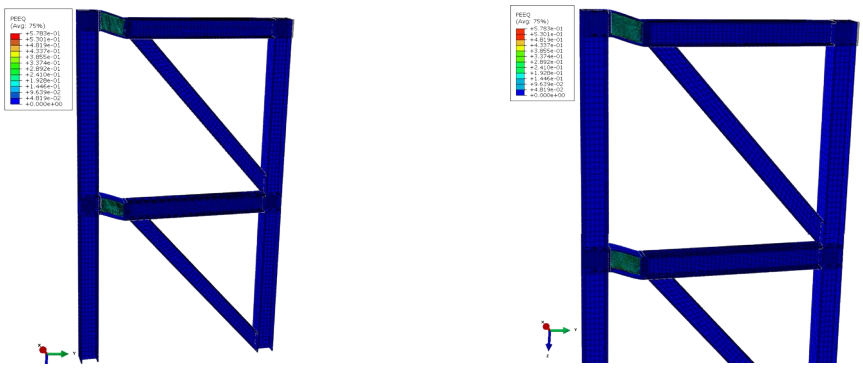

(d) Deformed shape with equivalent plastic strain distribution of 2-story, h/L=1 EBF with unreduced link

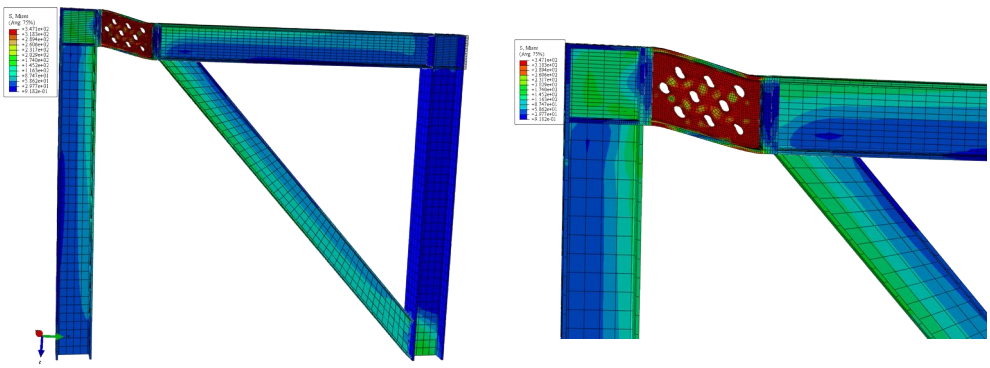

(e) Deformed shape with von Mise's stress distribution of 1-story, h/L=1 EBF with reduced link

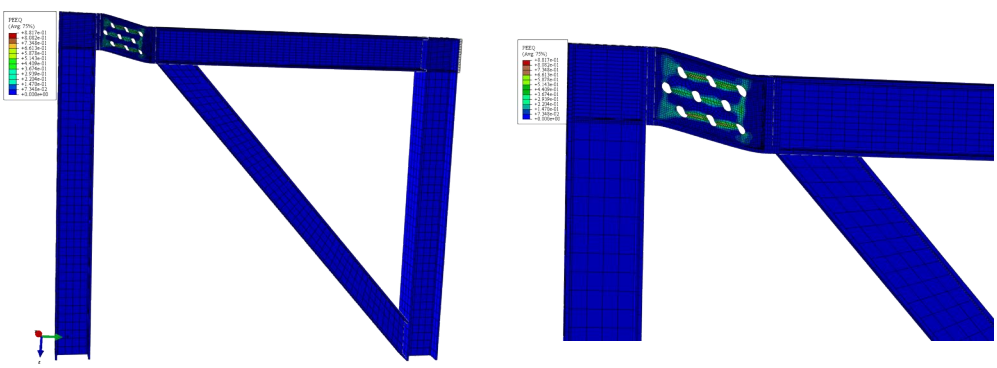

(f) Deformed shape with equivalent plastic strain distribution of 1-story, h/L=1 EBF with reduced link

Fig. D.4 Deformed shape of EBFs with von Mise's stress and equivalent plastic strain distribution *(Continued...)*

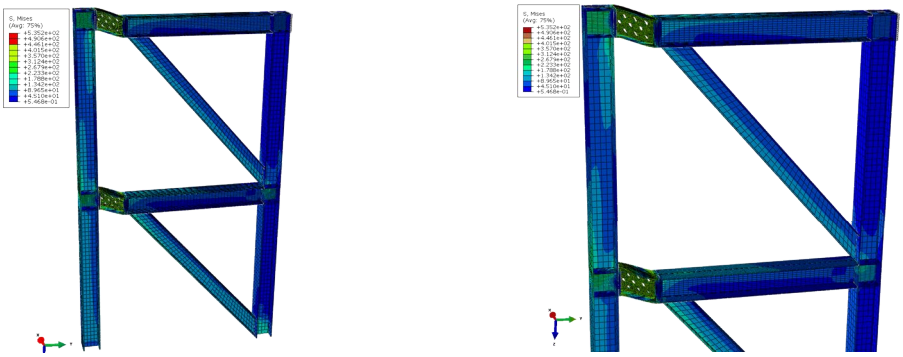

(g) Deformed shape with von Mise's stress distribution of 2-story, h/L=1 EBF with reduced link

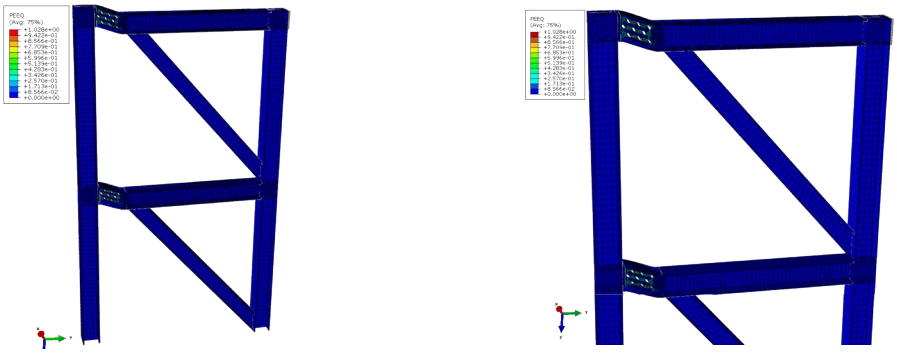

(h) Deformed shape with equivalent plastic strain distribution of 2-story, h/L=1 EBF with reduced link

Fig. D.4 Deformed shape of EBFs with von Mise's stress and equivalent plastic strain distribution *(Continued...)*

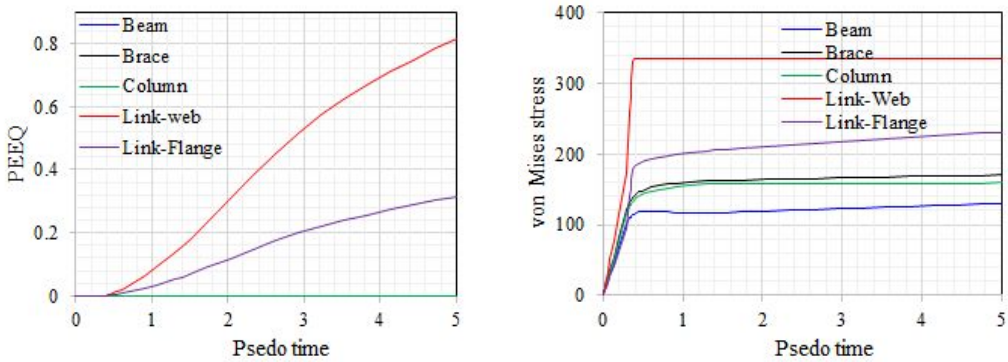

(a) PEEQ distribution in EBFs (b) von Mises stress distribution in EBFs

Fig. D.5 PEEQ and von Mises stress distribution in 1-story EBFs with reduced shear link

The relationship of base shear force-story drift of analysis result was shown in Fig. D.6. The parameters used link section type and h/L ratio of frame. As shown in Fig. D.2, as the h/L increase the bases shear decreases. As the story number increased the base shear is decreased. The base shear of reduced links in also less compared to unreduced links for both 1-story and 2-story frames.

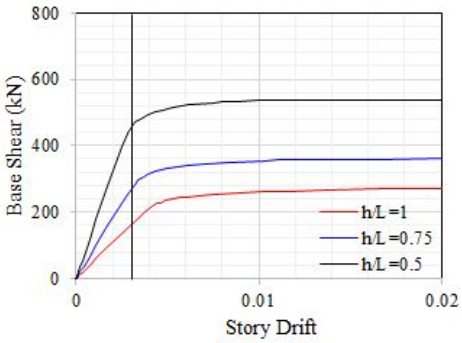

(a) 1-story frames with reduced web link

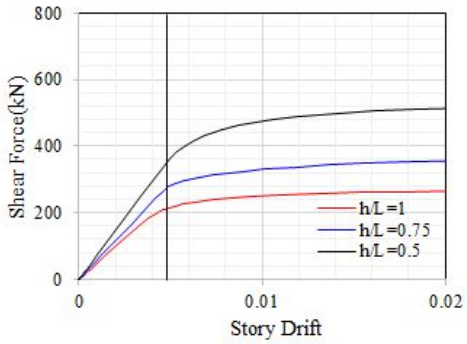

(b) 2-story frames with reduced web link

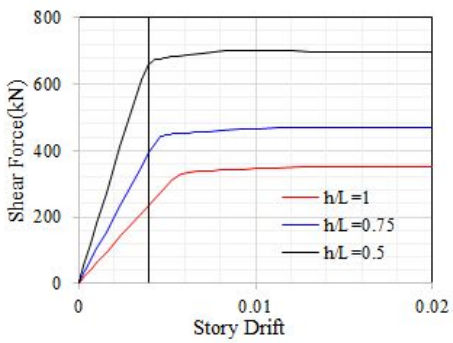

(c) 1-story frames with unreduced link

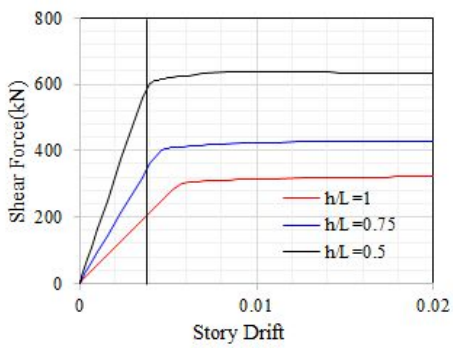

(d) 2-story frames with unreduced link

Fig. D.6 Base shear-story drift relationship of D-braced frame under monotonic

D.4 Estimation of initial stiffness EBFs

The stiffness calculated from the analysis result and calculated from the Richard's recommendation and edited for reduced link section is compared. The accuracy of the initial stiffness of EBFs given in Eq. (D.1) checked through calculated stiffness of FE analysis. The difference in the calculated stiffness using modified Eq. (D.1) and stiffness of analysis results is presented in Fig. D.7 for both unreduced and reduced web link sections. The analysis model recommended for conventional link was applied for reduced link section by replacing the link length e by e_{rw} in Eq. (D.1). Looking at the plot presented in Fig. D.7, the percent of stiffness difference of reduced and unreduced link has no significant differences. Comparing the results obtained and presented in Fig. D.7 and the result of Richard presented in Fig. D.2, no apparent difference is observed. Thus, it is fair to say that the initial stiffness of EBFs suggested by Richard can be applied for reduced link section as well.

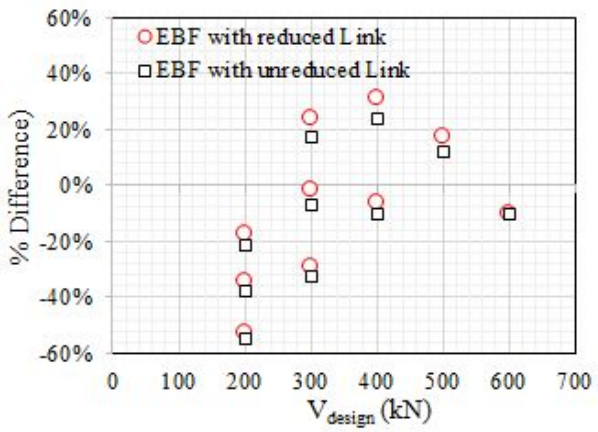

Fig. D.7 Difference in estimated stiffness and stiffness from FE analysis

APPENDIX E. Analytical Model of SDOF System of EBFs

The inelastic behavior of eccentrically braced frames depends on the behavior of links. Thus, correct modeling of link will determine the overall inelastic behavior of EBFs because in EBFs only link beam is assumed to go through plastic (inelastic deformation). Different analytical models have been proposed which includes: Roder and Popov (1977), Ricles and Popov (1987, 1994) Ramadan and Ghobarah (1995), Richards and Uang (2006) and Rozon and Tremblay, (2008). These models were used to describe the behavior of link beam during seismic excitations. The model of link element, proposed by Ramadan and Ghobarah (1995) and slightly modified by Richards and Uang (2006), appeared convenient in predicting maximum shear forces and deformation with respect to the experimental data of shear link (Okazaki et al., 2005 and Rozon et al., 2008). This element is an elastic beam element with lumped plasticity at each end Fig. E.1 (a). Three parallel bilinear springs are assigned between internal and external nodes at each end of the beam in order to achieve a multi-linear force deformation relationship, Fig. E.1 (b) (Richards and Uang 2006).

This model shown in Fig. E.1, was checked if it appears to be convenient in predicting maximum shear forces and deformation for experimental and analytical results of reduced link section. In the application of this model, the plastic shear strength suggested in Eq. (7.1) and the reduced web area using Eq. (7.2) in calculating the variables in Fig. E.1 (b). The analysis model for reduced link has been modeled and presented in Table E.1. The models presented in Table E.1 was compared for the reduced link RWS-S10S1. The comparison of each model is presented in Fig. E.2. As shown in the Fig. E.2, the analysis model suggested by Richard (Richard et al., 2006) and Rozon (Rozon et al., 2008) has difference in the initial stiffness and maximum shear force. The initial stiffness and maximum shear force of analysis model suggested by Ramadan et al, 1995, well agreed with the test result, however, the yield strength has a difference. Looking at the analysis model suggested in this study, well agreed in all initial stiffness, yield shear force and maximum shear forces compared other analysis model.

Table E.1 Analysis model proposed

	V_1 [V_p]	k_{v1}	V_2	k_{v2}	V_3	k_{v3}	k_{v4}
Ramadan and Ghobarah (1995)	1.00*	GA_v/e	1.26*	0.03k_{v1}	1.40*	0.015k_{v1}	0.002k_{v1}
Richards and Uang (2006)	1.10†	$2GA_v/e$	1.30†	0.03k_{v1}	1.50†	0.015k_{v1}	0.002k_{v1}
Rozon and Tremblay, (2008)	1.00*	$2GA_v/e$	1.20*	0.03k_{v1}	1.35*	0.015k_{v1}	0.002k_{v1}
This Study	1.10††	GA_v^*/e_{rw}	1.35††	0.03k_{v1}	1.45††	0.015k_{v1}	0.002k_{v1}

**V based on nominal resistance, $V_p = \phi 0.55 A_v R_y F_y$, with $\phi R_y = 1.0$*
†V based on expected resistance, $V_p = \phi 0.55 A_v R_y F_y$, with $\phi R_y = 1.1$
††V based on expected resistance, $V_p = \phi 0.6 A_v R_y F_y$, with $\phi R_y = 1.1$

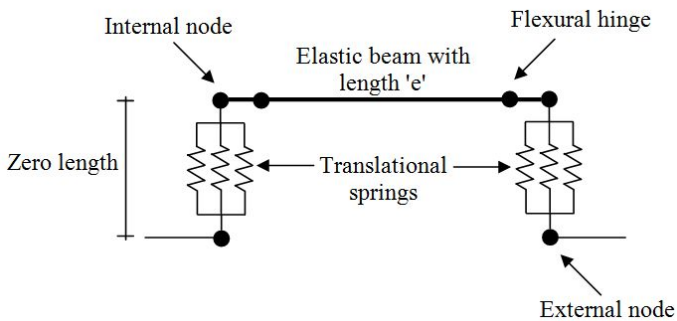

(a)

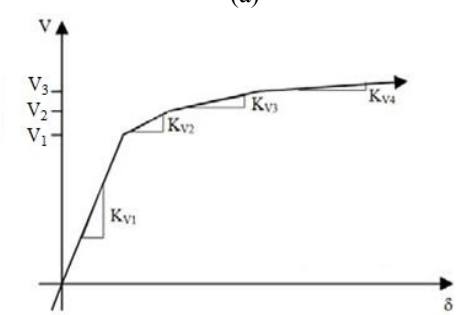

(b)

Fig. E.1 (a): EBF link element; (b): Combined behavior of parallel translational springs

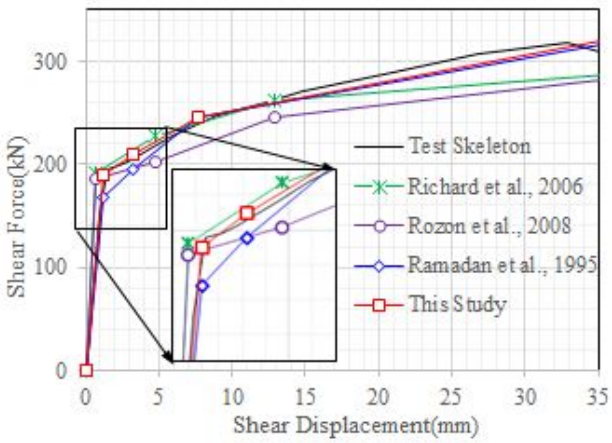

Fig. E.2 Comparison analysis models with Test skeleton for verification

Acknowledgements

ሁሉን ያረገ አምላክ ይክበር ይመስገን።
የእግዚአብሔር ጸጋ የማያስጨርሰው መንገድ የለም።

The financial support for this research was provided by Basic Science Research Program through the National Research Foundation of Korea (NRF) funded by the Ministry of Education, Science and Technology is highly appreciated.

First and for most I would like to express my most sincere gratitude to my supervisor Professor Jaehyouk Choi (Ph.D) for his guidance, support, patience and encouragement during the course of this research and though out my stay here in South Korea. I wish and hope that this is the end for the other beginning.

I thank distinguished Professors/Scientists for not only serving on my dissertation evaluation committee but also for giving me a valuable comments and suggestions on my research. Including: Prof. Jung-uog Park, Civil Engineering Department, Chosun University, Gwangju, Prof. Chang-geun Cho, Architectural Engineering Department, Chosun University, Gwangju, Prof. Sang-hoon Oh, Architectural Engineering Department, Pusan National University, Pusan, and Prof. Young-hyu Ju, Architectural Engineering Department, Korea University, Seoul.

I also thank professors and all faculty members of architectural engineering department including Prof. Hyouk-ki Kim (Ph.D), Prof. Kyu-man Cho (Ph.D) and Prof. Hwang Tea-young (Ph.D) for teaching, guidance and support during my Ph.D courses and research. Special appreciation and thank is addressed to Mr. Gyu-myong Gwak and Dr. Si-jeong Jeong for their support during the experimental works of this research. I also thank all members of SSEEL and Smart green research center including Hyun-soo Kim, Jong-hyun Jank, Jin-hyang Kim, Ji-hoon Hwang, Eun-soo Park, Jung-woo Jong, Meron W. Lemma, Joung-hwa Cho, Hae-ryoung, Ji-hoon An and Ju-hwi kim and all others who I forgotten to mention their name for their cooperation throughout my research works at Chosun University. I extend my thanks to Prof. Fujinaga and Prof. Asada of Kobe University, Japan for their valuable comments on my research.

Hwang-mo Park and Dr. Jin-woo Kim thank you both very much for your friendship and encouragement throughout my stay here in Korea. I extend my special thanks to all friends including: Fikadu, Mingizem, Dr. Girum, Million, Najira, Prof. Borhanian, Mayor, Steve, Dinberu* (for all those papers you sent me*), Hyong-jang Kim, Dr. Mesfin, Chris, Grishima, Roza, Martins, Dr. Annand, Selamu, Dr. Binu, Anish, and Sabin.

I thank my fiance Widist for her understanding and support. Acknowledgments are also due for all my family members my parents Deye and Yaye and all my sisters and brothers, I thank you all very much. I would also like to thank Mrs Joo-hae Kim, Su-myoung Choi and Jong-myoung Choi for your love and for all those time we spent together.

Lat but not the least I thank Dr. Dawit for giving me a reason to come to the Korea and all my friends in Deagu, in Chosun University, in Ethiopia, in USA...

Finally I would like to dedicate this dissertation for my parents W/ro Senait Nigussie (데예) and Mamire Yeshewawork Abebe (야예).

Daniel Y. Abebe
Chosun University
Department of Architectural Engineering
Major: Steel Structure and Earthquake Engineering
January, 2017